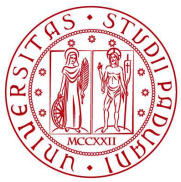

UNIVERSITÀ
DEGLI STUDI
DI PADOVA

Sede Amministrativa: Università degli Studi di Padova

Dipartimento di Fisica Tecnica

SCUOLA DI DOTTORATO DI RICERCA IN INGEGNERIA INDUSTRIALE
INDIRIZZO: FISICA TECNICA
CICLO: XXIV

ENERGY PERFORMANCE, COMFORT AND VENTILATION EFFECTIVENESS OF RADIANT SYSTEMS COUPLED WITH MECHANICAL VENTILATION

Direttore della Scuola: Ch.mo Prof. Paolo Bariani
Coordinatore d'indirizzo: Ch.ma Prof.ssa Luisa Rossetto
Supervisore: Prof. Michele De Carli

Dottoranda : Roberta Tomasi

UNIVERSITÀ
DEGLI STUDI
DI PADOVA

Sede Amministrativa: Università degli Studi di Padova

Dipartimento di Fisica Tecnica

SCUOLA DI DOTTORATO DI RICERCA IN INGEGNERIA INDUSTRIALE
INDIRIZZO: FISICA TECNICA
CICLO: XXIV

ENERGY PERFORMANCE, COMFORT AND VENTILATION EFFECTIVENESS OF RADIANT SYSTEMS COUPLED WITH MECHANICAL VENTILATION

Direttore della Scuola : Ch.mo Prof. Paolo Bariani
Coordinatore d'Indirizzo: Ch.ma Prof.ssa Luisa Rossetto
Supervisore :Ch.mo Prof. Michele De Carli

Dottoranda : Roberta Tomasi

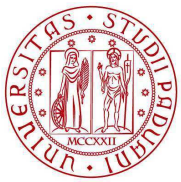

UNIVERSITÀ
DEGLI STUDI
DI PADOVA

Università degli Studi di Padova

Dipartimento di Fisica Tecnica

Doctorate School in Industrial Engineering – Course in Applied Physics

DOCTORATE THESIS

ENERGY PERFORMANCE, COMFORT AND VENTILATION EFFECTIVENESS OF RADIANT SYSTEMS COUPLED WITH MECHANICAL VENTILATION

Director of the School: Prof. Paolo Bariani

Coordinator of the School: Prof. Luisa Rossetto

Supervisor: Prof. Michele De Carli

Co-Advisor: Prof. Bjarne W. Olesen

Ph.D.: Roberta Tomasi

TABLE OF CONTENTS

SOMMARIO

In questo lavoro di dottorato vengono presentati i risultati di uno studio sui sistemi radianti per il raffrescamento ed il riscaldamento in ambito civile e sulla loro integrazione con opportuni sistemi di ventilazione meccanica. Le prestazioni energetiche in regime stazionario e transitorio, così come le prestazioni di comfort termico e di qualità dell'aria garantita, sono state studiate mediante l'ausilio di prove sperimentali, di simulazioni fluidodinamiche e di altri codici di calcolo.

Gli studi sperimentali sono stati realizzati in parte in Italia, presso i laboratori dell'azienda RHOSS S.p.A di Codroipo (Udine), e in parte presso i laboratori dell'ICIEE (International Centre for Indoor Environment and Energy), dell'Università Tecnica di Danimarca, (DTU) a Lyngby (DK).

L'aspetto più rilevante di questo lavoro è legato alla sempre maggiore diffusione dei sistemi radianti come soluzione per il riscaldamento ed il raffrescamento di ambienti interni, in quanto combinano vantaggi energetici ad elevati livelli di comfort termico. Per ragioni dovute alla piccola differenza di temperatura tra l'ambiente e il fluido termovettore, i sistemi radianti si interfacciano molto bene con caldaie a condensazione, pompe di calore, sistemi free cooling, collettori solari e altre sorgenti rinnovabili e soluzioni ad alta efficienza energetica.

Il calcolo della resa termica di tali sistemi viene eseguito mediante le equazioni valide per la convezione in regime stazionario, come quelle fornite dalle norme Europee EN 1264 ed EN 15377. In letteratura esistono numerose correlazioni valide per il calcolo della potenza convettiva di superfici orizzontali e verticali e di superfici interne di stanze reali; le norme EN 1264 ed EN 15377 consigliano correlazioni diverse e lo stesso accade per codici si simulazione energetica degli edifici. Ad oggi non è disponibile una chiara definizione di coefficiente di scambio termico convettivo per i sistemi radianti, specialmente per quanto riguarda pavimenti freddi e soffitti caldi. Il primo obiettivo di questa tesi è stato di realizzare un'analisi critica delle correlazioni disponibili in letteratura adatte ai sistemi radianti e di proporre delle equazioni per ogni configurazione di riscaldamento o raffrescamento da soffitto, pavimento o parete.

In ambito residenziale il pavimento radiante rappresenta una delle soluzioni più richieste grazie all'elevato livello di comfort termico garantito; tuttavia, al fine di migliorare la qualità dell'aria

e specialmente a causa della necessità di deumidificare l'aria in estate per evitare formazione di condensa, accanto al sistema radiante andrebbe installato un sistema di ventilazione meccanica.

L'aria primaria in estate è solitamente a temperatura più bassa della temperatura della stanza e dotata di una certa velocità; nel caso di immissione da bocchette installate vicino ad una superficie radiante, lo scambio convettivo potrebbe venire variato rispetto ad una soluzione senza ventilazione. Mediante uno studio con simulazioni fluidodinamiche CFD è stato possibile valutare l'incremento dello scambio convettivo da un soffitto freddo mediante lo sfruttamento di aria primaria.

I sistemi radianti, in particolare i sistemi a soffitto, rappresentano un'ottima soluzione per rimuovere i carichi termici degli uffici durante il periodo estivo, ma allo stesso tempo possono essere usati per il riscaldamento invernale degli stessi con buone prestazioni energetiche e di comfort termico. La differenza sostanziale è che durante la stagione invernale il sistema radiante si trova a lavorare prevalentemente in regime stazionario, mentre durante la stagione estiva i carichi esterni dovuti alla radiazione solare e all'escursione diurna, accompagnati da carichi interni dovuti all'occupazione umana, determinano condizioni piuttosto variabili durante la giornata. Il comportamento di sistemi radianti a regimi stazionari e transitori sono state studiate mediante prove in camera climatica; inoltre un modello di calcolo chiamato Digithon, sviluppato all'interno del Dipartimento di Fisica Tecnica dell'Università di Padova, è stato validato mediante un confronto con dati sperimentali. Seguendo un'opportuna procedura, riportata nella tesi, è stato possibile impostare dei profili di carico che simulano una tipica giornata estiva o invernale su una parete della stanza ed è stato studiato come il soffitto radiante reagisca per cercare di mantenere una certa temperatura di comfort nella stanza.

Al fine di mantenere una buona qualità dell'aria, evitare la formazione di condensa, ma anche per incrementare la capacità di raffrescamento quando richiesto, i sistemi radianti per gli uffici andrebbero sempre associati a sistemi di ventilazione meccanica. Accanto ai tradizionali sistemi a soffitto con ventilazione a miscelazione, le soluzioni con ventilazione a dislocamento accoppiate a sistemi a pavimento o a soffitto sono alternative di crescente interesse per gli uffici. In edifici dove sia bassa la quantità di inquinanti emessi dai materiali edili, dai mobili e dalle attrezzature, la quantità di bioeffluenti dagli occupanti, dei quali l'anidride carbonica CO_2 è normalmente usata come principale indicatore, è determinante per la qualità dell'aria interna. La capacità di rimozione dei contaminanti e, parallelamente, la capacità di immettere aria pulita negli ambienti sono espresse dall'efficienza di ventilazione (ventilation effectiveness). Mediante simulazione fluidodinamiche CFD è stato possibile confrontare l'efficienza di

rimozione dei contaminanti utilizzando diverse soluzioni di ventilazione a dislocamento piuttosto che soluzioni tradizionali a miscelazione.

La qualità di un ambiente interno andrebbe misurata in termini sia di comfort termico garantito all'occupante che di qualità dell'aria. Attraverso prove sperimentali in laboratorio, i principali indici di comfort termico e di efficienza di ventilazione sono stati determinati per diverse configurazioni di ventilazione a miscelazione e di ventilazione a dislocamento in ambienti rappresentativi di applicazioni residenziali o del terziario. I risultati sono stati in seguito utilizzati per effettuare una validazione di un modello fluidodinamico (CFD) creato per la previsione del movimento dell'aria in ambienti residenziali o uffici.

ABSTRACT

This work presents the results of different numerical and experimental studies about energy performance, thermal comfort and ventilation effectiveness of radiant systems combined with different types of mechanical ventilation. Experimental studies have been carried out in Italy, in a test room in the laboratories of the company RHOSS S.p.A in Codroipo (Udine) and in Denmark, in a test room in the laboratories of the International Centre for Indoor Environment and Energy (ICIEE), at DTU (Danish Technical University), in Lyngby.

Radiant systems in residential and in office buildings are increasingly used because of the low heating or cooling demand and, at the same time, for the good thermal comfort they assure.

The thermal output estimation of radiant system in steady state condition needs the determination of the convective heat transfer coefficient from the surface to the room; a critical review among the correlations available in literature have been carried out and correlations for heated ceiling and cooled floor have been presented. Furthermore the variation of convective heat transfer coefficients, depending on the considered ventilation systems, has been estimated by means of the Computational Fluid Dynamics (CFD) technique.

The energy performance and thermal behavior of radiant systems during transient conditions have been predicted by using experimental tests and numerical calculations with the software Digithon that was developed by the University of Padua. In this work the validation of this software by comparison with experimental data has been presented.

In new and renovated buildings the high tightness and high insulation determine a potential risk of poor indoor air quality and condensation at the surfaces; for this reason an efficient ventilation system is necessary to provide for fresh air in the rooms. In a low polluted building air quality depends on human bioeffluents, among which carbon dioxide is considered the most significant one. By using numerical simulations (CFD) the effects of the supply and extract air terminals on contaminants distribution in offices equipped with a cooled ceiling has been investigated. Besides, in order to fully characterize the indoor climate of residential rooms or offices, an extensive experimental study has been carried out in a test room to determine both thermal comfort and ventilation effectiveness for different solutions of mixing ventilation and displacement ventilation combined with floor radiant systems. In particular, the effects of supply and extract air terminals positions by using low air change rates in mixing ventilation

and the effects of different ventilation rates with displacement ventilations terminals have been analyzed. Results from experiments have been used for the validation of a CFD model for the prediction of air distribution in rooms equipped with mixed or displacement ventilation, combined with heating/cooling floor systems.

1 - Introduction

Radiant systems for heating and cooling are becoming increasingly popular since they represent a good solution for both energy savings and thermal comfort. The low temperature difference between the surface and the room fits well with high efficiency boilers, heat pumps, free cooling, thermal solar collectors and other renewable sources or high efficiency energy solutions.

Floor radiant systems are recommended for residential environments, because the low temperature difference between the floor and the room could guarantee high thermal comfort. Cooled ceiling panels are suitable to remove the heat loads normally present in offices; they can be combined with mixed ventilation or displacement ventilation systems in order to provide for primary air and to increase the cooling capacity when necessary. As an alternative, cooled floors combined with displacement ventilation systems can be used in offices.

The determination of thermal performance of water based surface heating and cooling systems requires the definition of heat transfer coefficients between indoor surfaces and the room. Standards EN 1264 and EN 15377 give the methods to calculate the thermal heating/cooling output under steady state conditions from floor, ceiling and wall. The convective heat transfer coefficients are different in the two Standards. Dynamic simulation models for evaluating energy demand of buildings consider also different heat exchange coefficients. Different equations, based on measurement procedures or on detailed calculations, have been developed in the past for determining convective heat transfer coefficients of vertical and horizontal internal surfaces in the room. Some reviews exist in literature, but no clear decision on heat transfer coefficients values is available, in particular for floor cooling and heated ceiling. One of the goals of Chapter 2 is a critical review on convective heat exchange coefficients and try to check available expressions for calculating these coefficients for each case of heating/cooling from floor, ceiling and wall.

The radiant systems performance and thermal behavior under transient conditions are extremely important since daily solar radiation, internal gains and human occupancy have to be considered in usual applications in residential rooms or offices. For this reason a numerical model able to perform the detailed simulation of the dynamic behaviour of water based surface embedded heating and cooling systems has been already developed by the research group. So far anyway

it was not possible to compare the model against measurements. In this work a validation of the model by using experimental data is going to be presented. In order to perform the validation under real use boundary conditions, a specific procedure to set heating/cooling load profiles aimed to simulate different climatic conditions which have to be faced by ceiling radiant panels has been carried out, as described in Chapters 3 and 4.

Radiant systems need to be assisted by a primary air system, especially when used for cooling purposes, in order to avoid condensation on surfaces at low temperatures. Primary air coming from Air Handling Unit (AHU) is usually colder than room temperature in summer period. In order to investigate on the possible performance enhancement of radiant ceiling coupled with ventilation, convective heat transfer coefficient has been investigated based on CFD (Computational Fluid Dynamics) analysis, as shown in Chapter 5.

As for ventilation, the higher the air flow rates the better the air quality level, but, at the same time, local discomfort could increase, due to draught risk. In addition, high flow rates of primary air require to increase cooling capacity of the AHU and consequently energy consumptions and costs. In low energy buildings the heating demand for space is decreasing, therefore ventilation systems can be used also for heating purposes. If radiant floor systems for cooling are installed without AHU, external warm air could remove contaminant efficiently, but at the same time affect thermal comfort. In order to evaluate indoor climate in a typical room or office when mechanical ventilation is combined with floor heating/cooling systems, an experimental study has been carried out in a fully scale test room. In Chapter 6 thermal comfort parameters, air temperature vertical gradients, velocity vertical profiles and different ventilation effectiveness parameters like contaminant removal effectiveness and air change index have been determined on a residential room indoor climate equipped with different sets of mixed ventilation. On the other hand, the effect of different ventilation rates on indoor climate in a typical office room with a displacement ventilation system has been examined.

In a low polluted building air quality is strongly dependent on the human presence and carbon dioxide is normally used as indicator of human bioeffluents. The effect of the supply and exhaust locations on the contaminant distributions in an office equipped with cooled ceilings has been predicted using numerical simulations (CFD) in Chapter 7. Mixed ventilation was compared with different displacement ventilation solutions (floor outlets or a displacement unit from a wall). Contaminant removal effectiveness, percentage dissatisfied PD% in different positions of occupied zone and a discomfort index for the whole office have been calculated.

Computational fluid dynamic technique is an important tool for the prediction of air flow and contaminant distribution in ventilated spaces. Computational time and simulation costs are constantly reducing, therefore it becomes more convenient using CFD technique to predict indoor climate in rooms. However fully scale experiments are nowadays determinant in order to validate a new CFD model, because the representation of different complex phenomena taking place in the room needs to be compared with measurements.

A CFD model for air distribution in rooms equipped with mixed or displacement ventilation combined with heating/cooling floor systems has been carried out in Chapter 8. It was validated by comparison with experimental measurements in a fully scale test room representing a typical residential room or a typical office with heat gains inside.

2 - A critical review on heat transfer coefficients between heated and cooled horizontal and vertical surfaces and the room

Abstract

Heating and cooling thermal output of surface systems (floor, ceiling and walls) have been recently debated in the standards EN 1264 and EN 15377. Currently, different surface heat transfer coefficients between surfaces and rooms are used. Literature reports different equations, based on measurement procedures or on detailed calculations. Moreover dynamic simulation models for evaluating energy demand of buildings also consider different heat transfer coefficients, like TRNSYS or EnergyPlus. In this work a critical review on convective heat transfer coefficients is presented and available expressions for calculating these coefficients for heated ceiling or cooled floor are presented. The determination of convective heat transfer coefficients is of great help both in radiant systems and in building simulation, due to their interesting use in practice.

2.1 Introduction

Heat transfer coefficients between indoor surfaces and room are very important, since they affect the heat flow and the resulting temperatures. This is a very important issue, since room simulation models are increasingly used. The problem is even more critical, as radiant heating and cooling systems are becoming more and more popular and there is the need to correctly predict their performance in different operating conditions. In the last years, different procedures have been carried out for evaluating the heating/cooling capacity of radiant systems. Depending on the calculation method used, different heat transfer coefficients may be found in literature. Especially for cooled floors and heated ceilings there is an ongoing discussion on which values have to be considered. Heating and cooling thermal output of surface systems (floor, ceiling and walls) have been recently debated in the European Standards EN 1264 [1] and EN 15377 [2] as well as in the new draft of ISO standard on radiant systems. Recently, a review has been carried out by Khalifa [3], but no clear decision on heat transfer coefficients values is available. The present work aims at comparing various expressions for heat transfer coefficients available in literature.

2.2 Literature review

Both natural convective and radiant heat transfer have to be considered in heat transfer analysis within an enclosed room. In natural convection the flow may be laminar or turbulent depending on the geometry properties, the distance and the temperature difference between the surface and the fluid. Since transition occurs in the range $10^7 < Ra < 10^9$, in building application generally the problem of fluid motion is turbulent (Rayleigh numbers are about 1×10^{10}).

There are different ways to consider the heat exchange between a surface and its surroundings. One possibility is to look in detail at the heat flows between each surface and the other ones through radiation and convection between each surface and the air. This problem is shown in Figure 2. 1 (a) for a simplified case where three surfaces (floor, ceiling and one wall) are considered. In the more comprehensive description of the problem, at least six surfaces appear. Another possibility is to deal with the problem considering the radiation between the examined surface and the other surfaces at an equivalent temperature (T_{aust}) and the convection between the considered surface and the air. This case is reported in Figure 2. 1 (b) for the heat transfer between the floor and the surrounding environment. The third case represents the heat exchange between the surface and the room at a unique temperature, which is the operative temperature (T_{op}), as reported in Figure 2. 1 (c) for the heat transfer between the floor and the room.

In all these cases different coefficients can be evaluated, due to the choice of reference temperatures, as debated by Olesen et al. [4].

Another aspect to be considered is the evaluation of heat transfer coefficients and values which can be found in literature. As a matter of fact, three types of correlations to estimate internal heat transfer coefficient for natural convection can be found in literature: correlations for isolated horizontal and vertical plates, for enclosed spaces and from studies in three-dimensional rooms. The description of these three possible correlations is described hereafter and a selection of correlations from various different works available in literature is presented.

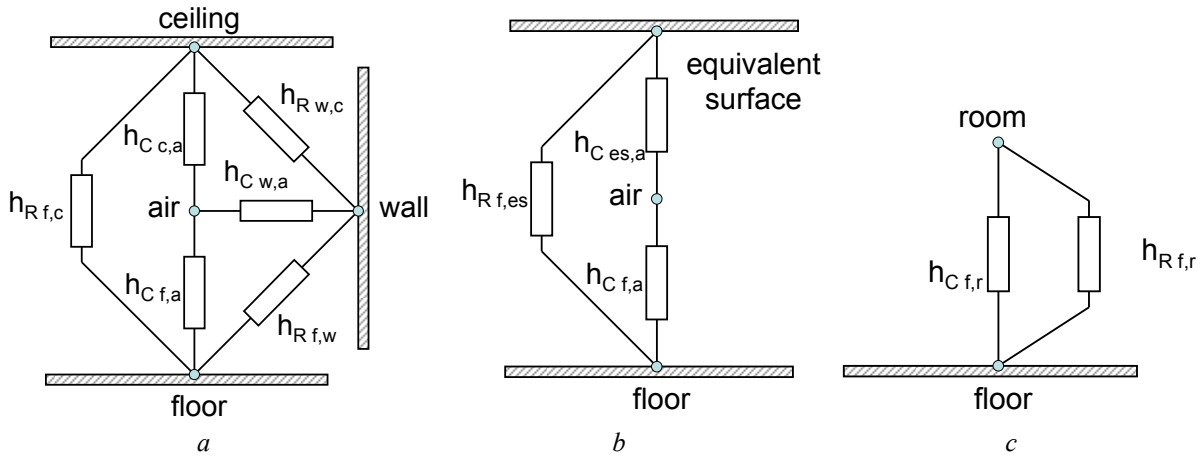

Figure 2. 1 Example of heat exchange between floor and surroundings; a) overall balance (including heat flows to walls and ceiling), b) considering radiation with an equivalent surface and convection with the air, c) synthetic approach (heat flow with the room)

2.2.1 Isolated horizontal and vertical plates

The general relationship for natural convection for an isolated horizontal and vertical plate is:

$$Nu = C \cdot (Gr \cdot \mathrm{Pr})^n \qquad \textit{Eq. 2. 1}$$

For calculating the Grashof number, the plate length is considered as characteristic length. Physical film properties are valued at the average film temperature (T_f) between the surface temperature (T_s) and the undisturbed free stream temperature (T_∞). When dealing with air movement from horizontal plates facing downwards when heated (or upwards if cooled), the effect of convection is in principle very limited, since warm air in the upper part of the space tends to stagnate. Some convection is caused, however, by secondary influences such as temperature differences at the edges of plates. The mechanism of heat loss by conduction and convection from vertical surfaces has been studied starting by numerous air temperature measurements at various location near the surface. Empirical correlations are suggested by Fishenden and Saunders [5] in air atmospheric pressure and at room temperature of 21°C. For heated plates facing upwards the following equations are reported:

$$h_c = 1.32 \cdot \left(\frac{\Delta T}{L} \right)^{0.25} \qquad \textit{Eq. 2. 2}$$

for laminar flow (10^5 <Gr Pr < 2×10^7), while, for turbulent flow (2×10^7 < Gr Pr < 3×10^{10}):

$$h_c = 1.52 \cdot (\Delta T)^{0.33} \qquad \textit{Eq. 2. 3}$$

For heated plates facing downwards, or cooled plates facing upwards (3×10^5 < Gr Pr < 10^{10}), the proposed correlation is:

$$h_c = 0.59 \cdot \left(\frac{\Delta T}{L} \right)^{0.25} \qquad \textit{Eq. 2. 4}$$

For vertical surfaces in turbulent regime (10^9 < Gr Pr < 10^{12}), for air at ordinary temperature and at atmospheric pressure, Weise and Saunders [5] recommend the following relation:

$$h_c = 1.31 \cdot (\Delta T)^{0.33} \qquad \textit{Eq. 2. 5}$$

Similar correlations for natural convection for plane surfaces, in air atmospheric pressure and similar room temperature are proposed by King, Wilkes and Peterson, Giesecke, as reported in [6].

2.2.2 Equations for enclosed spaces

An extensive study of the phenomena associated with heat transfer in enclosed air spaces has been carried out by Mull and Reiher [7, 8], who measured the overall heat transfer coefficient between two parallel plates enclosed around their edges to form a box. For Grashof numbers larger than 2×10^5 the flow is fully turbulent and it is possible to deduce Nusselt value for vertical and for horizontal layers through two correlations obtained by measurements. Mull and

Reiher used plane surfaces 1.0 m by 0.6 m and air layer thickness from 0.0127 m to 0.2 m (i.e. small boxes). The extensive data of Mull and Reiher for air between parallel plates (with upward heat flow) have been correlated by Jakob [5] by equation (2.1), where *C* an *n* are given for different Grashof numbers. The correlation is valid if $Gr < 10^7$ for horizontal plates, while in case of vertical enclosed space, correlation is valid if $Gr < 1.1 \times 10^7$, as reported in Table 2. 1.

Table 2. 1. Parameters C and n used in equation (2.1) valid for enclosed space with natural convection according to Jakob [5]

	Grashof	**C**	**n**
horizontal enclosed space, laminar heat flow	$10^4 < Gr < 3.2 \times 10^5$	0.21	1/4
horizontal enclosed space, turbulent heat flow	$3.2 \times 10^5 < Gr < 10^7$	0.075	1/3
vertical enclosed space , laminar heat flow	$2 \times 10^4 < Gr < 2.1 \times 10^5$	0.20	1/4
vertical enclosed space, turbulent heat flow	2.1×10^5 $Gr < 1.1 \times 10^7$	0.071	1/3

2.2.3 Equations for three-dimensional rooms

Beginning from 1956, with the research of Min [6], a lot of studies have been carried out on heat transfer in a three dimensional room, with the purpose to deduce some correlations describing natural convection phenomena. The heat exchange through radiation is sometimes measured, but often calculated or neglected (if aluminium foil are used on the walls to minimize the effect of long wave radiation). Six experimental test room studies, one numerical and one theoretical method are discussed below.

Min's studies resulted in the following equations for floor convection in a floor-heated space (2.6) and for ceiling convection in a ceiling-heated space (2.7) for a given hydraulic diameter D_e:

$$h_C = 2.416 \cdot \frac{\Delta T^{0.31}}{D_e^{0.08}} \qquad \textit{Eq. 2. 6}$$

$$h_C = 0.2002 \cdot \frac{\Delta T^{0.25}}{D_e^{0.25}} \qquad \textit{Eq. 2. 7}$$

Schutrum and Parmelee [9] studied heat flow distribution for an uniform environment, such as air temperatures at centre of the room and, for each surface, the measured average temperature, heat flow and view factor $F_{c,i}$ (between ceiling surface and the other surfaces). The heat flow from ceiling for different ceiling temperatures and for different average unheated surface temperatures (T_{aust}) is presented.

Khalifa [10] developed 36 correlations describing the convective heat transfer coefficient for nine of the most widely used heating configurations in building: among these the heated floor and the heated vertical wall. During the experimental tests radiant contribute was neglected.

When the floor is heated, Khalifa developed two correlations for the heat transfer coefficient for the other interior surfaces, vertical wall (2.8) and ceiling (2.9).

$$h_C = 2.02 \cdot \Delta T^{0.24} \qquad \textit{Eq. 2. 8}$$

$$h_C = 2.52 \cdot \Delta T^{0.15} \qquad \textit{Eq. 2. 9}$$

When a vertical wall is heated, Khalifa developed the following correlation (2.10):

$$h_C = 2.27 \cdot \Delta T^{0.25} \qquad \textit{Eq. 2. 10}$$

Awbi [11,12] used experimental results to validate the numerical predictions of CFD codes. Surface heat transfer coefficients, valid for floor heating, for ceiling heating and for heated wall, are calculated from measurements at various temperature differences. The proposed equations are:

$$h_C = \left(2.175 \Big/ D_e^{0.076} \right) \cdot \Delta T^{0.308} \qquad \textit{Eq. 2. 11}$$

for floors and

$$h_C = \left(0.704 \Big/ D_e^{\,0.601} \right) \cdot \Delta T^{0.133} \qquad \textit{Eq. 2. 12}$$

for ceiling and

$$h_C = \left(1.823 \Big/ D_e^{\,0.121} \right) \cdot \Delta T^{0.293} \qquad \textit{Eq. 2. 13}$$

for walls.

In Olesen et al. [4] heat transfer coefficients for floor cooling are calculated with different reference temperatures by four different approaches. In the first approach, radiant heat exchange is calculated using 5.5 W m^{-2} K^{-1} as radiant heat transfer coefficient and the reference temperature T_r for the convection is the air temperature at two different heights (0.6 m and 1.1 m), for 9 test conditions. In the third approach both radiant and convective heat transfer between floor surface and space are calculated with the operative temperature as reference temperature T_r (at the same heights) and the constant value 5.5 W m^{-2} K^{-1} is used as radiant heat transfer coefficient.

Karadağ [13] determines radiant and convective ceiling heat transfer coefficients using a commercial computational fluid dynamics tool. Convective heat transfer is simulated numerically for the cooling case, avoiding radiant heat transfer (ε =0); the resulting equation is:

$$h_C = 3.1 \cdot \Delta T^{0.22} \qquad \textit{Eq. 2. 14}$$

Fohanno and Polidori [14] use the integral formalism for modelling laminar and turbulent heat transfer in a free convection boundary layer along a vertical surface heated with a uniform heat flux density. For building applications, if $\Delta T = T_w - T_\infty$ is the average temperature difference between the wall surface and the ambient fluid, Fohanno and Polidori give two equations for convective heat transfer coefficient:

$$h_C = 1.332 \cdot \frac{\Delta T^{0.25}}{H^{0.25}} \qquad \textit{Eq. 2. 15}$$

for the laminar regime Ra < 6.3 x 10^9, and

$$h_C = 1.235 \cdot e^{(0.0467 \cdot H)} \cdot \Delta T^{0.316} \qquad \textit{Eq. 2. 16}$$

when both laminar and turbulent flow regimes exist (Ra > 6.3 x 10^9).

Causone et al. [15] evaluate the heat transfer coefficients between radiant ceiling and room in typical conditions of occupancy of an office or residential building. Analysis were performed in a real test chamber equipped with radiant panels and a radiant floor. Internal gains were simulated using heated cylinders and heat losses using cooled surface. Temperature differences are in the range of about 7÷10 °C for cooling conditions, in the range of about 3÷4 °C for heating conditions. Authors recommend operative temperature at a height of 1.1 m as reference temperature.

Table 2. 2 and Table 2. 3 report the main characteristic for the examined works for natural convection in three dimensional room.

Table 2. 2. Description of the main characteristics for the examined works in rooms with real dimensions. Part 1

AUTHOR	**MIN [6]**	**SCHUTRUM [9]**	**KHALIFA [10]**	**AWBI [11,12]**
Date	1956	1953	2000	1998
Cases examined	Heated floor and ceiling	Heated ceiling	Heated wall	Heated floor, wall and ceiling
Conditions	Uniform environment, no infiltration, empty room, unlighted room	Uniform environment, no infiltration, empty room, unlighted room	Steady-state conditions Test cell empty, unlighted, tightly	20°C constant in room
Test room [m]	7.47 × 3.66 × 2.44 7.47 × 3.66 × 3.66 7.47 × 3.66 × 2.44	7.47 × 3.65 × 2.44	2.95 × 2.35 × 2.08	2.78 × 2.78 × 2.3
Walls materials	Aluminium panels painted with semi gloss grey paint	Aluminium panels, painted with semi gloss grey paint	Walls/roof: Isocyanurate board covered with aluminium. Floor: styrofoam board with chipboard	12mm Plywood, 50mm expanded polystyrene slab and polithene sheet
Temperature surfaces control	Liquid circulation	Liquid circulation	Cold air in adjacent room	Cold air in adjacent room
Radiation	Measured and calculated	Calculated	Neglected	Calculated
Apparatus	Floor and ceiling panels	Ceiling panels	Seven strips as heated elements	Heating plates
Reference temperature	Air temperature at 1.52 m level	Air temperature at 1.52 m level	Air temperature	Air temperature

Table 2. 3. Description of the main characteristics for the examined works in rooms with real dimensions. Part 2

AUTHOR	OLESEN [4]	KARADAĞ [13]	FOHANNO [14]	CAUSONE [15]
Date	1999	2008	2005	2009
Cases examined	Floor cooling	Cooled ceiling	Heated wall	Heated and cooled ceiling
Conditions	Different combinations of water flow rate, supply temperatures, outside temperatures. Empty room	Floor temperature fixed (25°C); Wall and ceiling temperatures variables	Theoretical analysis based on the integral formalism	Different combinations of water flow rate, supply temperatures, outside temperatures. Empty room
Test room [m]	6 × 4 × 2.8 with a window	3 × 3 × 3 4 × 3 × 4 6 × 3 × 4	Heights up to 3 m	4.3 × 2.7 × 2.56 with a window, a door and four metallic cylinders
Walls materials	Floor: concrete and 0,06 m polystyrene Walls: insulating board covered with grey paint	GAMBIT for room plotting, forced condition: ε =0	Not considered	Insulating boards 120 mm, plaster board panel 15 mm.
Temperature surfaces control	Conditioned space surrounding the room	Forced with CFD	-	Radiant floor and radiant panels on ceiling (n°8) and on three vertical walls (n° 14)
Radiation	Calculated	Neglected	Not considered	Calculated
Apparatus	Hydraulic system below the floor	FLUENT	-	Hydraulic system
Reference temperature	Air and operative temperature at 0.6 and 1.1 m)	Air temperature at the centre of room	Room well stirred air at 20°C	Air and operative temperature at 0.1m, 1.1 m and 1.7 m height

2.3 Development of new correlations

2.3.1 Method

Correlations for isolated horizontal and vertical plates have been chosen when referring to turbulent region or, if specified, for streamline region for facing downward plates. Correlations for enclosed spaces, such as Jakob, have been excluded since they refer to too small boxes or they are valid for Grashof numbers lower than 10^7. Correlations from studies in three-dimensional room have been chosen when referring to similar room conditions, i.e. uniform heating or cooling of the internal air, no infiltration, empty room.

Two or three temperature differences ΔT (between the surface temperature T_s and the reference temperature T_r) have been considered for each situation: 9°C and 16°C for floor heating (FH), 7°C and 10°C for ceiling heating (CH), 4°C and 7°C for floor cooling (FC), 4°C and 9°C for ceiling cooling (CC), 4°C, 10°C and 20°C for vertical wall heating (WH). These values have been considered, since they represent usual values and maximum operational limits for comfort conditions in the occupied space in moderate environments [16] or for usual possible condensation problems. Two equivalent diameters have been chosen: 3 m and 6m.

Since the objective is to compare results from different equations and try to obtain an average value, Min's equations and in general all the results are converted in International Units. Correlations for isolated horizontal and vertical plates and correlations from three-dimensional room studies are treated in separate way. When possible, correlations are grouped on the basis of the reference temperature.

Schutrum results are elaborated as follows. Assuming that the average unheated surface temperature (T_{aust}) coincides with the real surface floor and wall temperature, the heat flow (q) from ceiling at five different ceiling temperatures is deduced. View factors are available for each surface, as to calculate the radiant heat flow via the surface internal temperatures (T_i) and the radiant heat transfer coefficient (h_R= 5.5 W m^{-2} K^{-1}),

$$h_C = \frac{q - \sum_n [F_{c,i} \cdot h_R \cdot (T_c - T_i)]}{(T_c - T_{op})} \qquad \textit{Eq. 2. 17}$$

Khalifa floor heating results are not considered because an expression for the floor in this configuration is not available. Instead results for vertical walls (2.10) are considered in the present work.

Olesen results are elaborated to obtain an expression depending on temperature difference and on the characteristic length considering the mean value of the first 9 tests, which seem to be more accurate, as mentioned by authors. The general expression is:

$$h_C = k \cdot \frac{\Delta T^{0.25}}{D_e^{0.25}} \qquad \textit{Eq. 2. 18}$$

Using the first approach and considering 1.1 m height as reference, k is 1.26 W $m^{-1.75}K^{-1.25}$ using the third method, k is 3.03 W $m^{-1.75}K^{-1.25}$.

Causone results are elaborated to obtain two different values depending on the chosen reference temperature. From the 8 tests in ceiling cooling condition an average convective heat transfer coefficient of 4.4 W m^{-2} K^{-1} has been obtained using air temperature at 1.1 m height as reference, while the value of 5 W m^{-2} K^{-1} has been found if operative temperature (at 1.1 m) is considered. Instead, from the 9 tests in ceiling heating condition the value of 0.3 W m^{-2} K^{-1} for both reference temperatures has been deduced. Only temperature differences included in the range of experimental tests are considered (7, 10 °C for heating and 4°C for cooling).

2.3.2 Results

In Table 2. 4 the calculated heat transfer coefficients for three-dimensional rooms when air temperature is considered as reference are listed. In the last column of Table 2. 4, the mean value among the convective coefficients found for each ΔT and equivalent diameter is reported. Even if relations for a vertical wall are found for heating conditions, it is possible to extend them for cooling; in fact heat flow direction (ascendant or descendant) should not influence heat transfer phenomena due to convection. In Table 2. 5 the heat transfer coefficients for three-dimensional rooms are presented when using the operative temperature as reference. In this case calculations based on reported values were possible only for heating/cooling ceiling and for floor cooling. It is possible to notice how mean radiant temperature can influence the room: operative temperature has a different value compared to air temperature, therefore choosing T_{op} as reference, the convective heat transfer coefficients changes.

In Table 2. 6 the comparison between plates and three-dimensional rooms heat transfer coefficients, when air temperature is considered as reference, is reported. Relations derived for plates and expressions resulting from three dimensional enclosure tests lead to quite close altogether values in the case of floor heating, ceiling cooling and wall heating. Relevant differences are found for the ceiling heating case, where experimental values are significantly lower than the corresponding horizontal plates values. Also results in the case of floor cooling are different compared to the plates studies. It is important to notice that cooling floor situations is represented by only one work [4].

Based on the above described evaluations, the equation (2.19) has been found for floors and ceilings while equation (2.20) is valid for vertical walls:

$$h_C = k \cdot \frac{\Delta T^a}{D_e^{\ b}} \qquad \textit{Eq. 2. 19}$$

$$h_C = k \cdot \frac{\Delta T^a}{H^b} \qquad \textit{Eq. 2. 20}$$

where coefficient *k* and exponents *a* and *b* are reported in Table 2. 7 (if air temperature is used as reference) and Table 2. 8 (if operative temperature is used as reference), D_e. is the hydraulic diameter of the surface and H the height of the room.

Equations (2.19) and (2.20) are represented in Figure 2. 2 if the air temperature is considered as reference and equation (2.19) is represented in Figure 2. 3 if the operative temperature is considered as reference, in the considered temperature difference ranges ΔT.

Table 2. 4 Heat transfer coefficient [W m^{-2} K^{-1}] for three-dimensional room, at corresponding reference temperature differences and for two hydraulic diameters of the floor (3 m and 6 m) and one height of the room (3 m). Air is the reference temperature for the room. Average values (Av.) and standard deviation (St.d) are reported.

Case	**Δt**	**De = 3 m**						**De = 6 m**						**Av.**
Floor	**[°C]**	**[6]**	**[11]**			**Av.**	**St.d**	**[6]**	**[11]**			**Av.**	**St.d**	
heating	9	4.37	3.94			**4.15**	0.31	4.14	3.73			**3.94**	0.28	**4.05**
(FH)	16	5.23	4.70			**4.96**	0.37	4.95	4.46			**4.70**	0.34	**4.83**
Ceiling	**[°C]**	**[6]**	**[9]**	**[11]**	**[15]**	**Av.**	**St.d**	**[6]**	**[9]**	**[11]**	**[15]**	**Av.**	**St.d**	
heating	7	0.25	0.43	0.47	0.30	**0.36**	0.12	0.21	0.43	0.31	0.30	**0.31**	0.11	**0.34**
(CH)	10	0.27	0.51	0.49	0.30	**0.39**	0.13	0.23	0.51	0.32	0.30	**0.34**	0.14	**0.37**
Floor	**[°C]**	**[4]**				**Av.**	**St.d**	**[4]**				**Av.**	**St.d**	
cooling	4	1.20				**1.20**		1.20				**1.20**		**1.20**
(FC)	7	1.39				**1.39**		1.39				**1.39**		**1.39**
Ceiling	**[°C]**	**[13]**	**[15]**			**Av.**	**St.d**	**[13]**	**[15]**			**Av.**	**St.d**	
cooling	4	4.21	4.40			**4.30**	0.14	4.21	4.40			**4.30**	0.14	**4.30**
(CC)	9	5.03	4.40			**4.71**	0.44	5.03	4.40			**4.71**	0.44	**4.71**
	[°C]	**[10]**	**[11]**	**[14]**		**Av.**	**St.d**	**[10]**	**[11]**	**[14]**		**Av.**	**St.d**	
Wall	4	3.21	2.40	2.20		**2.60**	0.58	3.21	2.31	2.20		**2.58**	0.63	**2.59**
heating	10	4.04	3.13	2.89		**3.36**	0.64	4.04	3.03	2.89		**3.32**	0.71	**3.34**
(WH)	20	4.80	3.84	3.66		**4.10**	0.68	4.80	3.71	3.66		**4.06**	0.77	**4.08**

Table 2. 5 Heat transfer coefficient [W m^{-2} K^{-1}] for three-dimensional room, at corresponding reference temperature differences. Operative temperature is the reference for the room.

Case	**Δt [°C]**	**De = 3 m**
Ceiling		**[15]**
heating	7	0.3
(CH)	10	0.3
Floor		**[4]**
cooling	4	2.9
(FC)	7	3.3
Ceiling		**[15]**
cooling	4	5.0
(CC)	9	-

Table 2. 6 Average convective heat transfer coefficients [W m^{-2} K^{-1}] for plane surfaces and real sized room, for D_e = 3 m and H = 3m.

	Plane horizontal surfaces					Real sized room				
CASE	**FH**	**FC**	**CH**	**CC**	**WH**	**FH**	**FC**	**CH**	**CC**	**WH**
ΔT [°C]	**W m^2 K^{-1}**					**W m^2 K^{-1}**				
4		1.62		3.97	2.90		1.20		4.30	2.60
7		1.80	1.80				1.39	0.36		
9	4.79			4.79		4.15			4.71	
10			1.93		3.63			0.39		3.36
16	5.49					4.96				
20					4.31					4.12

Table 2. 7 Equations suggested for floor and ceiling heating or cooling and for wall heating/cooling. Air temperature is the reference for the room.

	FH	**FC**	**CH**	**CC**	**WH**
k	1.78	0.72	0.18	2.29	1.71
a	0.4	0.4	0.4	0.4	0.3
b	0.05	0.08	0.10	0.03	0.01

Table 2. 8 Equations suggested for floor cooling and ceiling heating or cooling. Operative temperature is the reference for the room.

	FC	**CH**	**CC**
k	1.74	0.14	2.56
a	0.4	0.4	0.4
b	0.08	0.10	0.03

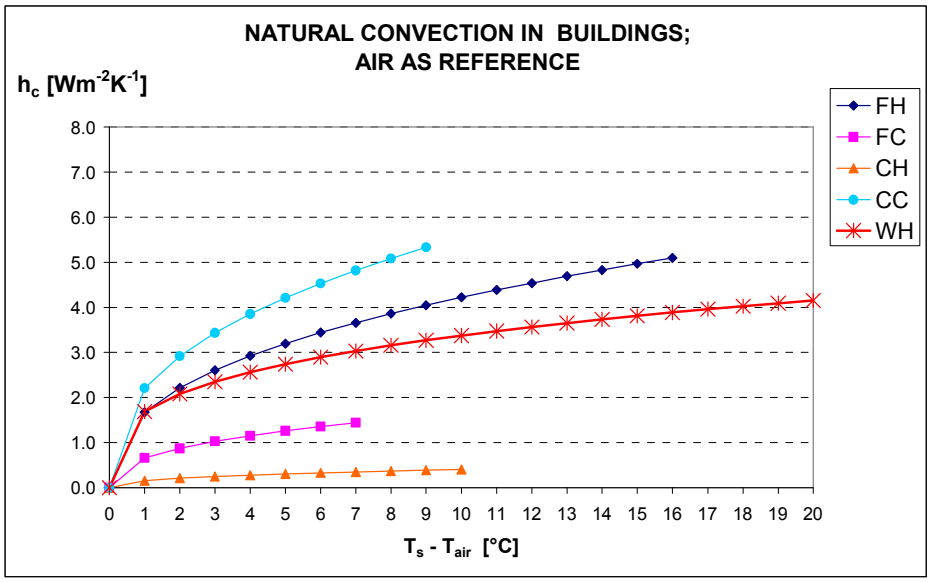

Figure 2. 2 Convective heat transfer coefficient equation from equations (2.19) and (2.20) found in the present work for buildings application. Air temperature is considered as reference for the room.

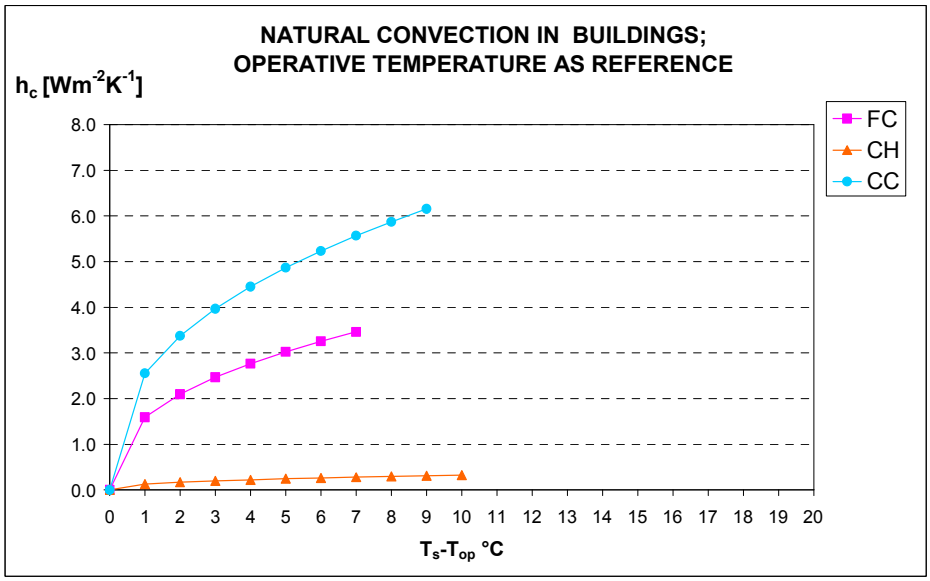

Figure 2. 3 Convective heat transfer coefficients from equation (2.19) found in the present work for buildings application. Operative temperature is considered as reference for the room.

2.3.3. Discussions

Despite the general agreement between plates and three dimensional enclosure relations, convective coefficients resulting from real or simulated rooms would have to be preferred, since they take into account two important aspects: the mutual radiant heat exchange among internal surfaces and the upwards or downwards flow of air during its warming or cooling due to contact with surfaces at different temperatures.

The use of aluminum foil can minimize but not avoid the effect of radiation heat exchange; this assumption may introduce errors in considering the convective heat exchange coefficient in a room. For radiant ceiling, different evaluations in defining a right convective coefficient may occur, when looking at results from horizontal plates and from experimental test room studies (Table 2. 6). This demonstrates that ascendant flow through heated floor may differ from the descendent one through cooled ceiling. Also the behavior of flow from floor cooling differs from the flow of heated ceiling. It looks like that cooling surfaces may induce higher convection movements than heated surfaces. It has anyway to underline that only one study is present in literature on floor cooling. Moreover, studies conducted in similar rooms produce different values (for example, in ceiling heating Causone [15] and Min [6] results). Probably this is due to operating difficulty in radiation measurements [6] and to high relative weight of radiant component on total heat.

A more detailed comparison between different values in literature for plates and the proposed equation based on measurements is reported in Figure 2. 4 for floor heating and ceiling cooling, in Figure 2. 5 for floor cooling and ceiling heating and in Figure 2. 6 for heated and cooled walls. All those comparisons consider equations (2.19) and (2.20) with air as reference temperature (Table 2. 4 and Table 2. 7). As it can be seen, floor heating and ceiling cooling values are inside the range proposed by different values in literature for heated plates facing upwards (Figure 2. 4), as well as for walls (Figure 2. 6) and for floor cooling (Figure 2. 5) for warm plates facing downwards. Only proposed ceiling heating values are different compared to warm plates facing downwards (Figure 2. 5).

According to previous works [4, 15] another result is the influence of the chosen reference temperature for defining the convective heat transfer coefficient, especially for floor cooling configuration (Figure 2. 2 and Figure 2. 3).

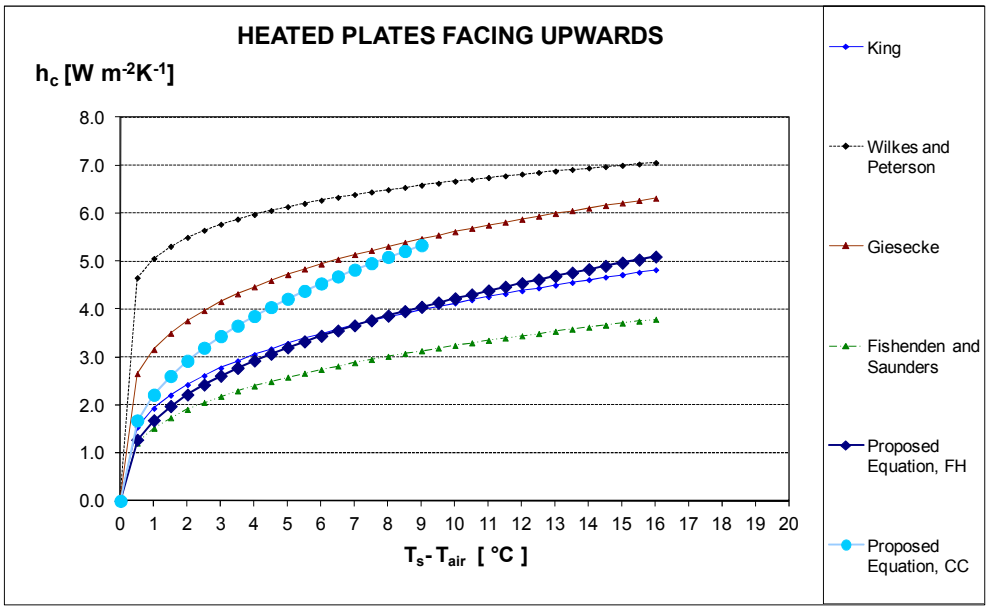

Figure 2. 4 Natural convection heat transfer coefficient equation found for floor heating (Eq.2.19, FH) and ceiling cooling (Eq.2.19, CC) compared with those for horizontal plane surfaces from literature for a room with D_e = 3 m.

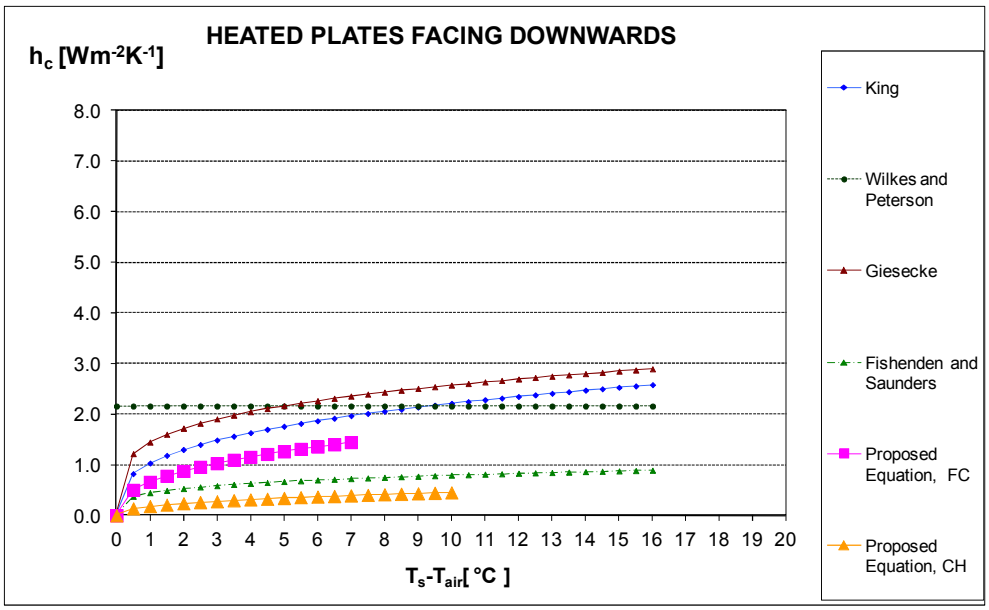

Figure 2. 5 Natural convection heat transfer coefficient equation found for floor cooling (Eq. 2.19, FC) and ceiling heating (Eq. 2.19, CH) compared with those for horizontal plane surfaces from literature for a room with D_e = 3 m.

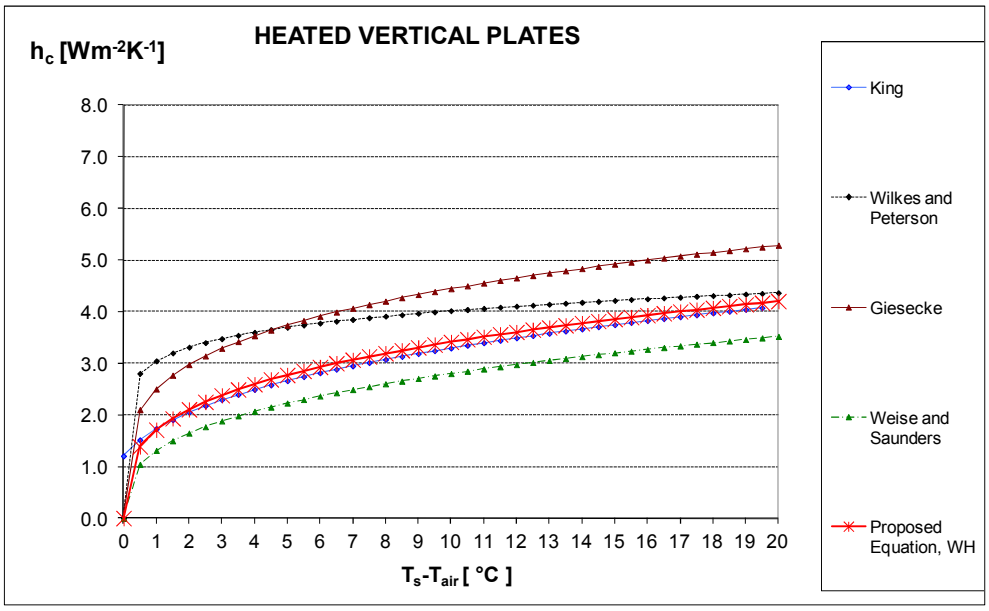

Figure 2. 6 Natural convection heat transfer coefficient equation found for wall (Eq. 2.20, WH) compared with those for vertical plane surfaces from literature for a room with H = 3 m.

Table 2. 9 Natural convective heat transfer coefficients [W m^{-2} K^{-1}] according to Trnsys15, Trnsys16 and Energy-Plus 6 for a room with D_e = 3 m. FIX means simplified default values

	TRNSYS 15					TRNSYS 16					ENERGY PLUS 6					Proposed correlation				
ΔT [°C]	FH	FC	CH	CC	WH	FH	FC	CH	CC	WH	FH	FC	CH	CC	WH	FH	FC	CH	CC	WH
4		0.73		0.73	0.59		1.66		1.66	2.43		1.21		2.40	2.08		1.20		4.30	2.61
7		0.84	1.07				1.97	3.66				1.45	1.45				1.39	0.36		
9	1.16			0.90		3.95			2.13		3.14			3.14		4.15			4.71	
10			1.20		0.74			4.08		3.19			1.64		2.87			0.39		3.37
16	1.38					4.72					3.80					4.96				
20					0.88					3.93					3.56					4.12
FIX											4.04	0.95	0.95	4.04	3.08					

Finally it is interesting to check the convective heat transfer coefficients values used in three dynamic simulation programs commonly used, i.e. TRNSYS-15 [17], TRNSYS-16 [18] and EnergyPlus-6 [19], for the same temperature differences used in experimental analysis (Table 2. 9). EnergyPlus-6 gives the user to choice between the "simple natural convection algorithm" (fixed temperature difference), or the "TARP algorithm", which derives from the Walton algorithm [20]. It is evident a great difference with the experimental results, especially for TRNSYS-15 and TRNSYS-16.

2.3.4. Conclusions

Despite the number of different studies in literature, it looks like that evaluation of convective heat transfer coefficients is not fulfilled yet. More work on measurement activity has to be done, in order to have more cases to collect and to analyze, especially for horizontal heated and cooled surfaces (floor and ceiling), since vertical heated and cooled walls seem to be in agreement with data found in literature.

Symbols

a exponent [-]
b exponent [-]
C constant [-]
D_e equivalent diameter of the room (hydraulic diameter) [m]
$F_{c\text{-}i}$ view factor between the ceiling and the i-th surface elements [-]
Gr Grashof number [-]
H height of the room [m]
h_C convective heat transfer coefficient [$W \cdot m^{-2} \cdot K^{-1}$]
h_R infrared radiation heat transfer coefficient [$W \cdot m^{-2} \cdot K^{-1}$]
L Geometrical factor [m]
k constant [-]
n exponent [-]
Nu Nusselt number [-]
Pr Prandtl number [-]
Ra Rayleigh number [-]
T_{air} air temperatures [°C]
T_{aust} unheated surface temperatures [°C]
Ti general surface internal temperatures [°C]
T_{op} operative temperature [°C]
T_r refence temperature of the room [°C]
T_s general surface temperature [°C]

T_W wall surface temperature [°C]
T_∞ undisturbed free stream temperature [°C]
ΔT Temperature difference between T_s and T_∞ *or* between T_s and the T_r
ε emissivity of surface for radiation [-]

Abbreviations:
CC ceiling cooling
CH ceiling heating
FC floor cooling
FH floor heating
WH wall heating

Subscripts:
C convective part
R radiant part
a air
c ceiling
es equivalent surface
f *floor*
r room
w *wall*

2.4 References

[1] UNI, EN 1264—1999. Floor heating - Systems and components - Definitions and symbols.

[2] UNI EN 15377—2008. Heating systems in buildings - Design of embedded water based surface heating and cooling systems.

[3] Khalifa, A J N. 2000. Natural convective heat transfer coefficient- a review II. Surfaces in two- and three-dimensional enclosures. Energy Conversion and Management, 42,(2000), pp. 505-517.

[4] Olesen, B W, Michel, E, Bonnefoi, F, De Carli, M. 2000. Heat Exchange coefficient between floor surface and space by floor cooling-Theory or a Question of Definition. ASHREE Transactions,2000, 106.

[5] McAdams, W H. Heat Transmission.1954. McGraw-Hill.

[6] Min, T C, Schutrum, L F, Parmelee G V , Vouris, J D. 1956. Natural convection and radiation in a panel-heated room. Heating, Piping & Air conditioning, May 1956, pp. 153-160.

[7] Kreith, F. Principles of Heat Transfer. 1965. Int. Textbook Co, pp 347-348.

[8] Jakob, M. Heat Transfer. Wiley & Sons. 1949. Vol 1, pp. 534-539.

[9] Schutrum, L F, Parmelee, G V, Humphereys, C M.1953. Heat Exchanges in a Ceiling Panel Heated Room. 1953. ASHVE Transactions.

[10] Khalifa, A J N, Marshall R H. Validation of heat transfer coefficients on interior building surfaces using a real-sized indoor test cell. Int. J. Heat Mass Transfer. Vol.33,(1998) No.10, pp.2219-2236.

[11] Awbi, H B. 1998.Calculation of convective heat transfer coefficients of room surfaces for natural convection. Energy and Building. 28,(1998), pp. 219-227.

[12] Awbi, H B. 1999. Natural convection from heated room surfaces. Energy and Buildings, 30 (1999), pp 233-244.

[13] Karadağ, R. 2009. New approach relevant to total heat transfer coefficient including the effect of radiation and convection at the ceiling in a cooled ceiling room. Applied Thermal Engineering.29 (2009) pp.1561-1565.

[14] Fohanno S, Polidori G. 2006 .Modelling of natural convective heat transfer at an internal surface. Energy and Buildings. 38, (2006). pp. 548-553.

[15] Causone F, Corgnati, S , Filippi, M, Olesen B W. 2009. Experimental evaluation of the heat transfer coefficients between radiant ceiling and room. Energy and Buildings. 41,(2009) pp. 622-628.

[16] ISO 7730 – 2005. Ergonomics of the thermal environment -- Analytical determination and interpretation of thermal comfort using calculation of the PMV and PPD indices and local thermal comfort criteria.

[17] Klein, SA, Beckman, WA, Mitchel, JW et al. TRNSYS 15 Manual, University of Wisconsin.2002.

[18] Klein, S.A., TRNSYS 16 Program Manual.SEL, University of Wisconsin, Madison USA. 2007.

[19] EnergyPlus Engineering Reference October 2010.

[20] Walton, G. N. 1983. Thermal Analysis Research Program Reference Manual. NBSSIR 83-2655. National Bureau of Standards.

3 - Test room for the performance analysis of radiant heating and cooling systems

Abstract

A full scale chamber with all six internal surface temperatures controlled by radiant systems has been set up in order to carry out tests of performance analysis of radiant heating and cooling system according to European Standard.

Type B uncertainty of different measurements were calculated from technical data sheets and calibration certificates, considering only the sensor or adding acquisition system uncertainty components. In case of temperature measurements also uncertainty due to calibration was considered. Finally the uncertainty related to the determination of the heating/cooling capacity of the radiant system tested has been evaluated. It was found that calibration uncertainty is determinant in the global uncertainty definition. Meanwhile the difference between thermocouples and resistor thermal detectors uncertainties have been highlighted.

3.1 Test room description

The full scale chamber that is going to be presented in this work is located in the laboratories of RHOSS S.p.A., an Italian company. Its dimensions in plan are 4 m by 7 m and the ceiling height can vary from 2.6 m to 3.6 m by means of a mechanical lifting system.

The test room is thermally insulated from the external environment, consisting in the hosting laboratory. The exterior vertical walls consist in two layers of insulation material (expanded polystyrene) separated by a still air cavity. The thermal resistance achieved by the structures is higher than 3.8 m^2 K W^{-1}. The internal sides of vertical walls and ceiling are covered with radiant panels embedded in gypsum board (doors excluded), arranged in series of three. The floor is equipped with a radiant floor system (5 circuits) with pipes embedded in the screed above a thermal insulation layer (total thermal resistance around 3 m^2 K W^{-1}).

Figure 3. 1 The chamber from outside

The chamber can be set up in conformity with Standard EN 14240 [1] through the separation in two parts, by means of a separating plaster wall. In this way two rooms (with dimensions in plan of 4 m by 4 m and 3 m by 4 m) can be formed. The height was fixed at 3.3 m. Standard EN 14240 gives the method to test and evaluate the cooling power of ceiling panels in a full scale chamber of certain features.

The bigger room has the size recommended by EN 14240, so it may become the effective test room. The other room can be kept at a certain temperature by means of radiant panels and heat flow rate through the separating wall can be controlled.

In the test room ceiling panels were installed in a false ceiling in order to obtain the height of 3 m from the floor as recommended from Standard.

Besides the room was equipped with 12 electrically heated dummies for simulating internal heat gains; the geometric features, the exact position on the floor and the amount of electric power have been chosen in order to satisfy the Standard requirements.

3.2 Sensors and equipments

Water flowing in the radiant systems of the test room comes from three independent circuits: the first one provides for warm water, one for cold water and the third can give warm or cold water.

In order to control the water supply temperature, 3 way valves mix the water from the cold or the warm water tanks with the water return.

Water flows and temperatures in the main hydronic circuits are measured by means of six Pt100 and three magnetic flow meters, while some probes are used to measure the temperature of the air surrounding the test room, at 10 cm distance from the external surface of walls.

Several direct reading flow meters allow to balance the total flow in the secondary circuits (to the radiant panel and to the floor) and thermocouples allow to control outlet temperatures for each group of panels. Around one hundred thermocouples T-type are placed on the internal surfaces.

According to the Standard EN 14240, a globe sensor was placed at the center of the test room at 1.1 m height; three probes for the air temperature with radiation shields were located at different heights (0.1 m, 1.1 m and 1.7 m). One air probe was positioned near a black globe thermometer, so as to calculate operative temperature according to ISO 7726 [2].

There are two types of acquisition systems: direct and indirect. In the direct acquisition system, signals reach the main control panel Compact Field Point (CFP), while in the indirect one signals go into a chassis SCXI and then, through a multimeter, to a computer. In case of resistor temperature detectors RTDs, signal conditioning modules (SCM) are used, while all thermocouples are connected to a cold junction sensor in a isothermal terminal block. A dedicate signal conditioning module is available for the resistor RTD, measuring the temperature in the terminal block, that is the reference for all the thermocouples.

a

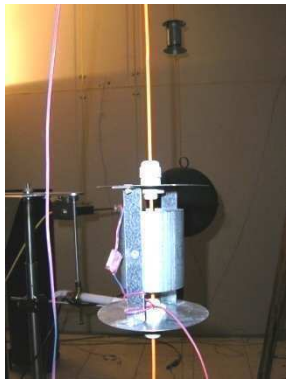

b

Figure 3. 2 Globe sensor and electric dummies(a) and air temperature sensor(b) in the test room

Table 3. 1: Measuring instruments available in the chamber for each category of measurement

Category	Physical quantity	Probe type	Signal
1	Internal air temperature	Thermocouples T	Tc class 2
2	Internal air temperature	RTD	Pt100 DIN 1/3
3	Superficial temperature	Thermocouples T	Tc class 2
4	Water temperature	Thermocouples T	Tc class 2
5	Globe temperature	Globe probe	Pt100 DIN-A
6	Inlet temperature for test panel	RTD	Pt100 DIN 1/10
7	Outlet temperature for test panel	RTD	Pt100 DIN 1/10
8	External temperature	RTD	Pt100 DIN 1/10
9	Main circuits water temperatures	RTD	Pt100 DIN 1/10
10	Terminal block temperature	RTD	Pt100 DIN 1/10
11	Water flow rate	Magnetic flow meter	[4÷20mA]-[1÷100] l/h
12	Electric power	Wattmeter	[4÷20mA [0÷6000] W

3.3 Measurements uncertainty

The formal definition of the term "uncertainty of measurement" developed for use in GUM (Guide to the expression of Uncertainty in Measurement [3]) is as follows:

"*parameter, associated with the result of a measurement, that characterizes the dispersion of the values that could reasonably be attributed to the measurand".*

The GUM introduces the type A and type B uncertainty concepts, that have been resumed in the ENV 13005 [4].

Type A evaluation of uncertainty can be carried out with a statistical analysis of series of observation.

If n observations of the same quantity X are carried out under the same condition, the mean value $\bar{x}$, the experimental variance of the observation $s^2(x_k)$, the experimental deviation $s(x_k)$ and the experimental standard deviation $s(\bar{x})$ should be calculated by applying equations (3.1), (3.2) and (3.3). The experimental standard deviation $s(\bar{x})$ can be used as a measure of the uncertainty of $\bar{x}$ (indicated with $u(x)$) and it is called Type A standard uncertainty.

$$\bar{x} = \frac{1}{n}\sum_{k=1}^{n} x_k \qquad \textit{Eq. 3. 1}$$

$$s^2(x_k) = \frac{1}{n-1}\sum_{k=1}^{n}\left(x_k - \bar{x}\right)^2 \qquad \textit{Eq. 3. 2}$$

$$s^2(\bar{x}) = \frac{s^2(x_k)}{n} \qquad \textit{Eq. 3. 3}$$

$$u(x) = s(\bar{x}) \qquad \textit{Eq. 3. 4}$$

For an estimate x_i of an input quantity X_i that has not been obtained from repeated observations, the associated estimated variance $u^2(x_i)$ or the standard uncertainty $u(x_i)$ is evaluated by scientific judgment based on all of the available information on the possible variability of X_i. This information could be obtained from previous measurements, manufacture's specifications, calibration and other certificates and general knowledge about the instrument properties. Uncertainty evaluated in this way is denominated Type B standard uncertainty.

Usually in manufacture's specification handbooks or calibration certificate the quoted uncertainty is expressed as a particular of standard deviation or alternatively it is given together with a level of confidence. In this way the standard uncertainty is the quoted uncertainty divided by the multiplier or for the appropriate factor for the normal distribution (unless otherwise indicated). For example, for a level of confidence of 95 %, 95.45% and 99,73%, multiplier factor are 1.96, 2.0 and 3.0.

Sometimes the upper and lower limits a_- to a_+ of the interval in which the quantity X_i lies are known and information about the probability distribution around the middle value are given. In other cases probability distribution should be assumed among normal, rectangular, triangular or trapezoidal distribution.

In case of rectangular distribution, the probability that X_i lies in the interval a_- to a_+ is uniform in all the interval, while with triangular (and trapezoidal) distribution the probability is higher in the centre of the interval.

Within an interval [-a, +a], the estimated variance $u^2(x_i)$ for a rectangular and triangular probability distribution are expressed by equations (3.5) and (3.6) respectively:

$$u^2(x_i) = \frac{a^2}{3} \qquad \textit{Eq. 3. 5}$$

$$u^2(x_i) = \frac{a^2}{6} \qquad \textit{Eq. 3. 6}$$

The standard uncertainty of y, where y is the estimate of Y =f (X_i) obtained as results of N quantities X_i, is determined by appropriately combining the standard uncertainties of the input estimates x_1, x_2, ..., x_N. This combined standard uncertainty of the estimate y is denoted by $u_c(y)$ and can be calculated with the following equation (3.7) if quantities X_i are independent.

$$u_c(y) = \sqrt{\sum_{i=1}^{N} \left(\frac{\partial f}{\partial x_i} \right)^2 u^2(x_i)} \qquad \textit{Eq. 3. 7}$$

If quantities X_i where correlated, equation (3.7) should be modified with additional terms, i.e. the second-order partial derivatives.

Although $u_c(y)$ can be universally used to express the uncertainty of a measurement result, it is often necessary to give a measure of uncertainty that defines an interval that may be reasonable for the measurand. If combined standard uncertainty is multiplied by an appropriate factor k, called coverage factor, the obtained uncertainty is the extended uncertainty U (equation 3.8). The result of a measurement Y is then conveniently expressed like in equation (3.9):

$$U = k \cdot u_c(y) \qquad \textit{Eq. 3. 8}$$

$$Y = y \pm U \qquad \textit{Eq. 3. 9}$$

The value of the coverage factor k is chosen on the basis of the level of confidence required; typical values are from 2 to 3, that corresponds to level of confidence between 95.5 % and 99.7%.

The aim of calibration is to improve the accuracy of a probe. It consists in the comparison between a probe with a reference probe and to correct signal in order to limit the difference with reference. Calibration of temperature sensor like thermocouples and resistor temperature detectors can be done by immersing this probes in a liquid bath together with the reference at

different temperatures; signals are read with an appropriate calibrator and difference between signals reduced.

SIT (Italian National calibration service) guideline [5] based on EA/402 [6] provides the method for analyzing temperature calibration uncertainty. Two types of uncertainty are to be considered:

- type 1: uncertainty due to the transfer of information from reference to sensor that should be calibrated. The instrumental uncertainties of the reference ("working standard"[6]) and of the probe, the uniformity and stability of the temperature in the liquid bath and other effects like hysteresis or drift of the reference temperature must be considered;
- type 2: uncertainty due to signal acquisition from the calibrator.

3.3.1 Instruments

This uncertainty analysis has focused on variables designed to control the heat balance and used to perform a possible test in the chamber. Measurements of temperature and water flow rates were therefore analyzed.

Five temperature measurements types have been individuated and they differed for the probes and/or the acquisition mode. In addition, a water flow rate measurement via a magnetic flow meter was considered. More details are shown in Table 3. 2.

For all instrumental uncertainties a triangular distribution was assumed, while for the components of uncertainty due to acquisition and signal conditioning, rectangular distribution was hypothesized. As required by Standards, the combined standard uncertainty $u_c(y)$ should be multiplied by the coverage factor k to define the expanded uncertainty U. A covering factor k = 2, corresponding to a confidence level of 95.45%, was chosen.

All thermocouples were affected by uncertainty due to the definition of the reference temperature, since the terminal block was not completely isothermal and temperature inside was not homogeneous and may change with the time. However the magnitude of these uncertainties components is limited and cannot be easily found in technical data sheet, so it has been ignored.

Instrumental type B uncertainties for all sensors available from technical data sheet or calibration certificate are reported in Table 3. 3. Unfortunately the accuracy for the electric power associated to dummies was not known (category 12).

As for RTDs, knowing the tolerance class, the tolerance values indicated by standard IEC 60751 [7] has been used. Tolerance limits for thermocouples were taken from IEC 60584-2 [8] assuming tolerance class n° 1 and choosing the bigger of two values. For the flow rate measurements, calibration certificates were used.

Instrumental uncertainty type B for all acquisition and conditioning system elements is reported in Table 3. 4: accuracy information is given for certain boundary conditions, as a function of the reading and the range of values.

For conditioning signal module only the temperature drift declared by the manufacturer and expressed as a percentage of the full scale was considered. The range was set between 0 °C and 95 °C.

Temperature factor for the multimeter was not considered for the uncertainty calculation, since it was assumed that all data have been evaluated in the range 23.0 ± 5.0 °C.

Table 3. 2 Measurement types available and corresponding acquisition system for all categories of measurement

Type of measurements	Probes	SCM+ SCXI+ multimeter	Terminal block+ SCM + SCXI + multimeter	CFP AI 110	CFP RTD 124	Categories
T1	Pt100 1/10 DIN	x				6, 7, 8 e 10
T2	Pt100 A DIN	x				5
T3	Thermocouples T		x			1, 3 e 4
T4	Pt100 1/10 DIN				x	9
T5	Pt100 1/3 DIN				x	2
m_w	Magnetic Flow meter			x		11

Table 3. 3 Instruments accuracy or tolerance (from technical data sheets), for all categories of measurement

Category	Physical quantity	Range multimeter	Tolerance/accuracy
1	Internal air temperature	0÷0.1V	±(0.5°C or 0.0075*|t|) °C
2	Internal air temperature	/	±(0.1°C + 0.00167*|t|) °C
3	Superficial temperature	0÷0.1V	±(0.5°C or 0.004*|t|) °C
4	Water temperature	0÷0.1V	±(0.5°C or 0.004*|t|) °C
5	Globe temperature	0÷10V	±(0.15+0.002*|t|) °C
6	Inlet temperature for test panel	0÷10V	±(0.03+0.0005*|t|) °C
7	Outlet temperature for test panel	0÷10V	±(0.03+0.0005*|t|) °C
8	External temperature	0÷10V	±(0.03+0.0005*|t|) °C
9	Main circuits water temperatures	/	±(0.03+0.0005*|t|) °C
10	Terminal block temperature	0÷10V	±(0.03+0.0005*|t|) °C
11	Water flow rate	/	±0.4%, vel > 1m/s
12	Electric power	0÷10V	N.D.

Table 3. 4 Accuracy (from technical data sheets) for all acquisition system elements

Element	Range [A]	Resolution [B]	Accuracy	Boundary conditions	Temperature factor
Multimeter	10V	$10*10^{-6}$ [V]	$\pm(90*VL*10^{-6} + 6*A*10^{-6})$	23°C±5°C	$\pm(5*VL*10^{-6} + 0.2*A*10^{-6})$
	1V	$1*10^{-6}$ [V]	$\pm(90*VL*10^{-6} +7*A*10^{-6})$	23°C±5°C	$\pm(5*VL*10^{-6} + 0.2*A*10^{-6})$
Signal conditioning module (SCM)	0-95 °C		0.01%F.S./°C	-	N.D.
CFP AI 110	4-20 mA	500 nA	$0.04\%*VL+1*10^{-3}$ [mA]	15÷35°C Typical	N.D.
CFP RTD 124	0-400 Ω	0.0061 Ω	0.06%VL +0.03 [Ω]	15÷35°C Typical	N.D.
VL = reading [V]					

Three uncertainty levels have been calculated:

- Level 1: instrumental uncertainty
- Level 2: instrumental + acquisition system uncertainty
- Level 3: instrumental + acquisition system + calibration (for temperature) uncertainty, that is global uncertainty

To simplify the calculation of the uncertainty it is was assumed that all components of uncertainty are independent; in this way the equation (3.7) can be used.

Calibration of temperature probes was carried out by means of a liquid bath and a Pt100 as reference in the typical temperature range of tests for the chamber (5 °C÷50 °C). Two types of uncertainty were considered:

- type 1: information transfer uncertainty; uncertainty of the working standard (Pt100) and of the probe and uncertainty due to radial uniformity and absolute stability of the bath were considered. Drift of the working standard temperature, hysteresis effects and temperature instability were neglected. Rectangular distribution has been assumed for all the components except the working standard uncertainty (from calibration report); details are in Table 3. 5.
- Type 2: uncertainty due to calibrator; 18 °C as temperature was assumed. Rectangular distribution has been assumed and details can be found in Table 3. 6.

The global calibration uncertainty calculated for a RTDs (Pt100) and for a thermocouples T-type at 18 °C is reported in Table 3. 7.

Table 3. 5 Uncertainty type 1 (information transfer)

Variable X_i	Estimated value x_i	Probability distribution	Standard uncertainty $u(x_i)$	Uncertainty contribution $u_i(y)$
Working standard uncertainty	0.05	Normal	0.02500	0.00063
Measurement probe uncertainty	0.1	Rectangular	0.05774	0.00333
Probe resolution	0.01	Rectangular	0.00577	0.00003
Radial uniformity of the bath	0.004	Rectangular	0.00231	0.00001
Absolute stability of the bath	0.02	Rectangular	0.01155	0.00013
Uncertainty (k = 1)				0.064
Extended uncertainty (k = 2)				0.129

Table 3. 6 Uncertainty type 2 (calibrator)

Variable X_i	Range	Reading	Declared uncertainty	Probability distribution	Standard uncertainty $u(x_i)$
Temperature TC T	-100°C + 300°C	18	0.076	rectangular	0.044
Temperature PT100	-100°C + 500°C	18	0.060	rectangular	0.034

Table 3. 7: Global calibration uncertainty (at 18°C)

Variable X_i	Reading	Uncertainty (k = 1)	Extended uncertainty (k = 2)
Temperature TC T	18	0.078	0.146
Temperature PT100 – 1/10 DIN	18	0.073	0.153

In Table 3. 8 the calculated uncertainties at three levels for all types of measurements are reported. Two water flow rates (150 l/h and 250 l/h) and two temperatures (20 °C and 40 °C) were chosen as representative of the normal operative range in the chamber.

In Figure 3. 3 and Figure 3. 4 the minimum and maximum extreme values of the error band around the reading value are shown, for all temperature measurement types and for each level of uncertainty.

It is evident the significant difference between resistor RTDs and thermocouples (T3), for which the instrumental uncertainty is more than 0.4 °C. Acquisition system does not affect significantly the uncertainty in any case, while calibration is determinant in the case of high accuracy sensors like PT100 1/10 DIN (T1 and T4).

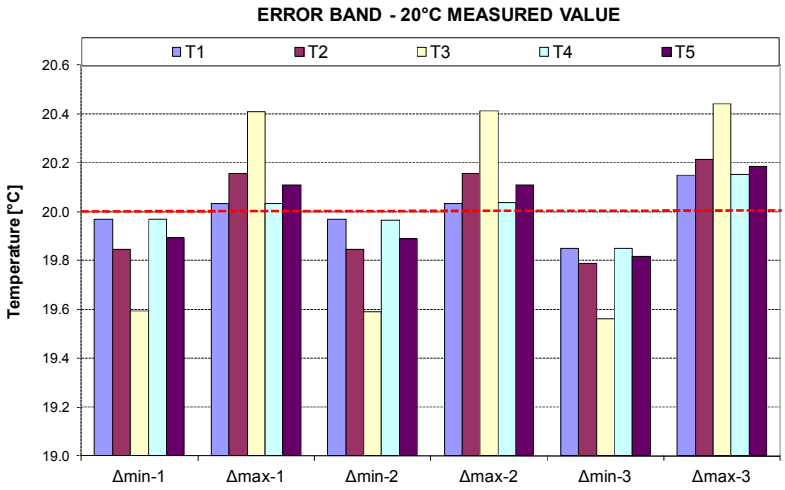

Figure 3. 3 Minimum (Δmin) and maximum (Δmax) values of the error band at 20°C, for all temperature measurement types and for the three levels of uncertainty.

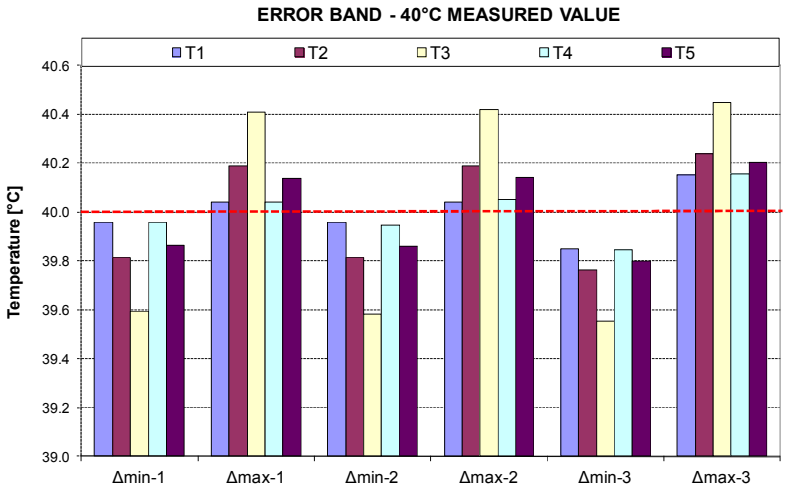

Figure 3. 4 Minimum (Δmin) and maximum (Δmax) values of the error band at 40°C, for all temperature measurement types and for the three levels of uncertainty.

Table 3. 8 Calculated uncertainties for sensor (level 1), for sensor +acquisition system (level 2) and for sensor + acquisition system + calibration (level 3), for six types of measurements and different measured values

Type	Variable	Units	Value	Instrumental uncertainty	Acquisition system uncertainty	Instrumental + acquisition system uncertainty	Global calibration uncertainty	Global uncertainty
				Level 1		Level 2		Level 3
T1	T	°C	20	0.033	0.003	0.033	0.146	0.150
T2	T	°C	20	0.155	0.003	0.155	0.146	0.213
T3	T	°C	20	0.408	0.046	0.411	0.156	0.439
T4	T	°C	20	0.033	0.017	0.037	0.146	0.151
T5	T	°C	20	0.109	0.017	0.110	0.146	0.183
T1	T	°C	40	0.041	0.007	0.041	0.147	0.152
T2	T	°C	40	0.188	0.007	0.188	0.147	0.238
T3	T	°C	40	0.408	0.093	0.419	0.155	0.446
T4	T	°C	40	0.041	0.032	0.052	0.147	0.156
T5	T	°C	40	0.136	0.032	0.140	0.147	0.203
m	m_w	l/h	150	0.490	0.096	0.499	0.0	0.152
m	m_w	l/h	250	0.816	0.152	0.830	0.0	0.830

3.3.2 Cooling capacity

Standard EN 14240 allows to evaluate the performance of a radiant ceiling cooling system in a test room with the surface at temperatures close to the reference environment and a number of artificial heat loads to balance the power of the cooling ceiling.

The cooling capacity is presented as a function of the temperature difference $\Delta\theta$ between the reference room temperature and the mean cooling water temperature. Globe temperature measured in the centre of the room and at 1.1 m height is used as reference temperature.

Specific cooling capacity can be express like:

$$P_a = k \cdot \Delta\theta^n \qquad \textit{Eq. 3. 10}$$

where:

- P_a [W/m^2]: specific cooling capacity;
- $\Delta\theta$ [°C]: temperature difference between the mean cooling water temperature, θ_w, and the reference temperature, θ_r ;
- k [W/(m^2 K^n)]: characteristic constant;
- n: exponent.

Specific cooling capacity shall be calculated from the equation:

$$P_a = \frac{q_m \cdot c_p \cdot (\theta_{w2} - \theta_{w1})}{A} \qquad \textit{Eq. 3. 11}$$

where:

- θ_{w1} [°C]: cooling water inlet temperature;
- θ_{w2} [°C]: cooling water outlet temperature;
- q_m [kg/s]: cooling medium mass flow rate;
- c_p [J/(kg K)]: specific heat capacity of water;
- A [m^2]: active area.

To express the overall uncertainty of the test, a clear distinction between temperature difference uncertainty (u_θ) and cooling capacity uncertainty (u_P) is needed. In this way it is possible to add the error bands on the curve that interpolates the experimental points.

Temperature difference uncertainty u_θ is calculated with equation (3.12), taking into account the globe temperature uncertainty (u_{glob}) and the mean cooling water temperature (u_{mean}) with the equation (3.7) for combined standard uncertainty. In particular u_{mean} is calculated with uncertainties u_{w1} and u_{w2} of water inlet and outlet temperature in the test panel with equation (3.13).

$$u_\theta = \sqrt{\left(u_{mean}^2 + u_{glob}^2\right)} \qquad \textit{Eq. 3. 12}$$

$$u_{mean} = \sqrt{\left(u_{w1}^2 + u_{w2}^2\right)} \qquad \textit{Eq. 3. 13}$$

Cooling capacity uncertainty u_P is calculated considering the flow rate q value and corresponding uncertainty u_q and the water temperature difference $\Delta\theta_w$ and corresponding uncertainty ($u_{\Delta\theta w}$). Applying the relationship for the combined standard uncertainty (Eq. 3. 7) the following equation can be found:

$$u_P = \text{const} \cdot \sqrt{\left[\left(u_{\Delta\theta w} \cdot q\right)^2 + \left(u_q \cdot \Delta\theta_w\right)^2\right]} \qquad \textit{Eq. 3. 14}$$

3.4 Example of test

It was decided to consider experimental results from a test in nominal condition, that is with 8 K of temperature difference $\Delta\theta$ and 2 K of water temperature raise $\Delta\theta_w$ (difference between supply and return temperature of the circuit of the radiant ceiling system tested). This test was carried out in the test room with a water flow rate of 185 l/h.

Temperature difference uncertainty u_θ and cooling capacity uncertainty u_P were calculated at three levels, that is considering only instrumental uncertainty, or adding acquisition system uncertainty and calibration uncertainty. All uncertainty components were calculated as uncertainty type B, using information from technical data sheet and calibration certificates. The extended uncertainty was calculated assuming 2 as covering factor k , corresponding to 95.5 % of confidence.

Results obtained for the nominal case were applied to the other cases required by the Standard, i.e. cases with temperature difference equal to 6 K and 10 K.

From results in Table 3.9 and 3.10 it is evident that level 1 and level 2 uncertainties are similar for both cooling capacity uncertainty u_P and temperature difference u_θ: this means that the acquisition system has a minimal effects on uncertainty. But if one considers also calibration, global uncertainty (level 3) reaches 4.86 % and 10.69 % for $u_{\theta,}$ and u_P respectively.

Another way to present results about uncertainty for a cooling capacity experimental test is through graphical representation of the characteristic curve, as shown in Figures 3.5, 3.6 and 3.7. Uncertainties on temperature difference and on cooling capacity are defined for each experimental point and for each uncertainty level.

Table 3. 9 Calculated extended uncertainties for sensor (level 1), for sensor + acquisition system (level 2) and for sensor + acquisition system + calibration (level 3) related to specific cooling capacity P_a , expresses in [%] of the calculated value

Uncertainty related to calculation of cooling capacity P_a				
Uncertainty [%]	**Confidence level**	**Instrumental uncertainty**	**Instrumental + acquisition system uncertainty**	**Global uncertainty**
		Level 1	**Level 2**	**Level 3**
Combined Standard uncertainty	68.27%	1.14%	1.15%	5.35%
Expanded uncertainty, k = 2	95.45%	2.28%	2.29%	10.69%

Table 3. 10 Calculated extended uncertainties for sensor (level 1), for sensor + acquisition system (level 2) and for sensor + acquisition system + calibration (level 3) related to temperature difference $\Delta\theta$, expresses in [%] of the calculated value

Uncertainty related to calculation of temperature difference $\Delta\theta$				
Uncertainty [%]	**Confidence level**	**Instrumental uncertainty**	**Instrumental + acquisition system uncertainty**	**Global uncertainty**
		Level 1	**Level 2**	**Level 3**
Combined Standard uncertainty	68.27%	1.08%	1.08%	2.43%
Expanded uncertainty, k = 2	95.45%	2.16%	2.16%	4.86%

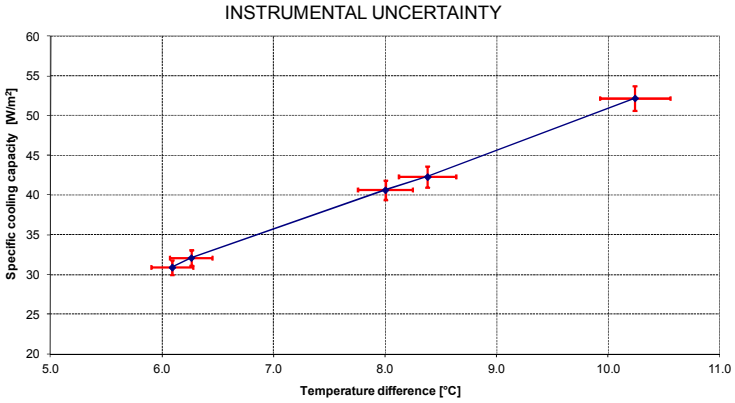

Figure 3. 5 Graphical representation of the characteristic curve according to EN 14240 and punctual uncertainties of level 1 on temperature difference and cooling capacity axes

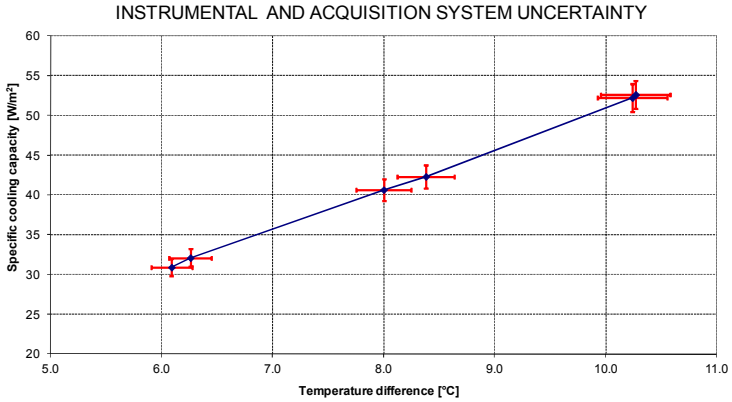

Figure 3. 6 Graphical representation of the characteristic curve according to EN 14240 and punctual uncertainties of level 2 on temperature difference and cooling capacity axes

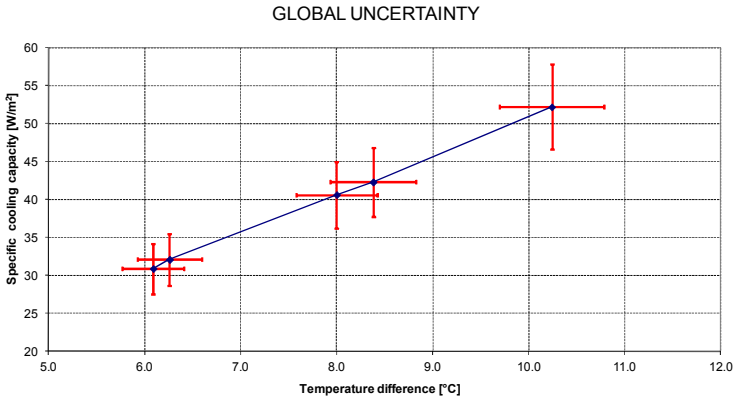

Figure 3. 7 Graphical representation of the characteristic curve according to EN 14240 and punctual uncertainties of level 3 on temperature difference and cooling capacity axes

3.5 Discussions

The fully scale chamber presented is suitable for different experimental tests, thanks to its equipment and instruments. The test for evaluating the cooling capacity of cooled ceiling according to Standard EN 14240 can be carried out in this chamber. The uncertainty analysis shows that type B uncertainties calculated for the only instruments differ from those calculated taking into account the acquisition system and the calibration. Actually, for this test room, the acquisition system does not affect significantly the uncertainty, (Figure 3. 5 vs. Figure 3. 6), but calibration uncertainty is very important in temperature measurements, particularly for high accuracy probes like Pt100 1/10 DIN (Figure 3. 3). When calibration is considered, high expanded global uncertainties can be obtained. For example, the expanded global uncertainties for the specific cooling capacity of a radiant ceiling P_a is 10.69%, while the expanded uncertainty is 2.28 % considering only probes (Table 3. 9).

The method for the uncertainty evaluation presented in this work was applied to a real test case of cooled ceiling, but can be easily adapted to a case of heated ceiling or cooling/heating from floor or wall radiant systems. In fact Standard EN 14240 allows to adapt the method to every case of radiant cooling/heating system.

Alternatively to this method, uncertainties about a test for the cooling performance determination of radiant systems could be evaluated by using the Type A standard uncertainty definition; the probes of main interest for the test could be calibrated together and the uncertainty calculated from statistical elaboration of repeated observations, using the appropriate equations.

3.6 References

[1] EN 14240- 2004. Ventilation for buildings - Chilled ceilings - Testing and rating.

[2] ISO 7726-1998, Ergonomics of the thermal environment- Instrument for measuring physical quantities.

[3] JCGM-2008. (GUM 1995 with minus corrections).Evaluation of measurement data- guide to the expression of uncertainty in measurement.

[4] ENV 13005-1999. Guide to expression of uncertainty in measurement.

[5] SIT/Tec-002/01. November 2001. Linee guida per la taratura dei misuratori di temperatura . SIT-Servizio di taratura in Italia (Italian National calibration service).

[6] EA 4/02. December 1999. Expression of uncertainty of measurement in calibration. European co-operation for accreditation.

[7] IEC 60751 -2008. Ed.2. Industrial platinum resistance thermometers and platinum temperature sensors.

[8] IEC 60584-2- 1982. Ed. 1.Thermocouples. Part 2: Tolerances.

4 - Digithon: a mathematical model for the thermal balance of rooms equipped with radiant heating and cooling systems

Abstract

Water based surface embedded heating and cooling systems have gained appreciable interest and success for a variety of applications in new buildings and renovations. Some problems related to the correct design of these systems were solved a long time ago, but some uncertainties still remain, especially as regards the thermal behaviour under transient conditions.

In this context a numerical model able to perform the detailed simulation of the dynamic behaviour of water based surface embedded heating and cooling systems developed by authors is presented in this chapter. It is validated versus test room measurements. In order to perform the validation under real use boundary conditions, the test room was subjected to heating/cooling load profiles aimed to simulate different climatic conditions which have to be faced by ceiling radiant panels.

The results achieved show that the presented model can predict the real room conditions and that results are not affected by the use of variable or fixed convective heat transfer coefficients.

4.1 Introduction

Water based surface embedded (hereafter simply referred as "radiant") heating and cooling systems have been used widely and for a long time for heating (Shoemaker [1]) and cooling (Olesen [2]) purposes. The most common type of radiant system is the radiant floor, even if radiant ceilings are increasingly used, especially for commercial applications.

Sizing radiant systems taking into account unsteady-state conditions is not a common practice, because few models are available to solve the thermal balance of the room as well as the heat balance inside the pipes embedded in the structure under unsteady state boundary conditions.

As regards the accuracy of simulation models with water based radiant systems, recently some papers demonstrated the accuracy of methods based on different approaches. A FEM program (frequency-domain) and a simplified RC-model (time-domain) were validated for Thermally Activated Building Systems (TABS) using measurement data (Weber et al.[3]). Another validation was carried out for the heat transfer response factor technique (De Carli and Tonon [4]): in this case the model was compared against a detailed numerical model based on FDM.

These works therefore show that the heat conduction through the radiant systems can be efficiently modelled in different ways. The problem becomes more complex when dealing with both conduction through the radiant systems and the overall thermal balance of the room at the same time.

As a matter of fact, a comprehensive validation should consider the entire room calculations, therefore measurements in a test room are needed. Works comparing tests and calculations are few, since it is difficult to achieve high-precision measurements in full scale test rooms and mock-ups.

In this context, the following main issues are usually considered in validating building energy simulation programs:

- Split of internal heat gains into radiant and convective heat transfer components
- Distribution of solar radiation within the enclosure
- Air temperature stratification
- Determination of the convective heat transfer coefficients

Internal heat gains may be split into radiant and convective parts by numerical calculations, by the use of CFD and detailed radiation calculations, or by means of default coefficients. The latter is the method mostly used in building energy simulations, since the consequent error is within the global uncertainty of results.

As regards the distribution of solar radiation, two studies investigated the effect both in heating (Athienitis and Chen [5]) and in cooling conditions (De Carli and Tonon [4]). In particular, in cooling conditions, the solar radiation can be assumed uniformly distributed on the surfaces of the room with no relevant consequence in the accuracy on the energy performance evaluation of radiant systems. For this reason the radiation in the present study will be considered uniformly diffused.

As for the air temperature stratification within enclosures, in rooms with conventional height (less than 3 m), air temperature can be assumed uniform both in heating (Berglund and Gagge [6]) and in cooling conditions (Külpmann [7]), in the case of radiant systems as well as in a wide range of situations that have been confirmed by other studies (Fischer and Pedersen [8]).

Finally, for convective heat transfer coefficients, no clear agreement on values can be found in the literature (Khalifa [9]), even if a recent review (De Carli and Tomasi [10]) shows that the most reliable analyses are those based on measurements in full scale test rooms. This particular aspect will be discussed in detail afterwards.

The present work has the goal to determine the accuracy in modelling light structure radiant systems by validation against data measured in a test room suitably tuned as shown hereafter.

4.2 The model Digithon

The building energy simulation model used in the present work is named DIGITHON and it is based on heat transfer functions method ([4]).

In this model the surfaces enclosing the room are subdivided into elements (named "tiles") and for each of them the surface and water temperatures are calculated, via the "response factor" technique (Stephenson and Mitalas [11], Kusuda [12]). The heat transfer response factors used in the model are calculated by using a commercial software, namely HEAT2 (Blomberg [13]), based on the Finite Difference Method (FDM) technique. Details on the method for calculating response factors in the model as well as the comparison with a detailed FDM are reported in ([4]).

The thermal nodes considered in the model are resumed in the following list (Figure 4. 1 and Figure 4. 2):

- the air thermal node, that represents the entire air volume of the room, mixed;
- the surface thermal nodes, at the inner and outer sides of each wall (named "inner surfaces" and "external surfaces");
- the water thermal nodes, representing the water flow rate inside the pipes (named "water volumes");
- the thermal nodes placed on the surfaces of the pipe segments (named "pipe surfaces").

Assuming a suitable discretization of the time domain by time intervals $\Delta\tau$, the general balance for the *h*-th sub-system, which is assumed to be at a uniform temperature, may be approximated as follows:

$$\left(\sum_i q_i\right)_h = \left(\frac{M\ c_p\left[T_M - (T_M)_{-\Delta\tau}\right]}{\Delta\tau}\right)_h + \left(\sum_v \dot{m}_v c_{pv} T_v\right)_h \qquad \textit{Eq.4. 1}$$

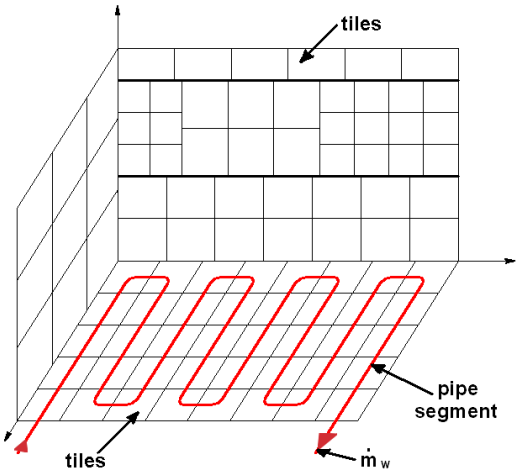

Figure 4. 1 Example of discretization of a room equipped with radiant system embedded in the floor

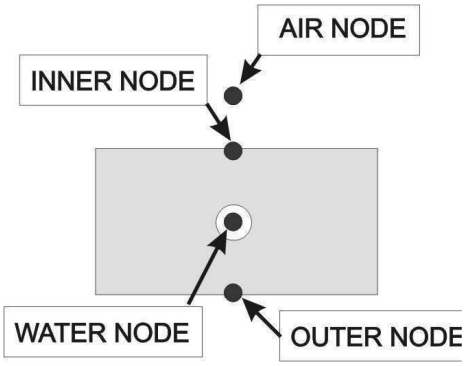

Figure 4. 2 Scheme of the modelization for a generic building element embedding pipes

The heat flows may be conductive, convective or radiative. As already mentioned, the response factor technique has been used to solve dynamic conduction problems through walls and building elements containing pipes.

The temperature difference between two adjacent building elements is very low. As a matter of fact, the length of the pipe is of several meters and the water temperature difference between supply and return is usually in the range of about 3-6°C. Therefore it is possible to assume that the trend of the temperature in each building element is linear and that the outlet water temperature of each segment can be assumed as the representative water temperature for the entire segment. Forced convection takes place inside the pipe and the relationships for the convective heat transfer coefficients both in laminar and turbulent conditions are well established ([14]).

The convective heat flows for the *j*-the general surface element facing air (outdoor and indoor) can be expressed as:

$$q_{c,j} = h_{c,j} S_j \left(T_{s,j} - T_{f,j}\right) \qquad \text{Eq.4. 2}$$

In natural convection the air flow may be laminar or turbulent, depending on the position of the surface and the temperature difference between the surface and the fluid. Since transition occurs in the range $10^7 < Ra < 10^9$, in building applications the problem of fluid motion is generally turbulent (Rayleigh numbers are circa 1 x 10^{10}).

As previously mentioned, the most reliable analyses are those based on measurements in full scale test rooms. In the past a lot of studies were carried out on heat transfer in test rooms, aimed at deriving correlations describing natural convection phenomena.

Awbi [15] used experimental results to validate the numerical predictions of CFD codes. Convective heat transfer coefficients, valid for heated floors, ceilings and walls, were calculated from measurements at various temperature differences. The following equations were proposed for heated floors, ceilings and walls respectively:

$$h_C = \left(2.175 \Big/ D_e^{\,0.076} \right) \cdot \left(T_s - T_f \right)^{0.308} \qquad \textit{Eq.4. 3}$$

$$h_C = \left(0.704 \Big/ D_e^{\,0.601} \right) \cdot \left(T_s - T_f \right)^{0.133} \qquad \textit{Eq.4. 4}$$

$$h_C = \left(1.823 \Big/ D_e^{\,0.121} \right) \cdot \left(T_s - T_f \right)^{0.293} \qquad \textit{Eq.4. 5}$$

In Olesen et al.[16] heat transfer coefficients for floor cooling are calculated with different reference measured temperatures by means of four different approaches. In the first approach, the reference temperature for the convection is the air temperature at two different heights (0.6 m and 1.1 m) and 5.5 W m^{-2} K^{-1} is assumed as radiant heat transfer coefficient for the radiant heat exchange calculation. Results of this work have been further elaborated ([10]) to obtain the following expression:

$$h_c = 1.26 \cdot \frac{\left(T_s - T_f \right)^{0.25}}{D_e^{\,0.25}} \qquad \textit{Eq.4. 6}$$

Karadağ [17] used a commercial computational fluid dynamics tool for the determination of radiant and convective ceiling heat transfer coefficients. Convective heat transfer was simulated

numerically for the cooled ceiling case, avoiding radiant heat transfer (ε =0); the resulting equation is:

$$h_C = 3.1 \cdot \left(T_s - T_f\right)^{0.22} \qquad \textit{Eq.4. 7}$$

As for mutual infrared radiation, assuming near-black surfaces in the infrared with small temperature differences, the following equation may be written:

$$q_{r,j-k} = F_{j-k}\, 4\sigma\left(T_m + 273.15\right)^3 S_j \left(T_{s,k} - T_{s,j}\right) = F_{j-k} h_{r,j-k} S_j \left(T_{s,k} - T_{s,j}\right) \qquad \textit{Eq.4. 8}$$

Due to the low amount of infrared radiation that is reflected by each surface (hypothesis of near-black surfaces) and the homogeneity of emissivity for all surfaces of the room, the contribution of mutual reflections of infrared radiation (hence radiosity) is not considered.

Since the surface discretization in the model is fine, view factors are calculated as follows (Figure 4. 3):

$$F_{j-k} \cong \frac{\cos\phi_j \cos\phi_k S_k}{\pi r^2} \qquad \textit{Eq.4. 9}$$

The mutual overall radiative heat flow exchanged by the surface and the other elements can be expressed as:

$$q_{r\,j} = \sum_{k=1,n} h_{r,j-k} S_j \left(T_{s,k} - T_{s,j}\right) \qquad \textit{Eq.4. 10}$$

where *n* is the number of surfaces radiatively coupled.

The gains due to solar radiation depend on glazing element characteristics. In the model solar gain through a reference window is considered as uniformly distributed in the space. As shown in [4] this assumption is accurate for defining the solar gain distribution in the room. The internal gains are supposed uniformly distributed as well. The resulting overall absorbed radiant gain due to solar radiation and internal radiant loads can be thus approximated as follows:

$$q_{s,j} = \frac{S_j}{S_T}\left[\sum_{G=1,n}(C\ S\ I)_G + q_{I,r}\right] \qquad \textit{Eq.4. 11}$$

The model calculates the temperatures of each thermal node by the solution of a linear system, via matrix inversion. The main output from the model consists in surface, water and air temperatures and in consequent heat flows.

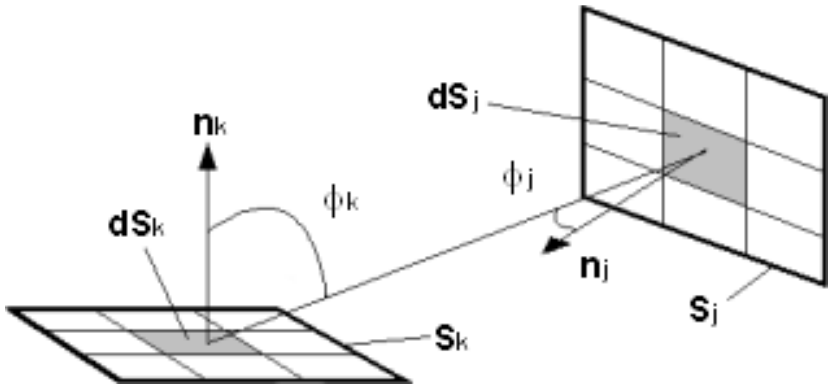

Figure 4. 3 Determination of the view factors between building elements

4.3 Test room: set up and equipments

A test room properly equipped has been set up (Figure 4. 4). Internal dimensions are 7 m (walls North and South) by 4 m (walls East and West) by 3 m (height); two doors are present along wall South side. The room features and details on instruments and acquisition system have been properly described in the previous Chapter 3.

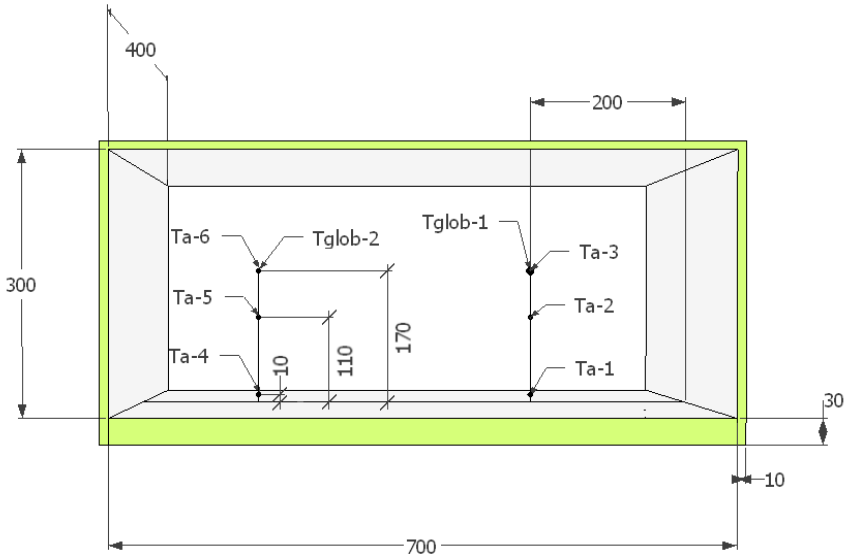

Figure 4. 4 Sketch of the room and positions of air temperature probes (T_a) and globe temperature probes (T_{glob})

Ten electrically heated dummies according to Standard EN 14240:2004 [18] requirements are available if needed for simulating internal heat gains. In order to obtain the heat flows as uniform as possible in the room, they are equally distributed on two rows on the floor.

Two globe thermometers and six air temperature probes placed at different heights permit to monitor the internal room environment (Figure 4. 4). One air probe is positioned near a black globe thermometer, so as to calculate operative temperature according to ISO 7726 [19].

Around one hundred thermocouples T-type are placed on the internal surfaces. Since surface temperature profiles may vary depending on the position of these probes (i.e. above the pipes, in the middle of the pipes, in non activated areas) errors may occur. Therefore such probes have been used only to have a feedback on surface temperatures profiles. The overall balance of the room has been checked by using the measured energy of the water circuits. Average surface temperatures have been used also for determining the convective variable heat exchange coefficients in the simulations, as shown afterwards. Details on the measurement system are reported in Table 4. 1. For each type of measure, the global expanded uncertainty according to EN ISO 13005 [20] with coverage factor k = 2, i.e. a level of confidence of approximately 95.5%, and basing on data from sensor and board producers, so as to find type B uncertainty. Then triangular (for sensors) or rectangular (for acquisition components) shapes of error distribution were assumed and all the uncertainties of components related to each measurement have been combined together, so as to calculate the global uncertainty due to both instruments and acquisition systems.

In this work three case studies are considered: a steady state condition (typical winter design day, namely case 1), a dynamic condition without internal heat gains (typical summer design day, namely case 2) and finally a dynamic condition with the presence of internal heat gains for a part of the day (typical summer design day with workers occupation, namely case 3).The related uncertainties are shown in Table 4. 2 and Table 4. 3 (case 2 and case 3 have the same reference temperature, thus the measurement accuracies are the same).

To improve the room measurement system precision, in particular for temperatures, a suited calibration procedure was carried out by means of a liquid bath and applied to all the probes considered in this test, thus achieving uncertainties lower than 0.025°C if type A uncertainty is evaluated.

Table 4. 1 Details on room measurement instruments

Cod.	Instruments	Measured variable	Unit
T1	Pt100 1/10 DIN	External air temperature under the floor construction	°C
T2	Pt100 1/10 DIN	External air temperature close to walls	°C
T3	Pt100 A DIN	Indoor globe temperature	°C
T4	ThermocoupleTC T	West surface temperature	°C
T5	ThermocoupleTC T	Walls or floor surface temperatures	°C
T6	ThermocoupleTC T	Ceiling surface temperature	°C
T7	ThermocoupleTC T	Air temperature	°C
T8	Pt100 1/10 DIN	West wall water temperatures	°C
T9	Pt100 1/10 DIN	Ceiling water temperatures	°C
T10	Pt100 1/10 DIN	Walls or floor water temperatures	°C
$\mathbf{m_{w1}}$	Magnetic flow meter	Walls or floor water volume flow rate	l/h
$\mathbf{m_{w2}}$	Magnetic flow meter	Ceiling water volume flow rate	l/h
$\mathbf{m_{w3}}$	Magnetic flow meter	West wall water volume flow rate	l/h

Table 4. 2 Evaluation of global sensor + acquisition system uncertainties for each type of measurement for case 1 (temperatures in [°C] and water flow rates [l/h])

Measure	Number of elements	Number of values per element	Reference value	Acquisition + sensor uncertainty
External air temperature under the floor construction	1	1	15	0.015
External air temperature close to walls	5	1	20	0.016
Indoor globe temperature	1	1	20	0.078
West surface temperature	1	3	16	0.205
Floor surface temperature	1	3	20	0.205
Walls or surface temperatures	5	3	20	0.205
Ceiling surface temperature	1	3	23	0.206
Air temperature	1	3	21	0.206
West wall water temperatures	1	2	11	0.015
Ceiling water temperatures	1	2	23	0.020
Walls or floor water temperatures	1	2	21	0.019
Walls or floor water flow rates	1	1	850	1.406
Ceiling water flow rates	1	1	700	1.158
West wall water flow rates	1	1	275	0.457

Table 4. 3 Evaluation of global sensor + acquisition system uncertainties for each type of measurement for cases 2 and 3 (temperatures in [°C] and water flow rates [l/h])

Measure	Number of elements	Number of values per element	Reference value	Acquisition + sensor uncertainty
External air temperature under the floor construction	1	1	15	0.015
External air temperature close to walls	5	1	18	0.016
Indoor globe temperature	1	1	26	0.082
West surface temperature	1	3	33	0.208
Floor surface temperature	1	3	26	0.206
Walls or surface temperatures	5	3	26	0.206
Ceiling surface temperature	1	3	18	0.161
Air temperature	1	3	27	0.214
West wall water temperatures	1	2	41	0.027
Ceiling water temperatures	1	2	18	0.018
Walls or floor water temperatures	1	2	27	0.021
Walls or floor water flow rates	1	1	1000	1.654
Ceiling water flow rates	1	1	970	1.604
West wall water flow rates	1	1	230	0.380

4.4 Method

The influence of the weather is set by means of the imposition of proper heat flows via the radiant panels installed in the internal side of the test room building constructions. In particular, in order to estimate winter and cooling loads through the assumed external surface (corresponding to wall West of the test room), the following phases took place:

- Calculation of heating/cooling loads for the defined room in settled weather conditions
- Calculation of water flows and temperatures to be used in the test room
- Test room measurements
- Comparison of DIGITHON versus test room measurements, under the same boundary conditions

The phases of the analysis procedure are further described in the following sub-sections:

Calculation of heating/cooling loads for the defined room in settled weather conditions

In this phase a room with the same size as the test room, but with typical office envelope constructions, was simulated via DIGITHON, to achieve heating/cooling loads in assessed weather conditions. This simulation is performed considering a convective system to heat/cool the room, since the aim of the phase consists in calculating heating/cooling loads received by the room through the external wall (here corresponding to wall West of the test room). As already mentioned, three case studies were considered: case 1 (steady state winter design day) , case 2 (dynamic conditions of a summer design day) and case 3 (dynamic conditions of a summer design day with internal heat gains). For all cases typical design days of Venice (North-East of Italy) were considered (45° latitude) and the room is supposed to be heated/cooled continuously 24 hours.

Case 1 refers to an internal air temperature of 20°C, while external air temperature is set to -2.8°C (assumption based on the EnergyPlus database [21], [22]). No solar radiation nor internal gains were considered, as usual when simulating a typical winter design day.

Case 2 refers to a clear sky day in July: internal air temperature is set to 26°C, outdoor air temperature was varied between 22.3°C and 31.1°C (based on EnergyPlus database [21], [22]). The external surface of the room consists in a fully glazed wall (12 m^2 surface), facing West, with U = 1.2 W m^{-2} K^{-1} and SHGC = 0.3. No heat gain was considered in this case.

Case 3 refers to the same external weather conditions of case 2, (clear sky day in July), but, since internal heat gains during 10 hours each day have been activated during measurements in the test room, in order to have approximately the same overall heat gain as in case 2 during tests, the fully glazed wall facing West has been considered with the same U-value used in cases 1 and 2, but SHGC = 0.21.

All the other surfaces enclosing the office were considered adiabatic. No infiltration was assumed in the model, since the only action of the external surface had to be predicted by this simulation. Moreover, the indoor air set-point temperature was constant throughout the day and no additional internal heat gain was considered.

In a few words, the profiles of convective load P_{conv} represent the heating and cooling heat flow rates necessary in order to keep comfort temperatures in the room when just climate loads (and eventual internal heat gains) are acting. Time step of simulations was set to 10 minutes. Results of the window internal surface temperatures and of the indoor air temperatures are shown in Figure 4. 5 (a) for winter, (b) for summer design days and (c) for summer design day with internal heat gains. The heat flow rate through the window and the one needed by the convective system are represented in Figure 4. 6 (a), (b) and (c) for the heating design day (case 1), for the cooling design day (case 2) and for the cooling design day with internal heat gains (case 3).

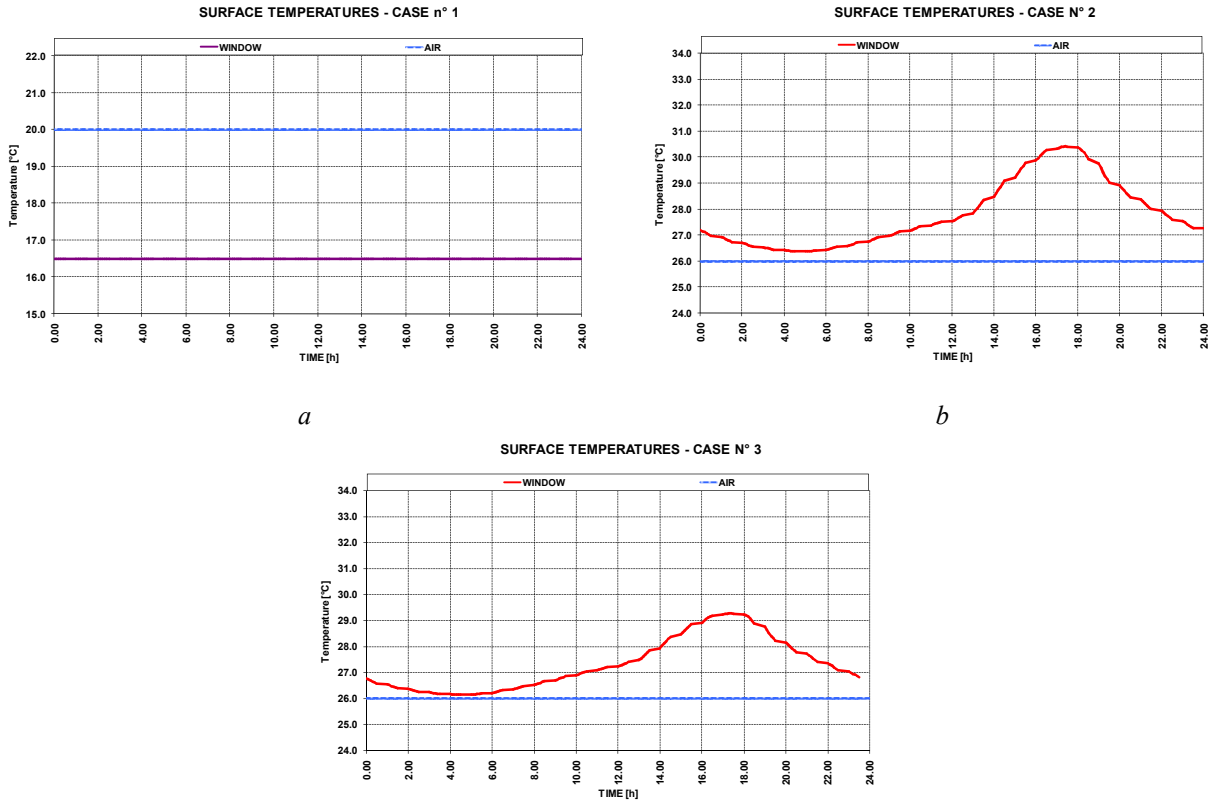

a *b*

c

Figure 4. 5 Calculated daily air temperatures and internal surface temperature of the window in the simulated room in case 1(a), in case 2 (b) and in case 3 (c)

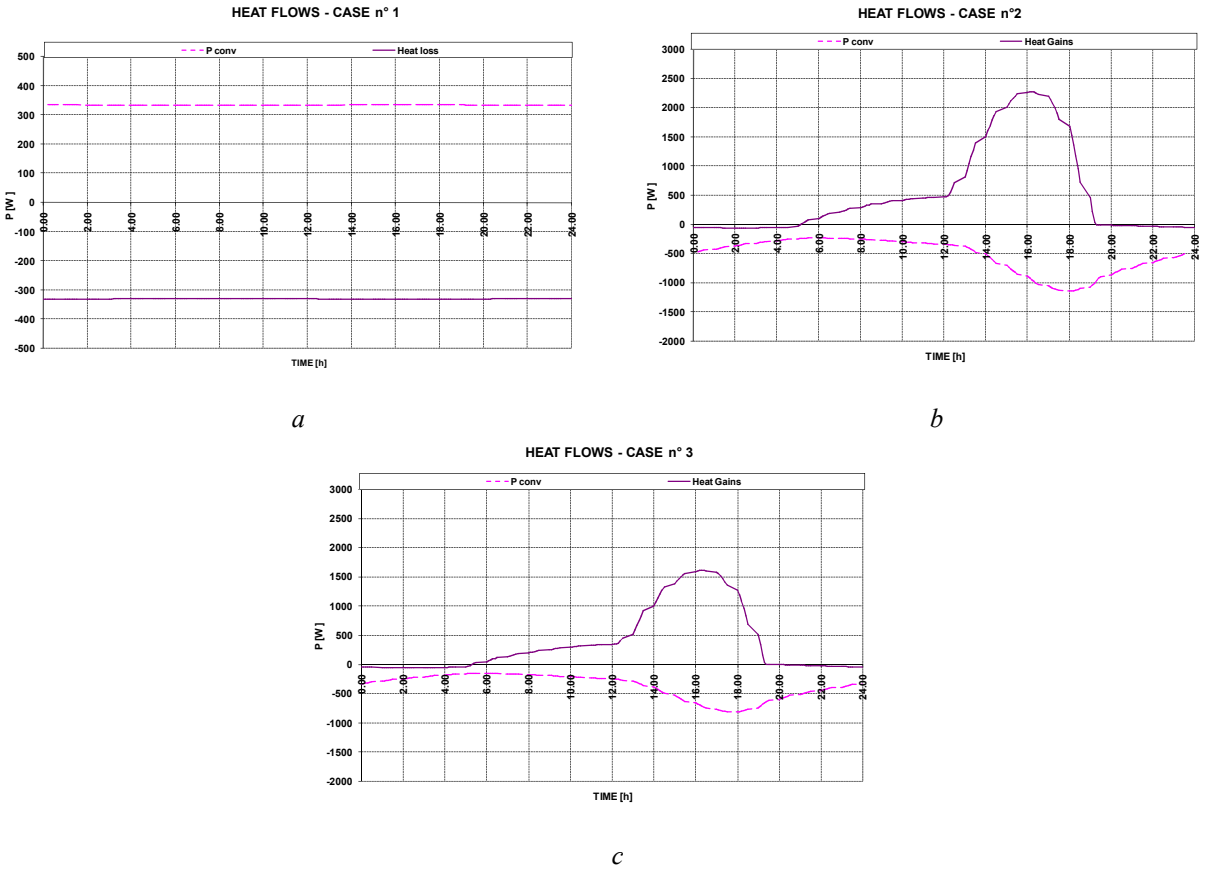

Figure 4. 6 Calculated daily winter heat loss, external heat gains and convective power (P_{conv}) in case 1(a), in case 2 (b) and in case 3 (c)

Calculation of water flows and temperatures to be used in the test room

In this phase, the results of the previous simulations have to be transferred as boundary conditions for the test room to represent typical winter and summer design days.

In fact, in the test room the presence of the assumed weather conditions have to be simulated by the imposition of proper water flows and temperatures in the radiant panels covering the internal side of wall West. The heat loads calculated via DIGITHON have to be therefore transformed into proper water inlet temperatures in the circuits of the West wall of the climatic chamber, considering the actual layers present in the test room building construction. For this purpose a finite difference method simulation tool was implemented to calculate the water inlet temperature to be imposed in wall West, and hence to the actual test room envelope, to get the previously estimated heat flows due to the outdoor weather.

This simulation model calculates the thermal behaviour of test room wall West depending on boundary conditions, under unsteady state boundary conditions. The program iterates until the

water inlet temperature necessary to get the calculated heat flows from the internal side of wall West is achieved. The calculation takes into account even the thermal inertia of the wall: the real construction of wall West is split into eight thermal nodes, as described in Figure 4. 7 and Table 4. 4.

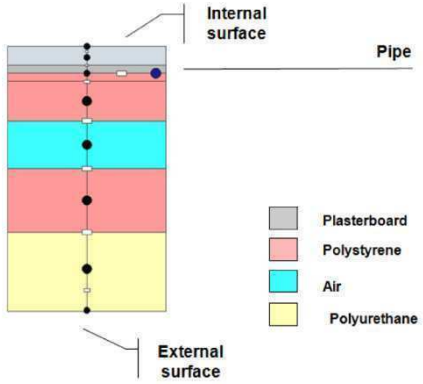

Figure 4. 7 Discretization of the wall West construction (see also Table 4.4))

Table 4. 4 Main characteristics of wall West of the test room (see also Figure 4. 7)

Node	**1**	**2**	**3**	**4**	**5**	**6**	**7**	**8**
Material Int*	Plaster board	Plaster board	Plaster board	Polystyrene	Air	Polystyrene	Polyurethane	Polyurethane
Material Ext**	Plaster board	Plaster board	Polystirene	Polystyrene	Air	Polystyrene	Polyurethane	Polyurethane
Thickness Int [mm]	0.005	5	5	12.5	15	20	10	15
Thickness Ext [mm]	0.005	5	5	12.5	15	20	10	15
R_{int} [$m^2K\ W^{-1}$]	0.000014	0.014	0.014	0.379	0.075	0.606	0.333	0.500
R_{ext} [$m^2\ K\ W^{-1}$]	0.000014	0.014	0.152	0.379	0.075	0.606	0.333	0.500
C [$J\ m^{-2}K^{-1}$]	9	9000	4754	1269	36	2030	870	1305
* Int: towards internal side **Ext: towards external side								

In this structure heat flows previously calculated by the software DIGITHON are imposed as target on the inner surface, while typical temperatures present in the laboratory are used as

boundary conditions on the outer surface. Summarizing, the model implemented is able to determine the water inlet temperature necessary to obtain, at wall West of the real test room, the heat flows previously calculated by DIGITHON.

In this model the radiant panels are linked to node 3 (representing the average conditions in a plane at pipes level) via a resistance network between node 3 and the mean water temperature. The overall resistance between node 3 and the mean temperature of the water in the circuit was calculated via HEAT2 and its value is equal to 0.07 m^2 K W^{-1}. In the end, the heat exchange between the water and the radiant panel is computed through ε-NTU method (Incropera and De Witt [23]). Such model can be used, since the temperature difference between water supply and return is appreciable, whereas the temperature at the pipes level is almost uniform (due to conductivity and thermal inertia of the material embedding the pipes) and subjected to lower increase/decrease compared to the average temperature of the water; it can be thus assumed that the equivalent pipe level has higher thermal capacity than the one of the water flow. The efficiency of this ideal heat exchanger can be therefore simplified as follows:

$$\varepsilon \cong 1 - e^{-NTU} = 1 - e^{-\frac{U \cdot A}{(\dot{m} \cdot c_p)_{Min}}} \qquad \textit{Eq.4. 12}$$

where U is the overall heat transfer coefficient and A is the heat transfer area.

Since the active area of wall West is 65% of the overall area, the heat gain entering from the window P_w, calculated in the first phase via the simulation, was referred to the active area, thus allowing to have the proper supply temperature on the real test facility.

Figure 4. 8 (a), Figure 4. 8 (b) and Figure 4. 8 (c) represent the profile of water inlet temperature and the expected theoretical active wall temperature over the day for cases 1, 2 and 3 respectively.

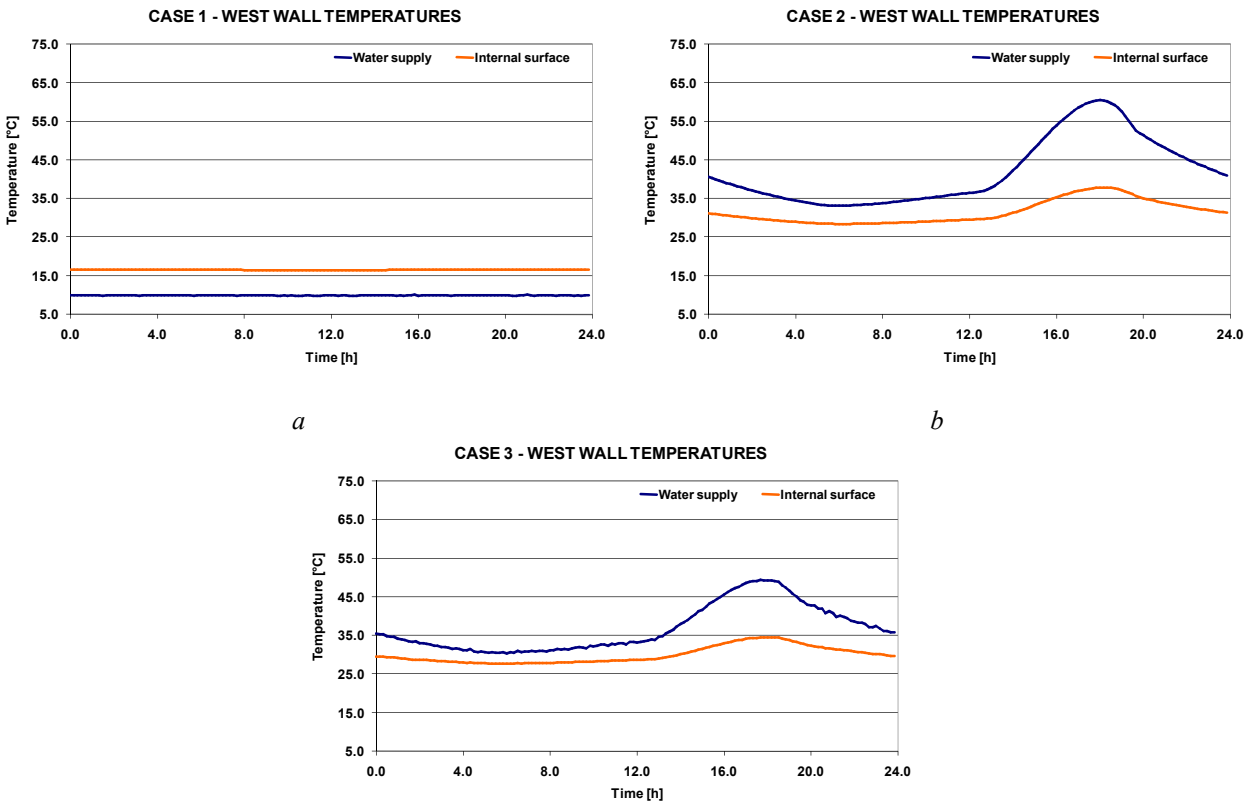

Figure 4. 8 Daily profiles of surface and water supply temperatures estimated for wall West in case 1 (a), in case 2 (b) and 3 (c)

Test room measurements

The tests in the real mock-up room were conducted under the previously defined conditions, via the estimated water inlet temperatures for wall West. The ceiling was used to meet the heating/cooling loads and achieve thermal comfort in the room. The water inlet temperatures for the remaining surfaces were 20°C and 26°C for heating and cooling typical design days respectively. The measurements lasted a suitable amount of days.

As already mentioned, for cases 1 and 2 the heating/cooling loads were imposed via water supply temperatures described in Figure 4. 8 (a), Figure 4. 8 (b) with no internal gains. In case 3 the temperature profile of wall West is the one reported in Figure 4. 8 (c) and internal loads have been imposed by means of dummies uniformly distributed in the room for simulating a typical office with 3 persons and 3 PC active from 9:00 AM to 7:00 PM, for a total of 680 W over the occupancy time.

4.5 The model construction

Water inlet temperatureprofiles were imposed in wall West, in order to simulate the influence of the specific outdoor environment. In the radiant panels embedded in the other surfaces enclosing the indoor environment, water inlet temperatures were set to 20°C for case 1 and 26°C for cases 2 and 3, in order to limit the amount of heat flow exchanged by these surfaces with the room. The consequent heating/cooling loads entering the room were balanced by the ceiling radiant panels through PID regulation, with indoor environment set points at 20°C for case 1 and 26°C for cases 2 and 3. The control strategy is out of the scope of the present work, since the aim of this work is to compare measured and calculated energies and indoor conditions. Water actual inlet temperature profiles measured in the test room are reported in Figure 4. 9 (a) for case 1, in Figure 4. 9 (b) for case 2 and in Figure 4. 9 (c) for case 3.

In Figure 4. 10 the measured surface temperatures profiles are shown. As can be seen, a slight difference between the internal surface temperatures and the profiles previously calculated can be observed. This happens mainly for the following reasons:

- as shown in Figure 4. 11 external air temperature in the laboratory is variable during the day, whereas, for assumption, it was considered constant in calculations, at 20°C in winter and 26°C in summer, because of the impossibility to know the actual laboratory temperatures in advance;
- in the prediction of water inlet temperatures, wall West is supposed to exchange heat with an indoor thermal node kept at a fixed operative temperature equal to 20°C in winter and 26°C in summer. Actually, the indoor operative temperature perceived by wall West is higher in winter and lower in summer, since wall West itself contributes to decrease and increase operative temperature of the room in winter and in summer conditions respectively;
- in the West wall simulation model the thermal inertia of the room (the other walls and the time delay of the control system of the radiant ceiling) is not considered;
- in the real test room the control system allows a temperature oscillation that could not be considered in the convective DIGITHON model and wall West model simulations.

Despite the above mentioned small differences on resulting boundary conditions, heat flow rates outcoming from wall West represent anyway a realistic load profile aimed to validate

DIGITHON by imposing real-use heat flows. In order to make negligible the influence of initial temperature of the test room and test room's building constructions, the measurements were taken for some days (nine days in case 1, eleven days in cases 2 and 3) under repeated boundary conditions.

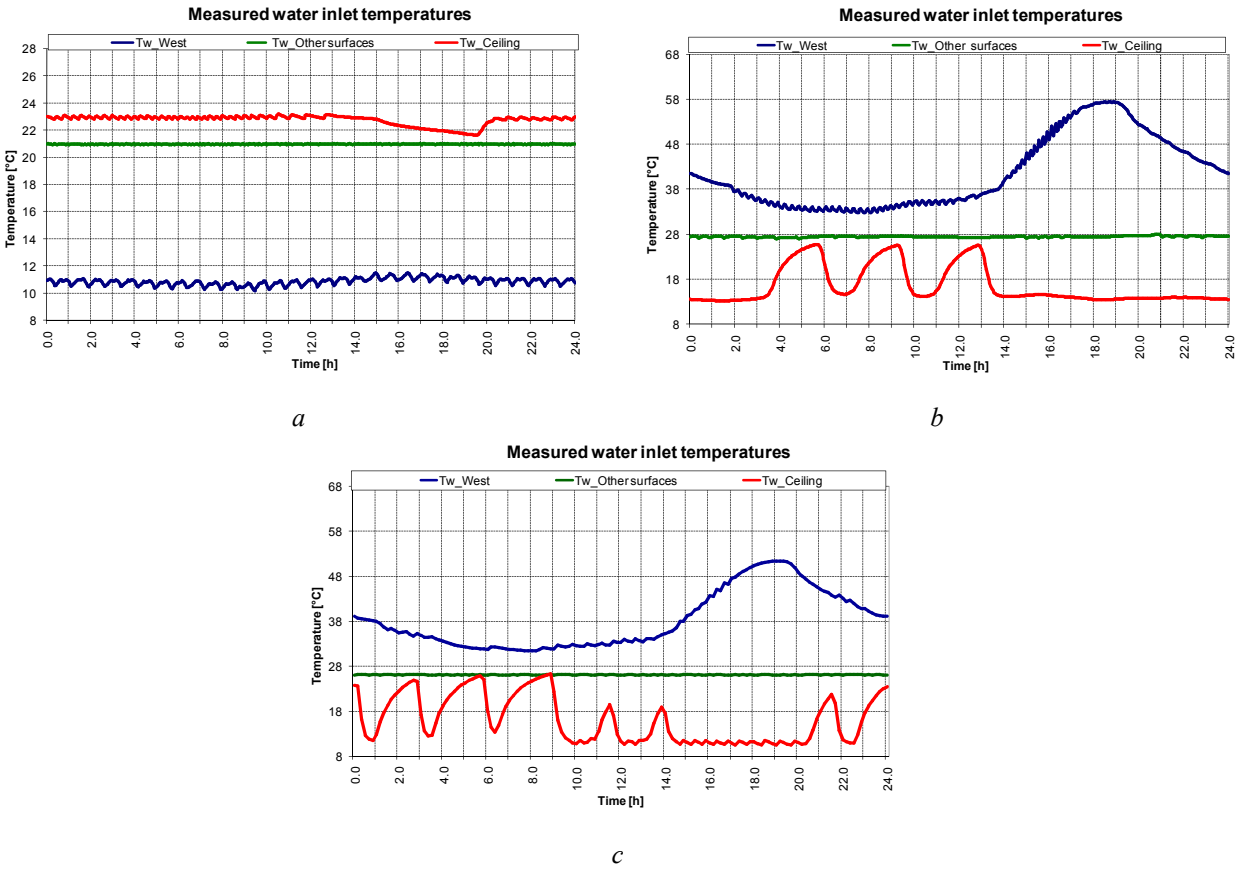

Figure 4. 9 Measured water inlet temperatures in case 1 (a), in case 2 (b) and case 3 (c) for wall West, for the ceiling and average of the other surfaces

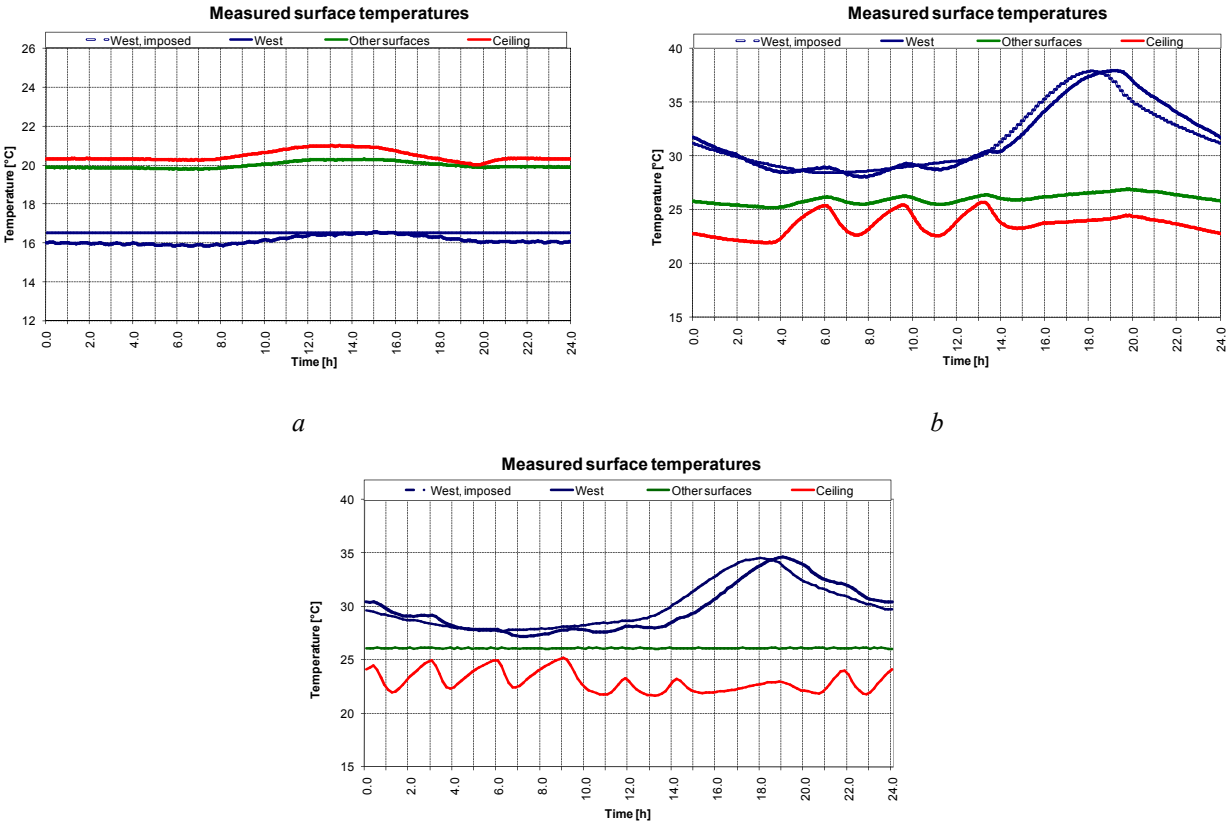

Figure 4. 10 Measured surface temperatures in case 1 (a), in case 2 (b) and case 3 (c) for wall West, for the ceiling and average of the other surfaces

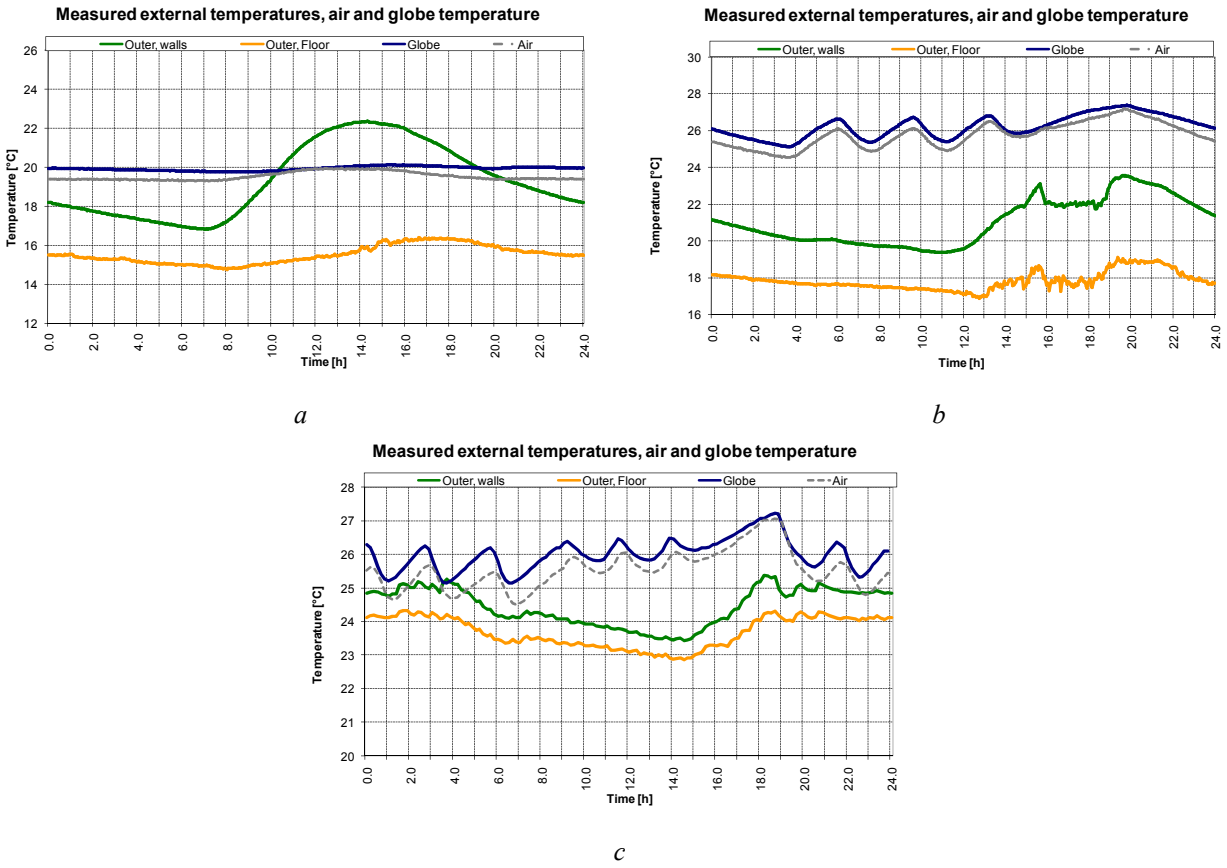

Figure 4. 11 Outdoor (i.e.: hosting laboratory) air temperatures close to the walls and under the floor, internal air and globe temperatures measured for case 1 (a), case 2 (b) and case 3 (c)

Comparison of DIGITHON versus test room measurements, under the same boundary conditions

DIGITHON was compared against the measurements under the same operating conditions, i.e. imposing the same geometry, the same thermal properties of the building materials as well as the same temperatures of the outdoor environment (i.e.: the hosting laboratory). Details on the discretization of the room surfaces are reported in Table 4. 5.

DIGITHON is used again for the ultimate contrast against test room measurements. For that purpose the same boundary conditions present during test room measurements must be used in DIGITHON simulations. These include the measured values of laboratory water inlet temperatures and water mass flow rates in the test room. But even other parameters might dramatically influence the validation, such as infiltration air mass flow rates in the test room and the assessment of convective heat transfer coefficients, indeed.

Table 4. 5 Details on the room discretization

	Number of regions	Number of tiles	Number of inactive regions	Number of active regions	Overall active surface[m^2]	Ratio of active area to the overall [%]
Floor	5	105	0	5	28	100%
South	21	60	6	15	21	51%
East	12	35	3	9	12	84%
North	21	60	6	15	21	86%
West	12	35	3	9	12	90%
Ceiling	35	96	20	15	28	77%
Tot	**106**	**391**	**38**	**58**	**122**	**81%**

An important issue in thermal simulations of enclosures consists in the knowledge of the air infiltration mass flow rate, which is related to the pressure difference between outdoor (i.e. the hosting laboratory, in the present case) and the indoor environment. The air-tightness of the test room was measured by a blower door test. As a result, the following equation was achieved, according with ASTM (2003) [24] to estimate air infiltration in the test room:

$$\dot{V}_L = 54.34 \cdot \Delta p^{0.63} \qquad \textit{Eq.4. 13}$$

$$\Delta p = g \cdot \Delta \rho \cdot z \qquad \textit{Eq.4. 14}$$

where the height of the room z = 3 m in the present case.

The resulting air flow rates are imposed in the simulations for DIGITHON validation in order to match real test room indoor conditions (surface, air, mean radiant and operative temperatures).

Convective heat transfer coefficients were calculated depending on the orientation of the surface and on the temperature difference between air and surface; using equations from (4.3) to (4.7) applied to the temperatures of the internal air and the average surface temperatures measured in the test room, for each simulation time step the consequent convective heat transfer coefficient was calculated.

DIGITHON allows to fix the convective and radiant part of internal heat gains; since the determination of the real phenomena of heat exchange between the 10 thermal dummies and

room internal surface is not easy, some assumptions are needed. Due to the particular shape of the dummy as well as to the presence of the holes on lateral surfaces, once measured and known the dummy surface temperature when switched on, a specific calculation lead to assuming that the convective part is 60% of the total amount of heat exchange.

4.6 Results

The comparison between measurements and simulations is shown from Figure 4. 12 to Figure 4. 16 for case 1, from Figure 4. 17 to Figure 4. 21 for case 2 and from Figure 4. 22 to Figure 4. 26 for case 3.

Figure 4. 12 shows the surface temperature profiles in case 1. As can be seen, some differences are present. That may happen for the following reasons:

- Surface temperatures are measured through punctual sensors; the value depends on the position, in particular on distances from pipes and water inlet. As a consequence the calculation of surface average measured temperatures is affected by the composition of such diverse punctual measures.
- An additional aspect to be considered in the comparison is due to the hypothesis in the simulation model (surface thermal uniformity in each tile is assumed).

The predicted air temperature (Figure 4. 13) shows some differences from measured values, from 10 a.m. to 4 p.m., but they are limited within 0.3°C. Mean radiant (Figure 4. 14) and operative (Figure 4. 15) calculated temperatures present a good agreement compared to the measured ones.

An overview of the correspondence between measured and predicted values of the operative temperature is shown in Figure 4. 16.

Measured and calculated surface temperatures are in agreement in case 2 as well, as shown in Figure 4. 17, even if there are some differences in ceiling surface temperature profiles, when sudden temperature variations occur.

Simulated air temperature is sometimes different from the measured one (Figure 4. 18), due to ceiling surface floating temperature.

The calculated value of mean radiant temperature (Figure 4. 19) is 1°C higher than the measured one during afternoon hours (around 6:30 p.m.), when the heat gain is maximum.

In case 2, simulated values of the operative temperature (Figure 4. 20) are very similar to the measured ones (the difference is smaller than 0.4°C). A better overview on correspondence between simulated and measured operative temperature values is reported in Figure 4. 21.

The calculated air temperature for case 3 follows the same trend of measured air temperature during the day, even if in the afternoon, when external radiation is significantly higher, calculated temperatures are higher than measurements (Figure 4. 23). Mean radiant and operative temperatures present a good agreement with measured values and the internal heat gains turned on do not affect meaningfully the results, as seen in Figure 4. 24, Figure 4. 25 and Figure 4. 26.

As for the surface temperatures simulated in case 3 (Figure 4. 22), a good agreement with measured values has been found, even if during the second part of the day the ceiling and the West wall slightly differ from measured values (about 1°C).

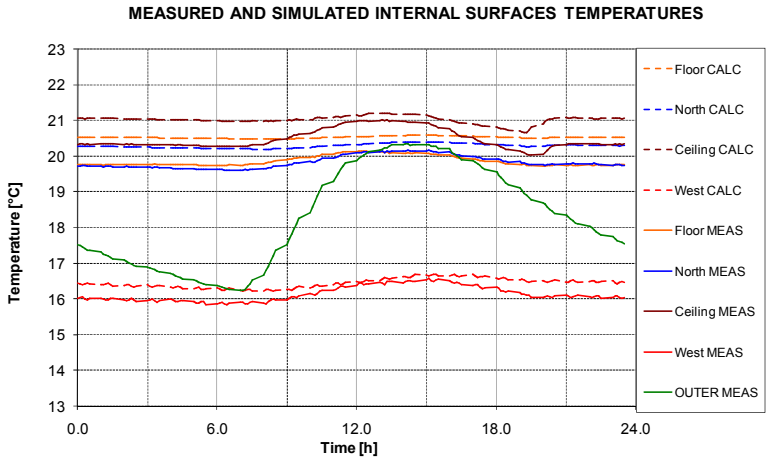

Figure 4. 12 Measured (continuous line) and simulated (dotted line) surface temperatures in case 1

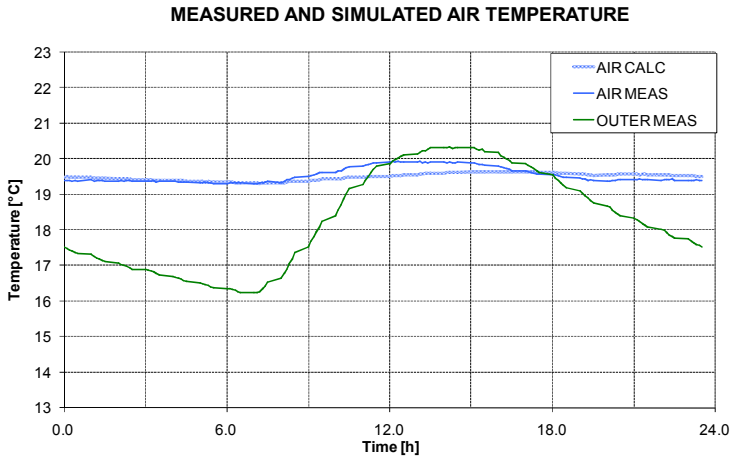

Figure 4. 13 Measured (continuous line) and simulated (dotted line) air temperatures in case 1

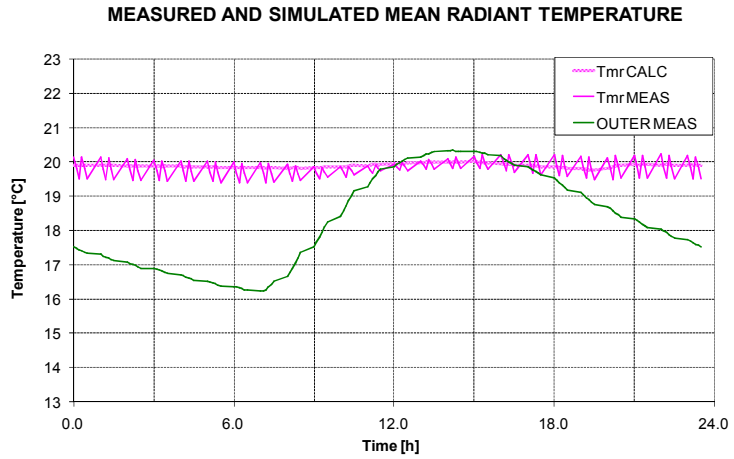

Figure 4. 14 Measured (continuous line) and simulated (dotted line) mean radiant temperature in case 1

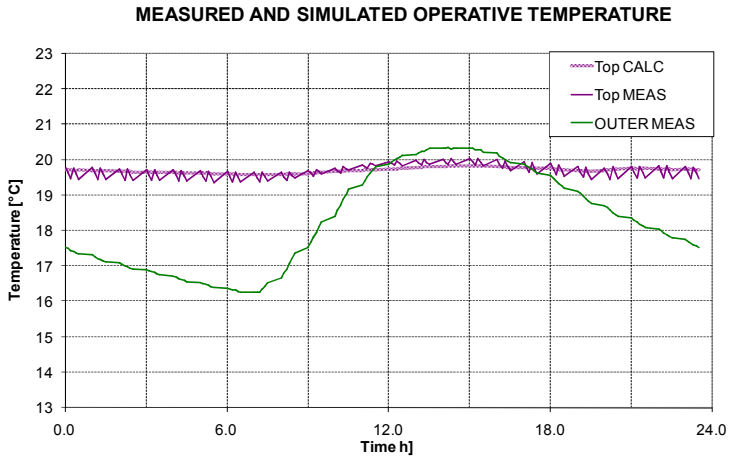

Figure 4. 15 Measured (continuous line) and simulated (dotted line) operative temperatures in case 1

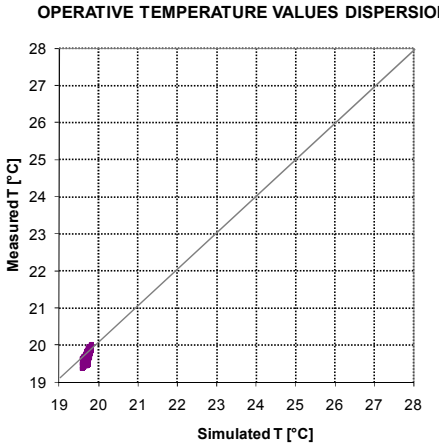

Figure 4. 16 Operative temperature values correspondence in case 1

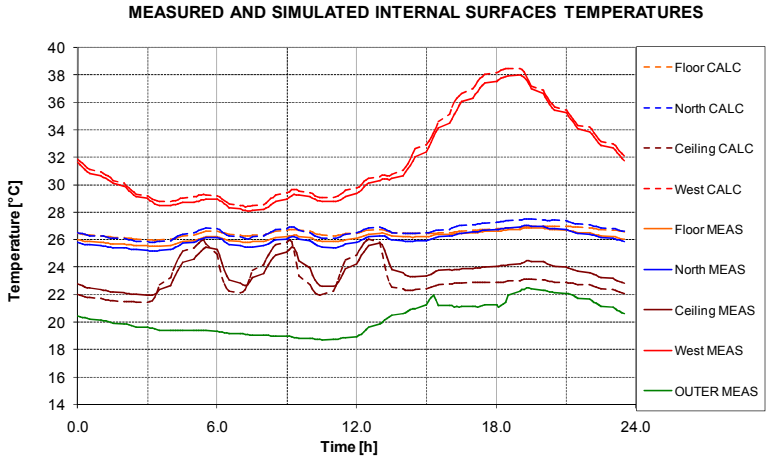

Figure 4. 17 Measured (continuous line) and simulated (dotted line) surface temperatures in case 2

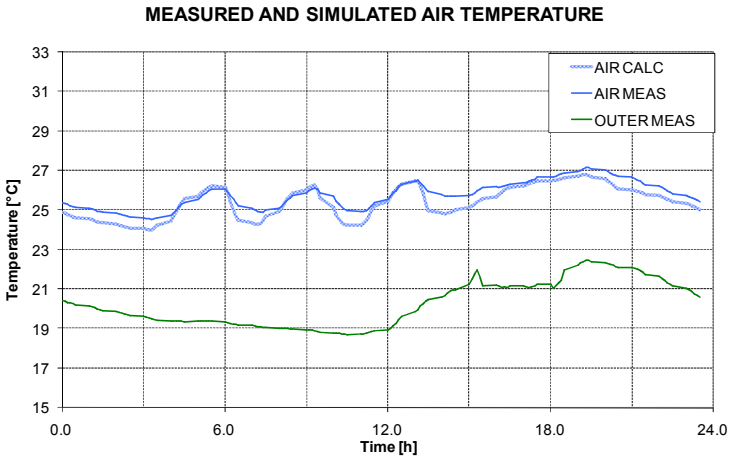

Figure 4. 18 Measured (continuous line) and simulated (dotted line) air temperature in case 2

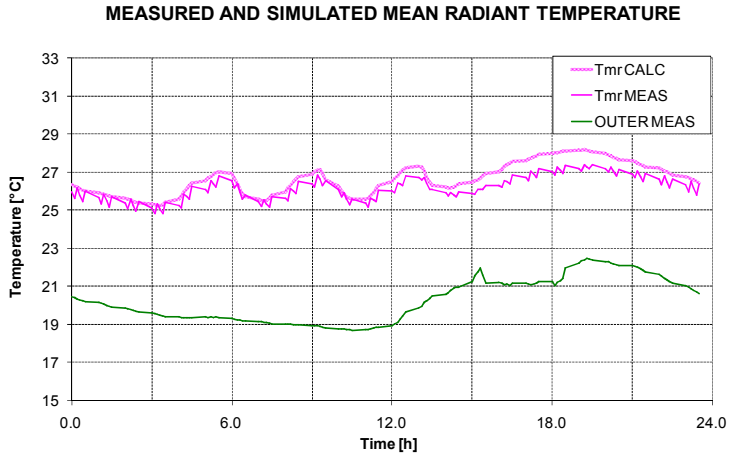

Figure 4. 19 Measured (continuous line) and simulated (dotted line) mean radiant temperature in case 2

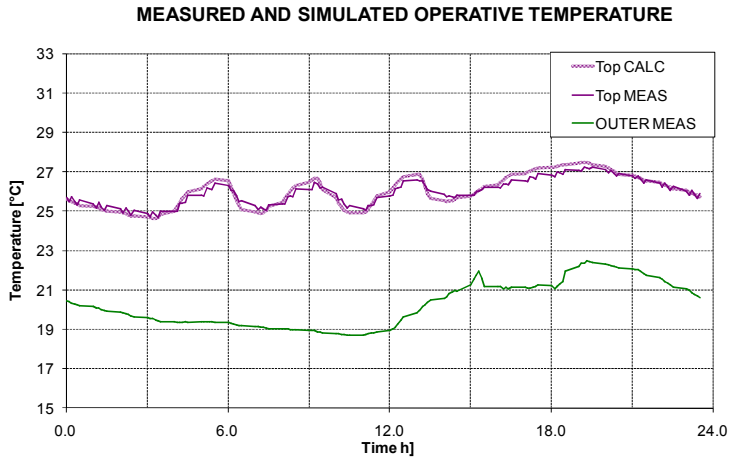

Figure 4. 20 Measured(continuous line) and simulated (dotted line) operative temperatures in case 2

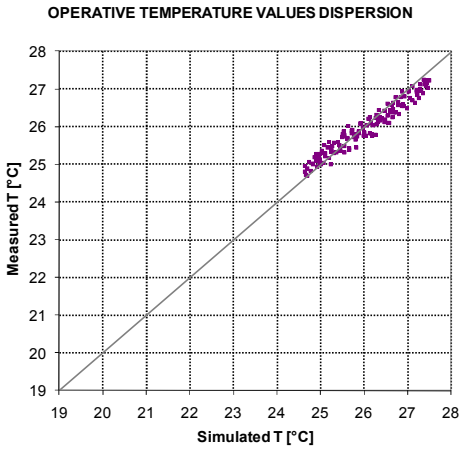

Figure 4. 21 Operative temperature values correspondence in case 2

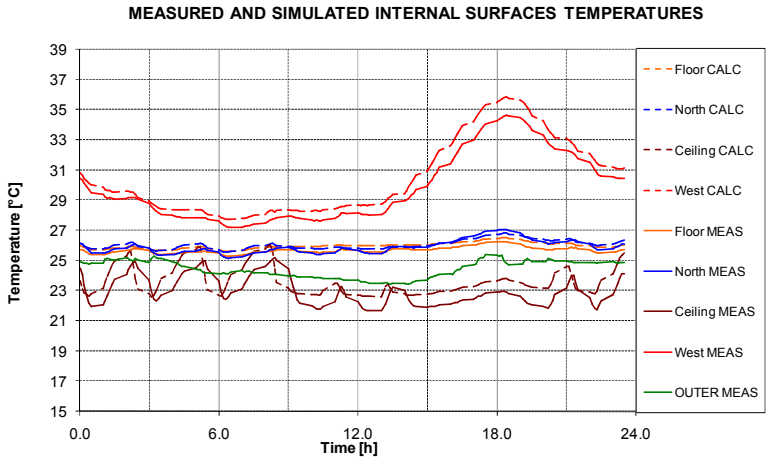

Figure 4. 22 Measured (continuous line) and simulated (dotted line) surface temperatures in case 3

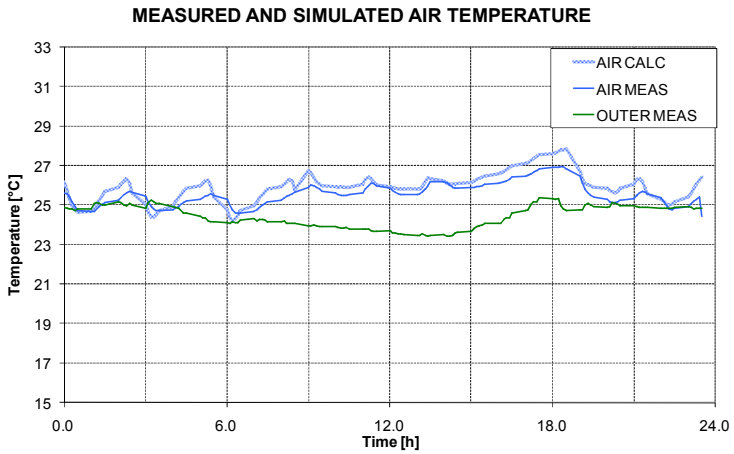

Figure 4. 23 Measured (continuous line) and simulated (dotted line) air temperature in case 3

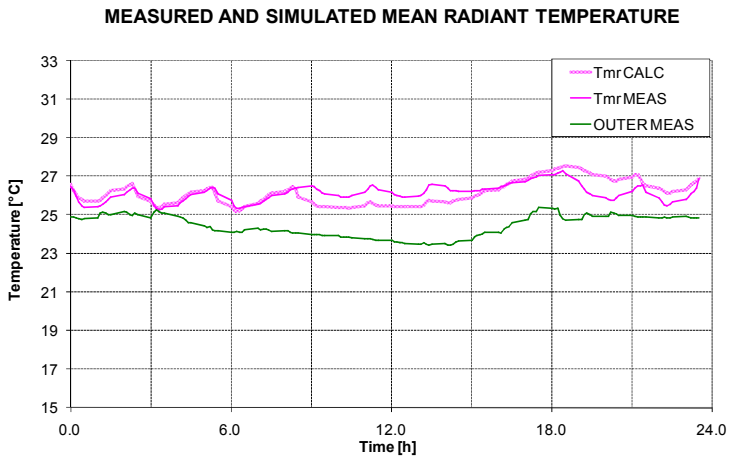

Figure 4. 24 Measured (continuous line) and simulated (dotted line) mean radiant temperature in case 3

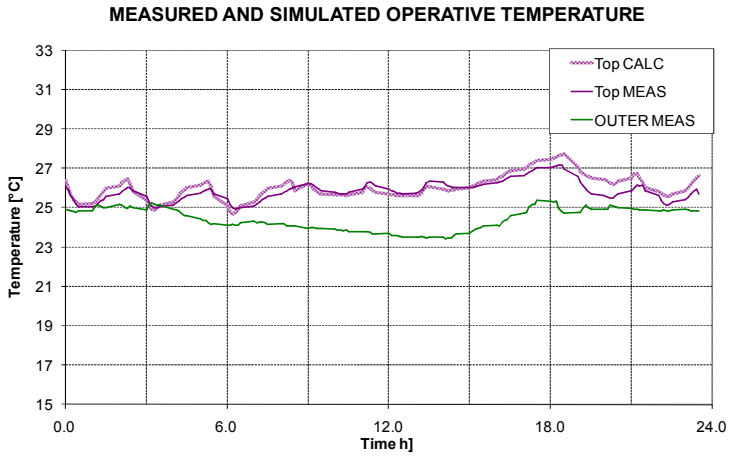

Figure 4. 25 Measured(continuous line) and simulated (dotted line) operative temperatures in case 3

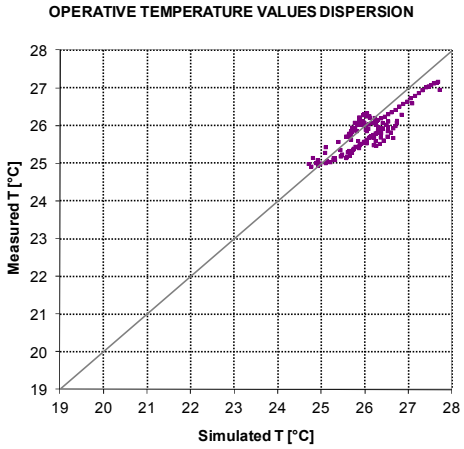

Figure 4. 26 Operative temperature values correspondence in case 3

An additional analysis carried out in the present work regards the sensitivity of the model to the convective heat transfer coefficients. For all cases (1, 2 and 3) a constant value of convective heat transfer coefficient has been assumed, according to European Standard EN 1264 [25]. In Table 4. 6 the constant values ($h_{c\text{-}const}$) and the daily average values of the convective heat transfer coefficients derived by measurements ($h_{c\text{-}v,av}$) are reported. In the same table the standard deviation of the derived variable heat exchange coefficients with respect to the average value is also reported. As can be seen, the difference in the average value is limited, since, if the aim is to maintain proper comfort conditions in the room, the indoor temperatures (surface and air) need to be in a small range.

In Figure 4. 27 the operative temperature profile derived by simulations when using constant heat transfer coefficients in case 1 is shown. The same parameter is reported in Figure 4. 28 for case 2 and Figure 4. 29 for case 3.

Figure 4. 30, Figure 4. 31 and Figure 4. 32 show the correspondence of values of operative temperature, when using constant values for the convective heat transfer coefficients. Comparing the results with Figure 4. 16, Figure 4. 21 and Figure 4. 26 it might be assessed that the choice of constant values for convective heat transfer coefficient does not affect results in an appreciable way. In fact all the simulated operative temperature values remain close to measured ones and do not differ from values calculated considering variable convective heat transfer coefficients. The results do not change if, instead of using coefficients present in EN 1264 [25], EN15377 [26] coefficients are used, i.e. 0.5 W/ (m^2 K) for ceiling heating and 1.5 W/(m^2 K) for floor cooling.

Table 4. 6 Constant value (from EN 1264) and daily average value based on measurements of the convective heat transfer coefficient assumed in cases 1, 2 and 3 for the internal surfaces [W/(m^2K)]

Surface	**Winter**			**Summer**					
	Case 1			Case 2			Case 3		
	$h_{c\text{-}const}$	**$h_{c\text{-}v,av}$**	**st dev.**	**$h_{c\text{-}cosnt}$**	**$h_{c\text{-}v,av}$**	**st dev.**	**$h_{c\text{-}cosnt}$**	**$h_{c\text{-}v,av}$**	**st dev.**
West wall	2.5	2.25	0.02	2.5	2.58	0.34	2.5	2.35	0.32
Other vertical walls	2.5	1.20	0.05	2.5	0.92	0.24	2.5	1.08	0.16
Floor	5.3	1.35	0.11	1.0	1.35	0.45	1.0	1.07	0.47
Ceiling	1.0	0.26	0.00	5.3	3.14	0.30	5.3	3.75	0.44

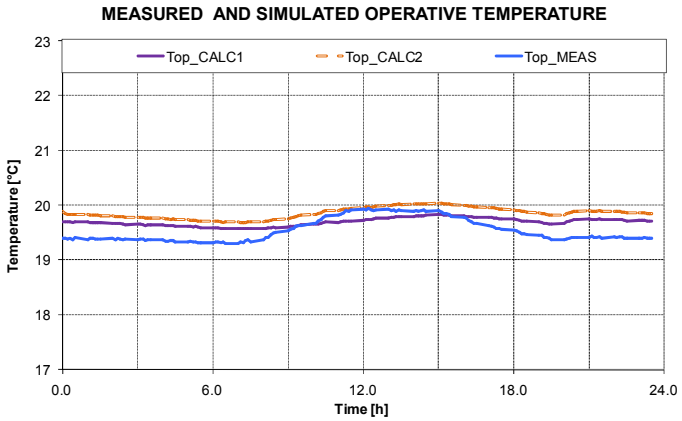

Figure 4. 27 Measured and simulated operative temperature in case 1 when using constant heat transfer coefficients(dotted line) and variable heat transfer coefficients (continuous line)

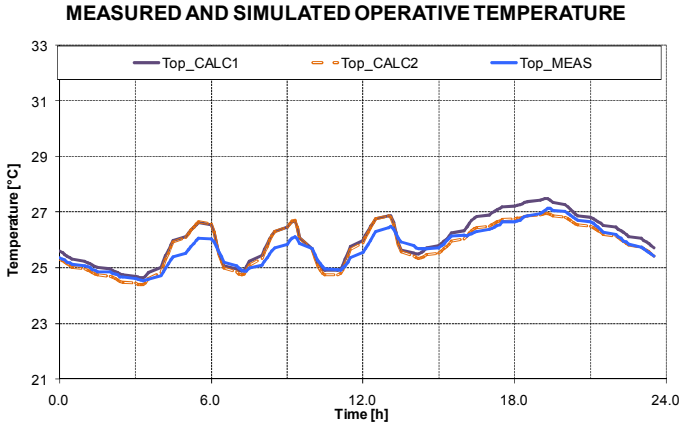

Figure 4. 28 Measured and simulated operative temperature in case 2 when using constant heat transfer coefficients(dotted line) and variable heat transfer coefficients (continuous line)

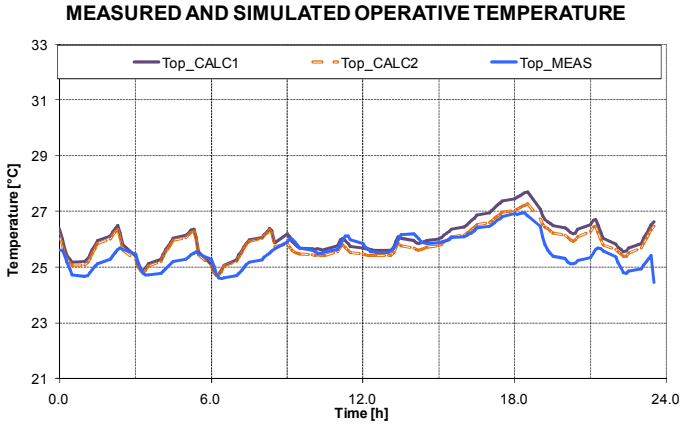

Figure 4. 29 Measured and simulated operative temperature in case 3 when using constant heat transfer coefficients(dotted line) and variable heat transfer coefficients (continuous line)

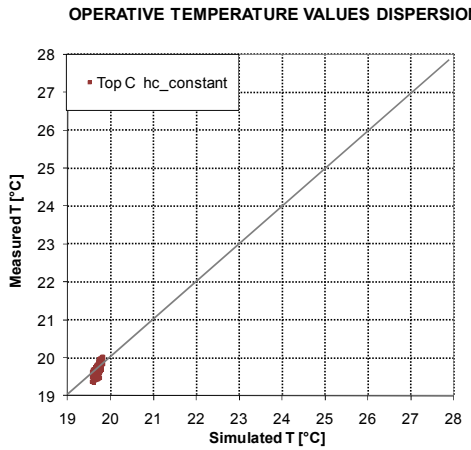

Figure 4. 30 Operative temperature values correspondence with constant convective heat transfer coefficients for case 1

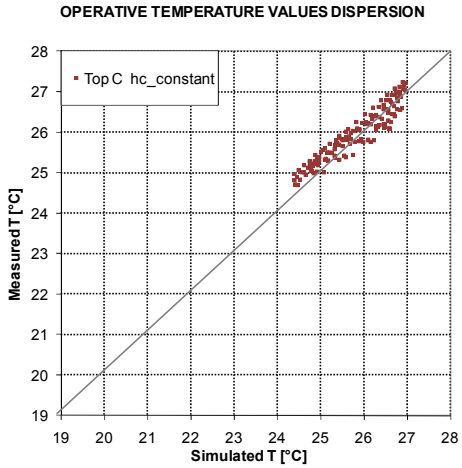

Figure 4. 31 Operative temperature values correspondence with constant convective heat transfer coefficients for case 2

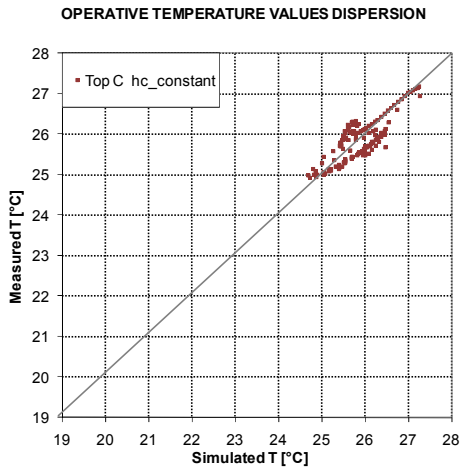

Figure 4. 32 Operative temperature values correspondence with constant convective heat transfer coefficients for case 3

4.7 Discussions and conclusions

The present work is based on the comparison between real test room measurements and calculations via a building energy dynamic simulation model based on response factor technique (namely DIGITHON) developed by authors.

As for the test room, the set up of the measurement data acquisition system allowed to reach an uncertainty of the temperatures lower than 0.025°C, while the global uncertainty for mass flow rate of the water was 0.33%.

For the comparison two different design weather conditions (representing heating and cooling design days respectively), based on a typical Mediterranean climate, have been simulated in the test room through the radiant systems embedded in all the inner side of the surfaces enclosing the test room.

The test room was set-up so that the heating/cooling load profiles were similar to the ones expectable under real use conditions. That was possible via a specific procedure shown in this work that is aimed to control the heat gain profiles which represent the weather conditions due to an external glazing wall facing West.

The global uncertainties of the procedure adopted were calculated and expressed as a fraction of the mean daily heat flow rate supplied by the water of the ceiling panels: the uncertainties are 2.19% with respect to 281 W for the winter case, 1.81% with respect to 668 W for the summer case without internal loads and 1.80% with respect to 1135 W for the summer case with internal heat gains.

The temperature daily profiles of the wall simulating the window were determined via the dynamic simulation program DIGITHON. Via an iterative finite difference wall simulation tool developed by authors, the resulting heating/cooling loads were used to define the water supply temperature in the real test room so as to reproduce the same weather conditions in the test room. The heating/cooling loads through the wall were removed by the water based radiant ceiling system and the test data were logged. Then DIGITHON simulations were carried out under the same boundary conditions as the real tests. The numerical model simulating the room equipped with radiant systems demonstrated good correspondence in terms of operative temperature profiles and the overall approaching method adopted in this work was validated. Some differences in surface temperatures appear, but measured values of surface temperatures are not very accurate, indeed.

A particular analysis based on convective heat transfer coefficients showed that the use of variable or constant convective heat transfer coefficients (between the air and the internal surfaces) implied negligible changes in calculated air temperature profiles.

A further analysis has been carried out in order to investigate the effect of the presence of internal heat gains in the cooling design day. Even in this case, despite some small differences in the inner surface temperatures (around 1°C in the ceiling) the dynamic simulation model can predict with good accuracy the operative temperature, which is the target design parameter when dealing with dynamic simulations.

Based on these results it is possible to assess that detailed dynamic energy simulation programs are accurate for determining heating/cooling load of the hydronic radiant systems as well as indoor operative temperature. As for calculations, it is accurate enough to run simulations based on convective heat exchange coefficients expressed by EN 15377 [26], or even to use fixed heat exchange coefficients present in EN 1264 [25].

As a final conclusion, the tests in the room demonstrated that, if the aim is to maintain indoor comfort conditions, the maximum cooling load which can be extracted by the gypsum board radiant ceilings is around 50-60 W m^{-2}, when looking at the active area, if the supply temperature is around 15 °C. When comfort conditions are achieved, the indoor parameters are close to each other and therefore small differences between the surface temperatures and air and operative temperatures are present. This explains why the calculations based on fixed or variable heat exchange coefficients do not differ in terms of calculated operative temperatures compared to the measured values.

Symbols

A heat transfer area [m^2]
C shading coefficient of the considered glazed surface [-]
c_p specific heat at constant pressure [$J \cdot kg^{-1} \cdot K^{-1}$]
D_e equivalent diameter of the room (hydraulic diameter) [m]
F_{j-k} view factor between the j-th and the k-th surface elements [-]
h_c convective heat transfer coefficient [$W \cdot m^{-2} \cdot K^{-1}$]
$h_{c\text{-}const}$ constant value of the convective heat transfer coefficient [$W \cdot m^{-2} \cdot K^{-1}$]
$h_{c\text{-}v,av}$ daily average value of the convective heat transfer coefficients derived by measured temperatures [$W \cdot m^{-2} \cdot K^{-1}$]
h_r infrared radiation heat transfer coefficient [$W \cdot m^{-2} \cdot K^{-1}$]
I reference transmitted solar radiation (transmitted through a single pane window) [$W \cdot m^{-2}$]
$\dot{m}$ mass flow rate [$kg \cdot s^{-1}$]
M mass [kg]
NTU number of transfer units [-]
n number of surfaces[-]
q heat flow [W]
q_c heat flow transferred by convection [W]
q_g total net heat flow transferred (positive when received) [W]
$q_{I,r}$ radiative internal gains [W]
q_r heat flow transferred by infrared radiation [W]
q_s overall absorbed radiant gain of the considered element [W]
r distance between two surface elements [m]
S surface area [m^2]
$SHGC$ Solar heat gain coefficient [-]
S_T overall internal surface of the room [m^2]
T_m mean temperature of surfaces in the room [°C]
T_M temperature at the present calculation time step [°C]
$(T_M)_{-\Delta\tau}$ temperature at the previous calculation time step [°C]
T_f reference temperature of the adjacent fluid [°C]
T_s surface temperature [°C]
T_v temperatures related to mass flow [°C]
T_w temperature of the water in the circuits [°C]
U overall heat transfer coefficient [$W/(m^2 K)$]
$\dot{V}_L$ air flow rate in the test room due to infiltration [$m^3 h^{-1}$]
z geodetic difference, assumed equal to the room height [m]
Δp pressure difference between outdoor and indoor [Pa]
$\Delta\rho$ difference between external and internal air densities (depending on air temperatures) [$kg \cdot m^{-3}$]
$\Delta\tau$ interval of the time step [s]
ε efficiency of the heat transfer in the considered heat exchanger [-]

ϕ angle between the segment connecting the centres of the two surface elements and the surface normal [rad]

σ Stefan-Boltzmann constant [$W \cdot m^{-2} \cdot K^{-4}$]

Subscripts:

h general h-th sub-system

i general i-th heat flow

j general j-th surface element

k general k-th surface element

Min fluid vector with minimum heat capacity in the considered heat exchanger

v general v-th element

G general G-th surface element for glazing

4.8 References

[1] Shoemaker, R. W. 1954. Le chauffage par rayonnement. Editions Eyrolles, Paris.

[2] Olesen, B.W. 1997. Possibilities and Limitations of Radiant Floor cooling. ASHRAE Transactions 103 (1997), Pt.1.

[3] Weber, T., Jóhannesson, G., Koschenz, M. , Lehmann, B., Baumgartner, T. 2005. Validation of a FEM-program (frequency-domain) and a simplified RC-model (time-domain) for thermally activated building component systems (TABS) using measurement data.

[4] De Carli, M., Tonon, M. 2011. Effect of modelling solar radiation on the cooling performance of radiant floors. Solar Energy 85 (2011). pp. 689–712.

[5] Athienitis, A. K., Chen, Y. 2000. The effect of solar radiation on dynamic thermal performance of floor heating systems. Solar Energy 69 (2000), No. 3, pp. 229–237.

[6] Berglund, L. G., Gagge, A. P. 1985. Human response to thermal conditions maintained in an office by radiant ceiling, baseboard, forced air and floor heating systems. ASHRAE Transactions 91 (1985). pp. 488 - 502.

[7] Külpmann, R. W. 1993. Thermal comfort and air quality in rooms with cooled ceilings - results of scientific investigations. ASHRAE Transactions, 99 (2) (1993),. pp. 488 - 502.

[8] Fisher, D. E., Pedersen, C. O. 1997. Convective heat transfer in building energy and load calculation, ASHRAE Transactions 103 (2) (1997).

[9] Khalifa, A. J. N., Marshall, R. H. 1998. Validation of heat transfer coefficients on interior building surfaces using a real-sized indoor test cell. Int. J. Heat Mass Transfer .33 (1998) No.10, pp.2219-2236.

[10] De Carli, M., Tomasi, R. 2009. A critical review on heat exchange coefficients between heated and cooled horizontal surfaces and room. 11th Roomvent 2009 Conference, May 2009, Korea.

[11] Stephenson, D. G., Mitalas, G. P. 1967. Cooling load calculation by thermal response factor method, ASHRAE Transactions 73 (1967).

[12] Kusuda, T. 1969. Thermal response factors for multi-layer structures of various heat conduction systems. ASHRAE semi-annual Meeting, 1969, Chicago, IL.

[13] Blomberg, T. 1999. Heat2 – A PC-program for heat transfer in two dimensions. Manual with brief theory and examples, Lund Group for Computational Building Physics, Sweden.

[14] Various Authors. 1983. Fluid Mechanics and Heat Transfer. Hemisphere Publishing Corporation, 1983, cap. 2.5.1-1.

[15] Awbi, H B. 1998. Calculation of convective heat transfer coefficients of room surfaces for natural convection. Energy and Building 28 (1998), pp. 219-227.

[16] Olesen, B. W., Michel, E., Bonnefoi, F., De Carli, M. 2000. Heat Exchange coefficient between floor surface and space by floor cooling - Theory or a Question of Definition. ASHREE Transactions 106 (2000).

[17] Karadağ, R. 2009. New approach relevant to total heat transfer coefficient including the effect of radiation and convection at the ceiling in a cooled ceiling room. Applied Thermal Engineering.29 (2009) pp.1561-1565.

[18] EN 14240-2004. Ventilation for buildings - Chilled ceilings - Testing and rating.

[19] ISO 7726-1998. Ergonomics of the thermal environment- Instrument for measuring physical quantities.

[20] ENV 13005-1999. Guide to expression of uncertainty in measurement.

[21] EnergyPlus Manual (Engineering Reference). U.S. Department of Energy, pp. 50-53.

[22] EnergyPlus – Weather Data- U.S.Department of Energy.

[23] F. P. Incropera,. D.P. DeWitt. 2002. Fundamentals of heat and mass Transfer, (5th Ed.), Wiley, New York.

[24] ASTM. 2003. ASTM E779-03. Standard Test Method for Determining Air Leakage Rate by Fan Pressurization.

[25] EN 1264-2008. Water based surface embedded heating and cooling systems.

[26] EN 15377-2008. Heating systems in buildings - Design of embedded water based surface heating and cooling systems.

5 - Evaluation of radiant systems performance enhancement by means of primary air

Abstract

Radiant ceiling panels are largely used for summer cooling, especially in offices, but they have to be assisted by a primary air system, aimed to dehumidify and prevent condensation on the cooled surfaces. In the present work, the interaction between the primary air inlet and the radiant ceiling is considered. In particular, the study regards how the inlet of primary air can be used to enhance the performance of the radiant ceiling, by means of the increase of convective heat transfer.

Via CFD (Computational Fluid Dynamics) simulations, the interaction of radiant ceiling panels and primary air has been analyzed in an office case study, with typical internal sensible heat gains and various ventilation conditions. Heat gains from occupants and computers are simulated by means of electrical cooling load simulators (dummies) distributed in the room.

Primary air inlet is considered both through typical vents and through induction air terminals. Different temperatures and air flows were chosen for different vents and the convective heat flow at the ceiling surface has been calculated for each configuration, in order to quantify the increase in the heat exchange.

The study showed that the exploitation of primary air allows just a modest enhancement of total heat transfer coefficients at the ceiling surface, even if induction air terminals are used, and consequently the ceiling cooling capacity is not increased.

5.1 Introduction

One of the most critical issues in the present study concerns the assessment of the convection heat transfer coefficient at the surface of the ceiling, since there both natural and forced air flows take place. As a consequence, a literature review was carried out, in order to quantify the enhancement in heat transfer coefficient due to increased air velocity on the surfaces. The main references on this topic are presented hereafter.

Awbi and Hatton [1] estimated that, in case of heated floor (10 K temperature difference between the surface and air supply, 0.5 m/s outlet velocity from the air terminal), the values of heat transfer coefficients consequent to mixed (natural + forced) convection are close to the ones obtained in the case of mere natural convection, whereas, in the case of heated wall and heated ceiling (10 K temperature difference between the surface and air supply, 2.0 m/s outlet velocity from the air terminal), the enhancement can reach 10% and 78% respectively.

Jeong and Mumma [2], using the existing correlations for natural and mixed convection, stated that, in case of cooled ceiling panels with nozzle diffusers close to the ceiling, the total cooling capacity of the panel is not enhanced significantly when outlet air velocity is lower than 2 m/s.

Beausoleil and Morrison [3] developed a new approach to model heat transfer coefficients for mixed convection in mechanically ventilated rooms, for heating and cooling modes: they used Churchill and Usagi's [4] approach to couple Alamdari and Hammond's [5] correlations, together with Fisher's[6] correlations, obtaining new correlations for mixed convection. This way the buoyancy forces, considered in Alamdari and Hammond, were joined to forced ventilation contribution, considered in Fisher's experiments.

Novoselac et al. [7], performing an experimental study using Churchill and Usagi's approach, developed new mixed convection correlations for a room provided with cooled ceiling panels and aspiration diffusers laying on the ceiling. The consequent increase in convection heat transfer coefficient at the surface, in the area directly influenced by the air terminal unit, was from 4% to 17%, for a 7 K temperature difference between the ceiling surface and the air and for volume flow rates in the range 1÷4 ACH.

The authors above mentioned focused on experimental results and on their elaborations, whereas the present work quantifies the enhancement in heat transfer of cooled ceilings via CFD simulations, in order to get a better understanding of the influence due to air diffusers position and layout.

5.2 Method

In the present study, CFD simulations were performed via FDS (Fire Dynamics Simulator [8]), in order to quantify how much the induced air stream influences the total heat transfer at the surface of cooled ceilings. FDS was developed to model fire-driven air flows, but it was demonstrated [9] that it is suitable for solving different air flow problems in rooms. Eight stationary configurations (summarized in Table 5. 1 and Table 5. 2) were simulated, in addition to case 0 (with no air inlet, used as a reference). Internal heat gains were simulated via 12 internal sources, arranged into two rows (Figure 5. 1). The present analysis refers to a room with internal heat gain of 680W, the ceiling surface temperature at 22°C and the floor surface and all the other wall surfaces at 26°C. The mean air temperature depends on the steady state equilibrium achieved by the contemporaneous action of the active surface and of the ventilation system and it is in the range 26°C÷26.8°C for each simulation. The convective heat transfer

coefficient is calculated by FDS itself as a function of the temperature difference between the ceiling surface and the nearest air node by FDS default correlations.

The fresh air flow rate is equal to 1.0 ACH (at 21°C) for each simulation (except case 0) and two types of inlet air terminal units are considered :

- traditional vents for the primary air, with a low induction rate (type A) according to the definition reported in EN 12792:2003 [10]; in this case the induction ratio (ratio of the internally induced air flow rate and the primary air flow rate) is equal to 1:1 (layout of (Figure 5. 1 a);
- vents for the primary air with high induction rate (type B), with a value of the induction ratio equal to 4:1 (for layouts of Figure 5. 1 (a,b,c)).

All vents (supply and exhaust) are considered placed on a short wall, corresponding to East side

In order to prevent calculation errors in the zone closest to the ceiling, where velocities and turbulence are higher for the presence of inlet vents, it was decides to reduce grid size in the upper part of volume, as shown in Figure 5. 2, for a total number of cells of 114,000.

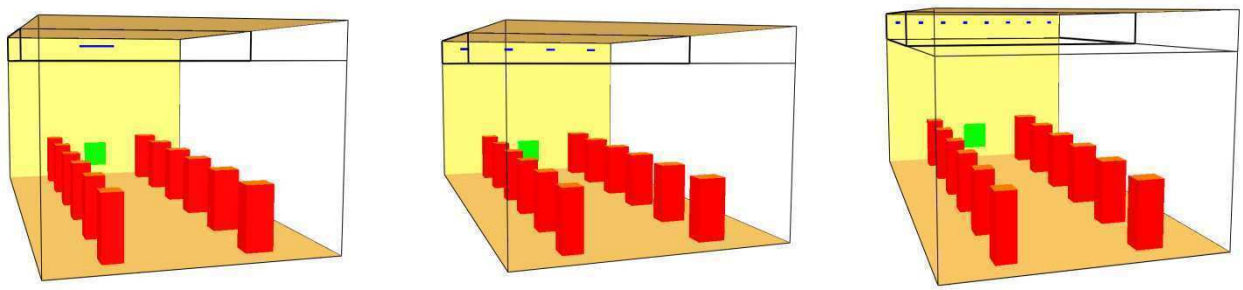

a) b) c)

Figure 5. 1 Representation of room layout, with 12 dummies, 1 outlet air vent and 1 inlet air vent (a – code 1.i), 4 inlet air vents (b - code 2.i), and 8 inlet air vents (c - code 3.i)

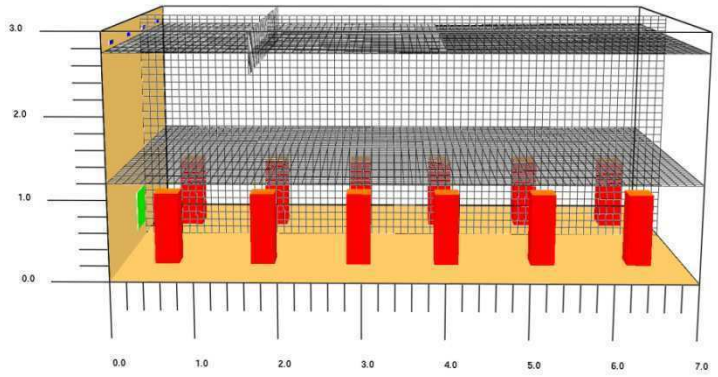

Figure 5. 2 Representation of grids adopted and sizes of the room in [m]

Table 5. 1 Cases description: boundary conditions, inlet air vent and outlet air vent codes

	Units	**Case**								
		0	**1**	**2**	**3**	**4**	**5**	**6**	**7**	**8**
Total internal heat load	[W]	680	680	680	680	680	680	680	680	680
Convective internal heat load	[W]	408	408	408	408	408	408	408	408	408
Wall and floor surface temperatures	[°C]	26	26	26	26	26	26	26	26	26
Ceiling surface temperature	[°C]	22	22	22	22	22	22	22	22	22
Primary air inlet temperature	[°C]	-	21	21	21	21	21	21	21	21
Inlet air pitch	[°]	-	0	3	0	3	0	3	0	3
Induction ratio*	[-]	-	1	1	4	4	4	4	4	4
Primary air volume flow	[ACH]	-	1	1	1	1	1	1	1	1
Inlet air vent code	[-]	-	1.i	1.i	1.i	1.i	2.i	2.i	3.i	3.i
Outlet air vent code	[-]	-	1.o	1.o	1.o	1.o	1.o	1.o	1.o	1.o
*: Induction ratio [-] = the ratio of the internally induced air flow rate and the primary air flow rate										

Table 5. 2 .Inlet and outlet air vent types

Inlet/Outlet	Code	N° vents	Sizes [cm]	Layout
Inlet	1.i	1	80 x 5	Short side wall , top at 15 cm from ceiling, central position on wall
	2.i	4	20 x 5	Short side wall, top at 15 cm from ceiling, uniform distribution on wall
	3.i	8	10 x 5	Short side wall, top at 15 cm from ceiling, uniform distribution on wall
Outlet	1.or	1	50 x 50	Short side wall, bottom at 20 cm from floor, central position on wall

5.3 Results

For each simulation the following parameters were obtained in steady state conditions and reported in Table 5. 4:

- T_{Air-1}, T_{Air-2}, and T_{Air-3}: average air temperatures near inlet air terminals (50 cm distant), outlet air terminals (50 cm distant) and at the centre of the room;
- v_1 and v_2: average air velocities at 2.0 m from the floor, at 2.0 m from long sides and at 0.5 m from East and West walls (short sides) respectively;
- $h_{c,av}$ is the average convective heat transfer coefficient for the whole ceiling;
- $h_{c-max-x}$, $h_{c-max-y}$, $h_{c-min-x}$ and $h_{c-min-y}$ are the maximum and minimum convective heat transfer coefficients calculated along longitudinal section (y = constant and x =[0 ÷7] m) and along cross-section (x = constant and y =[0 ÷4] m) as shown from Figure 5. 5 to Figure 5. 10;
- h_{c-max} and h_{c-min}: absolute maximum and absolute minimum convective heat transfer coefficient calculated on the ceiling area;
- Q_c and Q_r: average convective and radiant heat flows at the ceiling surface;
- Q_c' and Q_r': average convective and radiant heat fluxes at the ceiling surface.

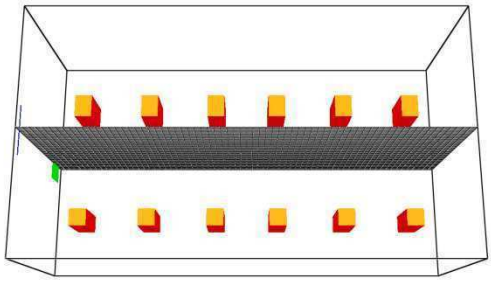

Figure 5. 3 Longitudinal section (y = constant) representation

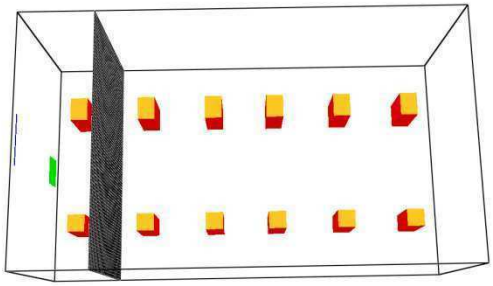

Figure 5. 4 Cross-section (x= constant) representation

Table 5. 3 Simulation results – Air temperatures and air velocity

Case	T_{Air-1}	T_{Air-2}	T_{Air-3}	v_1	v_2
	°C	°C	°C	m/s	m/s
0	-	-	26.80	0.065	0.083
1	24.57	26.03	26.49	0.119	0.081
2	24.56	26.06	26.47	0.129	0.118
3	25.95	26.32	26.31	0.096	0.116
4	26.12	26.27	26.26	0.069	0.102
5	26.01	26.32	26.42	0.059	0.210
6	26.03	26.22	26.29	0.072	0.209
7	26.12	26.33	26.46	0.070	0.236
8	26.11	26.23	26.33	0.077	0.205

Table 5. 3 shows that air temperatures near the inlet vents are lower in case of low induction, but no significant differences are near the exhaust and in the centre of the room with respect to high induction rate vents. However air temperature in the centre is higher for case 0 without primary air. Air velocities v_1 and v_2 under the ceiling (1.0 m distant) are from 0.06 to 0.24 m/s, and higher values are noticed on the west side (v_2) when the inlet vents number is increased, because the horizontal jet falls farther from the supply vents.

The average values and related standard deviations of the convective heat transfer coefficients are shown in Table 5. 4. It s evident that the configurations with 4 and 8 jets instead of a single nozzle, maintaining the same speed and temperature, ensure a lower overall dispersion of the values of convective heat transfer coefficient around the mean value, increasing the uniformity of the heat exchange under the ceiling. Distributions of heat transfer coefficients along the room axes are shown in Figure 5. 5 and Figure 5. 6 for case 4 (with 1 vent), in Figure 5. 7 and Figure 5. 8 for case 6 (with 4 vents) and in Figure 5. 9 and Figure 5. 10 for case 8 (with 8 vents).

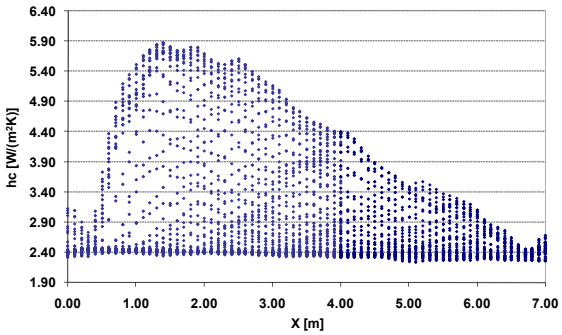

Figure 5. 5 Case 4, local convective heat transfer coefficient h_{c-x} representation

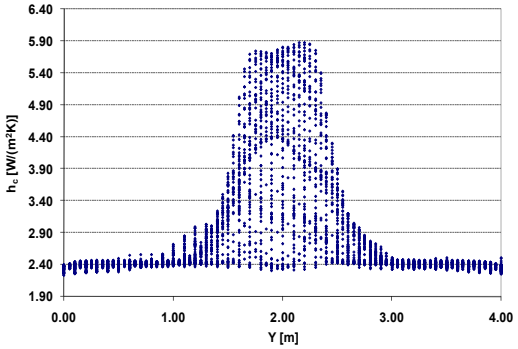

Figure 5. 6 Case 4, local convective heat transfer coefficient h_{c-y} representation

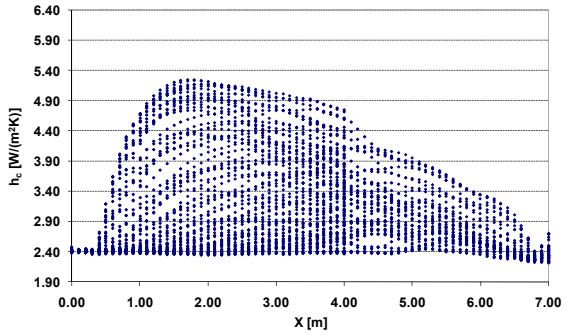

Figure 5. 7 Case 6, local convective heat transfer coefficient $h_{c\text{-}x}$ representation

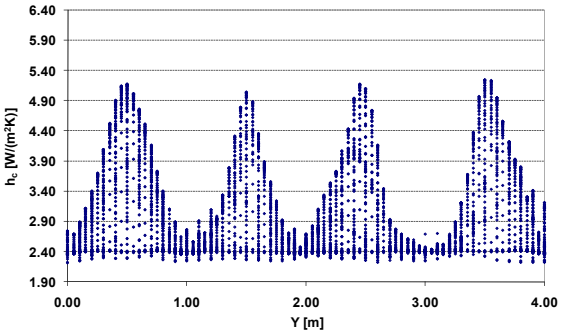

Figure 5. 8 Case 6, local convective heat transfer coefficient $h_{c\text{-}y}$ representation

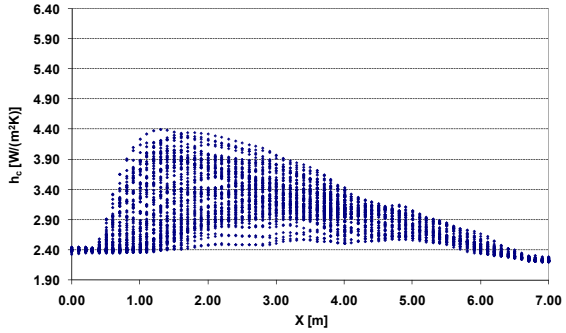

Figure 5. 9 Case 8, local convective heat transfer coefficient $h_{c\text{-}x}$ representation

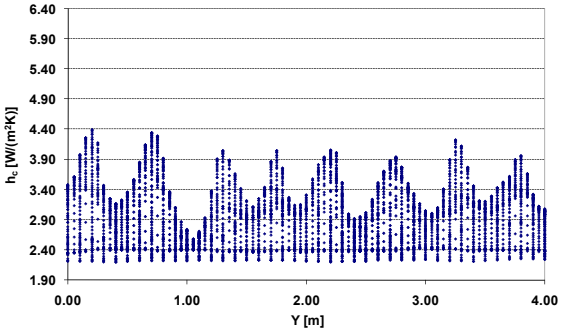

Figure 5. 10 Case 8, local convective heat transfer coefficient $h_{c\text{-}y}$ representation

In the case of jet inlet air terminal units tilted upward (pitch = 3°), no significant changes outcome when low induction rate air terminal units are used (case 2 vs. case 1) in the average convective heat transfer coefficient $h_{c\text{-}av}$ compared to horizontal jets; on the contrary, when high induction rate air inlet terminal units are used, an increase in the convective heat transfer coefficient values results, especially in the case of 4 jets (+12.8%) and 8 jets (7.1%). In the case of a single nozzle, the increase is very modest (+1%).

In Figure 5. 11 the average values of convective heat transfer coefficients at the ceiling surface are shown, together with the related standard deviation, whereas Figure 5. 12 shows the maximum and minimum values for the local convection heat transfer coefficient over the ceiling surface, along axes x and y.

Table 5. 4 Simulation results – Convective heat transfer coefficients and heat flows

Case	$h_{c\ av}$	$h_{c\text{-}max,x}$	$h_{c\text{-}min,x}$	$h_{c\text{-}max,y}$	$h_{c\text{-}min,y}$	$h_{c\text{-}max}$	$h_{c\text{-}min}$	Qc'	Q_c	Qr'	Qr
	$W/(m^2K)$							W/m^2	W	W/m^2	W
0	2.51	2.54	2.46	2.55	2.42	2.58	2.35	11.3	317	21.6	604
1	2.42	2.46	2.29	2.47	2.33	2.51	2.06	9.8	274	21.5	603
2	2.42	2.46	2.28	2.47	2.26	2.51	2.17	9.8	274	21.5	603
3	2.80	3.19	2.45	4.72	2.30	5.88	2.24	10.6	297	22	603
4	2.83	3.09	2.40	5.14	2.34	5.98	2.25	10.5	293	21.5	603
5	2.67	2.96	2.42	3.75	2.39	4.47	2.25	10.2	284	21.5	603
6	3.01	3.43	2.41	4.53	2.38	5.25	2.21	10.9	305	21.5	603
7	2.70	3.38	2.40	3.73	2.47	4.40	2.20	10.5	295	21.5	603
8	2.90	3.01	2.42	3.76	2.40	4.43	2.21	10.2	285	21.5	603

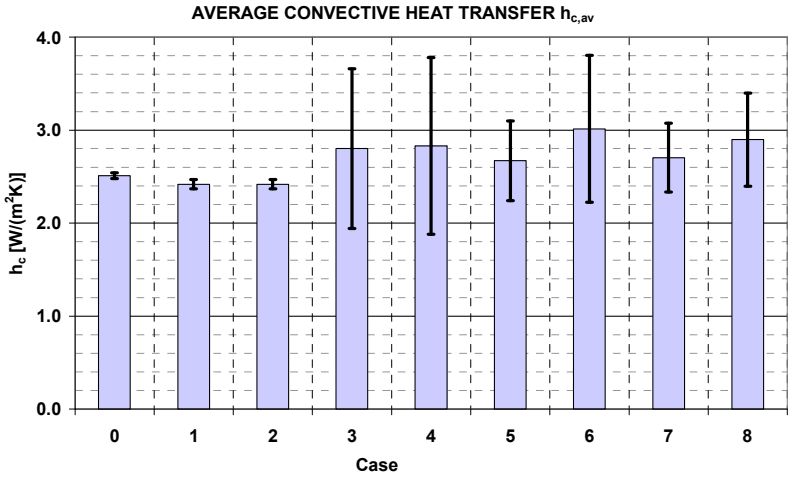

Figure 5. 11 Average convective heat transfer coefficients and standard deviation for all cases

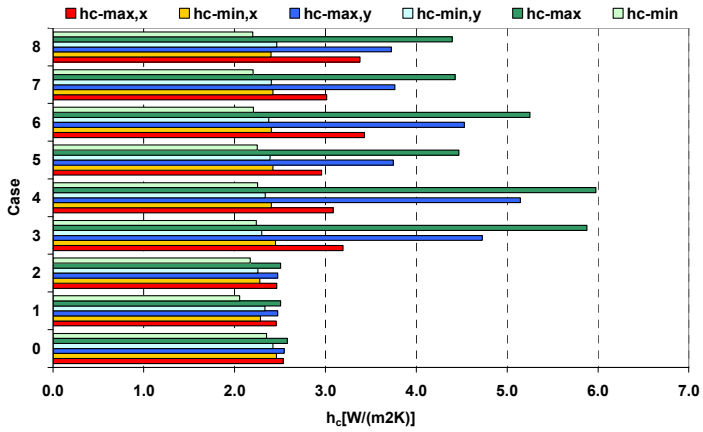

Figure 5. 12 Local x and y sections and absolute maximum and minimum convective heat transfer coefficients for all cases

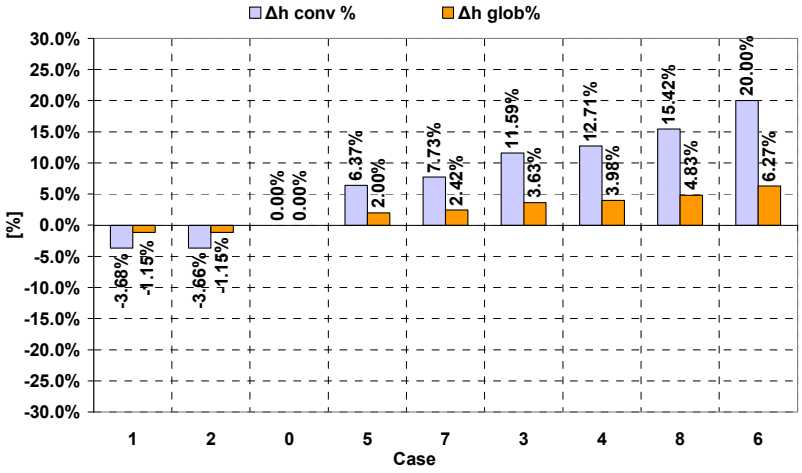

Figure 5. 13 Convective and global heat transfer coefficients enhancement vs. Case 0

The average convective heat transfer coefficients for all cases are compared with that of the reference case without ventilation (case 0) in Figure 5. 13. It shows that the choice of low induction ratios (case 1 and case 2) and consequent air flow temperatures below the room temperature determine convection heat transfer coefficient values lower than in the reference case (without ventilation), whereas high induction rate air terminal units increase the convective heat transfer coefficient at the surface of cooled ceilings. This happens because when vents type B are adopted, air velocities under the ceiling are higher for almost all the room, and consequently forced convection becomes important. Anyway, the influence of inlet air terminal units on the performances of cooled ceilings have to be calculated basing on the total heat transfer rate taking place at the ceiling surface. In fact, even if the largest increase in the convective heat transfer coefficient is around 20% (for case 6, the average convective heat transfer coefficient is 3.0 W/(m^2 K) against 2.5 W/(m^2 K) of the reference case), convective heat flows and total heat transfer flows are lower than in the reference case, as shown in Figure 5. 14.

In fact, in the case of low induction inlet air terminal units, the air that comes into contact with the surface of the ceiling has a low temperature difference with respect to the ceiling surface temperature. As a consequence, whatever is the value of the convective heat transfer coefficient, the resulting heat flow is still lower than in the case of mere cooled ceiling.

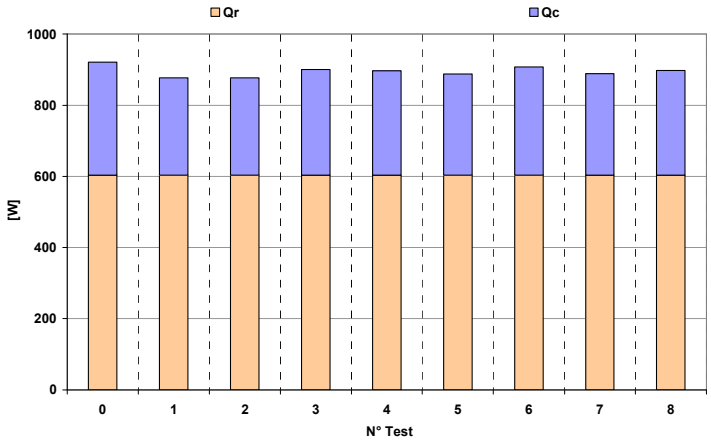

Figure 5. 14 Convective and radiant heat flows at the ceiling for all cases

5.4 Conclusions

In this work a study on the enhancement in heat transfer at the surface of cooled ceilings due to sweeping inlet air is presented. The study consists in CFD simulations for various configurations of inlet air vents placed near the ceiling, including both low induction rate and high induction rate inlet air terminals. The study shows that no relevant increase in cooling ceiling capacity takes place. In fact, in the case of low induction inlet air terminals, the air that comes into contact with the surface of the ceiling has a low temperature difference with respect to the ceiling surface temperature. As a consequence, whatever the value of the convective heat transfer coefficient value, the resulting heat flow is still lower than in the case of mere cooled ceiling. The heat transfer coefficient is increased in the case of inlet air terminals tilted towards the ceiling (3°), but only with high induction rate air terminals (type B) and significant speeds. The improvement in the convective heat transfer coefficient is low and, compared to the total amount of heat flows exchanged by the ceiling, this is even more evident.

If the inlet terminal units are near the ceiling, the global heat flow exchanged from the ceiling shows little dependence on the ventilation system.

5.5 References

[1] Awbi, H.B., Hatton. 2000. A. Mixed convection from heated room surfaces. Energy and Buildings 32, (2000), pp. 153-166.

[2] Jeong, J.W., Mumma, S.A. 2003. Ceiling radiant cooling panel capacity enhanced by mixed convection in mechanically ventilated spaces. Applied Thermal Engineering 23, pp. 2293–2306.

[3] Beausoleil-Morrison, I. 2001.An algorithm for calculating convection coefficients for internal building surfaces for the case of mixed flow in rooms. Energy and Buildings 33, pp. 351-361

[4] Churchill, S.W., Usagi, R. 1972. A general expression for the correlation of rates of transfer and other phenomena. AIChE Journal 18 (6) (1972), pp. 1121-1128.

[5] Alamdari, F., Hammond, G.P. 1983. Improved data correlations for buoyancy-driven convection in rooms, Building Services Engineering Research and Technology 4 (3) (1983), pp.106-112.

[6] Fisher, D.E. 1995. An experimental investigation of mixed convection heat transfer in a rectangular enclosure, Ph.D. Thesis, University of Illinois, Urbana, USA.

[7] Novoselac, A., Burley B.J., Sbrebric, J. 2006. New convection correlations for cooled ceiling panels in room with mixed and stratified airflow, HVAC&R RESEARCH, Volume 12, Number 2, pp. 279-294.

[8] McGrattan, K. B., Klein, B., Hostikka, S. and Floyd, J. E. 2007. Fire Dynamics Simulator (Version 5), User's Guide, NIST Special Publication 1019-5, National Institute of Standards and Technology, Building and Fire Research Laboratory, Gaithersburg, Maryland, USA.

[9] A. Musser, K. McGrattan, J. Palmer, Evaluation of a fast, simplified, Computational Fluid Dynamic Model for solving Room Airflow Model, NISTIR 6760, NIST, 2001.

[10] EN 12792 -2003. Ventilation for buildings - Symbols, terminology and graphical symbols.

6 - Mechanical ventilation in combination with radiant heating/cooling systems: experimental studies on thermal comfort and ventilation effectiveness for a residential and an office room

Abstract

Different experiments have been carried out in a full scale test room in order to evaluate indoor climate in a typical residential room and in a typical office equipped with mechanical ventilation and a floor heating/cooling system.

The effect of low ventilation rates (one or half air change per hour) on thermal comfort and ventilation effectiveness parameters in a residential room has been studied. Various positions of supply and extract air terminals and different winter and summer boundary conditions have been tested.

Moreover, the effect of different ventilation rates with a displacement ventilation system on thermal comfort and ventilation effectiveness in an office for two occupants have been examined.

Vertical air temperature, operative temperature and air velocity profiles were measured in different positions in the room, in order to determine possible causes of discomfort for each condition. Besides the ventilation effectiveness expressed by the contaminant removal effectiveness and local air change index have been measured in the space to characterize the system's ability to clean the air and distribute fresh supply air.

Results show that mixing ventilation with low flow rates guarantees high level of thermal comfort, even if local discomfort is possible during cooling season when the radiant floor is maintained at low temperature in order to balance significant internal heat loads or high supply air temperatures. Ventilation effectiveness strongly depends on the extract air terminal position and some differences between air change index and contaminant removal effectiveness have been noticed.

Displacement ventilation guarantees excellent ventilation effectiveness, particularly with higher flow rates; but at the same time the increase of ventilation rates implies higher risk of local discomfort.

Radiant temperature asymmetry due to warm ceiling is a serious risk of discomfort during summer if the floor temperature is more than 4 °C lower than the reference temperature in the room, regardless of the type of ventilation system (displacement or mixing ventilation).

6.1 Test room and equipment description

The experimental measurements have been carried out in a full scale chamber with the dimensions 4.2 m by 4.0 m by 2.4 m at the International Centre for Indoor Environment and Energy of Technical University of Denmark [1].

The chamber is equipped with a radiant heating /cooling floor and a radiant heating/cooling wall simulating a window of 8 m^2. Two control units were built to supply warm or cold water to the floor system and to the panels simulating the windows. Moreover the chamber can be equipped with primary air with flow rate from 6 to 170 l/s (0.5-14 ACH) at different temperatures (from 10 °C to 40 °C) and the percentage of outdoor air can be set through a PC control system.

Displacement air diffuser (Lindab CBA 1607), circular ceiling diffuser and wall mounted air terminal devices (Uponor) were used in order to provide mechanical ventilation in the chamber.

A thermal manikin [2] composed by 17 body parts was used in order to complete the information of thermal comfort.

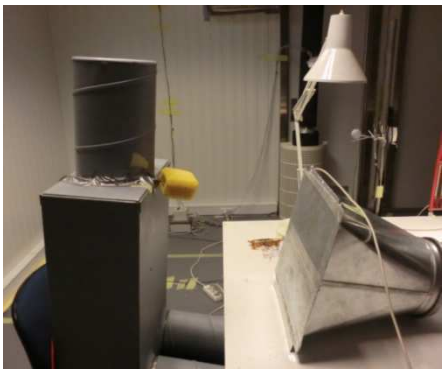

a

b

c

d

Figure 6. 1 Room equipment details: heated dummy, metal box simulating a PC, desk lamp, contaminant source (a), thermal manikin (b), wall supply air terminal (c) and displacement ventilation air terminal (d)

Sensors type Craftemp Astra were used to measure surface temperatures.

Sensors were connected to a single ended relay multiplexer with 60 channels type 44706A, which was connected to a data-logger type HP 3852A Data acquisition/control unit. The thermistor sensors were calibrated in the range between 15 and 35 °C, in order to assure an accuracy of ±0.3 °C in temperature measurements.

Air velocity measurements were carried out by means of nine omnidirectional hot sphere anemometers (Dantec), connected to a 54N10 Multichannel Flow Analyzer. The anemometers had been calibrated in the range between 0.02 and 2.82 m/s, and after that the uncertainty of $\pm(0.02 + 0.01 \cdot v)$ m/s, where v is the actual measurement, was reached [3].

To control the amount of heat gains in the chamber, one or two desk lamps with different electric power, two metal boxes with bulbs inside simulating PC monitors and one heated dummy was used to reproduce human occupancy (Figure 6. 1)

Hobo data logger were used to measured relative humidity, air and globe temperature with particular probes: air sensor was protected by radiation with a cylindrical metal device while globe temperature was inserted in a grey sphere (Figure 6. 2). The grey color chosen simulates people dressed in light colored clothing while the small dimensions of the sphere allow that the mean radiant temperature and air temperature have the same weighted influence on the transducer as on a person, like reported in [4]. Therefore the globe temperature measured with this sensors at 0.6 m and 1.1 m height can be considered as operative temperature. The two external probes, measuring one the globe temperature and the other the air temperature, have an accuracy of ± 0,3 °C.

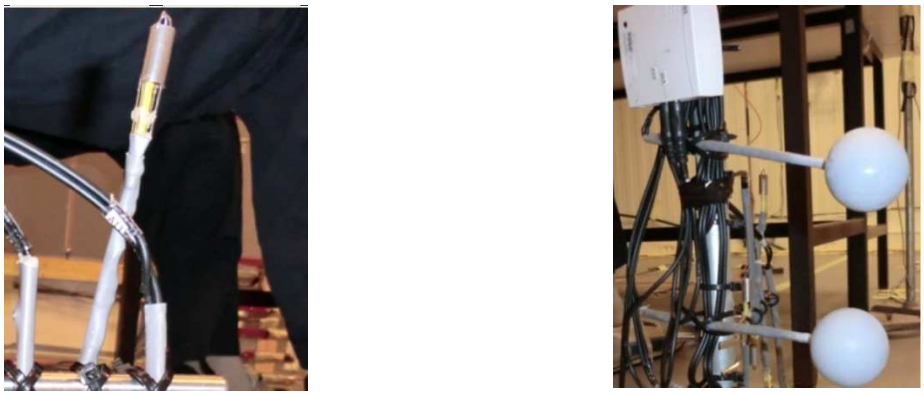

a b

Figure 6. 2 Air temperature sensor (a) and globe sensor connected to Hobo data logger(b) used in the occupied zone

Carbon dioxide and R134a were the tracer gases used in the experiments; concentration measurements and gas dosing in the room were carried out through two Innova 1312 Photoacoustic Multigas and two Innova 1303 Multipoint Sampler and Doses. The measuring device was placed outside the chamber and small plastic tubes allowed to take samples of air from the room or release gas in the room.

A smoke generator was used in order to visualize the airflow pattern in the chamber under different boundary conditions

6.2 Experimental method

6.2.1 Case studies

Mixing ventilation in a residential application and displacement ventilation in an office application are investigated, both for heating and for cooling conditions.

For mixing ventilation, the effect of the position of the supply air terminal and of the extract air terminal is studied.

Supply air terminal is placed in a central position on the upper part of a wall (0.15 m distant from the ceiling) or in the middle of the ceiling. The extract air terminal can be placed or on a wall (the same wall where the supply air terminal is placed), or on the ceiling on the opposite side of the window. As regard the position on the wall, the extract air terminal would be in central position or just below the supply or next to the floor (0.1 m height). Therefore 4 different combinations of supply/extract air terminals, named system M1, system M2, system M3 and system M4, are considered as shown in Figure 6. 3.

With systems M1 and system M2, the amount of internal heat gains (90 W) corresponding to the situation of one occupant (using the thermal manikin) and one low energy desk lamp (20 W) is adopted. For systems M3 and M4 the internal heat gain is 200 W, corresponding to one occupant, one desk lamp (30 W) and one PC (100W). Details about the position of furniture and of heat gains are in Figure 6. 4 and Figure 6. 5.

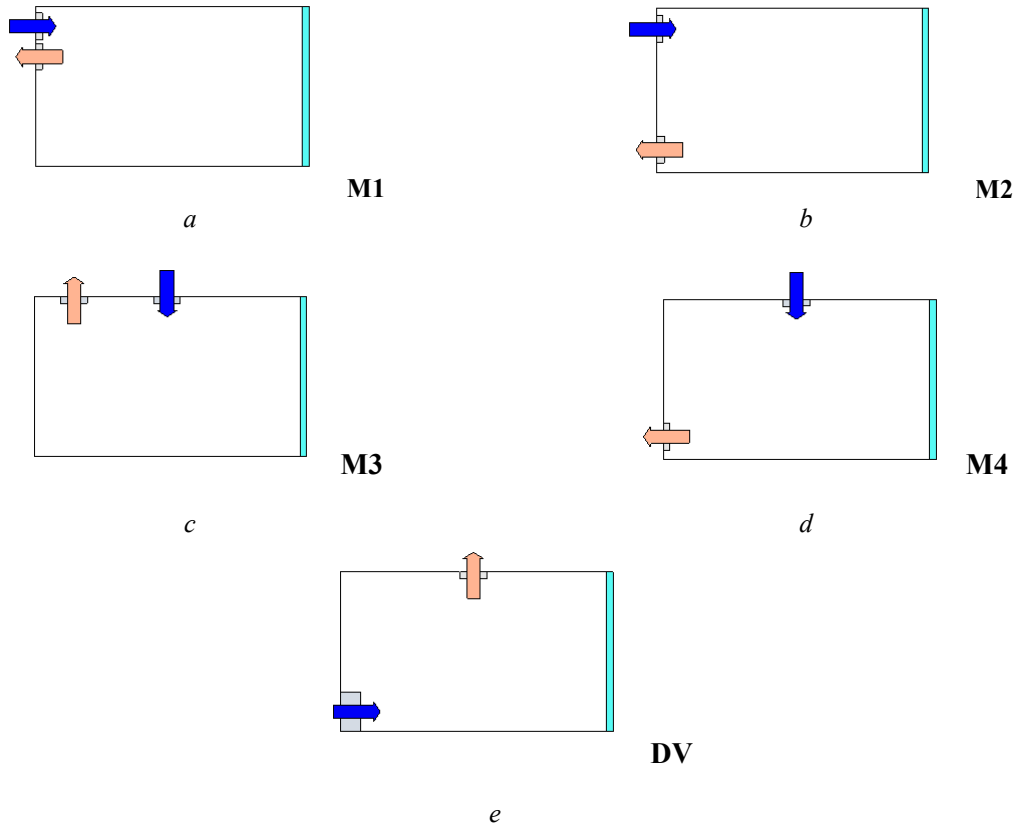

Figure 6. 3 Position of supply air terminal (blu arrow) and extract air terminal (orange arrow) for system M1 (a), system M2 (b), system M3 (c), system M4 (d) and system DV (e). The window is on the right (blue)

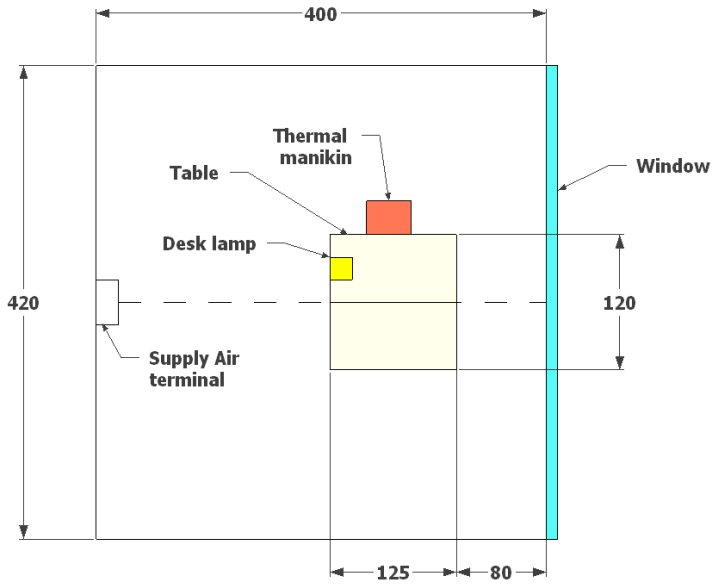

Figure 6. 4 Room representation for systems M1 and M2 (mixing ventilation from the wall for a residential room)

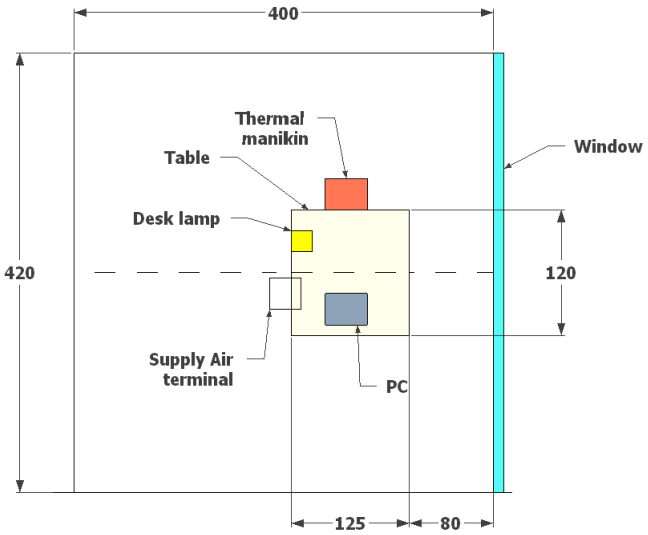

Figure 6. 5 Room representation for systems M3 and M4 (mixing ventilation from the ceiling for a residential room)

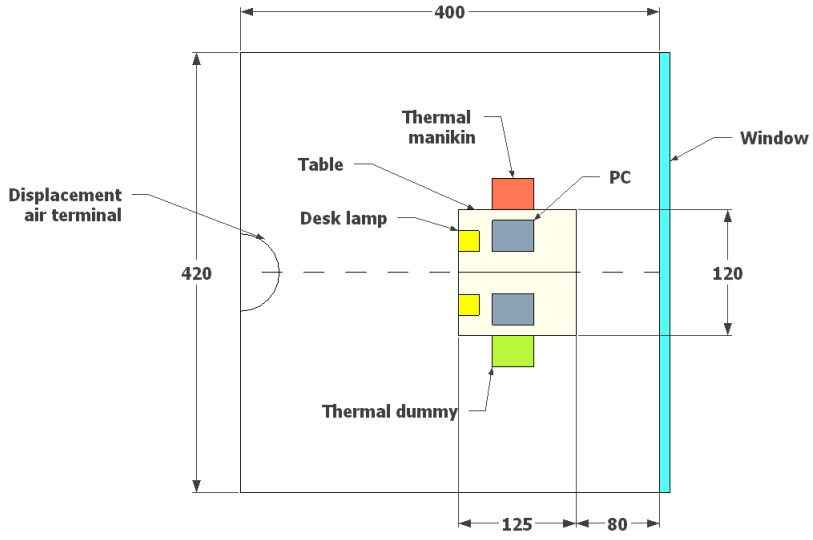

Figure 6. 6 Room representation for systems DV with displacement ventilation (office)

With displacement ventilation, the supply air terminal is at the middle of the wall opposite to the window and the extract air terminal is placed in the middle of the ceiling. In order to investigate a typical office with 2 occupants, a thermal manikin, a thermal dummy, 2 desk lamps and 2 personal computers (PC) are considered. The room lay-out is named system DV and shown in Figure 6. 6.

For each system different cases are chosen. Two air set point temperatures have been chosen for the room, that is 22 °C on winter condition and 26 °C in summer condition. In detail, operative

temperature at 1.1 m height in the centre of the room was chosen as set point θ_{sp} for the system, but in the same position the air temperature $\theta_{sp,air}$ was measured and used for the heat balance calculations.

Each case differs from the other for air flow rate and supply air temperature and surface temperature of the simulated window; in other words each case is characterized by own heat flows from the ventilation Q_v , from the window Φ_w and from the floor Q_F.

Φ_w is the heat flow transmitted through an 8.0 m^2 window assuming that the internal air temperature is uniform and equal to the set point temperature. Heat transfer coefficient for walls h_w is assumed to be 8 W/(m^2K), so the equation for Φ_w should be:

$$\Phi_W = h_W \cdot A_W \cdot \left(\theta_W - \theta_{sp,air}\right) \qquad \textit{Eq 6. 1}$$

Where A_w is the window area, θ_W the internal surface of window and $\theta_{sp,air}$ the reference air temperature at 1.1 m height in the centre of the room.

The assumed thermal transmittance of the window is U=1.2 W/(m^2K) or 2 W/(m^2K). In summer case the solar radiation Φ_{solar} has to be taken in account for the calculation of Φ_w according to equation (6.2): values from 180 W to 420 W are chosen.

$$\Phi_W = U \cdot A_W \cdot (\theta_{Ext} - \theta_W) + \Phi_{solar} \qquad \textit{Eq 6. 2}$$

Assuming a solar heat gain coefficient SHGC equal to 0.24, the chosen Φ_{solar} corresponds to a solar irradiation between 93 W/m^2 and 219 W/m^2, corresponding to the solar irradiance of central Europe and Mediterranean area respectively. Knowing Φ_w from the previous equation, the external surface temperature of the window θ_{Ext} could be estimated with equation (6.2). For a certain internal surface temperature of the window θ_W, when lower thermal transmittance U [W/(m^2K)] are assumed, more critical outside conditions can be hypothesized for winter and summer conditions. For example, if the window temperature is 33.2 °C during a summer day and the solar heat load is 420 W, external air temperature with overall heat transfer coefficient U equal to 1.2 W/(m^2K) is 30.3 °C instead of 28.2 °C obtained with U equal to 2.0 W/(m^2K).

The ventilation heat load Φ_v is calculated by equation (6.3) where Q_v is the supply air flow rate (m^3/s), ρ is the air density (1.20 kg/m^3), c_p is the specific heat of air (1006 J/kg·K), θ_e and θ_s are the extract and supply air temperatures (°C). The extract air temperature θ_e (°C) is calculated according to the 50% rule [5] for displacement ventilation while it is assumed 1 degree Celsius higher than set point for mixing ventilation.

$$\Phi_v = q_v \cdot \rho \cdot c_p \cdot (\theta_e - \theta_s) \qquad \textit{Eq 6. 3}$$

Heat losses from the room Φ_{loss} are calculated assuming the temperature in the environment in which the room is placed and the average thermal transmittance of the room, that is U= 0.25 $W/(m^2K)$ [3].

By calculation of heat flow rates from window Φ_W and from ventilation Φ_v and heat losses towards the external environment of the room Φ_{loss}, knowing the internal heat gains Φ_i, it is possible to estimate the required cooling/heating capacity of the floor Φ_F. Heat transfer coefficient h_F is assumed to be 7 $W/(m^2K)$ when floor is cooled, 11 $W/(m^2K)$ when floor is heated, as recommended in Standard EN 15377 [6], therefore the calculated floor temperature is obtained from equation (6.5).

$$\Phi_F = \Phi_v + \Phi_W + \Phi_i + \Phi_{loss} \qquad \textit{Eq 6. 4}$$

$$\theta_F = \theta_{sp} + \frac{\Phi_F}{h_F} \qquad \textit{Eq 6. 5}$$

The procedure is similar to that described in [7] and [8].

Table 6. 1 Boundary conditions and calculated heat flow rates for the 5 cases of mixing ventilation with supply air terminal from the wall and extract air terminal at high level (system M1)

Mixing ventilation from wall			**CASE M1-1**	**CASE M1-2**	**CASE M1-3**	**CASE M1-4**	**CASE M1-5**
Symbol	**Definition**	**Unit**					
$\theta_{sp,air}$	Set point air temperature	°C	22	22	26	26	26
Φ_w	Heat load from window	W	-218	-218	416	416	416
Φ_w'	Specific heat load from window	W/m^2_{floor}	-13.0	-13.0	24.8	24.8	24.8
θ_w	Surface temperature of the window	°C	18.6	18.6	32.5	32.5	32.5
Φ_i	Internal heat load	W	90	90	90	90	90
$\Phi i'$	Specific internal heat load	W/m^2_{floor}	5.4	5.4	5.4	5.4	5.4
q_v	Supply air volume flow	l/s	5.6	5.6	5.6	11	5.6
N	Air change per hour (ACH)	h^{-1}	0.5	0.5	0.5	1.0	0.5
θ_s	Supply air temperature	°C	30.0	17.0	30.0	30.0	18.0
θ_e	Extract air temperature	°C	23.0	23.0	27.0	27.0	27.0
Φ_v	Ventilation heat load	W	47.3	-40.5	20.3	40.5	-60.8
Φ_v'	Specific ventilation heat load	W/m^2_{floor}	2.8	-2.4	1.2	2.4	-3.6
Φ_f	Floor heat load	W	80.3	168.1	-582.4	-490.4	-501.3
Φ_f'	Specific floor heat load	W/m^2_{floor}	4.8	10.0	-34.7	-29.2	-29.8
θ_f	Floor temperature	°C	22.4	22.9	21.0	21.8	21.7
U	Overall heat transfer coefficient	W/m^2K	1.2	1.2	1.2	1.2	1.2
Φ_{solar}	Solar heat load	W	0	0	380	380	380
θ_{ext}	External temperature	°C	-0.6	-0.6	29.8	29.8	29.8

Table 6. 2 Boundary conditions and calculated heat flow rates for the 5 cases of mixing ventilation with supply air terminal from the wall and extract air terminal at low level (system M2)

Mixing ventilation from wall			CASE M2-1	CASE M2-2	CASE M2-3	CASE M2-4	CASE M2-5
Symbol	**Definition**	**Unit**					
$\theta_{sp,air}$	Set point air temperature	°C	22	22	26	26	26
Φ_w	Heat load from window	W	-218	-218	416	416	416
Φ_w'	Specific heat load from window	W/m^2_{floor}	-13.0	-13.0	24.8	24.8	24.8
θ_w	Surface temperature of the window	°C	18.6	18.6	32.5	32.5	32.5
Φ_i	Internal heat load	W	90	90	90	90	90
$\Phi i'$	Specific internal heat load	W/m^2_{floor}	5.4	5.4	5.4	5.4	5.4
q_v	Supply air volume flow	l/s	5.6	5.6	5.6	11	5.6
N	Air change per hour (ACH)	h^{-1}	0.5	0.5	0.5	1.0	0.5
θ_s	Supply air temperature	°C	30.0	17.0	30.0	30.0	18.0
θ_e	Extract air temperature	°C	23.0	23.0	27.0	27.0	27.0
Φ_v	Ventilation heat load	W	47.3	-40.5	20.3	40.5	-60.8
Φ_v'	Specific ventilation heat load	W/m^2_{floor}	2.8	-2.4	1.2	2.4	-3.6
Φ_f	Floor heat load	W	80.3	168.1	-582.4	-490.4	-501.3
Φ_f'	Specific floor heat load	W/m^2_{floor}	4.8	10.0	-34.7	-29.2	-29.8
θ_f	Floor temperature	°C	22.4	22.9	21.0	21.8	21.7
U	Overall heat transfer coefficient	W/m^2K	1.2	1.2	1.2	1.2	1.2
Φ_{solar}	Solar heat load	W	0	0	380	380	380
θ_{ext}	External temperature	°C	-0.6	-0.6	29.8	29.8	29.8

For systems M1 and M2 the same 5 cases are chosen.

Cases 1 and 2 refer to a heating condition, with a window surface temperature of 18.6 °C and a low ventilation rate (0.5 ACH); in the first case heating is due to the ventilation system while in the second case heating is due to a radiant floor system.

Cases 3 and 4 refer to a summer condition with a window surface of 32.5 °C, floor cooling and ventilation with supply air temperature equal to outside temperature. Two levels of ventilation rate, 0.5 ACH and 1.0 ACH, are investigated.

Case 5 refers to a cooling condition with a window surface of 32.5 °C, low ventilation rate (0.5 ACH) and cooling due to both ventilation and to floor radiant system.

For all this cases the internal heat gains are low (5.4 W/(m^2 K)$_{floor}$) as for a residential room.

Table 6. 3 Boundary conditions and calculated heat flow rates for the 4 cases of mixing ventilation with supply air terminal from the ceiling (systems M3 and M4)

Mixing ventilation from ceiling			**CASE M3-1**	**CASE M3-2**	**CASE M4-1**	**CASE M4-2**
Symbol	**Definition**	**Unit**				
$\theta_{sp,air}$	Set point air temperature	°C	26	26	26	26
Φ_w	Heat load from window	W	512	512	512	512
Φ_w'	Specific heat load from window	W/m^2 $_{floor}$	30.5	30.5	30.5	30.5
θ_w	Surface temperature of the window	°C	34	34	34	34
Φ_i	Internal heat load	W	200	200	200	200
Φi'	Specific internal heat load	W/m^2 $_{floor}$	11.9	11.9	11.9	11.9
q_v	Supply air volume flow	l/s	5.6	5.6	5.6	5.6
N	Air change per hour (ACH)	h^{-1}	0.5	0.5	0.5	0.5
θ_s	Supply air temperature	°C	20.0	26.0	20.0	26.0
θ_e	Extract air temperature	°C	27.0	27.0	27.0	27.0
Φ_v	Ventilation heat load	W	-47.3	-6.7	-47.3	-6.7
Φ_v'	Specific ventilation heat load	W/m^2 $_{floor}$	-2.8	-0.4	-2.8	-0.4
Φ_f	Floor heat load	W	-706.8	-747.4	-706.8	-747.4
Φ_f'	Specific floor heat load	W/m^2 $_{floor}$	-42.1	-44.5	-42.1	-44.5
θ_f	Floor temperature	°C	20.0	19.6	20.0	19.6
U	Overall heat transfer coefficient	W/m^2K	1.2	1.2	1.2	1.2
Φ_{solar}	Solar heat load	W	420	420	420	420
θ_{ext}	External temperature	°C	35.6	35.6	35.6	35.6

For systems M3 and M4 the same 2 cases are chosen.

The aim is to investigate the effect of a hot window surface (34 °C) in a residential room with low ventilation rate (0.5 ACH) and significant heat gains (11.9 W/(m^2 K)$_{floor}$) in cooling mode.

Case 1 refers to a floor cooling condition with supply air temperature of 20 °C while for Case 2 the primary air enters the room at the same temperature of the reference air temperature θ_{sp}.

Table 6. 4 Boundary conditions and calculated heat flow rates for the 6 cases of displacement ventilation (DV)

Displacement ventilation			CASE DV-1	CASE DV-2	CASE DV-3	CASE DV-4	CASE DV-5	CASE DV-6
Symbol	**Definition**	**Unit**						
$\theta_{sp,air}$	Set point temperature	°C	26	26	26	26	26	26
Φ_w	Heat load from window	W	461	461	461	461	218	461
Φ_w'	Specific heat load from window	W/m^2_{floor}	27.4	27.4	27.4	27.4	13.0	27.4
θ_w	Surface temperature of the window	°C	33.2	33.2	33.2	33.2	29.4	33.2
Φ_i	Internal heat load	W	520	520	520	520	520	520
$\Phi i'$	Specific internal heat load	W/m^2_{floor}	31.0	31.0	31.0	31.0	31.0	31.0
q_v	Supply air volume flow	l/s	35.8	50.4	33.6	23.5	23.5	16.8
N	Air change per hour (ACH)	h^{-1}	3.2	4.5	3.0	2.1	2.1	1.5
θ_s	Supply air temperature	°C	16.0	16.0	22.0	20.0	24.0	17.0
θ_e	Extract air temperature	°C	29.7	29.7	27.5	28.2	26.7	29.3
Φ_v	Ventilation heat load	W	-592.5	-833.1	-222.4	-233.5	-77.8	-250.2
Φ_v'	Specific ventilation heat load	W/m^2_{floor}	-35.3	-49.6	-13.2	-13.9	-4.6	-14.9
Φ_f	Floor heat load	W	-444.5	-203.8	-814.6	-803.4	-715.9	-786.8
Φ_f'	Specific floor heat load	W/m^2_{floor}	-26.5	-12.1	-48.5	-47.8	-42.6	-46.8
θ_f	Floor temperature	°C	22.2	24.3	19.1	19.2	19.9	19.3
U	Overall heat transfer coefficient	W/m^2K	2	2	1.2	1.2	1.2	1.2
Φ_{solar}	Solar heat load	W	420	420	420	420	180	420
θ_{ext}	External temperature	°C	28.6	28.6	30.3	30.3	30.0	30.3

For displacement ventilation system 6 cases of cooling are adopted. The aim is to investigate the effect of different ventilation rates and supply air temperatures on thermal comfort and ventilation effectiveness in an office with very high heat gains (31 W/m^2_{floor}).

The chosen ventilation rates correspond to the recommended Standard EN15251 [9] values for a single office with default occupant and different categories of pollution from the building itself.

Case 1 and Case 2 refer to a cooling condition in which the main part of the cooling is due to ventilation: the ventilation rates are respectively 3.2 an 4.5 ACH, corresponding to 2.1 and 3.0 l/(s m^2), Standard limit for non low polluted building, category II and I.

Case 3, Case 4 and Case 6 refer to cooling conditions with similar floor temperature (in the range from 19.1 °C to 19.3 °C) but different ventilation rates: from 3.0 ACH to 1.5 ACH, corresponding to 2.0 l/(s m^2) and to 1.0 l/(s m^2), limits respectively for low polluted building category I and very low polluted building category II.

Case 5 refers to a case with high supply temperature (24 °C), floor surface temperature near 20°C and lower window surface temperature (29.4 °C) with 1.4 l/(s m^2) (Standard limit for low polluted building category II).

6.2.2 Thermal comfort evaluation: method

Thermal comfort for each condition has been investigated by measurements in seven points, the same used in previous studies in the same chamber [3] and [10].

As shown in Figure 6. 7, there are 4 points in the occupied zone (S3, S4, S5 and S6) and 3 points near the window (S1, S2 and S7). S6 is the point closest to the supply air terminal when installed on the wall, S1 is the point closest to the window.

In order to obtained air temperature, globe temperature and air velocity vertical profiles in all the points, measurements were done by means of movable stands to which probes were fixed. In particular, temperatures were measured at 12 heights and velocities at 9 heights (Table 6. 5) for all the conditions. Because of the characteristics of the probes, globe temperature measured at 0.6 m and 1.1 m might be considered as operative temperature. Mean air velocity and mean air temperatures were calculated using an integration time of 3 minutes. In the case of velocity also Standard deviation was calculated.

During each test the conditions of the center of the room were monitored: not only temperatures and air velocities but also relative humidity RH%.(maintained in the range of 16 % ÷42 % ±2.5%) were measured.

All the internal surfaces temperatures were measured with 53 probes equally distributed and the average of the temperatures during each test condition was considered for the calculation of each average surface temperature. Two more probes measured the surface temperature on the external surface of the room, in order to assess the heat losses by conduction through the walls.

Supply air temperature and air temperature close to the extract air terminal were monitored with two sensors during each experiment.

Besides, for each condition the following thermal comfort parameters (according to Standard ISO 7730:2005 [11]) have been determined:

- Surface temperature of the floor; according to ISO 7730 the range of surface temperature for category A should be 19÷29 °C.
- Temperature difference between head and feet for a sitting person Δθ (1.1 m and 0.6 m above the floor) and a standing person (1.7 m and 0.6 m above the floor); according to ISO 7730 the vertical difference between 1.1 m and 0.6 m should be less than 2 °C for category A, less than 3 °C for category B and less than 4 °C for category C.
- Draught rating DR [%] (at 1.1 m and at 0.1 m height). The limits according to ISO 7730 are 10 %(category A), 20 % (category B) and 30 % (category C).
- Operative temperature at 0.6 m and 1.1 m height for each position within the occupied zone (position S3, S4, S5 and S6).
- Radiant temperature asymmetry caused by the window and by the ceiling in the position occupied by the manikin. A small element at 0.6 m height was assumed and shape factors have been calculated according to ISO 7726-1998 [12]. The limit for category A and B according to ISO 7730 are 5 °C for warm ceiling, 14 °C for cold ceiling, 23 °C for warm wall and 10 °C for cold wall.

Temperature differences between head and floor and air velocity have been measured in 7 positions (Figure 6. 7) for each case, so the calculation of Δθ and DR [%] was carried out in different points of the occupied zone and near the window.

Besides, for all the conditions the local equivalent temperature has been determined thanks to the thermal manikin. The equivalent temperature relates to the dry heat loss from the body. It expresses the combined effect of air temperature, mean radiant temperature and air velocity and it is derived from the operative temperature, which considers the first two parameters only. Measurements with thermal manikin provide information on the dry heat loss, Q_{si}, and the surface temperature, t_{sk} for each body segment. According to Fanger's comfort equation [13], the mean skin temperature, t_{sk}, under thermal neutrality can be estimated as:

$$t_{sk} = 35.7 - 0.28 \cdot Q_t \qquad \textit{Eq 6. 6}$$

where Q_t is the total heat loss from the human body. The thermal manikin can measure only the sensible heat loss but it can't simulate the latent heat loss, so another correlation is necessary, with the assumptions of a vapour pressure of 1,5 kPa, equivalent to typical indoor conditions at 24 ºC and relative humidity of 50% [14].

Therefore surface temperatures t_{sk} can be determined with the following equation:

$$t_{sk} = 36.4 - 00.054 \cdot Q_s \qquad \textit{Eq 6. 7}$$

Then, the local equivalent temperature for each part t_{eqi} can be calculated by the following equation:

$$t_{eqi} = t_{ski} + \frac{Q_{si}}{h_{cal}} \qquad \textit{Eq 6. 8}$$

where h_{cal} is the heat transfer coefficient [W/(m^{2}K)] for each body segment, determined during the calibration of the thermal manikin in a standard uniform environment (at different temperatures) before the experiment with the clothes chosen for the experiments [15].

Finally PMV and PPD [%] for winter and summer conditions have been calculated with ASHRAE Thermal Comfort Tool [16] based on ASHRAE 55-2004 [17] assuming 0.6 clo for summer and 1.0 clo as clothing resistance, 1 met in summer and 1.1 met in winter and as metabolic rate, corresponding to a sedentary activity in dwellings or offices. The average measured relative humidity RH [%], air velocity, air temperature and operative temperature at 1.1 m height in the centre of the room have been considered in the calculation.

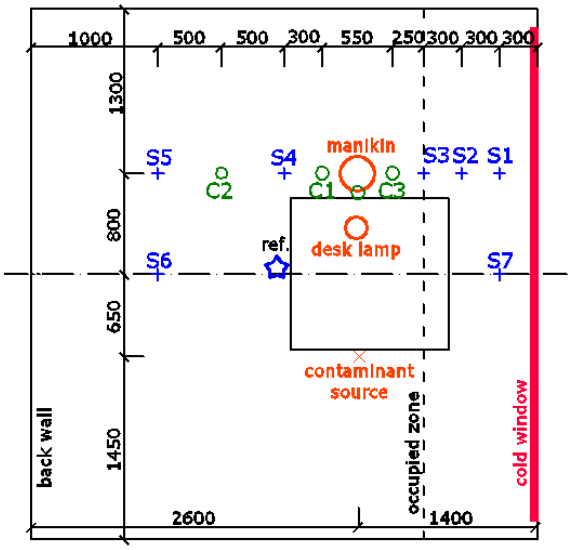

Figure 6. 7- Room representation with points of measurement of temperature and velocity (from S1 to S7) and points of measurement of ventilation effectiveness (C1,C2 and C3)

Table 6. 5 Number of sensors and corresponding heights for air temperature, T_a, globe temperature, $T_{globe,}$ and air velocity, v_a

	T_a [°C]	**T_{globe} [°C]**	**v_a [m/s]**
N° sensor	height, [m]	height, [m]	height, [m]
1	0.05	0.05	0.03
2	0.1	0.1	0.05
3	0.15	0.15	0.10
4	0.2	0.2	0.15
5	0.3	0.3	0.20
6	0.6	0.6	0.30
7	0.85	0.85	0.60
8	1.1	1.1	1.10
9	1.4	1.4	1.70
10	1.7	1.7	-
11	2	2	-
12	2.3	2.3	-

6.2.3 Ventilation Effectiveness evaluation: method

Ventilation effectiveness expresses the degree to which a ventilation system can satisfy the ventilation requirements in a room. In other words, ventilation effectiveness expresses the ability of the system to remove contaminants and at the same time to provide fresh air in all the volume. A ventilation system characterized by higher ventilation effectiveness can guarantee higher level of air quality within an environment, since the air-borne contaminants are removed more efficiently and fresh air reaches the occupants earlier.

Ventilation effectiveness for each condition has been investigated by measurements in different points and at different heights, the same used in previous studies in the same chamber [10].

Contaminant removal effectiveness and local air change index are determined by means of two different tracer gases, respectively carbon dioxide and R134a.

Contaminant removal effectiveness CRE indicates the ability of the room ventilation system to remove air-borne contaminants when the position of contaminant source is known.

Contaminant removal effectiveness CRE according to [18] is defined as:

$$CRE = \frac{c_e - c_s}{< c > - c_s} \qquad \textit{Eq 6. 9}$$

while local air quality index ε^a_P is defined as:

$$\varepsilon^c_P = \frac{c_e - c_s}{c_i - c_s} \qquad \textit{Eq 6. 10}$$

where c_e is the contaminant concentration in the exhaust, <c> is the mean contaminant concentration in the room, c_i is the concentration in the point and c_s is the contaminant concentration in the supply air. In a fully mixed situation the concentration is the same in all the points of the volume, therefore CRE is 1.0.

Since the concept of local air quality index ε^c_P and contaminant removal effectiveness CRE are close to each other, in this work local air quality in the point ε^c_P is defined contaminant removal effectiveness CRE in order to simplify the presentation of results.

The CRE measurements have been carried out with carbon dioxide as tracer gas using a contaminant omnidirectional source (constant dosing) on the other side the table right opposite the manikin (Figure 6. 7). The source was mounted on a stand at 1.1 m height during mixing ventilation tests, while it was attached to the thermal dummy at the same height in case of displacement ventilation. When steady state gas concentration was reached, c_i were measured from positions C1, C2 and C3 at (0.6 m, 1.1 m and 1.7 m height), near the manikin (at 1.1 m height) and in the extract air terminal, then CRE parameters were calculated. The initial concentration of the room before starting with tracer gas was taken as the contaminant concentration in the supply air.

Air change efficiency is defined as the ratio between the lowest possible mean age of air ($\tau_n/2$) and the room mean age of air $<\tau>$.

$$\varepsilon^a = \frac{\tau_n}{2 \cdot <\tau>} \qquad \textit{Eq 6. 11}$$

The upper limit is 100% for ideal piston flow, 50% for fully mixed flow and <50% in case of short-circuit.

The local air change index is defined as the nominal age of air τ_n and the age of air in the point τ_P and it assumes value 100% for fully mixed flow and ≥ 100% for displacement ventilation. In this work the nominal age of air τ_n was assumed to be the local age of air in the exhaust τ_e as recommended by [18].

$$\varepsilon_P{}^a = \frac{\tau_n}{\tau_P} \qquad \textit{Eq 6. 12}$$

Local air change index measurements have been carried out with R134a as tracer gas with step up method [18]. When equilibrium was reached, concentrations were measured [19] near the manikin at 1.1 m and in the exhaust, at 1.1 m height (positions C1 and C2), at 1.7 m height (position C1) and the corresponding local ages of air were calculated [18].

Smoke test, carried out at the end of the measurements with the appropriate instruments, was a valid instrument to visualize the air flow pattern in the test room.

6.3 Results

6.3.1 Thermal comfort results

The planned boundary conditions of window temperatures, ventilation rates, supply air temperatures, simulated window temperatures were imposed in the test room. All the sensors were connected to the central data acquisition system and recorded.

Differences between planned temperatures and measured temperatures are due to limitations of the control system.

Table 6. 6 Boundary conditions and calculated heat flow rates for the 5 cases of mixing ventilation with supply air terminal from the wall and extract air terminal at high level (M1) during the experiments

Mixing ventilation from wall			**CASE M1-1**	**CASE M1-2**	**CASE M1-3**	**CASE M1-4**	**CASE M1-5**
Symbol	**Definition**	**Unit**					
$\theta_{sp,air}$	Set point temperature	°C	22.0	22.0	26.0	26.4	26.0
Φ_w	Heat load from window	W	-217.9	-217.9	419.2	396.5	546.2
Φ_w'	Specific heat load from window	W/m^2_{floor}	-13.0	-13.0	25.0	23.6	32.5
θ_w	Surface temperature of the window	°C	18.6	18.6	32.6	32.6	34.5
Φ_i	Internal heat load	W	90.0	90.0	90.0	90.0	90.0
$\Phi i'$	Specific internal heat load	W/m^2_{floor}	5.4	5.4	5.4	5.4	5.4
q_v	Supply air volume flow	l/s	5.6	5.6	5.6	11.1	5.6
N	Air change per hour (ACH)	h^{-1}	0.5	0.5	0.5	1.0	0.5
θ_s	Supply air temperature	°C	30.3	17.1	30.3	30.8	18.9
θ_e	Extract air temperature	°C	24.1	21.3	26.8	27.3	25.4
Φ_v	Ventilation heat load	W	42.1	-28.7	23.5	46.5	-43.9
Φ_v'	Specific ventilation heat load	W/m^2_{floor}	2.5	-1.7	1.4	2.8	-2.6
Φ_f	Floor heat load	W	-27.3	343.2	-755.4	-850.6	-522.0
Φ_f'	Specific floor heat load	W/m^2_{floor}	-1.6	20.4	-45.0	-50.6	-31.1
θ_f	Floor temperature	°C	21.8	23.8	19.6	19.1	21.6

Table 6. 7 Boundary conditions and calculated heat flow rates for the 5 cases of mixing ventilation with supply air terminal from the wall and extract air terminal at low level (M2) during the experiments

Mixing ventilation from wall			**CASE M2-1**	**CASE M2-2**	**CASE M2-3**	**CASE M2-4**	**CASE M2-5**
Symbol	**Definition**	**Unit**					
$\theta_{sp,air}$	Set point air temperature	°C	22.2	22.0	26.3	26.3	26.1
Φ_w	Heat load from window	W	-227.0	-218.9	388.8	347.4	422.4
Φ_w'	Specific heat load from window	W/m^2_{floor}	-13.5	-13.0	23.1	20.7	25.1
θ_w	Surface temperature of the window	°C	18.6	18.6	32.4	31.7	32.7
Φ_i	Internal heat load	W	90.0	90.0	90.0	90.0	90.0
$\Phi i'$	Specific internal heat load	W/m^2_{floor}	5.4	5.4	5.4	5.4	5.4
q_v	Supply air volume flow	l/s	5.6	5.6	5.6	11.1	5.6
N	Air change per hour (ACH)	h^{-1}	0.5	0.5	0.5	1.0	0.5
θ_s	Supply air temperature	°C	31.6	17.0	29.9	30.0	19.1
θ_e	Extract air temperature	°C	22.4	21.6	24.2	24.2	24.5
Φ_v	Ventilation heat load	W	61.9	-31.0	38.8	77.6	-36.2
Φ_v'	Specific ventilation heat load	W/m^2_{floor}	3.7	-1.8	2.3	4.6	-2.2
Φ_f	Floor heat load	W	-36.3	314.2	-833.9	-854.6	-341.6
Φ_f'	Specific floor heat load	W/m^2_{floor}	-2.2	18.7	-49.6	-50.9	-20.3
θ_f	Floor temperature	°C	21.8	23.7	19.2	19.0	23.2

Table 6. 8 Boundary conditions and calculated heat flow rates for the 4 cases of mixing ventilation with supply air terminal from the ceiling (M3 and M4) during the experiments

Mixing ventilation from wall			CASE M3-1	CASE M3-2	CASE M4-1	CASE M4-2
Symbol	**Definition**	**Unit**				
$\theta_{sp,air}$	Set point air temperature	°C	26.4	26.4	26.6	26.4
Φ_w	Heat load from window	W	490.4	450.4	487.1	450.5
Φ_w'	Specific heat load from window	W/m^2_{floor}	29.2	26.8	29.0	26.8
θ_w	Surface temperature of the window	°C	34.1	33.4	34.3	33.5
Φ_i	Internal heat load	W	200.0	200.0	200.0	200.0
$\Phi i'$	Specific internal heat load	W/m^2_{floor}	12.0	12.0	12.0	12.0
q_v	Supply air volume flow	l/s	5.6	5.6	5.6	5.6
N	Air change per hour (ACH)	h^{-1}	0.5	0.5	0.5	0.5
θ_s	Supply air temperature	°C	19.9	25.8	19.9	25.5
θ_e	Extract air temperature	°C	27.1	27.3	25.2	24.4
Φ_v	Ventilation heat load	W	-48.6	-10.3	-35.3	7.8
Φ_v'	Specific ventilation heat load	W/m^2_{floor}	-2.9	-0.6	-2.1	0.5
Φ_f	Floor heat load	W	-523.8	-726.7	-569.1	-727.8
Φ_f'	Specific floor heat load	W/m^2_{floor}	-31.2	-43.3	-33.9	-43.3
θ_f	Floor temperature	°C	22.0	20.2	21.8	20.3

Table 6. 9 Boundary conditions and calculated heat flow rates for the 6 cases of displacement ventilation (DV) during experiments

Displacement ventilation			CASE DV-1	CASE DV-2	CASE DV-3	CASE DV-4	CASE DV-5	CASE DV-6
Symbol	**Definition**	**Unit**						
$\theta_{sp,air}$	Set point air temperature	°C	26.0	26.2	26.0	26.2	26.0	26.4
Φ_w	Heat load from window	W	458.0	460.0	461.0	455.5	215.9	425.2
Φ_w'	Specific heat load from window	W/m^2_{floor}	27.3	27.4	27.4	27.1	12.9	25.3
θ_w	Surface temperature of the window	°C	33.2	33.3	33.2	33.3	29.4	33.1
Φ_i	Internal heat load	W	520.0	520.0	520.0	520.0	520.0	520.0
$\Phi i'$	Specific internal heat load	W/m^2_{floor}	31.3	31.3	31.3	31.3	31.3	31.3
q_v	Supply air volume flow	l/s	36.0	50.3	33.6	23.5	23.5	16.8
N	Air change per hour (ACH)	h^{-1}	3.2	4.5	3.0	2.1	2.1	1.5
θ_s	Supply air temperature	°C	15.7	16.1	22.3	20.1	24.0	16.5
θ_e	Extract air temperature	°C	27.4	28.4	28.2	28.2	27.8	28.2
Φ_v	Ventilation heat load	W	-506.4	-744.6	-242.4	-232.3	-110.2	-235.5
Φ_v'	Specific ventilation heat load	W/m^2_{floor}	-30.1	-44.3	-14.4	-13.8	-6.6	-14.0
Φ_f	Floor heat load	W	-691.6	-94.2	-741.3	-754.0	-716.1	-828.4
Φ_f'	Specific floor heat load	W/m^2_{floor}	-41.2	-5.6	-44.1	-44.9	-42.6	-49.3
θ_f	Floor temperature	°C	20.1	25.4	19.7	19.8	20.0	19.4

In appendix A, measured vertical air temperature profiles and air velocity profiles are reported. Since the globe temperatures were very close to the air temperatures and the differences between them were not noticeable in the graphics of vertical profiles, it was decided to not report them.

Conditions in the centre of the room at 1.1 m height have been monitored for each case in order to check the thermal comfort levels in both summer and winter conditions according to Standard ISO 7730 [16] and ISO 55-2004 [17]. For the calculation, the average air temperature, operative temperature, air velocity and relative humidity have been adopted. In Table 6. 10 the predicted mean vote PMV and the percentage of people dissatisfied PPD [%] in winter and summer condition is presented; it was found that test room satisfied the category A limit for both situations.

Table 6. 10 Calculated PMV and PPD [%] for winter and summer condition

Condition	RH%	T_{air}	T_{op}	v_{air}	T_{mr}	Assumptions		ISO 55-2004	
	%	°C	°C	m/s	°C	met	clo	PMV	PPD%
Winter	24	22.0	22.0	0.07	22.1	1.1	1.0	-0.26	6%
Summer	30	26.3	26.8	0.06	27.3	1.0	0.6	0.26	6%

The following show the results related to thermal comfort (vertical air temperature differences, air velocities, draught rate and radiant temperature asymmetry) in a room with mixing ventilation (residential) or displacement ventilation (office) systems .

Mixing ventilation in winter

When mixing ventilation is used in winter for heating purpose (cases M1-1 and M2-1) the vertical air difference $\Delta\theta$ is about 0.8 °C, a very low value since the limit for category A according to ISO 7730 is 2 °C. When mixing ventilation is used combined with floor heating, that is cases M1-2 and M2-2, vertical air difference $\Delta\theta$ changes the sign but the absolute value remains low, less than 0.5 °C.

For the same cases, measured air velocities are low at head level (Table 6. 13 and Table 6. 19) but higher than 0.1 m/s at ankle level, particularly in the position of the occupied zone nearest to the window (position S3); as a results draught rating DR [%] at ankle levels are locally higher than 10 %, even if the average draught rating DR [%] in the occupied zone both at ankle level and at head level is lower than 10 % (limit for category A according to ISO 7730), as shown in Figure 6. 14 and Table 6. 20. The fact that DR [%] is influenced by the distance from the window is confirmed by the draught rating values in the positions S1, S2 and S7 out of the occupied zone and near the window. When mixing ventilation is used in combination with floor heating (cases M1-2 and M2-2) the draught rating risk is slightly higher than in cases of only ventilation (cases M1-1-and M1-2).

Operative temperature in the occupied zone is enough constant for all cases of mix ventilation in summer (

Table 6. 15 and Table 6. 21).

The equivalent temperature for the body is in the range between 23.2 °C and 23.7 °C for all cases of mixing ventilation in winter (Table 6. 35). Local equivalent temperature is in the range between 21 °C and 25 °C (Figure 6. 9 and

Figure 6. 11) and some differences are visible when the same boundary conditions are adopted with different positions of the extract air terminal (for ex: case M1-1 in comparison with M2-1). The cold window influences the thermal manikin on the left side: all the left segments of the body are up to 3 °C colder than the corresponding right parts.

Anyway radiant temperature asymmetry due to the cold widow is lower than 10 °C, that is the Standard limit for category A. Also the radiant asymmetry due to the cold ceiling (and the warm floor) is low enough to fall in category A according to ISO 7730, as reported in Table 6. 16 and in Table 6. 22.

Mixing ventilation in summer

When mixing ventilation with low supply temperature (19 °C) from the wall is used in summer in combination with floor cooling (cases M1-5, M2-5) and low internal load (5.4 W/m^2_{floor}), the vertical air difference $\Delta\theta$ between head (1.1 m) and ankle (0.1 m) level is enough low to satisfy the limit for category A according to ISO 7730 for case M2-5 and that for category B for case M1-5 (Table 6. 12 and Table 6. 18). For both cases M1-5 and M2-5 the floor temperatures are higher than 19 °C, lower limit for thermal comfort according to ISO EN 7730 (as shown in Table 6. 6 and Table 6. 7) and measured air velocities are low in all the volume. Consequently draught rating DR [%] calculated at ankle levels (0.1m) and at head level (1.1 m) in the occupied zone are low enough (< 3 %) to fall within the limit of category A according to ISO 7730 (Table 6. 14 and Table 6. 20).

Operative temperature in the occupied zone is influenced by the proximity of the supply air terminal, both at 0.6 m height and at 1.1 m height: measured temperatures in position S3 are about 1 °C higher than those measured in position S6 (

Table 6. 15 and Table 6. 21).

The equivalent temperature for the body is in the range between 26.5 °C 5 and 27.3 °C (Table 6. 35). Local equivalent temperature is in the range between 24 °C and 29 °C (Figure 6. 9 and Figure 6. 11) even if all temperatures of case M1-5 are lower than those of case M2-5 because of the lower floor temperature (21.6°C instead of 23.2°C).

Radiant temperature asymmetry due to the cold ceiling (and the warm floor) in case M1-5 is 5.14 °C, slightly higher than the limit of category A according to ISO 7730. On the contrary the corresponding radiant asymmetry of case M2-5 is lower than the limit of category A. Radiant

asymmetry due to the warm wall does not represent a risk of local discomfort for any case, as reported in Table 6. 16 and in Table 6. 22.

When mix ventilation from the ceiling at different supply air temperatures (20 °C or 26 °C) is used in summer in combination with floor cooling (cases M3-1, M3-2, M4-1, M4-2) with a modest internal heat load (12 W/m^2 K_{floor}), the vertical air differences between head level and ankle level for a sitting person are higher than 3°C or higher than 4 °C (case M3-2), as reported in Table 6. 24. This means that all the conditions are in category C of thermal comfort or out of category C. Higher values are obtained for a standing person and for the positions closest to the window (S1, S2 and S7).

Draught rating DR [%] calculated at ankle levels (0.1 m) and at head level (1.1 m) are enough low (< 3 %) to fall within the limit of category A according to ISO 7730 (

Table 6. 26). Since the supply air terminal position for systems M3 and M4 is in the centre of the ceiling, DR [%] was calculated also in the centre, but the low values obtained (less than 4 %) reveals that draught is not a risk for these cases.

Operative temperature in position S3 (near the manikin) is up to 1.1 °C higher than the measured temperatures in the other points of the occupied zone, except when a high supply temperature (26 °C) is adopted with extract air terminal near the floor (case M4-2); for this case operative temperature in S3 is the lowest (Table 6. 27).

Figure 6. 12 highlights the differences in air temperature when similar conditions are used with different positions of extract air terminal: with a high supply air temperature, the air temperature in the occupied zone increases of about 0.5 °C if air is extracted near the floor (case M4-2 vs. case M3- 2).

The equivalent temperature for the body is in the range between 27.2 °C and 27.9 °C for case M3-1 and M3-2 (Table 6. 35), while local equivalent temperature is in the range between 23 °C and 29 °C, as shown in Figure 6. 13. Besides, the same figure underlines the influence of the floor surface (about 2 °C colder in case M3-2 than in case M3-1) on the lower parts of the manikin (feet, legs) and the influence of the warm window on the heat transfer of the manikin toward the environment: the average of segments temperatures on the left (group B) is at higher temperature of the average of segments temperatures on the right (group A). In effect the radiant temperature asymmetry due to the warm ceiling with respect to the cold floor is for all cases higher than 5 °C, Standard limit for category A and B according to ISO 7730. Instead, the

cold window does not cause a significant radiant asymmetry and the Standard limit of category A was satisfied for all cases of systems M3 and M4.

When mixing ventilation with warm supply air temperature (30 °C) is used in summer in combination with floor cooling (cases M1-3, M1-4, M2-3 and M2-4), the vertical air differences between head level and ankle level for a sitting person are higher than 3 °C or higher than 4 °C (for case M1-4), as reported in Table 6. 12 and Table 6. 18. Therefore the conditions of cases M1-3, M2-3 and M2-4 fall in category C, while that of case M1-4 falls out of category C. This is due to the cold floor temperature, that is between 19 °C and 19.6 °C, even if it is within the limit for thermal comfort according to Standard ISO 7730.

Draught rating DR [%] are low at ankle level (0.1 m) and particularly at head level (1.1 m), therefore the limit of category A is satisfied in the occupied zone and also in the positions S1, S2 and S7 near the window.

Operative temperature is higher in position S3, placed between the window and the manikin, than the other positions of the occupied zone for all the considered cases (

Table 6. 15 and Table 6. 21). The only exception is the case M2-4, characterized by a great uniformity of operative (and air temperatures) in all the volume.

The equivalent temperature for the body is in the range between 26.2 °C and 26.5 °C (Table 6. 35), while local equivalent temperature is in the range between 21 °C and 28 °C (Figure 6. 9 and Figure 6. 11), with an evident temperature gradient from the upper parts of the body and the lower parts like legs and feet. Radiant temperature asymmetry due to the warm ceiling with respect to the cold floor for all the considered cases is higher than 6.7°C, that is out of Categories A and B according to ISO 7730. The warm window does not cause local discomfort since radiant temperature asymmetry is low compared to Standard limit value (Table 6. 16 and Table 6. 22).

Displacement ventilation in summer

When displacement ventilation is used in summer in combination with floor cooling (cases DV) the vertical air differences between head level and ankle level for a sitting person can be different with respect to the boundary conditions; while case DV-3 falls within the limit of category A of ISO 7730, case DV-5 falls in category C and the other cases fall out of the limit of category C, as reported in Table 6. 30.

Draught rating DR [%] at low level (0.1 m height) can be high (above 10 %, limit of category B), in particular when high air flow rates are adopted (cases DV-1 and DV-2), because air velocities near the supply air terminal (position S5 and S6) can be significantly high, up to 0.26 m/s. But at 1.1 m above the floor DR [%] calculated are below 10 %, so the category A for thermal comfort is satisfied in the whole occupied zone. Near the window (positions S1, S2 ad S7) draught rating is high (even higher than10 %) only for the case with the highest air flow rate, that is case DV-2.

As regards the distribution of operative temperature in the occupied zone, results in Table 6. 33 show that when medium air flow rates (3 ACH or 3.2 ACH) at low temperature (below 20.1 °C) are adopted (cases DV-1 and DV-3), the zone near the internal heat gains (represented by positions S3 and S4) is characterized by higher operative temperature with respect to the rest of the room. But when high air flow rates (4.5 ACH of case DV-2) or very low air flow rates (1.5 ACH of case DV-6) are adopted, measured operative temperatures at 0.6 m and 1.1 m height are similar in all the considered positions.

The equivalent temperature for the body is in the range between 24.8 °C and 26.0 °C (Table 6. 35). Local equivalent temperature is in the range between 20.8 °C and 29 1°C (Figure 6. 15) and a clear distinction between the lower parts of the body (cold) and higher parts (warmer) can be easily highlighted. With the same floor temperature near 20 °C and decreasing the ventilation rate from 3.2 ACH to 2.1 ACH (cases DV-1. DV-3 and DV-4), a translation of the curves toward higher temperature is evident. Besides, increasing the floor temperature up to 25°C allows warmer legs and feet also with a consistent ventilation cooling power (case DV-2).

Radiant temperature asymmetry due to the warm ceiling is higher than the limit of category A and B according to ISO 7730 for all the cases of displacement ventilation, with the only exception of case DV-2 (with the highest floor temperature). Even for these cases, the warm window does not cause local discomfort since radiant temperature asymmetry is low compared to Standard limit value (Table 6. 34).

System M1

Table 6. 11 Temperature difference [°C] between head level and ankle level for a sitting (1.1 m) and a standing person (1.7 m), in 7 points of measurements, for all cases of system M1

		S6	S5	S4	S3	S2	S1	S7
M1 Case 1	$\Delta\theta_{(1\text{-}1m\text{-}0.1m)}$ [°C]	0.4	0.3	0.4	0.5	0.4	0.2	0.5
	$\Delta\theta_{(1\text{-}7m\text{-}0.1m)}$ [°C]	0.8	0.6	0.6	0.7	0.7	0.6	0.9
M1 Case 2	$\Delta\theta_{(1\text{-}1m\text{-}0.1m)}$ [°C]	-0.2	-0.2	-0.3	-0.2	-0.1	-0.2	0.0
	$\Delta\theta_{(1\text{-}7m\text{-}0.1m)}$ [°C]	-0.3	-0.3	-0.4	-0.2	-0.1	-0.1	0.0
M1 Case 3	$\Delta\theta_{(1\text{-}1m\text{-}0.1m)}$ [°C]	3.2	3.3	3.5	3.7	4.0	4.3	4.1
	$\Delta\theta_{(1\text{-}7m\text{-}0.1m)}$ [°C]	3.9	3.9	4.2	4.3	4.6	4.9	4.5
M1 Case 4	$\Delta\theta_{(1\text{-}1m\text{-}0.1m)}$ [°C]	3.5	3.5	3.9	4.1	4.5	4.9	4.6
	$\Delta\theta_{(1\text{-}7m\text{-}0.1m)}$ [°C]	4.2	4.3	4.5	4.8	5.2	5.5	5.4
M1 Case 5	$\Delta\theta_{(1\text{-}1m\text{-}0.1m)}$ [°C]	1.8	1.8	2.1	2.5	2.4	2.8	2.5
	$\Delta\theta_{(1\text{-}7m\text{-}0.1m)}$ [°C]	2.2	2.3	2.6	2.8	2.7	3.2	2.9

Table 6. 12 Temperature difference [°C] between head level and ankle level for a sitting (1.1 m) and a standing person (1.7 m), in the worse position for thermal comfort , in the whole room and in the occupied zone, for all cases of system M1

	Whole room		**Occupied zone**	
	Max Δθ, sitting	**Max Δθ, standing**	**Max Δθ, sitting**	**Max Δθ, standing**
	1.1 m-0.1m	*1.7m-0.1m*	*1.1 m-0.1m*	*1.7m-0.1m*
M1 Case 1	0.5	0.9	0.5	0.8
M1 Case 2	-0.3	-0.4	-0.3	-0.4
M1 Case 3	4.3	4.9	3.7	4.3
M1 Case 4	4.9	5.5	4.1	4.8
M1 case 5	2.8	3.2	2.5	2.8

Table 6. 13 Air velocity [m/s] measured at 0.1 m and 1.1m height for all cases of M1 for all the points

		Air velocity				
Position	Height	M1 1	M1 2	M1 3	M1 4	M1 5
S1	0.1 m	0.11	0.14	0.06	0.05	0.07
	1.1 m	0.05	0.05	0.05	0.05	0.05
S2	0.1 m	0.11	0.14	0.05	0.08	0.06
	1.1 m	0.05	0.05	0.05	0.05	0.05
S3	0.1 m	0.10	0.14	0.06	0.08	0.06
	1.1 m	0.04	0.09	0.05	0.05	0.04
S4	0.1 m	0.08	0.10	0.06	0.06	0.06
	1.1 m	0.05	0.08	0.05	0.04	0.04
S5	0.1 m	0.06	0.09	0.07	0.08	0.06
	1.1 m	0.05	0.07	0.05	0.04	0.05
S6	0.1 m	0.08	0.10	0.07	0.07	0.06
	1.1 m	0.05	0.06	0.05	0.05	0.06
S7	0.1 m	0.11	0.15	0.06	0.08	0.07
	1.1 m	0.05	0.06	0.05	0.07	0.05

Table 6. 14 Draught rating DR [%] calculated at 0.1 m and 1.1m height for all cases of M1 for all the points and for the occupied zone

Draught rating						
Position	Height	M1 1	M1 2	M1 3	M1 4	M1 5
S1	0.1 m	7.9	10.9	2.0	0.4	2.9
	1.1 m	0.1	0.0	0.0	0.8	0.9
S2	0.1 m	7.8	10.4	1.0	4.8	2.4
	1.1 m	0.0	1.5	0.0	0.0	0.4
S3	0.1 m	7.2	9.8	2.8	5.2	2.1
	1.1 m	0.0	7.3	0.0	0.0	0.0
S4	0.1 m	4.8	7.1	1.8	2.6	2.0
	1.1 m	0.0	5.1	0.4	0.0	0.0
S5	0.1 m	3.2	6.4	3.6	4.6	2.0
	1.1 m	0.0	4.3	0.0	0.0	0.0
S6	0.1 m	5.4	7.2	3.2	3.9	1.5
	1.1 m	0.0	2.4	0.0	0.0	2.0
S7	0.1 m	7.8	10.7	1.5	4.6	2.7
	1.1 m	0.1	2.6	0.0	3.0	0.0
Average-occupied zone						
Average	0.1 m	5.1	7.6	2.9	4.1	1.9
	1.1 m	0.0	4.8	0.1	0.0	0.5

Table 6. 15 Operative temperature [°C] at 0.6 m and 1.1m height for all points in the occupied zone, for all cases of M1

Operative temperature					
CASE	H [m]	Position			
		S3	S4	S5	S6
M1-1	**0.6**	21.7	21.8	21.7	21.8
	1.1	22.1	22.0	22.1	22.1
M1-2	**0.6**	22.0	22.2	22.1	22.1
	1.1	22.0	22.1	22.1	22.0
M1-3	**0.6**	25.1	24.4	24.3	24.3
	1.1	26.2	25.4	25.2	25.2
M1-4	**0.6**	25.3	24.6	24.5	24.5
	1.1	26.5	25.7	25.5	25.6
M1-5	**0.6**	26.2	25.3	25.0	25.0
	1.1	26.8	25.6	25.4	25.4

Table 6. 16 Radiant asymmetry cased by the window and by the ceiling, for all cases of M1

CASE	M1-1	M1-2	M1-3	M1-4	M1-5
Δt_{pr} – ceiling [°C]	0.1	-2.4	6.7	7.3	5.1
Δt_{pr} -window [°C]	-1.6	-1.7	3.9	3.8	4.6

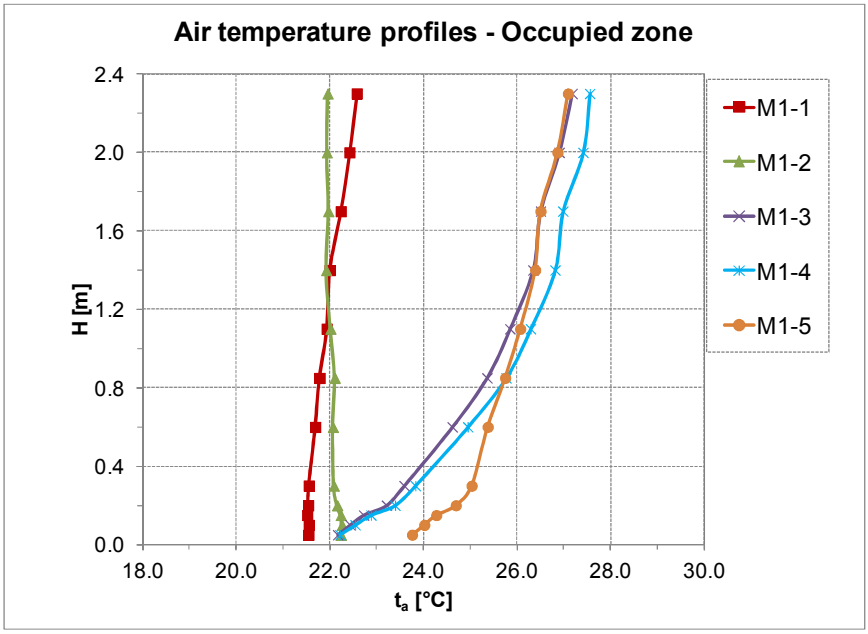

Figure 6. 8 Average air temperature profiles in the occupied zone, for all cases of system M1

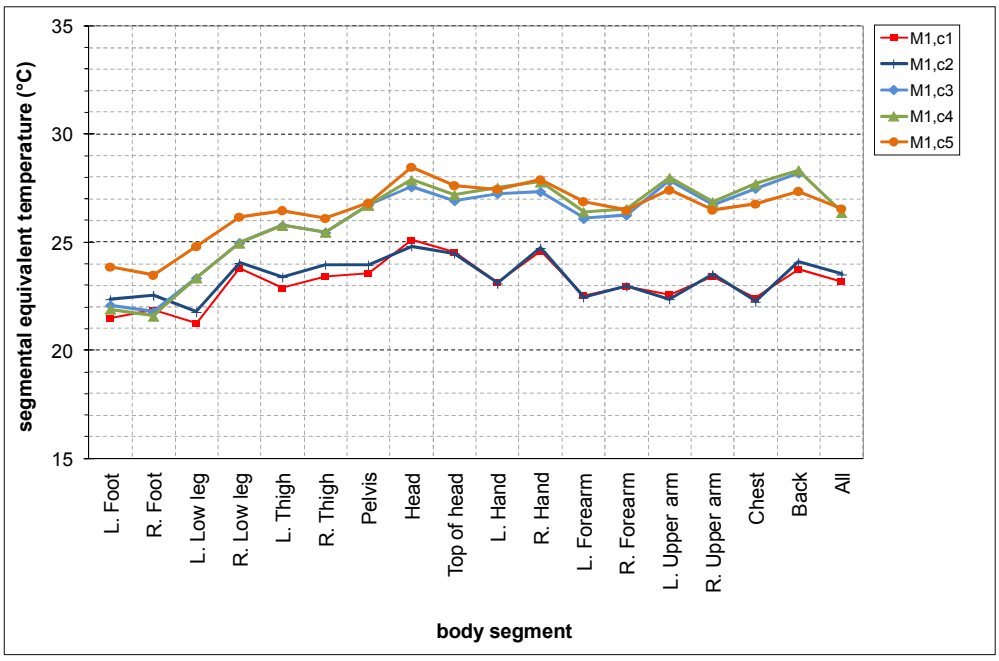

Figure 6. 9 Local equivalent temperature [°C] for all the body parts of the manikin and for the whole body (all) calculated for all cases of M1

System M2

Table 6. 17 Temperature difference [°C] between head level and ankle level for a sitting (1.1 m) and a standing person (1.7 m), in 7 points of measurements, for all cases of system M2

		S6	S5	S4	S3	S2	S1	S7
M2 Case 1	$\Delta\theta_{(1\text{-}1m\text{-}0.1m)}$ [°C]	0.4	0.4	0.5	0.5	0.4	0.3	0.5
	$\Delta\theta_{(1\text{-}7m\text{-}0.1m)}$ [°C]	0.7	0.7	0.8	0.8	0.9	0.8	0.9
M2 Case 2	$\Delta\theta_{(1\text{-}1m\text{-}0.1m)}$ [°C]	-0.2	-0.3	-0.3	0.0	0.0	-0.1	0.1
	$\Delta\theta_{(1\text{-}7m\text{-}0.1m)}$ [°C]	-0.3	-0.4	-0.4	0.0	0.0	-0.1	0.1
M2 Case 3	$\Delta\theta_{(1\text{-}1m\text{-}0.1m)}$ [°C]	3.2	3.3	3.6	3.8	3.9	4.5	4.0
	$\Delta\theta_{(1\text{-}7m\text{-}0.1m)}$ [°C]	3.5	3.8	4.0	4.1	4.3	4.9	4.5
M2 Case 4	$\Delta\theta_{(1\text{-}1m\text{-}0.1m)}$ [°C]	3.5	3.5	3.5	3.5	3.5	3.5	3.5
	$\Delta\theta_{(1\text{-}7m\text{-}0.1m)}$ [°C]	3.8	3.8	3.8	3.8	3.8	3.8	3.8
M2 Case 5	$\Delta\theta_{(1\text{-}1m\text{-}0.1m)}$ [°C]	0.8	1.1	1.3	1.3	1.5	1.7	1.6
	$\Delta\theta_{(1\text{-}7m\text{-}0.1m)}$ [°C]	1.0	1.3	1.5	1.5	1.9	2.2	1.9

Table 6. 18 Temperature difference [°C] between head level and ankle level for a sitting (1.1 m) and a standing person (1.7 m), in the worse position for thermal comfort , in the whole room and in the occupied zone, for all cases of system M2

	Whole room		**Occupied zone**	
	Max Δθ, sitting	**Max Δθ, standing**	**Max Δθ, sitting**	**Max Δθ, standing**
	1.1 m-0.1m	*1.7m-0.1m*	*1.1 m-0.1m*	*1.7m-0.1m*
M2 Case 1	0.5	0.9	0.5	0.8
M2 Case 2	-0.3	-0.4	-0.3	-0.4
M2 Case 3	4.5	4.9	3.8	4.1
M2 Case 4	3.5	3.8	3.5	3.8
M2 case 5	1.7	2.2	1.3	1.5

Table 6. 19 Air velocity [m/s] measured at 0.1 m and 1.1 m height for all cases of M2 for all the points

		Air velocity				
Position	Height	M2 1	M2 2	M2 3	M2 4	M2 5
S1	0.1 m	0.11	0.13	0.07	0.09	0.07
	1.1 m	0.05	0.05	0.05	0.06	0.05
S2	0.1 m	0.11	0.14	0.10	0.08	0.06
	1.1 m	0.05	0.05	0.05	0.05	0.05
S3	0.1 m	0.11	0.16	0.06	0.08	0.06
	1.1 m	0.05	0.07	0.04	0.05	0.06
S4	0.1 m	0.10	0.10	0.07	0.07	0.05
	1.1 m	0.05	0.08	0.05	0.05	0.05
S5	0.1 m	0.07	0.11	0.09	0.07	0.05
	1.1 m	0.05	0.06	0.04	0.04	0.05
S6	0.1 m	0.09	0.09	0.04	0.05	0.06
	1.1 m	0.05	0.06	0.03	0.05	0.10
S7	0.1 m	0.12	0.17	0.08	0.09	0.06
	1.1 m	0.05	0.05	0.05	0.06	0.05

Table 6. 20 Draught rating DR [%] calculated at 0.1 m and 1.1 m height for all cases of M2 for all the points and for the occupied zone

Draught rating						
Position	Height	M2 1	M2 2	M2 3	M2 4	M2 5
S1	0.1 m	8.1	9.6	3.1	5.0	2.8
	1.1 m	0.6	0.0	0.1	1.5	0.7
S2	0.1 m	8.1	10.2	5.4	4.5	2.3
	1.1 m	1.1	0.1	0.0	0.6	0.1
S3	0.1 m	7.5	10.5	1.5	5.1	2.4
	1.1 m	1.4	4.6	0.0	0.0	2.1
S4	0.1 m	6.9	7.6	3.0	3.6	1.0
	1.1 m	0.0	5.7	0.0	0.1	0.6
S5	0.1 m	4.5	7.9	5.2	4.0	0.0
	1.1 m	0.0	2.5	0.0	0.0	0.4
S6	0.1 m	5.7	6.8	0.0	0.7	2.4
	1.1 m	0.1	2.3	0.0	0.6	6.3
S7	0.1 m	8.5	12.3	4.7	5.5	1.9
	1.1 m	0.0	1.0	0.0	2.0	0.6
Average-occupied zone						
Average	0.1 m	6.1	8.2	2.4	3.4	1.4
	1.1 m	0.4	3.8	0.0	0.2	2.4

Table 6. 21 Operative temperature [°C] at 0.6 m and 1.1 m height for all points in the occupied zone, for all cases of M2

Operative temperature					
CASE	**H [m]**	**Position**			
		S3	**S4**	**S5**	**S6**
M2-1	**0.6**	21.7	21.9	21.8	21.8
	1.1	22.3	22.1	22.0	22.0
M2-2	**0.6**	21.9	22.2	22.1	22.1
	1.1	22.2	22.2	22.2	22.2
M2-3	**0.6**	25.5	24.8	24.7	24.7
	1.1	26.4	25.7	25.5	25.5
M2-4	**0.6**	24.8	24.8	24.8	24.8
	1.1	25.6	25.6	25.6	25.6
M2-5	**0.6**	26.2	25.4	25.2	25.2
	1.1	26.5	25.8	25.6	25.5

Table 6. 22 Radiant asymmetry cased by the window and by the ceiling, for all cases of M2

CASE	**M2-1**	**M2-2**	**M2-3**	**M2-4**	**M2-5**
Δt_{pr} – ceiling [°C]	0.2	-2.2	7.2	7.2	3.4
Δt_{pr} -window [°C]	-1.7	-1.7	3.7	3.5	3.6

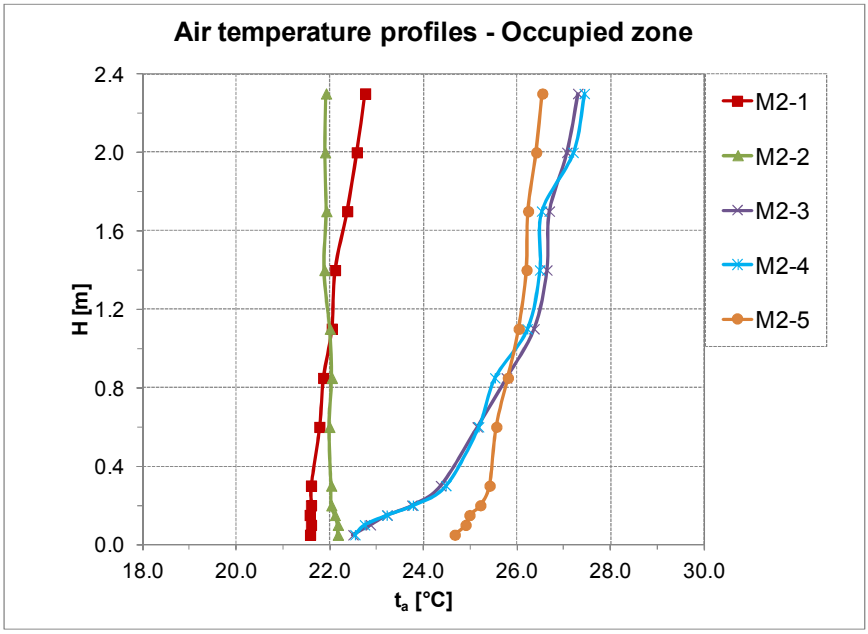

Figure 6. 10 Average air temperature profiles in the occupied zone, for all cases of system M2

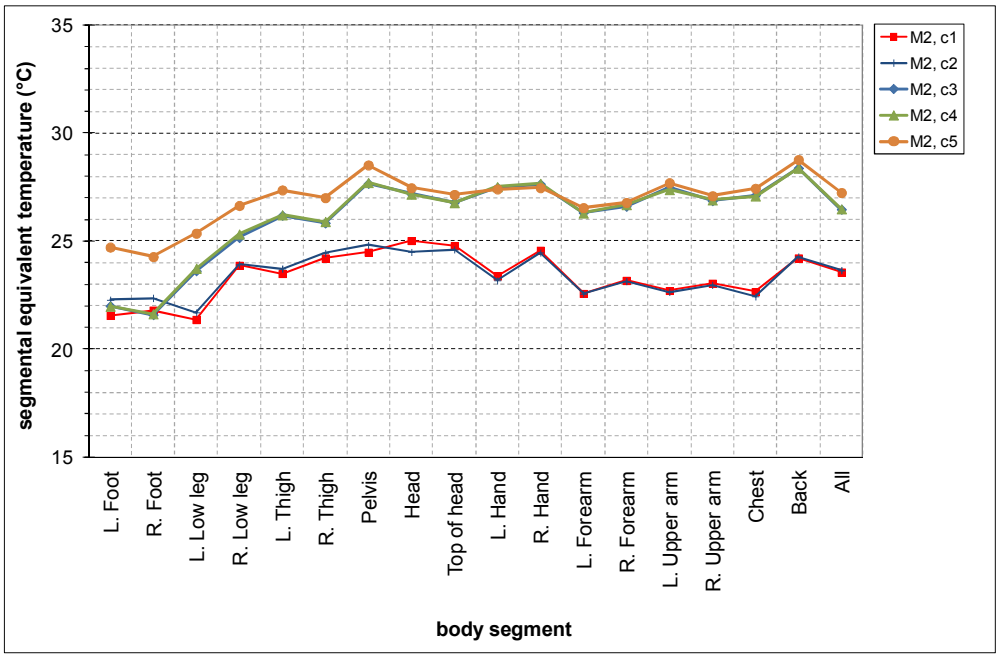

Figure 6. 11 Local equivalent temperature [°C] for all the body parts of the manikin and for the whole body (all) calculated for all cases of M2

Systems M3 and M4

Table 6. 23 Temperature difference [°C] between head level and ankle level for a sitting (1.1 m) and a standing person (1.7 m), in 7 points of measurements, for all cases of system M3 and M4

		S6	S5	S4	S3	S2	S1	S7
M3 Case 1	$\Delta\theta_{(1\text{-}1m\text{-}0.1m)}$ [°C]	2.4	2.4	2.6	3.1	3.1	3.7	3.2
	$\Delta\theta_{(1\text{-}7m\text{-}0.1m)}$ [°C]	2.8	2.9	3.1	3.3	3.4	3.9	3.5
M3 Case 2	$\Delta\theta_{(1\text{-}1m\text{-}0.1m)}$ [°C]	3.2	3.4	3.7	4.1	4.3	4.5	4.1
	$\Delta\theta_{(1\text{-}7m\text{-}0.1m)}$ [°C]	4.0	4.2	4.5	4.7	4.9	5.2	4.6
M4 Case 1	$\Delta\theta_{(1\text{-}1m\text{-}0.1m)}$ [°C]	2.6	2.5	2.8	3.2	3.5	3.8	3.5
	$\Delta\theta_{(1\text{-}7m\text{-}0.1m)}$ [°C]	3.0	3.2	3.3	3.6	3.8	4.3	3.8
M4 Case 4	$\Delta\theta_{(1\text{-}1m\text{-}0.1m)}$ [°C]	3.2	3.2	3.5	3.9	3.9	4.3	3.9
	$\Delta\theta_{(1\text{-}7m\text{-}0.1m)}$ [°C]	3.6	3.9	4.1	4.3	4.6	4.9	4.4

Table 6. 24 Temperature difference [°C] between head level and ankle level for a sitting (1.1 m) and a standing person (1.7 m), in the worse position for thermal comfort , in the whole room and in the occupied zone, for all cases of system M3 and M4

	Whole room		**Occupied zone**	
	Max Δθ, sitting	**Max Δθ, standing**	**Max Δθ, sitting**	**Max Δθ, standing**
	1.1 m-0.1m	*1.7m-0.1m*	*1.1 m-0.1m*	*1.7m-0.1m*
M3 Case 1	3.7	3.9	3.1	3.3
M3 Case 2	4.5	5.2	4.1	4.7
M4 Case 1	3.8	4.3	3.2	3.6
M4 Case 2	4.3	4.9	3.9	4.3

Table 6. 25 Air velocity [m/s] measured at 0.1 m and 1.1 m height for all cases of M3 and M4 for all the points

		Air velocity			
Position	Height	M3 1	M3 2	M4 1	M4 2
S1	0.1 m	0.06	0.06	0.06	0.07
	1.1 m	0.05	0.05	0.05	0.05
S2	0.1 m	0.06	0.07	0.10	0.07
	1.1 m	0.04	0.05	0.05	0.05
S3	0.1 m	0.06	0.06	0.06	0.06
	1.1 m	0.05	0.03	0.05	0.06
S4	0.1 m	0.05	0.06	0.06	0.06
	1.1 m	0.06	0.05	0.05	0.05
S5	0.1 m	0.07	0.07	0.07	0.07
	1.1 m	0.05	0.05	0.05	0.04
S6	0.1 m	0.06	0.07	0.06	0.04
	1.1 m	0.04	0.07	0.06	0.05
S7	0.1 m	0.07	0.07	0.07	0.07
	1.1 m	0.05	0.01	0.05	0.01

Table 6. 26 Draught rating DR [%] calculated at 0.1 m and 1.1 m height for all cases of M3 and M4 for all the points and for the occupied zone and in the centre

Draught rating					
Position	Height	M3 1	M3 2	M4 1	M4 2
S1	0.1 m	2.1	2.2	1.8	3.1
	1.1 m	0.0	0.0	0.1	0.1
S2	0.1 m	1.9	2.7	1.8	3.0
	1.1 m	0.0	0.0	0.3	0.0
S3	0.1 m	1.8	2.1	2.2	2.4
	1.1 m	0.0	0.0	0.0	0.8
S4	0.1 m	1.0	2.7	2.1	3.3
	1.1 m	0.6	0.0	0.3	0.3
S5	0.1 m	3.0	3.7	3.0	2.8
	1.1 m	0.6	0.0	0.0	0.0
S6	0.1 m	2.4	3.0	2.3	0.0
	1.1 m	0.0	2.3	1.2	0.6
S7	0.1 m	3.2	3.3	2.9	3.1
	1.1 m	0.0	0.8	0.3	0.0
Average-occupied zone					
Average	0.1 m	2.0	2.9	2.4	2.1
	1.1 m	0.3	0.6	0.4	0.4
centre					
centre	0.1 m	1.4	1.5		3.3
	1.1 m	0.9	1.7		1.8

Table 6. 27 Operative temperature [°C] at 0.6 m and 1.1 m height for all points in the occupied zone, for all cases of M3 and M4

Operative temperature					
CASE	H [m]	Position			
		S3	S4	S5	S6
M3-1	**0.6**	26.7	26.0	25.8	25.8
	1.1	27.4	26.4	26.3	26.3
M3-2	**0.6**	26.2	25.6	25.4	25.4
	1.1	27.1	26.3	26.1	26.2
M4-1	**0.6**	27.0	26.3	26.0	26.0
	1.1	27.5	26.7	26.5	26.5
M4-2	**0.6**	25.9	26.5	26.6	26.8
	1.1	26.4	27.2	27.4	27.6

Table 6. 28 Radiant asymmetry cased by the window and by the ceiling, for all cases of M3 and M4

CASE	M3-1	M3-2	M4-1	M4-2
Δt_{pr} – ceiling [°C]	5.4	6.9	5.7	6.9
Δt_{pr} -window [°C]	4.1	3.9	4.1	3.9

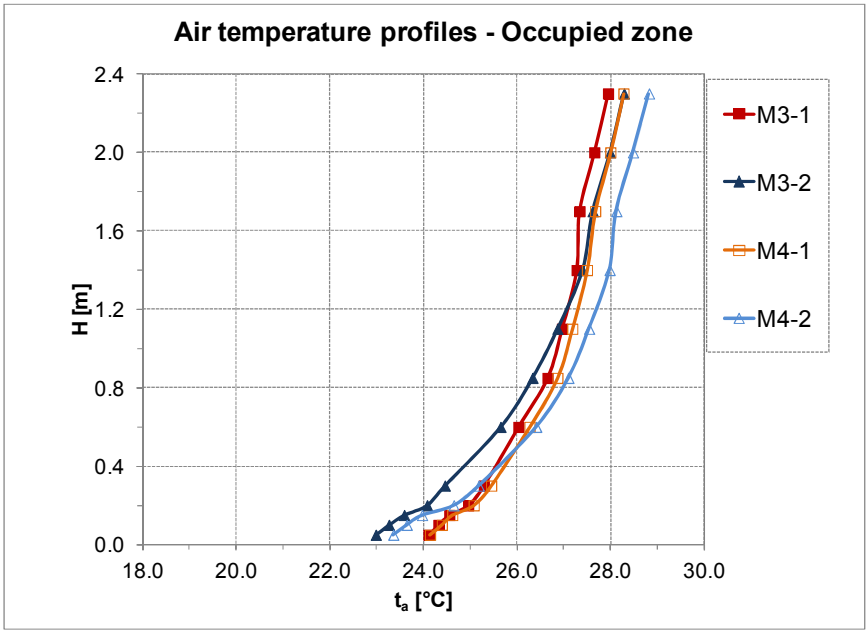

Figure 6. 12 Average air temperature profiles in the occupied zone, for all cases of system M3 and M4

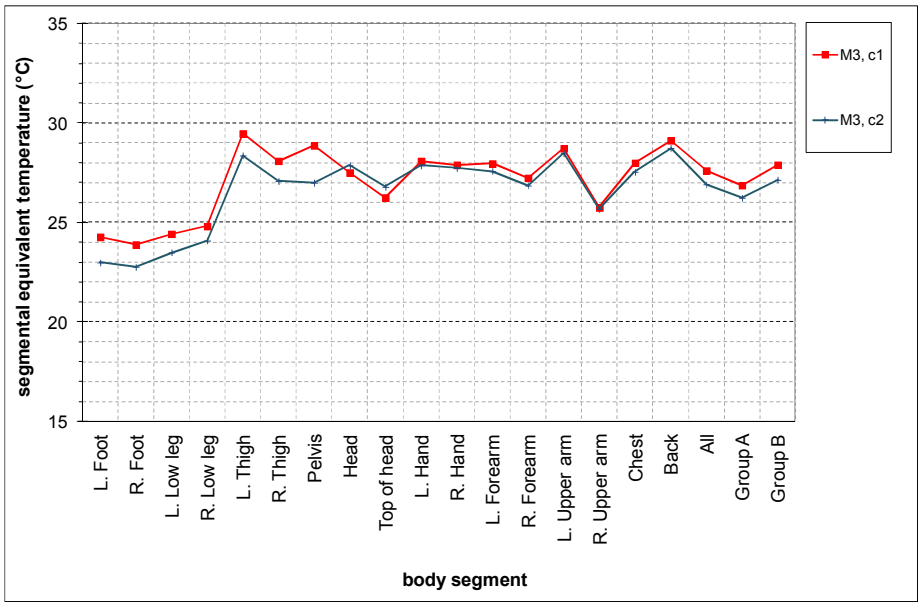

Figure 6. 13 Local equivalent temperature [°C] for all the body parts of the manikin, for the whole body ("all"), for the right part of the body (A) and for the left part (B) for all cases of M3

System DV

Table 6. 29 Temperature difference [°C] between head level and ankle level for a sitting (1.1 m) and a standing person (1.7 m), in 7 points of measurements, for all cases of system DV

		S6	S5	S4	S3	S2	S1	S7
DV Case 1	$\Delta\theta_{(1\text{-}1m\text{-}0.1m)}$ [°C]	6.0	5.8	5.5	5.7	5.7	5.7	5.7
	$\Delta\theta_{(1\text{-}7m\text{-}0.1m)}$ [°C]	7.1	7.0	6.9	6.9	6.9	6.9	6.9
DV Case 2	$\Delta\theta_{(1\text{-}1m\text{-}0.1m)}$ [°C]	5.4	5.4	5.4	5.4	5.2	4.0	4.2
	$\Delta\theta_{(1\text{-}7m\text{-}0.1m)}$ [°C]	7.0	7.0	7.1	7.0	6.9	5.6	5.6
DV Case 3	$\Delta\theta_{(1\text{-}1m\text{-}0.1m)}$ [°C]	1.1	0.9	1.2	0.9	4.2	3.7	4.0
	$\Delta\theta_{(1\text{-}7m\text{-}0.1m)}$ [°C]	0.9	0.8	1.1	0.7	5.1	4.8	5.2
DV Case 4	$\Delta\theta_{(1\text{-}1m\text{-}0.1m)}$ [°C]	4.7	5.0	5.0	5.3	5.3	3.7	5.4
	$\Delta\theta_{(1\text{-}7m\text{-}0.1m)}$ [°C]	5.7	5.9	5.8	6.0	6.1	4.8	6.0
DV Case 5	$\Delta\theta_{(1\text{-}1m\text{-}0.1m)}$ [°C]	3.1	3.1	3.5	3.5	3.6	3.7	3.8
	$\Delta\theta_{(1\text{-}7m\text{-}0.1m)}$ [°C]	3.8	4.0	4.3	4.1	4.2	4.4	4.5
DV Case 6	$\Delta\theta_{(1\text{-}1m\text{-}0.1m)}$ [°C]	6.3	6.3	6.3	6.3	6.3	6.3	6.2
	$\Delta\theta_{(1\text{-}7m\text{-}0.1m)}$ [°C]	7.3	7.3	7.3	7.3	7.3	7.3	7.2

Table 6. 30 Temperature difference [°C] between head level and ankle level for a sitting (1.1 m) and a standing person (1.7 m), in the worse position for thermal comfort , in the whole room and in the occupied zone, for all cases of system DV

	Whole room		**Occupied zone**	
	Max Δθ, sitting	**Max Δθ, standing**	**Max Δθ, sitting**	**Max Δθ, standing**
	1.1 m-0.1m	*1.7m-0.1m*	*1.1 m-0.1m*	*1.7m-0.1m*
DV Case 1	6.0	7.1	6.0	7.1
DV Case 2	5.4	7.1	5.4	7.1
DV Case 3	4.2	5.2	1.2	1.1
DV Case 4	5.4	6.1	5.3	6.0
DV Case 5	3.8	4.5	3.5	4.3
DV Case 6	6.3	7.3	6.3	7.3

Table 6. 31 Air velocity [m/s] measured at 0.1 m and 1.1 m height for all cases of system DV, for all the points

Air velocity							
Position	Height	DV 1	DV 2	DV 3	DV 4	DV 5	DV 6
S1	0.1 m	0.08	0.12	0.07	0.06	0.08	0.08
	1.1 m	0.06	0.05	0.05	0.05	0.05	0.05
S2	0.1 m	0.08	0.14	0.08	0.07	0.08	0.08
	1.1 m	0.05	0.05	0.05	0.06	0.05	0.05
S3	0.1 m	0.09	0.13	0.07	0.07	0.08	0.08
	1.1 m	0.05	0.05	0.04	0.05	0.03	0.03
S4	0.1 m	0.13	0.17	0.07	0.07	0.08	0.08
	1.1 m	0.07	0.06	0.08	0.08	0.06	0.06
S5	0.1 m	0.15	0.17	0.11	0.11	0.05	0.05
	1.1 m	0.09	0.06	0.08	0.08	0.06	0.06
S6	0.1 m	0.16	0.26	0.05	0.12	0.06	0.06
	1.1 m	0.04	0.03	0.03	0.04	0.04	0.04
S7	0.1 m	0.08	0.13	0.06	0.06	0.07	0.07
	1.1 m	0.06	0.06	0.05	0.06	0.04	0.04

Table 6. 32 Draught rating DR [%] calculated at 0.1 m and 1.1 m height for all cases of system DV, for all the points and for the occupied zone

Draught rating							
Position	Height	DV 1	DV 2	DV 3	DV 4	DV 5	DV 6
S1	0.1 m	4.9	9.8	2.6	1.9	4.5	1.8
	1.1 m	1.5	0.0	0.9	0.8	0.8	0.7
S2	0.1 m	6.0	11.2	3.5	3.7	4.8	4.6
	1.1 m	0.9	0.0	0.0	1.1	0.4	0.3
S3	0.1 m	6.9	10.6	3.1	3.6	4.7	4.9
	1.1 m	0.6	0.0	0.0	0.6	0.0	0.0
S4	0.1 m	10.7	14.0	2.4	3.6	4.7	3.1
	1.1 m	2.5	1.4	3.0	2.6	1.8	2.8
S5	0.1 m	13.8	14.2	5.5	7.8	1.2	5.0
	1.1 m	3.8	1.7	3.2	3.1	1.7	2.8
S6	0.1 m	13.3	21.1	1.0	8.6	1.5	8.8
	1.1 m	0.0	0.0	0.0	0.0	0.0	0.0
S7	0.1 m	5.8	9.8	1.4	1.6	3.2	2.6
	1.1 m	1.3	1.0	0.9	1.0	0.0	1.2
Average-occupied zone							
Average	0.1 m	11.2	15.0	3.0	5.9	3.0	5.5
	1.1 m	1.7	0.8	1.5	1.5	0.9	1.4

Table 6. 33 Operative temperature [°C] at 0.6 m and 1.1 m height for all points in the occupied zone, for all cases of DV

Operative temperature					
CASE	H [m]	Position			
		S3	S4	S5	S6
DV-1	**0.6**	23.4	23.6	22.7	22.4
	1.1	26.9	26.8	25.7	25.1
DV-2	**0.6**	24.4	24.4	24.4	24.4
	1.1	26.1	26.1	26.1	26.1
DV-3	**0.6**	26.3	25.4	26.1	26.2
	1.1	26.6	25.8	26.4	26.5
DV-4	**0.6**	24.6	24.6	23.7	23.6
	1.1	27.3	27.0	25.9	25.7
DV-5	**0.6**	24.6	24.2	24.1	24.0
	1.1	26.3	25.8	25.6	25.6
DV-6	**0.6**	24.7	24.7	24.6	24.6
	1.1	27.7	27.7	27.7	27.7

Table 6. 34 Radiant asymmetry cased by the window and by the ceiling, for all cases of DV

CASE	DV-1	DV-2	DV-3	DV-4	DV-5	DV-6
Δt_{pr} - ceiling[°C]	6.3	2.8	7.2	7.1	6.1	7.4
Δt_{pr} -window [°C]	4.2	3.2	3.9	4.0	2.2	3.9

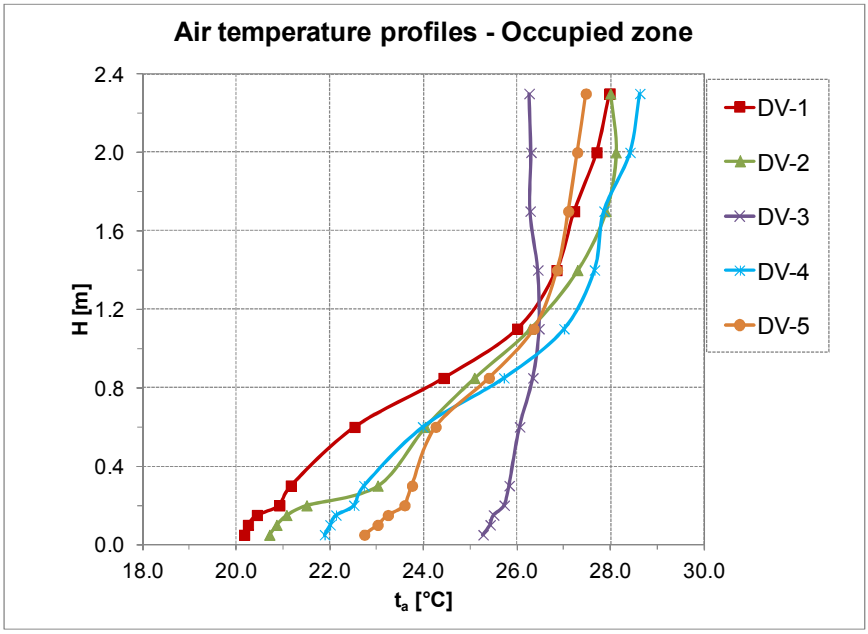

Figure 6. 14 Average air temperature profiles in the occupied zone, for all cases of system DV

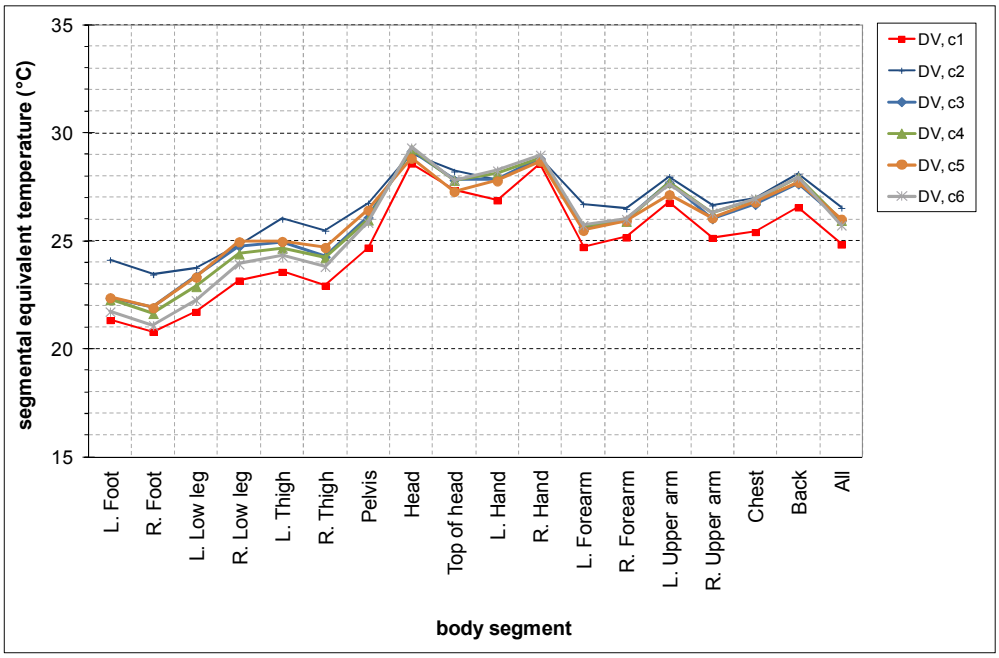

Figure 6. 15 Local equivalent temperature [°C] for all the body parts of the manikin and for the whole body ("all") calculated for all cases of DV

Table 6. 35 Calculated equivalent temperature [°C] for the body, as weighted average of local equivalent temperatures for all the cases

T_{eq}	Case 1	Case 2	Case 3	Case 4	Case 5	Case 6
M1	23.20	23.52	26.22	26.38	26.54	
M2	23.56	23.65	26.47	26.49	27.25	
M3	27.90	27.15				
DV	24.84	26.54	25.98	25.96	26.01	25.73

6.3.2 Ventilation effectiveness results

Contaminant removal effectiveness

The calculated contaminant removal effectiveness for sitting and standing persons, that are at 1.1 m and 1.7 m above the floor, is in the range between 0.77 and 1.41 for all the cases of mixing ventilation (Figure 6. 16) and a similar range of values is valid also at lower heights (0.6 m) as shown in Table 6. 36.

CRE values calculated at 1.1 m height are lower than 1.0 except for case M1-3, M1-4, M2-1 and M2-4, this means that fully mixed flow condition is rarely reached. The worse cases according to CRE criteria are cases M2-3 (warm air and floor cooling) and M4-1 (cold air and floor cooling), the better cases are M2-1 (heating) and M1-3 (warm air and floor cooling).

Figure 6. 18 and Figure 6. 19 show the influence of the extract air terminal (exhaust) position on contaminant removal effectiveness with the same boundary conditions: when ventilation is used for heating (supply air temperature at 30°C) the choice of exhaust near the floor is better, while when ventilation is used in combination with floor cooling at low ventilation rates (0.5 ACH) the choice of exhaust near the ceiling allows higher CRE values. Table 6. 37 clarifies the correspondence between the abbreviations in the previous figures and the cases of mixing ventilation used in the comparison.

The contaminant removal effectiveness calculated for all the cases of displacement ventilation is always higher than 1.0 and decreases with the height: at 0.6 m above the floor CRE can reach very high values, more than 10 (Table 6. 36 and Figure 6. 17).

The better conditions for ventilation effectiveness (using CRE as criteria) are in the case with the highest ventilation rate and the warmest floor surface (case DV-2), while the lower CRE, even if higher than 1.0, are determined with the lowest ventilation rate and the lowest floor temperature (case DV-6), as shown in Figure 6. 17.

If ventilation rate is increased from 2.1 ACH to 3 ACH with similar boundary conditions (cases DV-3 and DV-4), CRE at 1.1 m increases from 2.24 to 2.97, that is +32.9%; this improvement is more evident near the manikin, where CRE increases from 6.8 to 12.6.

Table 6. 36 Calculated air contaminant removal effectiveness [-] at the manikin and at different heights in the occupied zone for all the cases

Case	**Manikin**	**h = 0.6 m**	**h = 1.1 m**	**h= 1.7 m**
	CRE	**CRE**	**CRE**	**CRE**
M1-1	0.90	0.87	0.87	0.94
M1-2	0.85	0.94	0.89	0.89
M1-3	1.15	1.14	1.09	1.08
M1-4	0.92	0.82	1.00	1.01
M1-5	1.08	1.04	0.86	0.99
M2-1	1.36	1.41	1.31	1.30
M2-2	0.92	0.93	0.90	0.92
M2-3	0.78	0.73	0.75	0.74
M2-4	0.97	0.98	1.01	1.01
M2-5	0.93	0.90	0.79	0.81
M3-1	0.96	0.89	0.91	0.92
M3-2	0.85	0.87	0.92	0.90
M4-1	0.77	0.78	0.76	0.76
M4-2	0.71	0.68	0.81	0.78
DV-1	7.62	80.20	7.00	1.19
DV-2	18.58	27.15	10.53	1.12
DV-3	12.60	41.11	2.97	1.17
DV-4	6.79	22.56	2.24	1.22
DV-5	6.49	15.55	1.59	1.35
DV-6	3.01	10.10	1.52	1.16

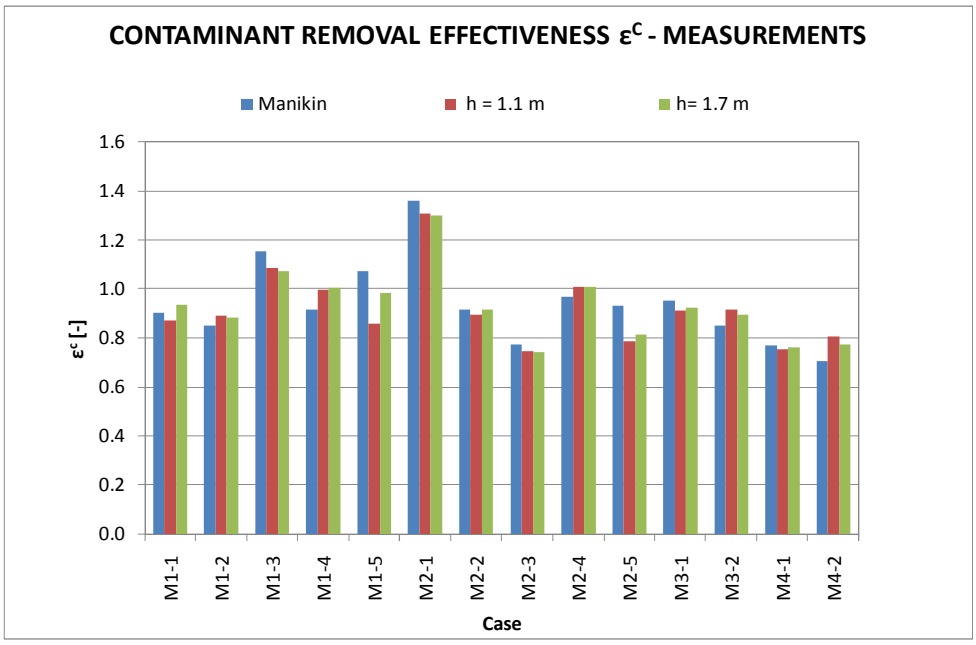

Figure 6. 16 Contaminant removal effectiveness [-] calculated near the manikin (1.1 m height), at 1.1 m height and at 1.7 m height for all the cases of mixing ventilation

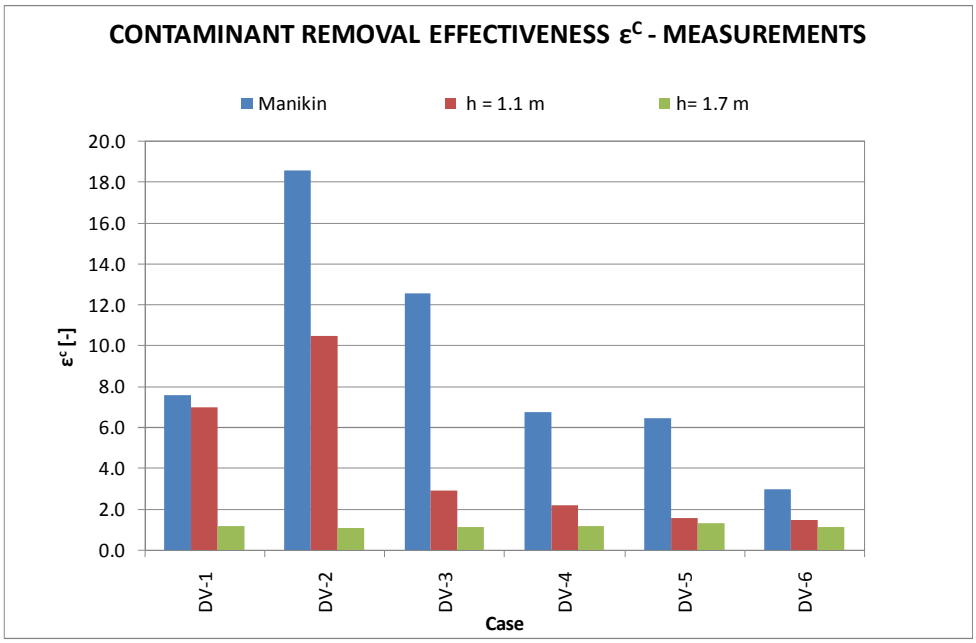

Figure 6. 17 Contaminant removal effectiveness [-] calculated near the manikin (1.1 m height), at 1.1 m height and at 1.7 m height for all the cases displacement ventilation

Table 6. 37 Correspondence between the boundary conditions abbreviations and the corresponding cases

BOUNDARY CONDITION	CASES
Wall- T supply 30°C, 0.5 ACH, Floor cooling	M1-3, M2-3
Wall- T supply 30°C, 1.0 ACH, Floor cooling	M1-4, M2-4
Wall- T supply 19°C, 0.5 ACH, Floor cooling	M1-5, M2-5
Ceiling - T supply 20°C, 0.5 ACH, Floor cooling	M3-1, M4-1
Ceiling -T supply 26°C Ts, 0.5 ACH, Floor cooling	M3-2, M4-2
Wall-T supply 30°C, 0.5 ACH	M1-1, M2-1
Wall-T supply 17°C, 0.5ACH, Floor heating	M1-2, M2-2

Table 6. 38 Contaminant removal effectiveness [-] with the same boundary conditions and different positions of extract air terminals (exhaust) and percentage difference between exhaust at low level and exhaust at high level.

BOUNDARY CONDITIONS	**Exhaust high level**	**Exhaust low level**	**difference**
Wall- T supply 30°C, 0.5 ACH, Floor cooling	1.09	0.75	-31.2%
Wall- T supply 30°C, 1.0 ACH, Floor cooling	1.00	1.01	1.1%
Wall- T supply 19°C, 0.5 ACH, Floor cooling	0.86	0.79	-8.2%
Ceiling - T supply 20°C, 0.5 ACH, Floor cooling	0.91	0.76	-17.2%
Ceiling -T supply 26°C, 0.5 ACH, Floor cooling	0.92	0.81	-12.0%
Wall-T supply 30°C, 0.5 ACH	0.87	1.31	49.5%
Wall-T supply 17°C, 0.5ACH, Floor heating	0.89	0.90	0.9%

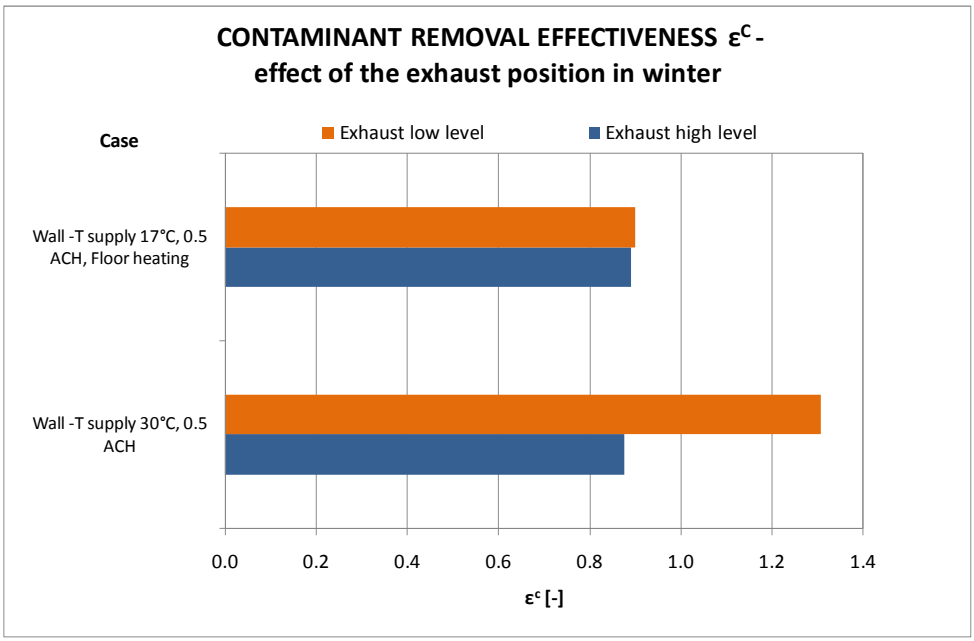

Figure 6. 18 Contaminant removal effectiveness[-] calculated at 1.1 m height for two cases of mixing ventilation from the wall in winter, with and without floor heating, 0.5 ACH, supply air temperature (T supply) at 17°C or 30°C and exhaust at high level near the ceiling or at low level near the floor.

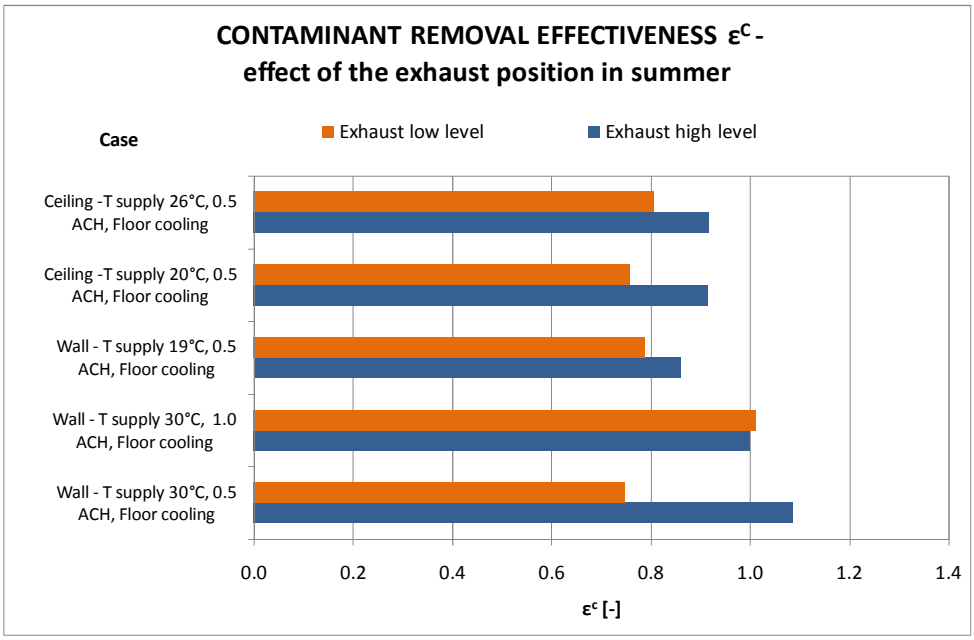

Figure 6. 19 Contaminant removal effectiveness [-]calculated at 1.1 m height for three cases of mixing ventilation in from the wall and two cases of mixing ventilation from the ceiling) in summer, with floor cooling , 0.5 ACH or 1.0 ACH, supply air temperature (T supply) from 19°C to 30°C and exhaust at high level or at low level near the floor

Air change index

Air change index for all cases of mixing ventilation is variable from 50 % to 125 % and this indicates that some cases allow ventilation effectiveness comparable with displacement ventilation while for other cases the risk of short circuit is present.

The better ventilation effectiveness using air change index as criteria is with system M2, when floor cooling and warm air at 1 ACH are adopted (case M2-4), but it is interesting to note that the same boundary conditions with extract air terminal (exhaust) near the ceiling (case M1-4) determine an evident risk of short circuit.

Air change index calculated at 1.7 m is generally lower or equal than that calculated at 1.1 m of height, except for the case M1-5. Moreover the air change index near the manikin differs only slightly from that measured at 1.1 m considering systems M1 and M2, but it is quite lower considering systems M3 and M4.

Figure 6. 23 and Figure 6. 24 show the influence of extract air terminal (exhaust) position on air change index with the same boundary conditions: when ventilation is used for heating (supply air temperature at 30°C), the choice of exhaust at high level is slightly better, while when ventilation is used in combination with floor cooling the convenience of exhaust near the floor for air change index is evident.

Table 6. 39 Calculated air change index [%] at the manikin and at different heights in the occupied zone for all the cases

ε^a	Manikin	h = 1.1 m	h= 1.7 m
M1-1	100.7%	96.8%	82.5%
M1-2	96.8%	98.0%	93.7%
M1-3	54.5%	59.1%	50.4%
M1-4	55.9%	63.6%	55.1%
M1-5	96.3%	92.8%	100.3%
M2-1	95.5%	94.9%	89.4%
M2-2	91.9%	89.9%	88.9%
M2-3	103.7%	101.9%	101.2%
M2-4	120.8%	125.1%	117.5%
M2-5	106.5%	104.1%	101.4%
M3-1	87.3%	111.0%	n.a.
M3-2	81.8%	99.8%	n.a.
M4-1	109.3%	119.4%	n.a.
M4-2	116.5%	124.6%	n.a.
DV-1	n.a.	127.3%	104.3%
DV-2	159.4%	136.0%	107.3%
DV-3	199.2%	142.5%	104.7%
DV-4	182.1%	128.8%	104.7%
DV-5	209.8%	115.2%	110.7%
DV-6	149.2%	102.9%	106.1%

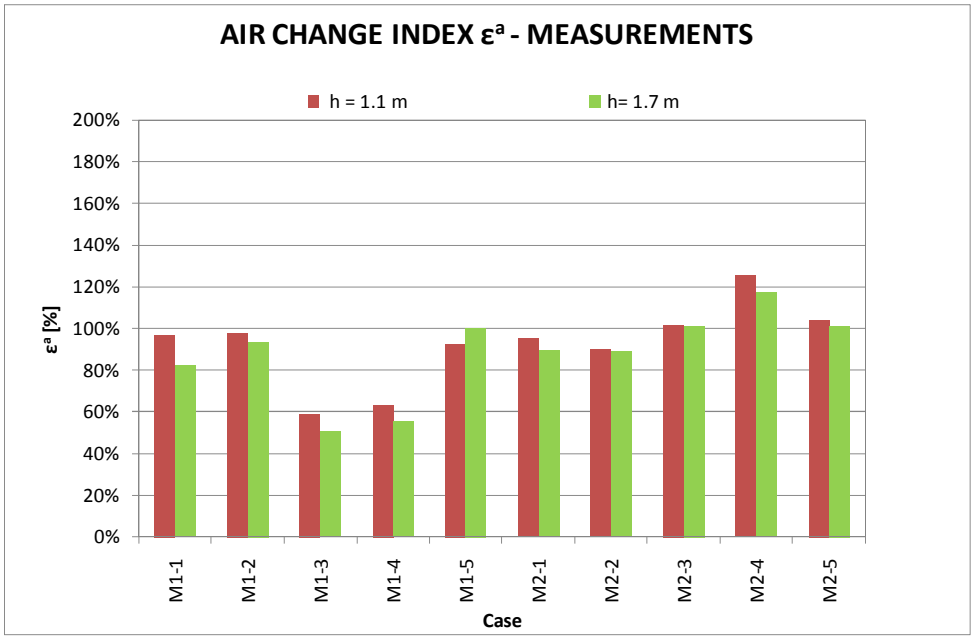

Figure 6. 20 Air change index [%] calculated at 1.1 m height and 1.7 m height for all the cases of mixing ventilation with inlet on the wall (systems M1 and M2)

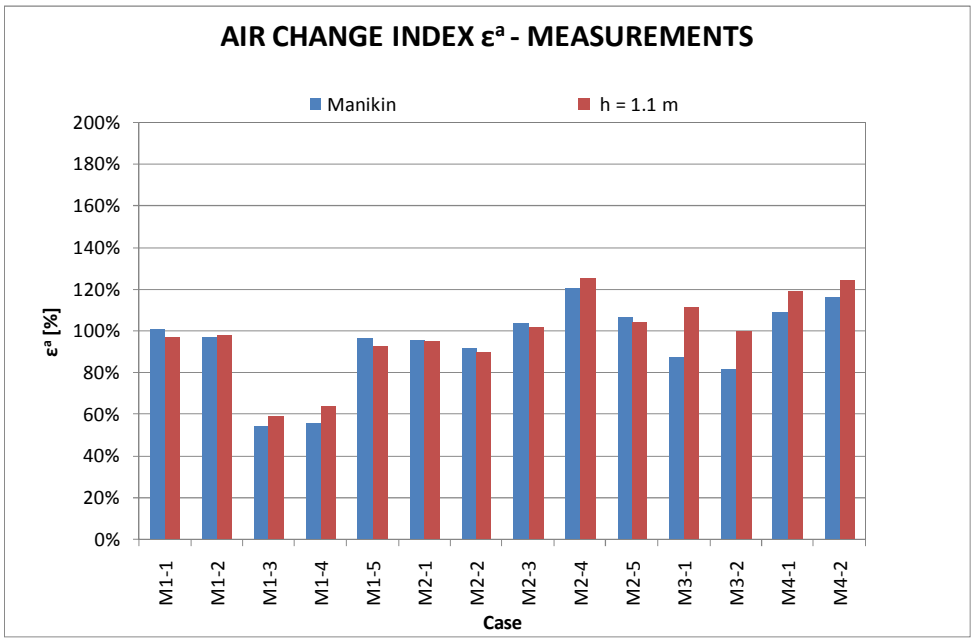

Figure 6. 21 Air change index [%]calculated near the manikin and at 1.1 m height for all the cases mixing ventilation

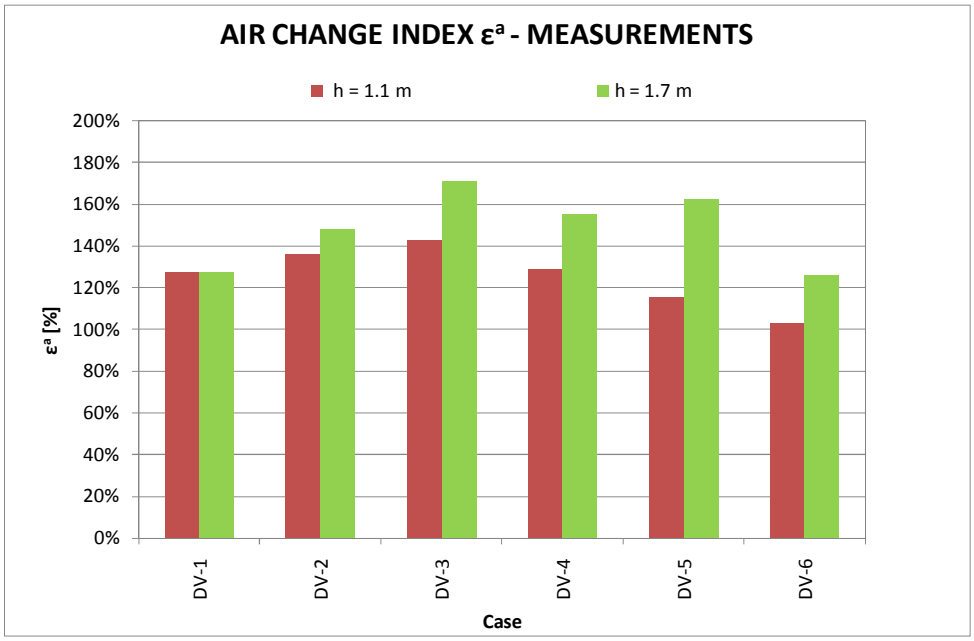

Figure 6. 22 Air change index [%] calculated at 1.1 m height and at 1.7 m height for all the cases displacement ventilation

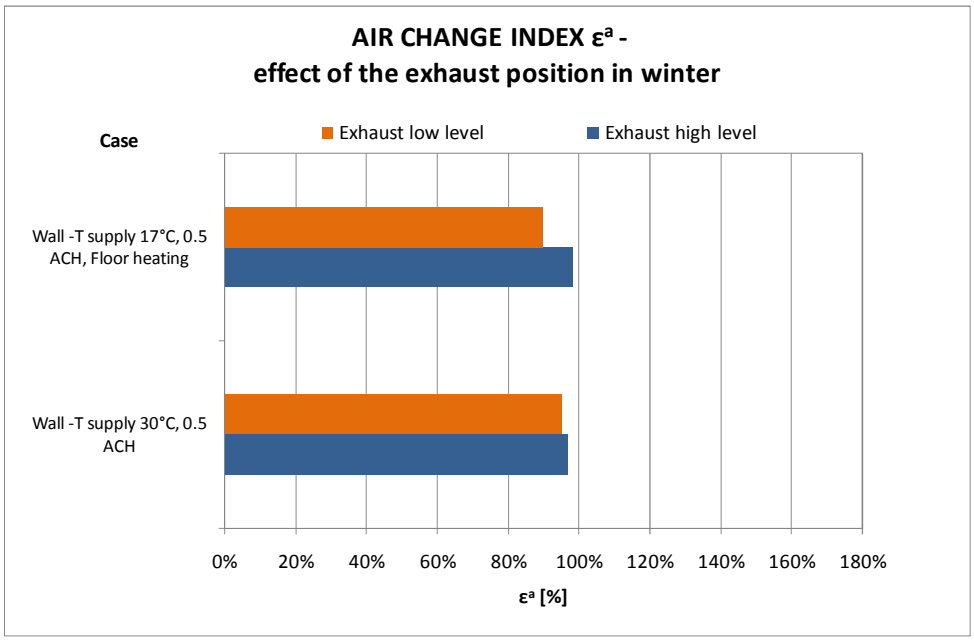

Figure 6. 23 Air change index [%]calculated at 1.1 m height for two cases of mixing ventilation from the wall in winter, with and without floor heating, 0.5 ACH, supply air temperature (T supply) at 17°C or 30°C and exhaust at high level near the ceiling or at low level near the floor

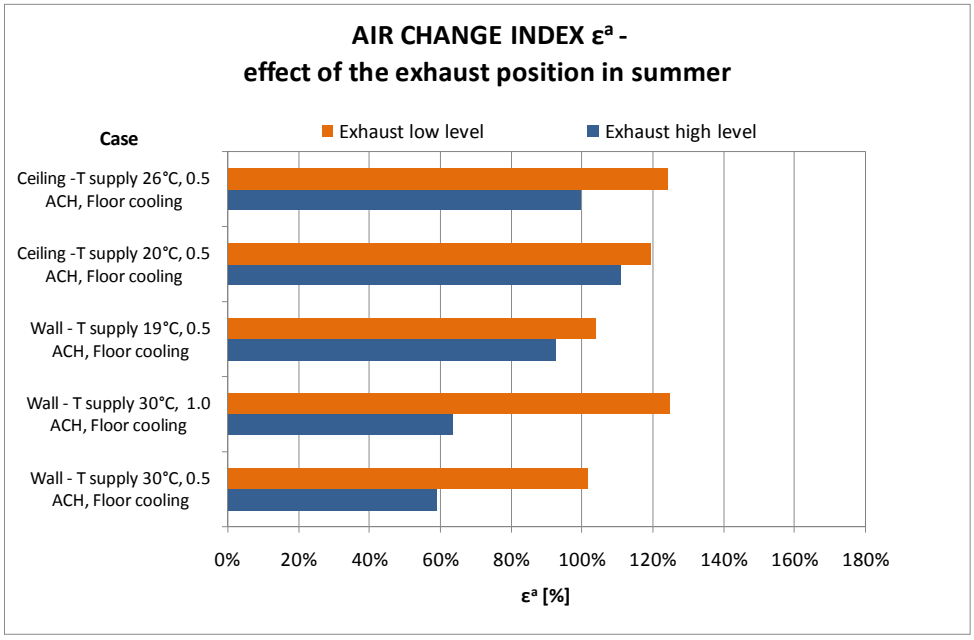

Figure 6. 24 Air change index [%] calculated at 1.1 m height for three cases of mixing ventilation from the wall and two cases of mixing ventilation from the ceiling in summer, with floor cooling, 0.5 ACH or 1.0 ACH, supply air temperature (T supply) from 19°C to 30°C and exhaust at high level or at low level near the floor.

Table 6. 40 Air change indices [%] with the same boundary conditions and different position of extract air terminal (exhaust) and percentage difference between exhaust at low level and exhaust at high level.

BOUNDARY CONDITIONS	**Exhaust high level**	**Exhaust low level**	**difference**
Wall- T supply 30°C, 0.5 ACH, Floor cooling	59.1%	101.9%	72.4%
Wall- T supply 30°C, 1.0 ACH, Floor cooling	63.6%	125.1%	96.8%
Wall- T supply 19°C, 0.5 ACH, Floor cooling	92.8%	104.1%	12.3%
Ceiling - T supply 20°C, 0.5 ACH, Floor cooling	111.0%	119.4%	7.6%
Ceiling -T supply 26°C Ts, 0.5 ACH, Floor cooling	99.8%	124.6%	24.8%
Wall-T supply 30°C, 0.5 ACH	96.8%	94.9%	-2.0%
Wall-T supply 17°C, 0.5ACH, Floor heating	98.0%	89.9%	-8.3%

6.4 Discussions

As regards the mixing ventilation cases, experiments show that the same configuration of supply and extract air terminals guarantees thermal comfort and ventilation effectiveness performances very different between summer and winter.

In winter the risk of draught rating DR[%] at ankle level can be significant high, particularly in the zones near the window, for the downdraught effect, while vertical air temperature gradients are very low. In this work it was assumed that the internal surface temperature of the window is 18.6 °C, corresponding to outside temperature of -0.6°C if the overall heat transfer coefficient U is 1.2 W/(m^2K). The window surface, 3.4 °C colder than reference temperature of the room, influences the thermal comfort of the manikin by causing an asymmetry of measured equivalent temperature between the left part facing the window (colder) and the right part (warmer). Anyway radiant temperature asymmetry calculated according to ISO 7726 in the zone occupied by the manikin satisfies the Standard limits of ISO 7730 for comfort.

According to this measurements, ventilation effectiveness in a room provided with heating ventilation is acceptable, in particular if extract air terminals are near the floor: case M2-1 not only guarantees air change index of 95 %, but contaminant removal effectiveness of 1.31, about +49.5% higher than the corresponding case M1-1 (Table 6. 38). If floor heating is used in combination with mixing ventilation, air change index results change depending on the extract air terminal position (the difference with extract air terminal at low level is -

8.3% as reported in Table 6. 40), while the contaminant removal effectiveness does not change significantly (Table 6. 38).

In summer the effect of the cold floor surface on the thermal manikin could be a risk for comfort because there could be a significant difference between air temperature at head level and at ankle level. The risk increases if, with the same reference room temperature, the floor temperature decreases because of the higher internal heat load (e.g.: case M3-2) or of the higher supply air temperature (e.g.: case M1-4). For all the cases of mixing ventilation in summer draught risk is very low and the limit of Category A for comfort is always satisfied in the occupied zone. The effect of radiation from the warm window on the manikin is evident in the local equivalent temperatures of the right and left part of the body for case M3-1 and M3-2, even if the calculated radiant asymmetry due to the warm window satisfies the Standard limit for comfort. On the contrary, the presence of the floor colder than the ceiling causes a local discomfort due to radiant asymmetry for all the summer cases of mixing ventilation for which the floor temperature is between 19°C and 22°C, that is more than 4°C less than reference room temperature.

Ventilation effectiveness results show that mixing ventilation in combination with floor cooling can guarantee high level of air quality when supply air temperature is less than or close to the reference air temperature in the room, that is for cases M1-5, M2-5, M3-1, M4-1, M3-2 and M4-2. Otherwise results show that the risk of short circuit is high (M1-3 and M1-4). The air change index is higher when the extract air terminal is placed near the floor: with the same boundary conditions the air change index is from +7.6% (M4-1 vs. M3-1) to +96.8% (M2-4 vs. M1-4) higher than the corresponding case with extract air terminal near the ceiling, as reported in Table 6. 40. The phenomenon is more evident when warm supply air (30 °C) and higher flow rate (11.1 l/s) are adopted; this situation corresponds to the case of summer warm air entering the room when a radiant floor cooling system is used.

If ventilation effectiveness of the internal environment is evaluated using the contaminant removal effectiveness results, mixing ventilation combined with floor cooling with extract air terminals at high level looks better than with extract air terminals near the floor, particularly with warm air at 30°C and low air flow rates (5.56 l/s), as seen in Figure 6. 19. This seems in contrast with what affirmed before about the air change index, so it is not possible define if for mixing ventilation in combination with floor cooling the extract air terminals should be near the ceiling or near the floor. Anyway the fact that contaminant removal effectiveness depends on the tracer gas source condition suggests that the air change index, depending only by the local age of air, should be taken as main criterion.

The same discussion could be done for mixing ventilation for heating or in combination with floor heating, for which ventilation effectiveness evaluated with the two different parameters leads to different conclusions.

As regard displacement ventilation, the main risk for thermal comfort seems to be the vertical gradient of temperature between 1.1 m and 0.1 m above the floor: if the flow rate is high and the supply air is very cold (e.g.: case DV-1) or if the floor surface temperature is very cold (case DV-6), vertical air temperature gradients higher than 6 °C can be easily reached. The high vertical gradient of air temperature can explain the significant difference in the equivalent temperature between the upper parts and the lower parts of the manikin (Figure 6. 15). Radiant temperature asymmetry due to the warm ceiling compared to the cold floor represents a potential risk of discomfort for all the cases of displacement ventilation except when high ventilation rates allow to increase the floor temperature (case DV-2).

The risk of draught rating DR [%] at ankle level (0.1 m height) is high when significant ventilation rates at low supply air temperatures are adopted, that is case DV-1 and DV-2. Both contaminant removal effectiveness and air change index results highlight the excellent ventilation effectiveness guaranteed by displacement ventilation. The lowest values of ventilation effectiveness are in case DV-6, but the air change index higher than 1 suggests that the system is good also with a so low air flow rate (1.5 ACH). Contaminant removal effectiveness seems to increase with the air flow rate (the maximum is for case DV-2 with 4.5 ACH), while air change index seems to be dependent on both air flow rate and floor temperature. In fact case DV-3 with 3 ACH and supply air temperature at 19.7 °C shows higher air change indices than both case DV-4, with a lower air flow rate (2.1 ACH) and similar floor temperature, and case DV-2, with a higher ventilation rate (4.5 ACH) and a higher floor temperature.

6.5 Conclusions

Different aspects of thermal comfort and ventilation effectiveness for 14 cases of mixing ventilation at low ventilation rates in a residential room and 7 cases of displacement ventilation in offices with 2 occupants have been studied.

Thermal comfort

Measurements have been carried out in different positions of the occupied zone in order to analyze air movement in the test room for different winter and summer cases. Thermal comfort parameters like draught rating DR [%] and vertical difference between head and ankle level have been calculated in each position and average values of the occupied zone have been determined.

Results showed that mixing ventilation with low ventilation rates could guarantees good levels for thermal comfort in winter, with and without floor heating, or in summer with cooled floor. Anyway the effect of downdraught in winter affects the thermal comfort in the zone near the window, because of the significant draught rating values DR [%] at ankle levels. When mixing ventilation is used combined with floor cooling during summer, radiant temperature asymmetry between floor and ceiling represents a potential risk of discomfort if the floor temperature is more than 4°C less than reference temperature of the room. Furthermore, if low floor temperatures are adopted due to high internal heat gains or to warm air entering the room, the risk of thermal discomfort due to vertical gradients increases.

In addition, results showed that local discomfort can be relevant with displacement ventilation cases since high vertical air temperature differences between head and ankle levels together with significant radiant temperature asymmetry values due to warm ceiling were obtained from measurements. The risk of discomfort due to draught rating DR [%] is present with displacement ventilation when high ventilation rates are adopted.

Ventilation effectiveness

Ventilation effectiveness parameters like contaminant removal effectiveness and air change index have been calculated with measurements in different positions and an average of values at the same height was used in order to characterize the occupied zone. It was found that mixing ventilation with low ventilation rates in residential rooms can guarantee acceptable ventilation effectiveness values both during heating season and during cooling

season. In addition, it was found that ventilation effectiveness is strongly dependant on the boundary conditions and on the positions of the extract air terminals. When summer warm air enters a room cooled by radiant floor system and extract air terminals are at low level, the risk of short circuit and, consequently, of poor air quality, is high.

Finally, results showed that displacement ventilation allows very high levels of ventilation effectiveness even using modest air flow rates.

6.6 References

[1] Toftum, J, Langkilde, G and Fanger, P O. 2004. New indoor environment chambers and field experiment offices for research on human comfort, health and productivity at moderate energy expenditure. Energy and Buildings 36, pp: 899–903

[2] Tanabe, S., E. Arens, F. Bauman, H. Zhang, and T. Madsen. et al. , 1994. Evaluating thermal environments by using a thermal manikin with controlled skin surface temperature. ASHRAE Transactions, Vol. 100, Pt. 1, pp. 39-48.

[3] Causone, F., Baldin F., Olesen B.W., Corgnati, S.P. 2010 Floor heating and cooling combined with displacement ventilation: Possibilities and limitations. Energy and Buildings 42 (2010) 2338–2352.

[4] Olesen, B.W., Babiak, J., Simone, A. 2007. How to measure operative temperature for control of radiant heating and cooling systems. Proceedings of Clima 2007,Helsinky, Finland.

[5] Skistad, H. 1994, Displacement ventilation. Research Studies Press, John Wiley &
Sons, Ltd., west Sussex. UK.

[6] EN 15377-2008.Heating systems in buildings. Design of embedded water based surface heating and cooling systems.

[7] Baldin , F. 2008. An experimental study of comfort and air distribution in a room with radiant floor heating/cooling and displacement ventilation. Master Thesis

[8] Zerpellon, F. 2009. Experimental Study of Air Flow Patterns in a Space with Radiant and Convective Heating / Cooling Systems. Master thesis

[9] EN 15251-2007. Indoor environmental input parameters for design and assessment of energy performance of buildings-addressing indoor air quality, thermal environment, lighting and acoustics. CEN, Brussels

[10] Krajčík, M, Simone, A, Bjarne, W.O., Petršás, D. Experimental evaluation of thermal environment and ventilation effectiveness in a room heated by warm air. Indoor air Conference Texas 2011

[11] ISO 7730-2005. Ergonomics of the thermal environment — Analytical determination and interpretation of thermal comfort using calculation of the PMV and PPD indices and local thermal comfort criteria

[12] ISO 7726-1998. Ergonomics of the thermal environment-Instruments for measuring physical quantities

[13] Fanger, P. O. Thermal Comfort, Danish Technical Press, 1970

[14] Matsunaga K, Sudo F, Tanabe S-I, Madsen. Evaluation and Measurement of Thermal Comfort in the Vehicles With a New Thermal Manikin. Sae Technical
Paper Series 931958 (1663) 339-403

[15] Manikin Manual. Version 3.1 for Windows August 2008 (http://www.byteline.dk)

[16] ASHRAE 1332-RP Revision to the ASHRAE thermal comfort tool to maintain consistency with Standard 55-2004. Final report 2006.

[17] ASHRAE. 2004, Standard 55-2004: Thermal Environmental Conditions for Human Occupancy. Atlanta:
American Society of Heating, Refrigeration, and Air-Conditioning Engineers

[18] RHEVA Guidebook n°2. 2004.Ventilation effectiveness

[19] Manual for application software 7620- LumaSense Technologies A/S

7 - Comparison of displacement ventilation and mixing ventilation systems with regard to ventilation effectiveness in offices

Abstract

Air quality in offices depends on the ventilation system skills to remove contaminants from the occupied zone. In a low polluted building air quality is dependent on the human presence and carbon dioxide is normally used as indicator of human bioeffluents.

The aim of this work is to investigate, by using numerical simulations (CFD), the effect of the supply and exhaust locations on the contaminant distributions in an office equipped with cooled ceiling. Mixed ventilation was compared with different displacement ventilation solutions, adopting floor displacement outlets around the occupied zone or a displacement air terminal unit from a wall. Exhaust vents in displacement ventilation were placed on the upper part of a wall or on the ceiling in different positions. Besides percentage of dissatisfied PD [%] and contaminant removal effectiveness, a discomfort index for the whole office was calculated.

Results showed that with displacement ventilation exhaust should be placed on the ceiling above the occupied zone: this could prevent high contaminant concentrations at the breathing level in the area of the office closest to wall where exhaust is placed.

7.1 Introduction

Computational fluid dynamics represents an appropriate instrument for the prediction of contaminant distribution in a room. Indoor air quality studies are very important for offices, where contaminant presence can affect both the health and productivity. Wargocki et al. [1] estimated that performance of office work increases on average by 1.5 % for every 10 % decrease in the percentage of persons dissatisfied with the air quality; they also studied the effects of pollution loads and outdoor air supply rates on Sick Building Syndrome (SBS) symptoms in office [2].

Within an office, even if furnishing, carpets, ventilation systems and computers should be considered, air quality is affected particularly by human presence. The occupants emit bioeffluents like carbon dioxide, carbon monoxide and water vapor in quantities variable with metabolic activity and age, as reported in [3] and [4]. Carbon dioxide is considered a good indicator of air quality in rooms with human presence even if it does not represent a serious health problem at concentrations that generally occur indoor. Furthermore it was found that

carbon dioxide concentration is connected to the acceptability of the space in terms of body odor (Persily, [5]). European standard EN 15251-2007 [6] recommends ventilation rates values in non residential buildings based on the floor area with a default occupant density and for different categories of pollution from building. In order to analyze the effective performance of ventilation system, it is useful to compare the concentration at exhaust with concentration in the room, by means of the contaminant removal effectiveness CRE defined by RHEVA [7]. CFD techniques allow to calculate contaminant removal effectiveness in rooms equipped with different ventilation systems and to make comparisons between them. Recently a study on contaminant removal effectiveness was carried out in order to compare three air distribution systems in a bar/restaurant assuming particulate and carbon monoxide as pollutant sources [8]. The effect of the air supply location on the performance of a displacement ventilation system in a big office was investigated by Lin [9], while Novoselac [10] studied vertical concentration of active pollutant sources (CO_2) and VOC from carpet in a conference room, with a cooled ceiling combined with displacement ventilation.

In this work the contaminant carbon dioxide concentration was calculated in an office for three people and equipped with cooled ceiling and mechanical ventilation. Mixed ventilation was compared with different displacement ventilation systems and the effects of both supply and exhaust positions were investigated.

7.2 Method

A typical office in summer conditions equipped with mechanical ventilation together with ceiling cooling panels was considered. CFD simulations were performed via FDS (Fire Dynamics Simulator), in order to analyze the effect of different ventilation systems on air quality levels. The present analysis refers to an office with an overall internal heat gain of 680W, the ceiling surface temperature at 22°C and the floor surface and all the other wall surfaces at 26°C. The office measures 7 m by 4 m by 3 m; the total internal heat gain is due to 3 persons and 3 computers modeled like simple shapes as shown in Figure 7. 1. Since workers were in sitting position, the maximum height of the modeled person is 1.1 m corresponding to the head level according to standard ISO 7730 [11].

It was supposed that each person was a source of 0.2 m^3/h of carbon dioxide (recommended value for an adult in sitting position [4]) and in the model the contaminant source was placed on the part of the person corresponding to the face.

The fresh air flow rate was 1.5 ACH (at 20°C) for each simulation and different types of inlet air terminal units were considered (Figure 7. 2):

- Wall mounted vents for mixed air flow (case 1)
- Floor displacement outlets (in raised floor or on floor plenums) with radial, horizontal jet (cases 2 and 4)
- Floor displacement outlets (in raised floor or on floor plenums) with inclined jet towards the occupied zone (case 3)
- Displacement ventilation unit from a wall (lateral), cases 5 and 6.

The air flow rate of 1.5 ACH corresponds to 1.25 (l/s m^2), above the recommended value for category II, very low polluted building, according to Standard [6].

As exhaust, grids of different sizes were adopted. They were placed either on a short side wall (at floor level or at ceiling level) or on the ceiling, along the longitudinal axis.

The six cases considered in this work differ from each other for the type, the number and the position of inlet and outlet air vents, as reported in Table 7. 1 and shown in Figure 7. 3. Details of all inlet and outlet vents are shown in Table 7. 2.

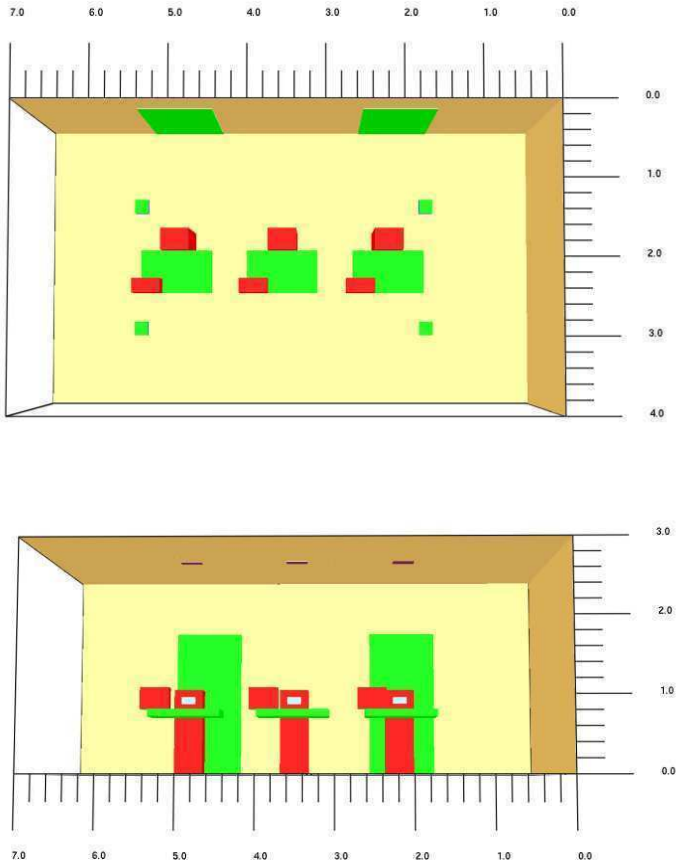

a

b

Figure 7. 1 Layout of the simulated office with 3 desks, 3 PC and 3 persons: floor map (a) and longitudinal section(b). Sizes are expressed in [m]. In (b) blue face is visible for each person.

a *b* *c*

Figure 7. 2 Examples of inlet air vents: wall mounted grids for mixed air flow (a), floor displacement outlets (b) and lateral displacement terminal (c)

Table 7. 1 The 6 cases description: boundary conditions, inlet vent and outlet codes

	Units	Case 1	Case 2	Case 3	Case 4	Case 5	Case 6
code		MIX	DV-1	DV-2	DV-3	DV-4	DV-5
Total Internal heat loads	[W]	680.0	680.0	680.0	680.0	680.0	680.0
Wall and floor surface temperature	[°C]	26.0	26.0	26.0	26.0	26.0	26.0
Ceiling surface temperature	[°C]	22.0	22.0	22.0	22.0	22.0	22.0
Primary air inlet temperature	[°C]	20.0	20.0	20.0	20.0	20.0	20.0
Inlet air velocity	[m/s]	0.29	0.22	0.22	0.22	0.20	0.20
Primary air volume flow	[ACH]	1.5	1.5	1.5	1.5	1.5	1.5
Inlet air vent code	[-]	1.i	2.i	3.i	2.i	4.i	4.i
Outlet air vent code	[-]	1.o	2.o	2.o	3.o	4.o	5.o

Table 7. 2 Inlet and outlet air vent types

Inlet/Outlet	Code	N° vents	Sizes [cm]	Layout
Inlet	1.i	3	40 x 10	Short side wall , top at 15 cm from ceiling, uniform distribution on the wall
	2.i	4	20 x 20	Floor, 100 cm from short sides, 140 cm from long sides, horizontal deflector 10 cm above the grid
	3.i	4	20 x 20	Floor, 100 cm from short sides, 140 cm from long sides, lateral deflector on 2 sides
	4.i	1	50 x 35	Short side wall, bottom at 10 cm from the floor, central position on wall
Outlet	1.o	1	50 x 50	Short side wall, bottom at 20 cm from floor, central position on wall
	2.o	2	40 x 20	Short side wall, top at 30 cm from ceiling, uniform distribution on the wall
	3.o	3	30 x 20	Ceiling, uniform distribution along the longitudinal axis
	4.o	1	60 x 30	Ceiling, longitudinal axis, central position
	5.o	1	60 x 30	Ceiling, longitudinal axis, 40 cm from the wall opposite to inlet vent

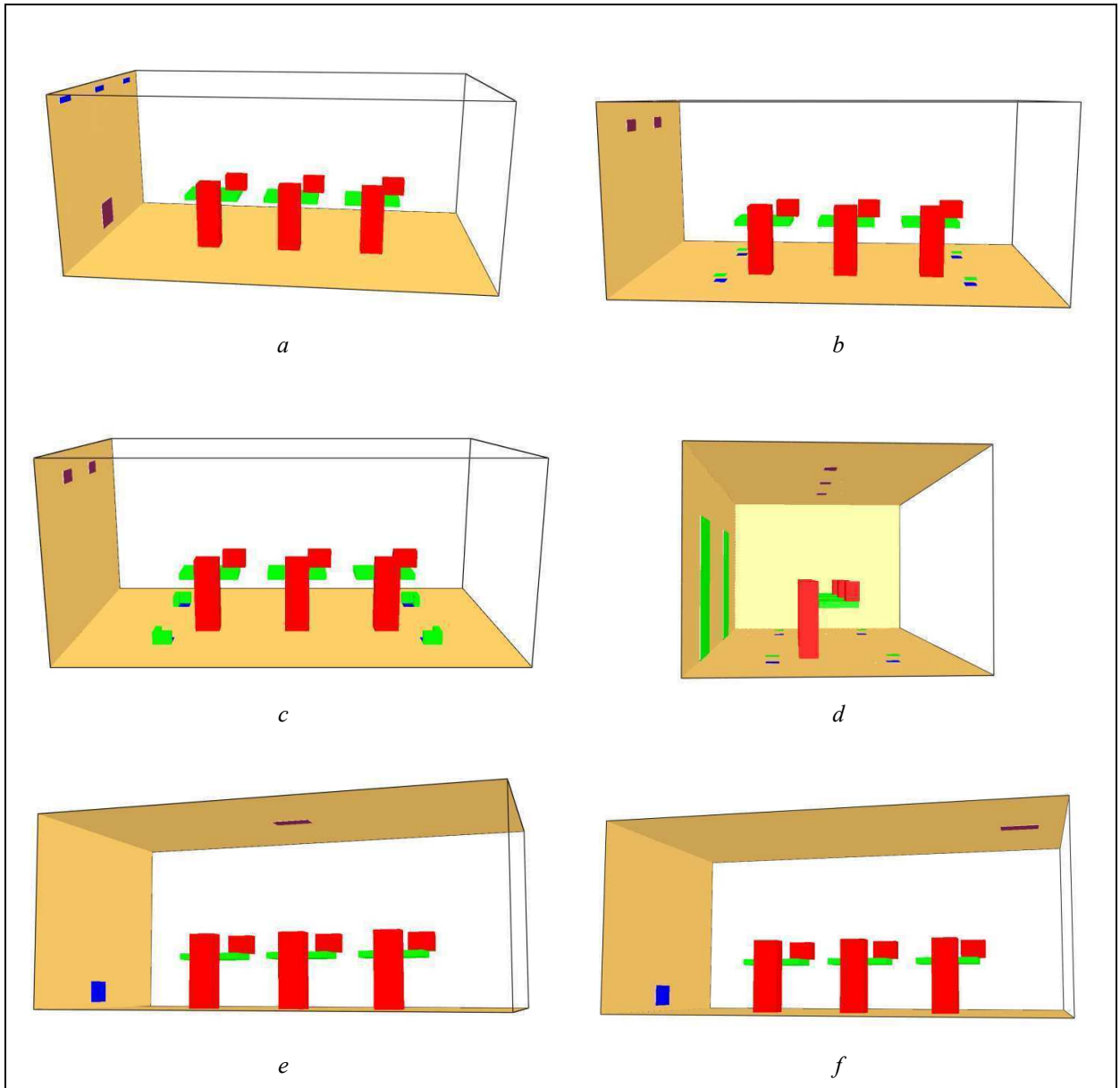

Figure 7. 3 Layout of the simulated office for all cases: inlet air vent (blue) and outlet air vents (violet) for case 1 (a), case 2 (b), case 3 (c), case 4 (d), case 5 (e) and case 6 (f)

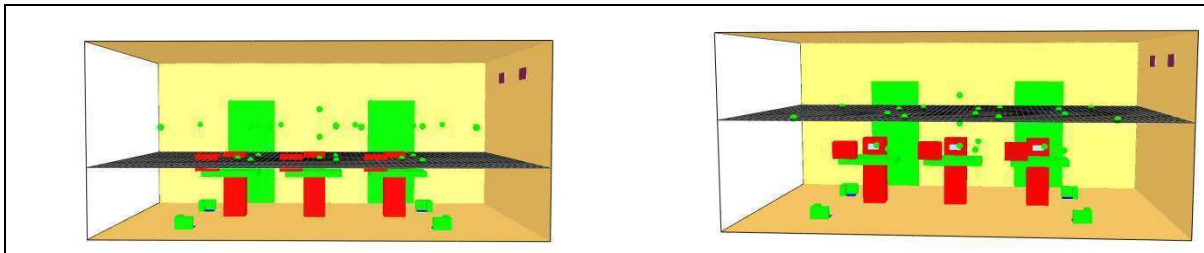

Figure 7. 4 Measurements points representation, grid at 1.1 m height (a) and 1.7 m height (b)

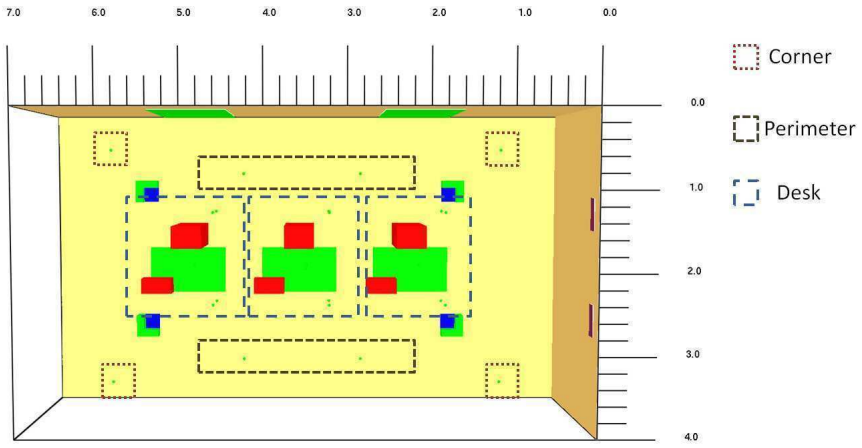

Figure 7. 5 Measurements points representation within the assumed zone in the room

Carbon dioxide concentration was calculated in 23 points, belonging to areas important for comfort, as shown in Figure 7. 4 and Figure 7. 5. They are:

- zone in front of the source, at 1.1 m height, 20 cm from the table; this zone is called "table" and includes 3 points;
- positions representative of standing persons around the desk, 80 cm from long sides and 1.7 m height. This zone is called "Perimeter" and includes 4 points;
- positions representative of standing person near the corners 1.7 m height. This zone is called "Corner" and includes 4 points;
- positions representative of standing or sitting person near the desk, at 1.1m and 1.7 m , at the same side of the source or on the opposite side. This zone is called "Desk1", Desk 2" and "Desk3" and 4 points are considered for each desk. Position Desk 1 is the closest to the short side wall with inlet vents or outlet vents while Desk 2 is in the centre.

Carbon dioxide is an indicator of human bioeffluents and if occupants are the exclusive pollution sources in a space it is possible determine the perceived air quality as percentage of dissatisfied PD [%] by using the ASTM D6245:98 [12] equation:

$$PD\% = 392 \cdot e^{(-15.5 \cdot dCO_2^{(-0.25)})} \qquad \text{Eq. 7. 1}$$

where dCO_2 is the difference between the external concentration and the internal concentration. In this case it was assumed that the external air entering the room is without contaminant, so dCO_2 coincided with the internal concentration.

In order to better compare the 6 cases, a discomfort index ID [%] representative for the whole room was determined using the percentage of dissatisfied PD [%] values for the 23 points multiplied for weighted coefficients (Eq. 7. 2). These coefficients varied from 3 to 10 and were assumed based on the importance of the zone with respect to the workers, that is points near the table had the higher coefficient values (Table 7. 4).

$$ID\% = \frac{\sum_{23}(c_i \cdot PD\%)}{\sum c_i} \qquad \textit{Eq. 7. 2}$$

Table 7. 3 Weighted coefficient c_i for the points belonging to each zone

Zone	N° points	Weight coefficient
table	3	10
Perimeter	4	5
Corner	4	3
Desk 1	4	10
Desk 2	4	10
Desk 3	4	10

Finally, contaminant removal effectiveness according to RHEVA [7] was calculated. This parameter expresses how quickly an air-borne contaminant is removed from the room, and it is defined as the ratio between contaminant concentration at exhaust c_e and in the room <c>, as expressed by equation (7.3). In this work <c> is the average of contaminant concentration in the different zones of the office while contaminant concentration at exhaust c_e is determined as the steady state concentration C_s in a volume V, with gas total emission G [m^3/h] and air change rate n [h^{-1}], by applying equation (7.4) derived from Standard ASTM D6245-98 [12].

$$\varepsilon^c = \frac{c_e}{< c >} \qquad \textit{Eq. 7. 3}$$

$$C_s = \frac{G}{n \cdot V} \qquad \textit{Eq. 7. 4}$$

7.3 Results

Results showed that contaminant concentrations in the room at equilibrium were quite different depending on the ventilation system. In Figure 7. 6 calculated carbon dioxide concentrations at 1.1 m height for the same cases are reported. It is evident that with mixed ventilation, concentrations are significant high in all the volume (Figure 7. 6 a): indeed calculated concentrations are about 800 ppm with the exception of the table zone (Table 7. 4). When displacement ventilation from floor is adopted with exhaust on a wall (Figure 7. 6 b), concentrations can be locally much higher than mixed ventilation cases; as reported in Table 7. 4, CO_2 concentration at desk n°1 near the exhaust is higher than 1000 ppm in case 2 and case 3 and decreases towards the centre of the room. With exhaust placed on the ceiling (cases 4, 5 and 6) contaminant concentration tends to be uniform in all the volume (Figure 7. 6 c, d); calculated values are about 550 ppm for case 4 and about 700 ppm for cases 5 and 6, except the table zone where values are slightly higher.

In this work it was found that cases 2 and case 3 presented the highest values for percentage of dissatisfied PD [%] and discomfort index ID [%], more than mixed ventilation case, as shown in Figure 7. 8 and Figure 7. 9, achieving very similar values. A significant improvement on air quality has been possible by placing exhaust on the ceiling (case 4) and by adopting displacement ventilation from a wall (case 5 and case 6). In this condition discomfort index ID [%] decreased from 23.0 % in the mix ventilation case (Case 1) to 9.3% of case DV-6, to 11.3% of the case DV-5 and to 17.0 % for the case 4.

Similar considerations can be carried out for contaminant removal effectiveness: it was found that, excluding the table zone, the highest values were assumed for case 4 ($\varepsilon^c > 0.8$) in all the volume, followed by case 5 and case 6 ($\varepsilon^c > 0.7$).

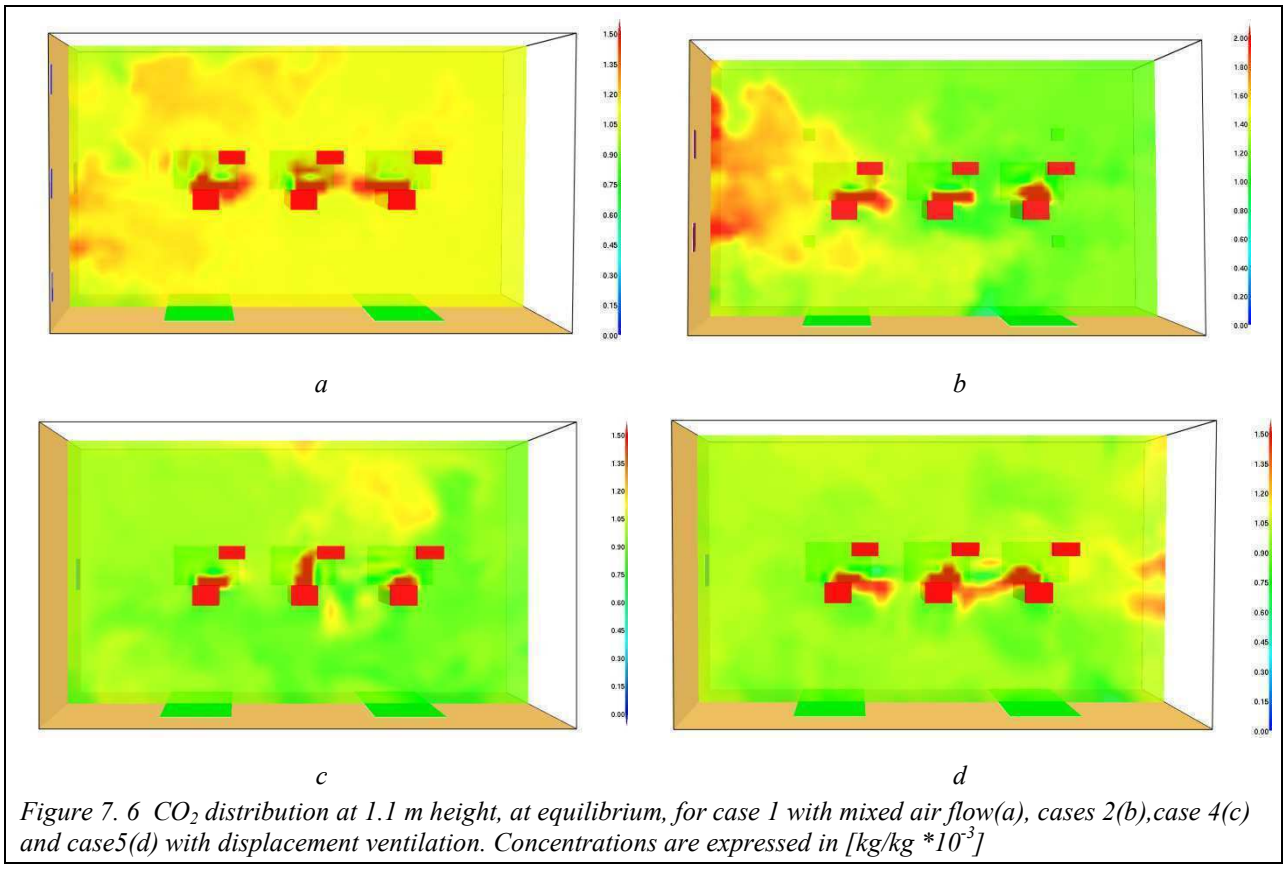

*Figure 7. 6 CO_2 distribution at 1.1 m height, at equilibrium, for case 1 with mixed air flow(a), cases 2(b),case 4(c) and case5(d) with displacement ventilation. Concentrations are expressed in [kg/kg *10^{-3}]*

Table 7. 4 Contaminant concentration [ppm] at steady state conditions in different zones of the volume, for all cases

POSITION	CASE					
N°	**1**	**2**	**3**	**4**	**5**	**6**
Code	**Mix**	**DV-1**	**DV-2**	**DV-3**	**DV-4**	**DV-5**
Table	896	1015	1032	616	804	810
Perimeter	792	884	874	533	674	694
Corner	785	897	896	539	663	699
Desk1	799	1019	1025	536	656	683
Desk2	790	912	907	526	671	686
Desk3	785	802	792	513	657	680

Table 7. 5 Percentage of dissatisfied PD [%] for the carbon dioxide concentration in different zones of the volume, for all cases

POSITION	CASE					
N°	**1**	**2**	**3**	**4**	**5**	**6**
Code	**Mix**	**DV-1**	**DV-2**	**DV-3**	**DV-4**	**DV-5**
Table	24.6	26.8	27.1	18.7	22.7	22.9
Perimeter	22.7	24.5	24.3	16.9	20.2	20.6
Corner	22.5	24.4	24.4	17.0	19.9	20.7
Desk1	22.8	26.7	26.6	16.8	19.8	20.4
Desk2	22.7	25.0	25.0	16.7	20.1	20.5
Desk3	22.6	22.9	22.7	16.4	19.8	20.3

Table 7. 6 Contaminant removal effectiveness in different zones of the volume, for all cases

POSITION	CASE					
N°	**1**	**2**	**3**	**4**	**5**	**6**
Code	**Mix**	**DV-1**	**DV-2**	**DV-3**	**DV-4**	**DV-5**
Table	0.53	0.47	0.46	0.78	0.60	0.59
Perimeter	0.60	0.54	0.55	0.89	0.71	0.69
Corner	0.61	0.53	0.54	0.88	0.72	0.68
Desk1	0.60	0.47	0.46	0.89	0.73	0.70
Desk2	0.60	0.52	0.53	0.90	0.71	0.69
Desk3	0.61	0.59	0.60	0.93	0.73	0.70

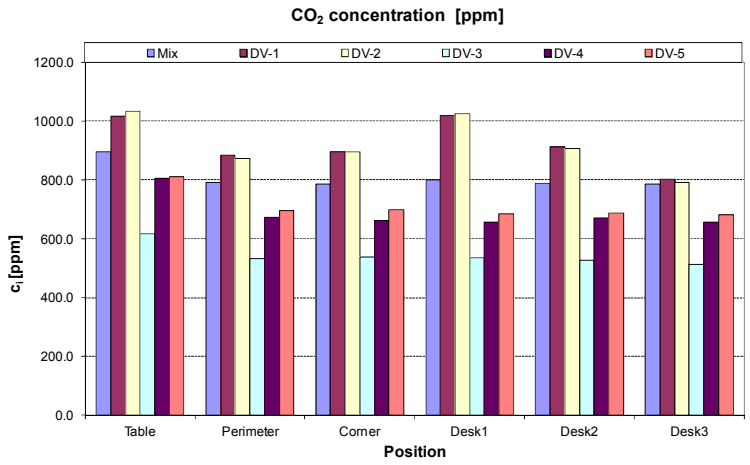

Figure 7. 7 CO_2 concentration [ppm] at steady state conditions in different zones of the volume, for all cases

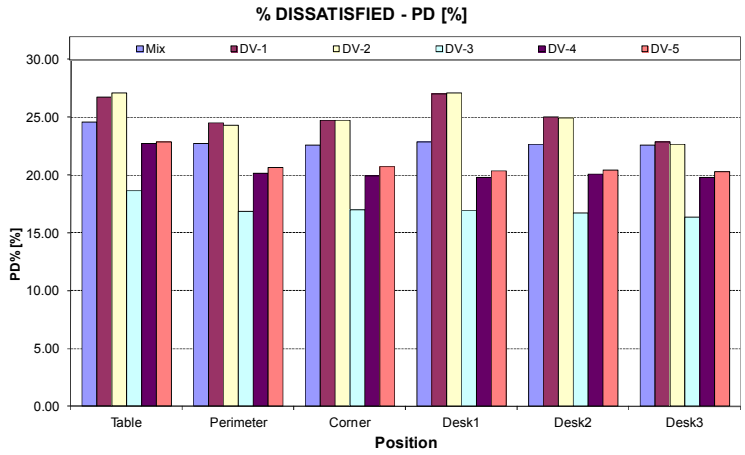

Figure 7. 8 Percentage of dissatisfied PD [%] for the carbon dioxide concentrations in different zones of the volume, for all cases

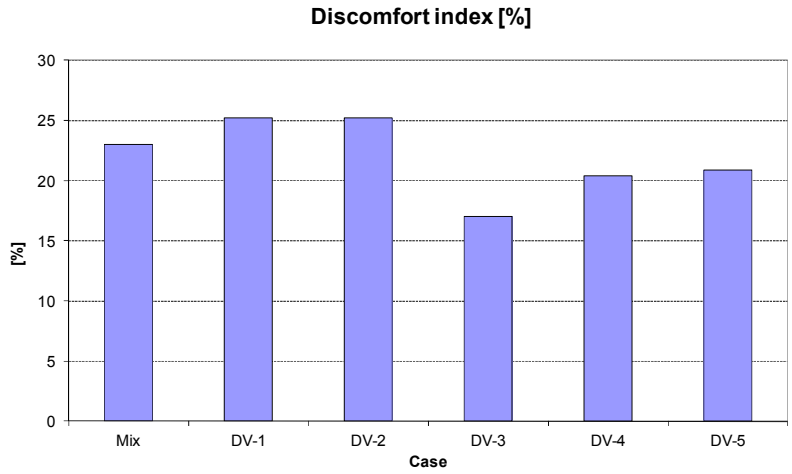

Figure 7. 9 Discomfort index ID [%] for the carbon dioxide concentration in different zones of the volume, for all cases

Table 7. 7 Discomfort index ID [%] for all cases and percentage difference with respect to case 1

	CASE					
N°	**1**	**2**	**3**	**4**	**5**	**6**
Code	**Mix**	**DV-1**	**DV-2**	**DV-3**	**DV-4**	**DV-5**
discomfort Index	23	25.2	25.2	17.1	20.4	20.86
Diff % with respect to case 1		9.6%	9.6%	-25.9%	-11.30%	-9.30%

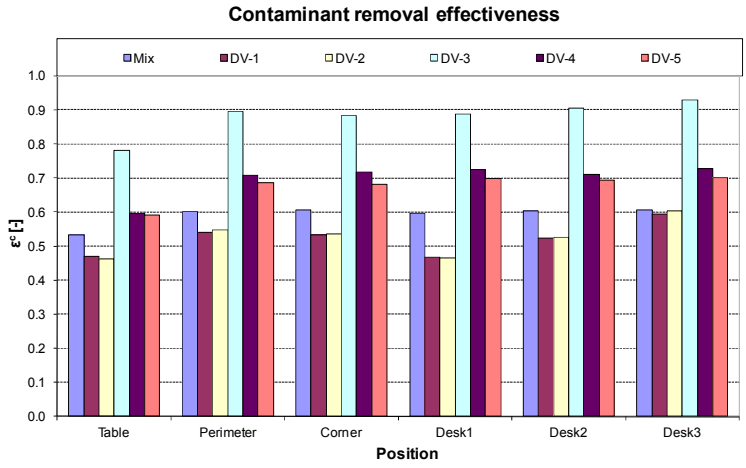

Figure 7. 10 Contaminant removal effectiveness [-] for the carbon dioxide concentration in different zones of the volume, for all cases

7.4 Discussions

The contaminant removal efficiency analysis carried out in this work showed that not always displacement ventilation is the best solution in an office with respect to traditional ventilation systems. The choice of floor displacement outlets with exhaust on a wall can cause an asymmetrical distribution of contaminant in the office, penalizing the person closest to the exhaust. The air jet direction from the floor does not affect the motion of air at the breathing zone (1.1 m height), because the velocities involved are low. As a matter of fact, case 2 and case 3, with tangential or directional air flow, were comparable for both contaminant removal effectiveness and for discomfort index.

When displacement ventilation is used with exhaust placed on the ceiling, contaminant efficiency increases significantly, particular if exhaust is in the centre rather than the side (case 5 vs. case 6) or above each contaminant source (case 4). In order to better understand the phenomenon, it is important to analyze velocity distribution in the volume: due to the thermal plume effect from heat gains, contaminants get warmer and raise upwards, reaching the cold ceiling surface. At this point if exhaust is placed on the ceiling contaminants are removed easily, on the contrary an additional air movement towards the exit starts. This study confirms Kobayashi and Chen [13] results about exhaust position on air quality in case of floor supply displacement ventilation: they demonstrated that contaminants can be removed faster when exhausts are placed above the contaminant sources rather than in lateral position on ceiling.

This study showed also that displacement units placed from a wall and extraction on the ceiling (case 5 and 6) could guarantee similar contaminant concentrations at the breathing zone both if extraction of air is in the centre of the ceiling or in near the wall opposite to the supply. With the chosen geometry features, a solution with displacement ventilation from floor (case 4) is slightly better than displacement units placed from a wall, even with the same boundary conditions, air flow rates and similar exhaust positions. This means that percentage of dissatisfied PD [%] in all the volume and discomfort indices ID [%] in an office equipped with displacement ventilation are influenced by the supply position. In fact in the interaction between the air flow at the floor level and the layout of the room is important for the contaminant removal efficiency: if cold air from floor is spread near the desk like as reported in Figure 7. 11 (a) or spread horizontally from the wall as shown in Figure 7. 11 (b), the movement upwards of contaminants for the thermal effect depends on the air velocity direction near the heat gains and on the presence of obstacles (e.g. the table).

The choice of contaminant sources position and objects near the source affects the results of the simulation: in this study a person with the face and mouth above the desk was assumed, but if the simulated person was distant from the desk, the primary air from the floor could reach earlier the source. However the aim of this work is to compare different systems with the same layout of the room, therefore only relative differences between contaminant concentrations for each case have been determined.

Concentration at exhaust position for all cases was assumed to be the steady state concentration in a fully-mixed air flow condition, therefore contaminant removal effectiveness has been calculated as the ratio between contaminant concentration in the points and theoretical concentration in complete mixing ventilation.

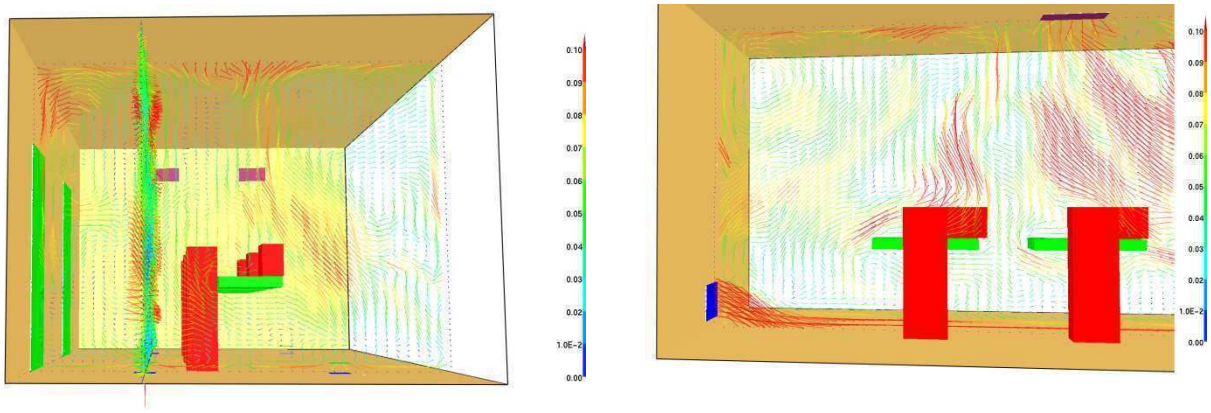

a *b*

Figure 7. 11 Air velocity [m/s]differences at the floor level with floor displacement outlets (a) and lateral displacement unit (b)

7.5 Conclusions

A numerical investigation about the effect of the supply and exhaust locations on the contaminant distributions in an office with cooled ceiling was carried out by using a numerical simulation (CFD). Mixing ventilation was compared with different displacement ventilation solutions with regards to contaminant concentration in 23 positions belonging to 6 zones, important for comfort and corresponding to sitting and standing positions. Percentage of dissatisfied for carbon dioxide concentration was calculated in the 6 zones and a discomfort index for the whole office was determined. Finally, contaminant removal effectiveness was calculated.

Results showed that, with the exhaust placed on a wall, the contaminant removal efficiency in displacement ventilation cases can be less than mixed ventilation and positions near the exhaust are penalized. The choice of exhaust on the ceiling, particularly in the centre or above each desk, allows higher air quality levels. Finally it was found that the position of displacement ventilation terminals can influence the contaminant removal efficiency for a certain office layout.

7.6 References

[1] Wargocki, P, Wyon, D. P., Baik, Y. K Fanger, P O. 2000. Productivity is affected by air quality in offices. Proceedings of Healthy Buildings 2000, Vol.1, pp 635-640.

[2] Wargocki, P, Wyon, D. P., Sundell, J., Clausen, G., Fanger, P. O. 2000. The Effects of Outdoor Air Supply Rate in a Office on Perceived Air Quality, Sick Building Syndrome (SBS) Symptoms and Productivity. Indoor Air 2000 (10), pp 222-226.

[3] CEN report CR 1752-1998. Ventilation for buildings - design criteria for the indoor environment. CEN/TC 156/WG 6.

[4] De Gids, W.F., Wouters, P. 2010. CO_2 as indicator for the indoor air quality - general principles. AIVC.VIP N°33 July2010.

[5] Persily, A.K., 1996.The relationship between indoor air quality and carbon dioxide, Proceedings of Indoor Air 1996, Nagoya, Japan, Vol. 2, pp 992-996.

[6] EN 15251-2007. Indoor environmental input parameters for design and assessment of energy performance of buildings addressing indoor air quality, thermal environment, lighting and acoustics.

[7] Mundt et al., RHEVA Guidebook n°2. 2004.Ventilation effectiveness.

[8] Hirnikel, D.J; Lipowicz, P.J.; Lau, R.W. Predicting contaminant removal effectiveness of three air distribution systems by CFD modeling. 2002. ASHRAE Transactions, Vol. 108, part 1, pp 350-359.

[9] Lin, Z., Chow, T.T., Tzang. C.F., Fong. K.F., Chan. L.S.2005.CFD study on effect of the air supply location on the performance of the displacement ventilation system. Building and Environment 40 (2005), pp 1051-1067.

[10] Novoselac, A., Sbrebric, J. 2002. A critical review on the performance and design of combined cooled ceiling and displacement ventilation systems. Energy and Buildings 34 (2002), pp 497-509.

[11] ISO 7730:2005. Ergonomics of the thermal environment — Analytical determination and interpretation of thermal comfort using calculation of the PMV and PPD indices and local thermal comfort criteria.

[12] ASTM D6245-98 -2002. Standard guide for using indoor carbon dioxide concentrations to evaluate indoor air.

[13] Kobayashi, N. and Chen, Q. 2003. Floor-supply displacement ventilation in a small office.
Indoor and Built Environment, 12(4), 281-292.

8 - Validation of a CFD model for the air distribution in rooms equipped with mechanical ventilation in combination with heating/cooling radiant systems

Abstract

An extensive study has been carried out in order to validate a CFD model for air distribution in rooms equipped with mixed or displacement ventilation combined with heating/cooling floor systems. Ten cases among those available from previous experiments in a full-scale-chamber representing a typical residential room or a typical office (described in Chapter 6) were chosen.

Geometry features, internal heat gains, supply air terminals and boundary conditions in the CFD model were chosen in order to maintain the model as much as possible similar to reality. But at the same time important simplifications of geometry were necessary due to the limit of the program to reproduce shapes and to limit the computing effort; in effect simulation time could be too high with very small sizes cell.

Vertical air temperature and air velocity profiles were calculated in the same positions where measurements have been carried out and some possible causes of discomfort were evaluated for each condition.

Besides to air change efficiency, that represents how quickly the air in the room is replaced, contaminant removal effectiveness and local air change index were calculated in the same positions where contaminant concentrations have been measured.

Results showed a good agreement of simulated and measured air velocity and temperatures; this means that the CFD model was able to evaluate a thermal environment and suitable to predict thermal comfort parameters for all the cases.

Contaminant removal effectiveness for mixed ventilation were higher than the corresponding values from experiments and different reasons for this have been hypothesized. In case of displacement ventilation the model guaranteed CRE on average similar to experimental values.

The predicted local air change index was in agreement with measurements for all cases, even if near the manikin the measured improvement of air quality was not well appreciated by the model.

8.1 Introduction

Computational fluid dynamic technique is an important tool for the prediction of air flow and contaminant distribution in ventilated spaces. The prediction is based on the solution of fundamental flow equations like equation of continuity, momentum, energy and transport. A numerical method is applied in order to solve differential equations and a volume division in limited numbers of cells is necessary.

First applications of CFD on indoor environment were made in the 1970s with Nielsen [1] and from that time a great development of CFD for ventilation applications started thanks to the constant increase of computer power and speed of calculation in the last decades. The practical use of flow simulations for air distribution in room increased also because the cost of numerical simulations decreased and they began to represent an alternative of fully scale experiments.

Anyway fully scale experiments are nowadays determinant in order to validate a new CFD model, because the representation of different complex phenomena taking place in the room needs to be compared with measurements. Recently a full-scale experimental campaign together with a computational fluid dynamics (CFD) study of a radiant cooling ceiling installed in a test room, under controlled conditions were carried out [2] and thermal comfort indices were investigated. Moreover, air quality in offices with floor heating and displacement ventilation was investigated by means of a CFD model [3] after experimental tests in a test room.

8.2 Method

8.2.1 The model

The aim of this work was to integrate the experimental studies on air distribution in a room with mechanical ventilation and radiant heating/cooling systems using a computational fluid dynamic model.

Experiments were carried out in a full scale chamber with the dimensions 4.2 m by 4.0 m by 2.4 m at the International Centre for Indoor Environment and Energy of Technical University of Denmark and the whole experimental procedure and results are reported in Chapter 6.

Fire dynamic simulator, FDS [4], is the software used for this study. Previous works ([5] and [6]) show that FDS could be used for air movement in room application.

The model should be as much as possible similar to the real test room during the experiments but at the same time the fluid dynamic techniques recommend to simplify the system, to focus on the parameters of main interest, limiting the computing effort and the simulation time. The importance of reducing the time for simulation is fundamental if an extensive study with many boundary conditions should be done, in order to individuate critics and benefits on indoor environment for each case.

In this work the final model was found after many attempts, using the information from experiments to build the model and to check if it was appropriate. This information is:

- the measured surface temperatures in steady state conditions;
- the measured air supply temperatures and air flow rates in the test room in steady state conditions;
- the measured air velocity profiles and vertical air temperature profiles;
- the experimental results about contaminant removal effectiveness and local air change index;
- The smoke test visualizations.

A selection of the cases available from experiments have been done, in order to focus on the main parameters characterizing mixing ventilation systems in residential rooms and displacement ventilation in offices.

In regards to mixing ventilation, experiments highlighted the effect of different positions of extract air terminal (exhaust) with the same supply air terminal and boundary conditions: for this reason simulations were carried out assuming supply air terminals on the upper part of a wall and extract air terminals just below the supply or at floor level, as described for systems M1 and M2 in Chapter 6. In order to assess the air distribution under typical residential winter and summer conditions, the same boundary conditions of cases M1-1 and M2-1 for heating, of M1-2 and M2-2 for mixing ventilation combined with a floor heating system, of M1-3 and M2-3 for warm air combined with a floor cooling system and finally the conditions of cases M1-5 and M2-5 for mixing ventilation coupled with a floor cooling system were adopted. Details of the cases are reported in Table 8. 1.

In regards to displacement ventilation, experiments showed that air flow rate affects the air quality and thermal comfort in different way: if high flow rate are adopted, air quality improves

but the risk of thermal discomfort increases as well. Even if many boundary conditions were tested during experiments, only two cases were adopted; they corresponded to a typical situation of office with ventilation rate of 3 ACH and 2.1 ACH (limit for low polluted building category I and II respectively according to Standard ISO 15251 [7]), that are cases DV-3 and DV-4.

Table 8. 1 Measured boundary conditions and calculated heat flow rates for the 10 cases used for CFD study

		Mixing ventilation from wall and with exhaust at high level				Mixing ventilation from wall and with exhaust at low level				Displacement ventilation	
CASE		CASE M1-1	CASE M1-2	CASE M1-3	CASE M1-5	CASE M2-1	CASE M2-2	CASE M2-3	CASE M2-5	CASE DV-3	CASE DV-4
θ_{sp}	°C	22.0	22.0	26.0	26.0	22.2	22.0	26.3	26.1	26.0	26.2
Φ_w	W	-217.9	-217.9	419.2	546.2	-227.0	-218.9	388.8	422.4	461.0	455.5
Φ_w'	W/m^2_{floor}	-13.0	-13.0	25.0	32.5	-13.5	-13.0	23.1	25.1	27.4	27.1
θ_w	°C	18.6	18.6	32.6	34.5	18.6	18.6	32.4	32.7	33.2	33.3
Φ_i	W	90.0	90.0	90.0	90.0	90.0	90.0	90.0	90.0	520.0	520.0
$\Phi i'$	W/m^2_{floor}	5.4	5.4	5.4	5.4	5.4	5.4	5.4	5.4	31.3	31.3
q_v	l/s	5.6	5.6	5.6	5.6	5.6	5.6	5.6	5.6	33.6	23.5
q_v	h^{-1}	0.5	0.5	0.5	0.5	0.5	0.5	0.5	0.5	3.0	2.1
θ_s	°C	30.3	17.1	30.3	18.9	31.6	17.0	29.9	19.1	22.3	20.1
θ_e	°C	24.1	21.3	26.8	25.4	22.4	21.6	24.2	24.5	28.2	28.2
Φ_v	W	42.1	-28.7	23.5	-43.9	61.9	-31.0	38.8	-36.2	-242.4	-232.3
Φ_v'	W/m^2_{floor}	2.5	-1.7	1.4	-2.6	3.7	-1.8	2.3	-2.2	-14.4	-13.8
Φ_f	W	-27.3	343.2	-755.4	-522.0	-36.3	314.2	-833.9	-341.6	-741.3	-754.0
Φ_f'	W/m^2_{floor}	-1.6	20.4	-45.0	-31.1	-2.2	18.7	-49.6	-20.3	-44.1	-44.9
θ_f	°C	21.8	23.8	19.6	21.6	21.8	23.7	19.2	23.2	19.7	19.8

The CFD model was built in FDS software, so all the decisions were done taking in account the specifics of the software. Anyway many assumptions and procedures followed in this work could be adapted to other CFD software whenever an experimental studies on indoor climate in a room should be completed with a computational fluid dynamic analysis.

The FDS software

FDS is a computational fluid dynamics program that was developed to model fires in enclosures, but it was demonstrated [5] that it is suitable for solving different airflow problems in a room (natural, forced and mixed convection airflow).

FDS solves numerically a form of the Navier-Stokes equations appropriate for low-speed (Mach number less than 0.3), thermally-driven flow. The partial derivatives of the conservation equations of mass, momentum and energy are approximated as finite differences and the solution is updated in time on a three-dimensional, rectilinear grid. Thermal radiation is computed using a finite volume technique on the same grid as the flow solver.

Turbulence is by default treated by means of Large Eddy Simulation (LES). LES is a technique used to model the dissipative processes (viscosity, thermal conductivity, material diffusivity) that occur at length scales smaller (subgrid- scale) than those that are explicitly resolved on the numerical grid; the dependent variables (e.g: velocity, pressure, temperature) are decomposed into a volume average part and a fluctuation. Turbulent viscosity is modeled according to Smagorinsky [8] and the default Smagorinsky constant is 0.2 [9], while turbulent Prandt number Pr_t and turbulent Schmidt number SC_t are 0.5.

Werner and Wengle model [10] is adopted for the treatment of viscous stress at the wall.

Visualization of FDS results is possible with another program, Smokeview [11], that produces images and animation.

The geometry

The CFD simulations were carried out in room with the same dimensions of the real test room, but with some necessary simplifications: the two doors were not considered and the six internal surfaces were considered to be perfectly flat.

The real experiments required a table, a thermal manikin sitting on a chair, one or two desk lamps, one or two computer-boxes and a thermal dummy with human shapes on a chair. Besides, different supply and extract air terminals for mixing ventilation or displacement ventilation were used to provide for the required air flow rate.

Each element was modeled for simulation in order to maintain the right proportions and the relative position with the other elements in the room.

The CFD program adopted does not allow circular shape in the geometry, so all shapes were reduced to cubes or parallelepipeds.

Details of geometry are described below.

The thermal manikin with human shape was simplified in four parts, corresponding to legs, thighs, trunk and head, or in six parts if the effect of the two arms should be included. Legs were considered united because of the sitting position of the manikin, while the two arms were considered separately and outstretched on the table, like in the real position. In order to simplify the model, feet and hands were not considered. The sizes of each part were chosen taking in account that the height of each part (in particular the head) and the relative positions of the elements (for example: the legs located under the table) could influence the air flow pattern near the manikin and the characteristic of thermal plume from it.

The total area (exposed to the environment) of the simulated manikin should be the same of the real manikin. Obviously a perfect match was not possible, also because the complex human shapes with winter or summer clothes was not well represented by using square shapes .

Besides, the discretization adopted in CDF model limited the minimum size of the shapes.

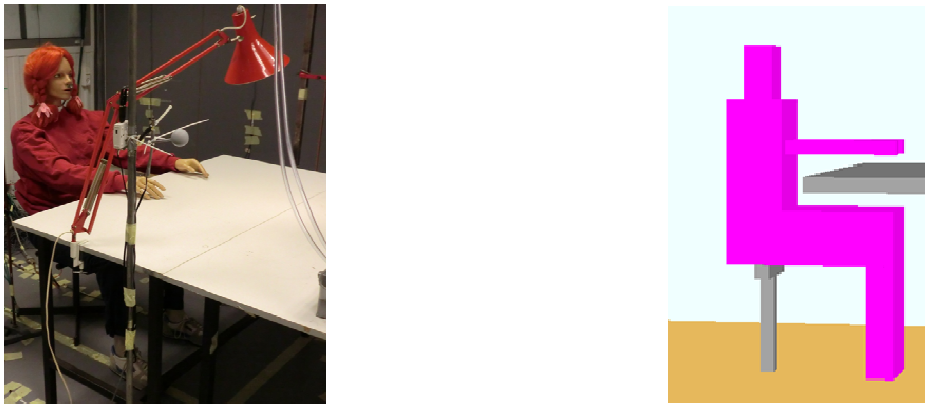

a *b*

Figure 8. 1 Thermal manikin used for experiments (a) and simplified for simulation in 6 parts (b)

The thermal dummy consists in four metal parts with approximately a human shape in sitting position. The parts are a parallelepiped for the trunk, a cylinder for the head and two cylindrical folded elements for the legs. The model considered four square shapes: besides the head and the trunk, the two legs are considered joined together but divided in two part (lower part near the floor and upper part connected to the body). As for the manikin, also for the thermal dummy sizes were chosen in order to maintain the total area (exposed to the environment), the right proportions and the relative positions of the parts with respect to the table and the floor.

a

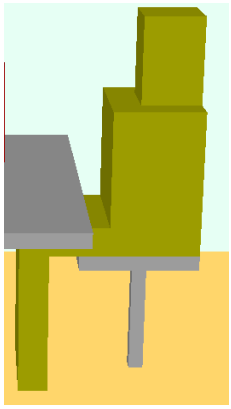

b

Figure 8. 2 Thermal dummy used for experiments (a) and simplified for simulation in 4 parts (b)

The two boxes representing the personal computer have cone shape and they are symmetrically placed on the table, in front of thermal manikin and of the thermal dummy. They were modeled like parallelepipeds maintaining the same area.

a

b

Figure 8. 3 Simulating PC boxes and desk lamps used for experiments (a) and simplified for simulation in parallelepiped shapes(b)

The desk lamp has a complex shape if it is considered with all the parts, but the only interesting part for the thermal effect is that one around the bulb; for this reason the desk lamp was considered as a cube suspended in the volume (Figure 8. 3).

About the table and the two chairs, they are passive elements on the thermal balance of the environment, they only could influence the air flow pattern. Anyway simplifications due to the small size of the table legs and the back of the chair were necessary.

The omnidirectional contaminant source used for the evaluation of the contaminant removal effectiveness from measurements in the test room is a parallelepiped sponge with the end of a tube inside (coming from Innova 1303, as reported in Chapter 6). The source was attached to a metal support (Figure 8. 4 a) or attached directly on the thermal dummy (Figure 8. 2 a) when present. The contaminant source for simulation was chosen with the smaller size possible, that is the cell size, and with only two faces spreading contaminant, the one toward the floor and the one toward the manikin (Figure 8. 4 b). This assumption was in order to simplify the phenomenon, also taking into account that the gas adopted tends to fall because of its weight (it is higher than air) and tends to be diffused toward the manikin because of the pressure in the plastic tubes from Innova Instrument.

The table geometry was slightly modified when additional studies about the contaminant source were carried out: in the model n° 2 the table is 20 cm smaller in order to leave the zone under the source free.

a *b*

Figure 8. 4 Contaminant source attached to a metal support used for experiments (a) and simplified for simulations(b); the faces spreading contaminant are in blue.

The grid

The prediction of the air flow is based on a solution of differential equations solved through a numerical method. The room is divided into grid points and the differential equations are formulated and solved around each grid point. A fine grid allows to reduce the risk of turbulence modeling errors but at the same time increases the computational effort and the simulation time. If the aim of the study was to evaluate the effect of turbulence in a particular zone, for example near the ventilation terminal or near the manikin, a fine grid or adaptive grid could be used. An adaptive grid is a grid which is modified according to different criteria, like

the distribution of different variables in the volume (e.g.: velocity) or according to the boundary [12]. Anyway the aim of this study is to evaluate indoor environment in the whole room equipped with different ventilation systems with several combinations of internal heat gains and boundary conditions. Many phenomena occur near the air diffuser, near the heat gains and near the window, so smaller size grids should be requested in too many positions to have an acceptable simulation time. At the same time each boundary condition changes the air flow pattern so the zone where the turbulence could be a problem for numerical calculations differs for each condition. For all this reasons in this work only three simple grid types were adopted, with cubic or rectangular cells like FDS allows. The difference in the cells size is due to different simulation times and to boundary conditions near the floor, as it will be explained later.

Grid type 1 (Figure 8. 5 a) was used in order to study the effect of ventilation combined with floor heating/cooling on air temperature and air velocity in the room. In particular it was used for mixing ventilation in winter (cases M1-1, M1-2, M2-1 and M2-2) and for both the cases of displacement ventilation (cases DV-3 and DV-4). Cell sizes were (0.05 x 0.05 x 0.05) m so the total number of cells was 322,560.

Grid type 2 (Figure 8. 5 b) was used for the case of floor cooling in a room with mixing ventilation, that is for case M1-3, M1-5, M2-3 and M2-5. Actually two different grids were adopted: rectangular cells with dimensions (0.1 x 0.1 x 0.2) m in the lower part of the volume up to 1.0 m from the floor, and cubic cells (0.05 x 0.05 x 0.05) m in the upper part of the volume, for a total of 196,560 cells.

Grid type 3 (Figure 8. 5 c) was used for all the 10 cases of mixing and displacement ventilation when simulations were carried out in order to evaluate the contaminant distribution in a room, that is for air quality studies. Since air quality studies require that steady state concentration has reached in all the volume and the time for this could be high (particularly with low air change rates), the chosen grid should be coarser with respect to type 1. Cell dimensions were (0.1 x 0.1 x 0.1) m, therefore the total number of cells was 161,280.

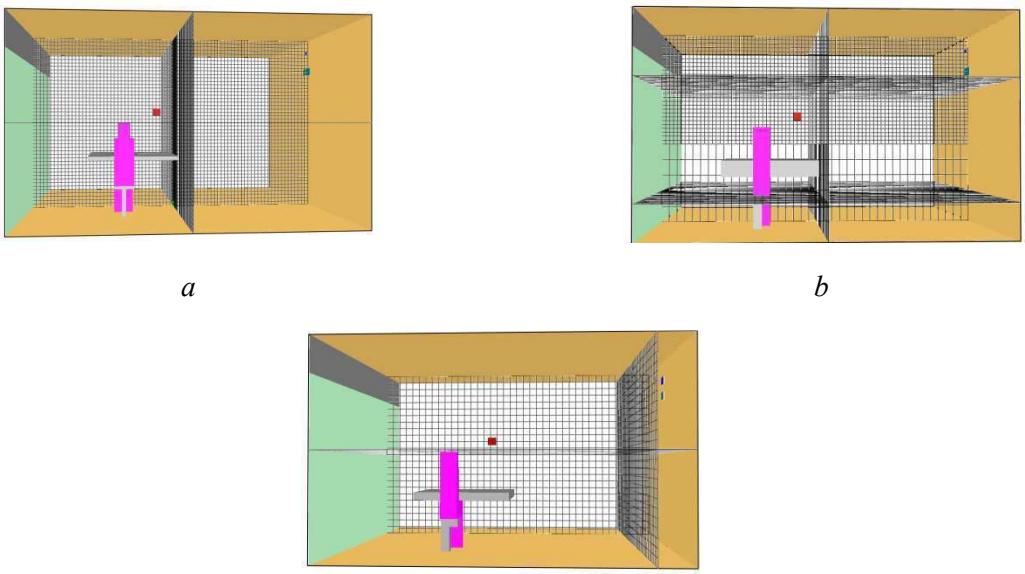

a *b*

c

Figure 8. 5 Different grids adopted: type 1 (a), type 2(b) and type 3(c)

The boundary conditions

Measured air flow rates and surface temperatures from experiments were used as input for CFD simulations.

In order to consider the vertical gradient temperature, each vertical wall (except window) was divided into a lower part (from floor to 1.5 m height) and an upper part (from 1.5 m height to the ceiling), and the corresponding average temperatures from sensors during test were calculated.

Since the panels simulating window did not cover completely the room wall, free spaces remained near the floor edge and near the ceiling, where water pipes have been accommodated. In the model the window was considered divided in two horizontal parts and until 2 m height from the floor. An adiabatic surface occupied the upper part of the wall where window was placed. In the real test the heat transfer in that area was quite complex, because pipes with hot or cold water directed to the radiant panels were not well insulated. Anyway, since the aim of the work was to evaluate the effect of a window on thermal environment in winter and in summer, the simplification of one adiabatic surface in that area was necessary.

The contaminant source was assumed adiabatic for all simulations (model n° 1) or with the same temperature of the floor (model n° 2); this in order to take into account that tubes with gas during real tests were in contact with the floor.

The supply air terminals and the extract air terminals

The positions of the supply air and extract air terminals were maintained in the model as far as possible similar to the actual positions.

The physical parameters at the supply diffuser should be known because they represent important boundary conditions for CFD simulations. The zone near the air supply terminal is characterized by turbulence, high pressure and velocities that should be specified. Anyway the flow from a diffuser is often determined by very fine details (for example, holes in a perforate surface) with sizes less than the other objects in the volume. This means that the grid should be very accurate near the diffuser, with a higher number of cells and with a significant increase of computing time and prediction cost. To avoid this problem, different methods are suggested.

The most simple method is called "Simplified Boundary Conditions" [12] and consists to replace the actual diffuser with one with less complicate geometry able to supply the same quantity of air maintaining the same momentum. This could be obtained if the total effective area of the diffuser is maintained in the new diffuser.

Boundary conditions could be applied at the diffuser using only a few grid points and velocity profiles could be prescribed for the volume in front of the supply air terminal: this method is called "Prescribed Velocity Method" and it was described in [13]. Velocity profiles can be based on measurements or analytical solution of the wall jet.

Another method is called "Box Method" [1] and consists to specify the air jet flow close to supply air terminal, along the surfaces of a box built around it; in this way it is not requested to describe the air flow in the immediate closeness of the supply diffuser and the grid could be not so fine in that area. This method can be based on measurements.

In this work the model of the supply air terminal was carried out with methods similar to the previous methods, using the input commands available by FDS software. The most appropriate method for each situation was chosen based on the measurements results and air flow features.

In regards to wall mounted supply air terminals, the real geometry of the diffuser was quite complex to be modeled in details: the small holes on the surface (Figure 8. 6 a) could be not reproduced with the chosen discretization. Meanwhile the small distance between supply and extract air terminals in some cases (system M1) and the low velocities (because of the low flow rates) could give problems with air flow pattern because of the risk of short circuit during simulations.

For this reasons the "Simplified Boundary Conditions", eventually with the implementation of a sort of "Prescribed Velocity Method" was used.

The effective area of the wall mounted diffuser is about 16% of the total area (about 0.02 m^2), because the air flow comes from little holes. The diffuser is placed on a box 20 cm thick and the surfaces are not completely flat. Since exhaust opening is on a box 20 cm thick (the same where supply is placed or on another near the floor), the first simplification was to eliminate this elements and placed both air supply and exhaust openings directly on the wall.

In order to maintain the same effective area, that is the same air jet momentum, the simulated supply opening should have the 0.16% of the actual diffuser (0.0032 m^2) and at the same time have size not less than grid size. Because of the adopted grid size, an effective area of 0.0050 m^2 for the supply opening was chosen. The smoke test visualizations carried out during experiments were used to check if the model was correct through comparison with simulation. Case M1-2, with cold air and floor heating, was chosen for this comparison, because the cold air falling down is easily visible during smoke test. It was found that the same air flow at the same temperature fell in the same area (near the desk lamp on the table), so the supply opening model was considered appropriate. Also the comparison of measured and calculated air vertical profiles was a valid control instrument (Appendix A and B).

The same method was used for air quality analysis; in this case the grid type 2 was adopted due to simulation time. The air flow rate was twice the air flow rate for thermal analysis, (1 ACH instead of 0.5 ACH) so the diffuser area was chosen twice the previous area, in order to maintain the same supply air velocity.

When exhaust is at high level, the risk of short circuit can be high both in measurements than in simulations and this can strongly influence the contaminant distribution. For this reason the model of supply air terminal was though with a barrier porous to the air 10 cm distant from the supply air terminal and with the same area (Figure 8. 7 b). Velocity was imposed to the barrier in order to define the turbulence 10 cm distant from the supply air terminal and to avoid the risk of short circuit. This method is conceptually near the Prescribed Velocity Method.

In regards to the displacement ventilation terminal, the complex geometry (perforated semi cylindrical device) was not easy to transform into a model. The circular shape allows an airflow diffusion angle of 180° from the terminal. Since circular shapes are not allowed with the program FDS, the simplified model shown in Figure 8. 9 (a) was adopted. The method here presented is similar to the “Box Method” described before.

For thermal analysis simulations, displacement ventilation terminal consisted of a box with five parts, with different orientations but the same area. For the three central parts the velocity directions were chosen in order to diffuse uniformly the air flow in the volume, that is with

angles of -0.45°, 0° and +0.45° with respect to the normal of the wall where the diffuser was placed. The other two parts were placed on the other vertical surfaces of the box and air flow was diffused with an angle of -90° and +90° with respect to the normal of the wall. After a comparison with measured air velocity and temperature profiles in front of the diffuser (position S6), it was assumed a ratio of 0.4 between holes area and global area of the diffuser. Smoke test visualizations did not give significant information when cold air entered near the floor from a displacement ventilation terminal. The factors limiting the area definition for this terminal were not only the discretization assumed (each change should be a multiple of the grid size), but also the division in five equal parts to have uniform diffusion. The resulting model was similar to what recommended in [12] for displacement ventilation systems.

For ventilation effectiveness and air quality analysis, displacement ventilation terminal consisted of a box with one opening, with area equal to the sum of the five parts described before. Since the air flow rate and the total area were constant, velocity and momentum did not change. This choice was because a different grid size has been adopted.

When necessary (if gas entered together with primary air), a barrier porous to the air, with the same function of that presented before (for wall supply air terminal) was adopted.

The models of the extract air terminals were more simple than those of supply air terminals: perforated surfaces or circular ceiling diffuser were simplified like rectangular shape. The most important parameter for exhaust openings was the air flow rate; the transverse velocity components were set to zero and the longitudinal exit velocity was calculated with mass balance. In order to reduce the complexity of the fluid pattern where the air is extracted and to limit the calculation effort in zones not so significant for indoor environment studies, it was decided to assume low velocities at the extract air terminals.

a *b*

Figure 8. 6 Wall mounted supply (up) and extract (down) air terminals for mixing ventilation (a) and displacement ventilation terminal (b) in the test room

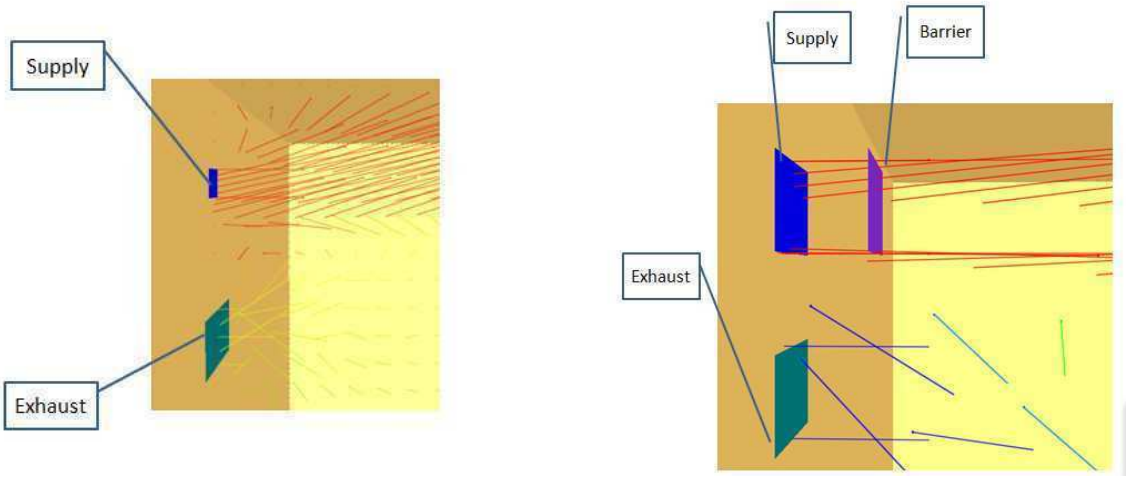

a *b*

Figure 8. 7 Different models of mixing ventilation terminals for system M1: for thermal analysis (a) and for ventilation effectiveness (b)

a *b*

Figure 8. 8 Different models of mixing ventilation terminals for system M2: for thermal analysis (a) and for ventilation effectiveness (b)

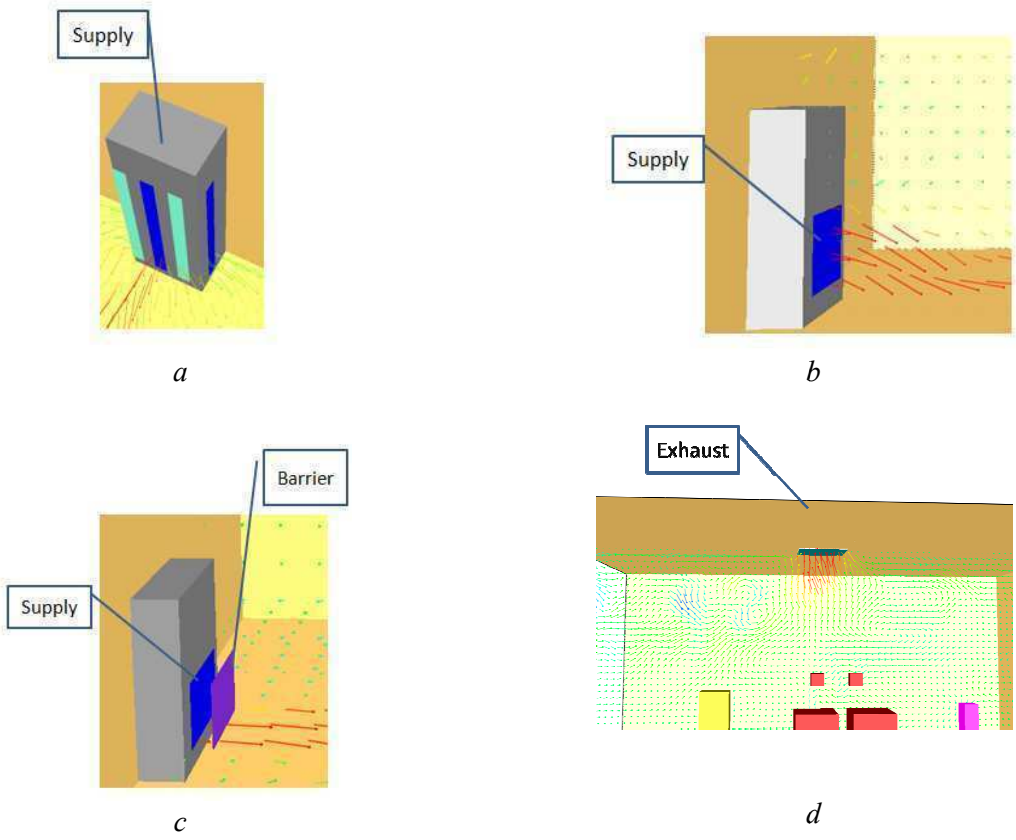

Figure 8. 9 Different models of displacement ventilation terminals (system DV): supply for thermal analysis (a), supply for ventilation effectiveness analysis without barrier(b) and with barrier (c) and extract air terminal (d)

The internal heat gains

The internal heat gains have a strong influence on the thermal condition of the room during experimental tests. Each element exchanges with the air and with the other surfaces in different way, depending also from the boundary conditions. In regards to the manikin, the specific heat transfer for the whole body was known for all the conditions (from experiments); for the others elements, that are PC boxes, desk lamps and thermal dummy, the electric power was known.

But in order to simplify the phenomena specific heat flow rates (expressed in kW/m^2) at the surface were considered independent from the boundary conditions. Once defined the geometry shapes for the manikin, thermal dummy, PC box and desk lamp, the specific heat flow from them was given as input.

The specific heat flow rate was given as net heat flow or as convective and radiant heat flow rate (but table and chairs were considered adiabatic for all cases).

In the first method 80 W from the manikin and 20 W from the desk lamp were imposed to the model and the program calculated by itself the distribution between convective and radiant heat flow rate according to the boundary conditions. It was applied to the model when mixing ventilation was studies for thermal analysis.

In the second method convective heat flow rate was assumed to be the 60 % of the total heat flow rate (or 80% for desk lamps), that is 80 W for manikin, 110 W for thermal dummy, 100 W for each PC box and 20 W or 60 W from desk lamp. The remaining radiant heat flow rate Q_{rad} was imposed through the definition of the surface after a simplified calculation of the surface temperature T_s. In equation (8.1) the mean radiant temperature of the room T_{mr}. is assumed equal to the measured operative temperature and the radiant heat transfer coefficient h_{rad} is assumed of 5.5 W/(m^2K).

$$T_s = T_{mr} + \frac{Q_{rad}}{h_{rad}} \qquad \textit{Eq. 8. 1}$$

Radiant emissivity was assumed of 0.9 for all the elements in the model.

This second method was applied to the model for ventilation effectiveness studies and for thermal analysis with displacement ventilation systems.

The convective heat flow rate from PC boxes, thermal dummy and manikin was assumed to be the 80% of the total heat flow rate for one case of displacement ventilation only and this configuration was called model n° 3.

Table 8. 2 Internal heat gains definition details for the 3 systems

System	Thermal analysis	Ventilation effectiveness
M1	Net heat flow rate imposed; 100 W tot	Convective and radiant heat flow rate imposed; 100W tot
M2	Net heat flow rate imposed; 100W tot	Convective and radiant heat flow rate imposed;100 W tot
DV	Convective and radiant heat flow rate imposed; 510W tot	Convective and radiant heat flow rate imposed; 510W tot

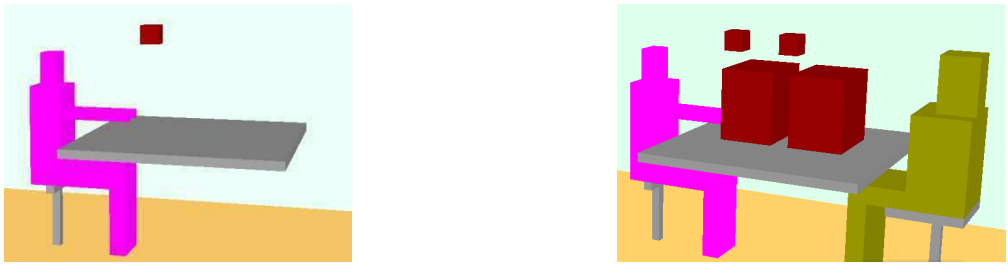

a *b*

Figure 8. 10 Global representation of the internal heat gains for residential room (a) and for office with 2 occupants (b) for thermal evaluation

Natural convection from cooled floors

A particular study about natural convection from floor cooling has been carried out; this because vertical temperature profiles at low heights when floor was cooled were quite different from experimental data, even if the same CFD model allowed a good agreement with measured values in the case of floor heating or floor cooling combined with displacement ventilation.

From experiments it was found that the decrease of the measured temperatures near the floor level did not follow a linear trend, as seen in Figure 8. 11 for case M1-3. The considered temperatures were the average of 13 thermocouples placed on the floor and insulated towards the environment and the averages of 12 air temperature probes moved in 7 positions in the room. The different sensors have been calibrated together in the same conditions, so the temperature values were not affected by systematic errors. But the CFD program calculates a linear interpolation of the temperature between two adjacent cells.

FDS adoptees for the natural convection heat transfer coefficient at the floor the ASHRAE [14] equation (8.2), where ΔT is the temperature difference between the room surface and fluid in the centre of the nearest cell.

$$h_c = 1.52 \cdot (\Delta T)^{0.33} \qquad \textit{Eq. 8. 2}$$

The program allows the user to change the convective heat transfer coefficient from the horizontal floor surface by changing the constant C_h in the following formula:

$$h_c = C\_h \cdot (\Delta T)^{0.33} \qquad \textit{Eq. 8. 3}$$

If the cell size is small, for example 0.05 m (as assumed for grid type 1), the centre of the cell closest to the floor is at 0.025m and, according to Figure 8. 11 for case M1-3, temperature at 0.025 m is less than temperature at higher level even if the temperature gradient in that zone is much higher than that at higher level.

In the model, the convective heat transfer rate Q_c [W/m^2] strongly depends on ΔT according to equation (8.4); this means that if small temperature differences are adopted, Q_c could be different from the real convective heat flow.

$$Q_c = h_c \cdot \Delta T = C\_h \cdot (\Delta T)^{1.33} \qquad \textit{Eq. 8. 4}$$

In order to improve the model when floor cooling was used with low air flows (case M1-3 and M2-3 with warm air or M1-5 and M2-5 with cold air), a particular study has been carried out.

Eleven simulations have been carried out with the same case (M1-3) changing the C_h coefficient and the grid size in the lower part of the room (until 1.0 m height).

A new coefficient C_h was found adapting the value recommended by Olesen et al. [15] to the results of 6 experimental cases with floor cooling (M1-3, M1-4, M1-5, M2-3, M2-4 and M2-5) reported in Chapter 6. The recommended convective heat transfer coefficient was 1.5 W/(m^2 K) for a sitting position, at 0.6 m height from floor, and this value was used to calculate the experimental convective heat flow rate Q_c from the floor for all the 6 tests; knowing the measured floor temperature and the air temperature at 0.05 m and 0.1 m for each test, equation (8.4) allowed to estimate C_h value at 2 different heights. Finally an average value C_h was calculated for each level.

C_h values calculated with this method were called C* and were 2.0 at 0.05 m height and 1.75 at 0.1 m height. Other values for C_h were chosen, multiplied by 2, 3 or 7 the C* values.

Three discretization models were adopted. The differences were only near the floor, because it was not possible to increase the size everywhere without changing the boundary conditions (supply air terminals had small size):

- discretization A - one grid with sizes (0.05x 0.05 x 0.05) m.
- discretization B - two grids: near the floor until 0.1 m the sizes were (0.1 x 0.1 x 0.1) m; the rest of the volume was with smaller sizes (0.05x 0.05 x 0.05 m).

- discretization C - two grids: near the floor until 0.1 m the sizes were (0.1 x 0.1 x 0.2) m; the rest of the volume was with smaller sizes (0.05x 0.05 x 0.05 m).

Convective heat transfer coefficients and convective heat flow rates at the floor were calculated in order to make a comparison between the experimental data and the simulation results. Four methods were adopted and described hereafter.

Method n° 0 consisted in the calculation of the heat transfer coefficient h_c and the heat flow rate Q_c with equations (8.3) and (8.4) assuming C_h= C* (corresponding to the cell-centre level) and considering the measured average temperature difference between the floor and the height corresponding the first node (the nearest to the floor).

Method n° 1 consisted in the calculation of the heat transfer coefficient h_c and the heat flow rate Q_c with equations (8.3) and (8.4) assuming C_h = C* (corresponding to the cell-centre level) and considering the measured average temperature difference between floor and the height corresponding the centre of the first cell (the closet to the floor).

Method n° 2 consisted in the calculation of heat transfer coefficient h_c and the heat flow rate Q_c by equations (8.3) and (8.4) taking the C_h value adopted for simulations; the temperature difference was between the floor and the average temperature of all the nodes closest to the floor (output of the simulation).

Method n° 3 consisted in the calculation of the heat transfer coefficient and of the heat flow rate Q_c directly by the CFD program. In this case the difference temperature was between the floor and the centre of the cells closest to the floor.

Table 8. 3 reports grid details (node distance from the floor), the C_h adopted (expressed as a multiple of the C* calculated for 0.05 m and 0.1 m) for the eleven tests carried out in this analysis.

Convective heat transfer coefficients and convective heat flow rates calculated by using measured values (methods n° 1 and n° 2) were compared with those obtained using calculation (methods n° 3 and n° 4). Particularly interesting was method n° 3, because it represents the real output of the simulation; the direct comparison with method n° 1 or, if not possible, with method n° 0 (with discretization n° 1), allowed to evaluate the quality of the simulation.

Another important parameter to consider was the difference temperature between the floor and the first node or the centre of the adjacent cell: the measured floor temperature was adopted in simulation, so temperatures near the floor should be as much as possible similar to experimental data. Since the convective heat flow from experiments with method n° 0 for test n° 1 was 112.4

W, as reported in Table 8. 4, strongly higher than that calculated from simulation (method n°3) with default C_h (42.6 W), the choice of a new C_h value and of a new grid was in order to limit this difference.

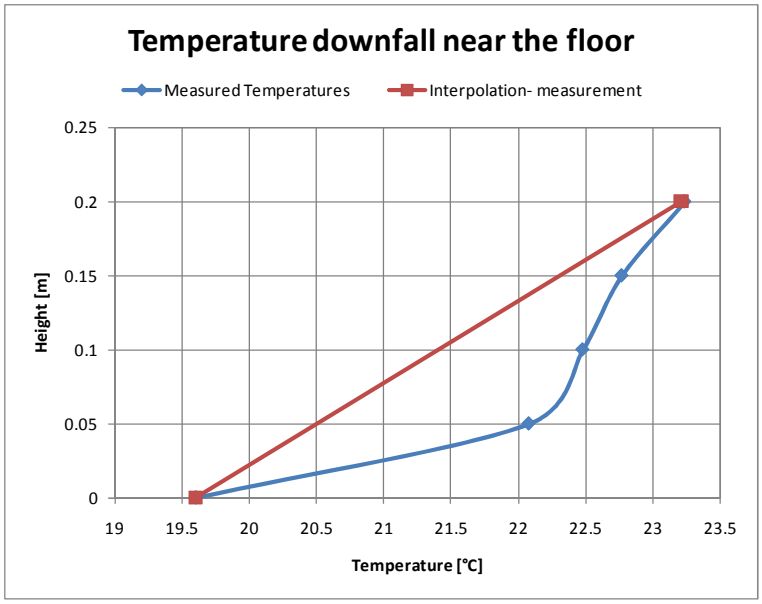

Figure 8. 11 Temperature downfall near the cooled floor from measurements and linear interpolation of the measured temperatures from 0.2 m height to the floor level for case M1-3

Table 8. 3 C_h adopted, C* considered and distance of the first node from the floor for the 11 simulations

test N°	constant C_h value	C value details	C*	Node distance from floor
				[m]
1	1.52	default		0.05
2	2	C*	2	0.05
3	6	C* x 3	2	0.05
4	14	C*x 7	2	0.05
5	2	C*	2	0.1
6	4	C*x 2	2	0.1
7	6	C*x 3	2	0.1
8	1.75	C*	1.75	0.2
9	3.5	C*2	1.75	0.2
10	5.25	C* x 3	1.75	0.2
11	7	C* x 4	1.75	0.2

Results show that by increasing C_h with the same grid, heat flow rates calculated with method n° 2 increase a lot, while with method n° 3, that is the real simulation output, not always this enhancement exists. Anyway it was found that with bigger cells, predicted heat flow rate increase.

Results from method n° 0 and method n° 1 show how much the convective heat flow calculated from measurements is influenced by the distance from the floor: if the same equation found for the centre- cell level is used with the temperature at the first node, the difference could be high: for example for case n° 8 the convective heat flows with methods n° 0 and n° 1 are respectively 163.8 W and 120.0 W.

The case that allows the minimum difference of heat flow rate with respect to measured heat flow rate is case n° 10 (-21 %), but the air temperature difference with respect to measurements at node level is very high.

Case n° 8 allows the minimum difference of air at node level (+0.17 °C) but the convective heat flow is enough distant from the measured value (-41.2%).

From cases n° 10 and n° 11 it is evident that by increasing the C_h value, the convective heat transfer coefficient increases from 5.27 to 6.59 W/(m^2K), but the convective heat flow rate Q_c decreases because also the temperature difference decreases. So the calculated heat flow rate comes from a combination of factors and the increase of the C_h value with the same discretization does not increase always the convective heat flows.

Case n° 9 represents the best compromise between air temperatures at node level simile and heat flow rate simile. Anyway the difference at 0.1 m height is still important for a reason due to the disagreement between simulations and measurements.

Case n° 9 model found for case M1-3 was adopted for the remaining cases of natural convection from cooled floor of this study, that are cases M1-5, M2-3 and M2-5 and discretization C, corresponding to grid type 2 of Figure 8. 5 (b) was used.

Table 8. 4. The 4 methods results for all cases- Convective heat flow rate Q_c [W] and convective heat transfer coefficient h_c [W/(m^{2}K]

test N°	mesh distance from floor	C*	C_h	Qc,0	Qc,1	Qc,2	Qc,3	hc,0	hc,1	hc,2	hc,3
				W	W	W	W	W/m^{2}K	W/m^{2}K	W/m^{2}K	W/m^{2}K
1	0.05	2	1.52	112.4		76.9	42.6	1.28	0.00	76.87	1.75
2	0.05	2	2	112.4		89.6	41.6	1.28	0.00	1.02	0.47
3	0.05	2	6	112.4		217.0	49.8	1.28	0.00	2.47	0.57
4	0.05	2	14	112.4		417.7	51.8	1.28	0.00	4.74	0.59
5	0.1	2	2	96.7	112.4	146.1	55.9	2.84	2.70	2.88	2.31
6	0.1	2	4	96.7	112.4	234.6	62.3	2.84	2.70	5.45	4.01
7	0.1	2	6	96.7	112.4	315.8	67.8	2.84	2.70	7.97	5.48
8	0.2	1.75	1.75	163.8	120.0	172.4	68.3	2.68	2.48	2.71	2.21
9	0.2	1.75	3.5	163.8	120.0	283.1	84.4	2.68	2.48	5.17	3.84
10	0.2	1.75	5.25	163.8	120.0	383.6	91.8	2.68	2.48	7.56	5.27
11	0.2	1.75	7	163.8	120.0	478.0	87.4	2.68	2.48	9.91	6.59

Table 8. 5 Distance from the floor of the closest node level and of the centre of the closest cell, air temperature difference between calculation (CFD) and measurements (M) at the closest node level and at the centre of the closest cell

test N°	Node distance	Centre cell distance	T-node M	T-cell M	T-node CFD	T-cell CFD	ΔT-node	ΔT- cell
	Z [m]	Z [m]	°C	°C	°C	°C	°C	°C
1	0.05		22.17		21.9		-0.28	
2	0.05		22.17		21.7		-0.48	
3	0.05		22.17		21.4		-0.79	
4	0.05		22.17		21.1		-1.03	
5	0.10	0.05	22.43	22.17	22.62	21.1	0.19	-1.03
6	0.10	0.05	22.43	22.17	22.16	20.6	-0.27	-1.56
7	0.10	0.05	22.43	22.17	21.96	20.4	-0.47	-1.81
8	0.20	0.10	23.21	22.43	23.38	21.61	0.17	-0.82
9	0.20	0.10	23.21	22.43	22.86	20.92	-0.35	-1.51
10	0.20	0.10	23.21	22.43	22.62	20.61	-0.59	-1.82
11	0.20	0.10	23.21	22.43	22.47	20.43	-0.74	-2.00

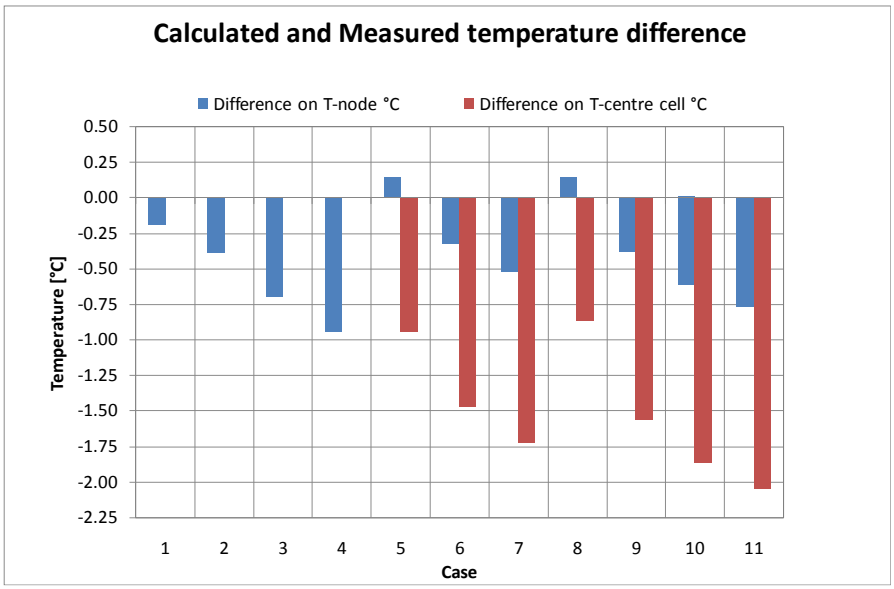

Figure 8. 12 Difference [°C] between calculated and measured temperatures of air. The air temperature refers to the closest node level and to the centre of the closest cell

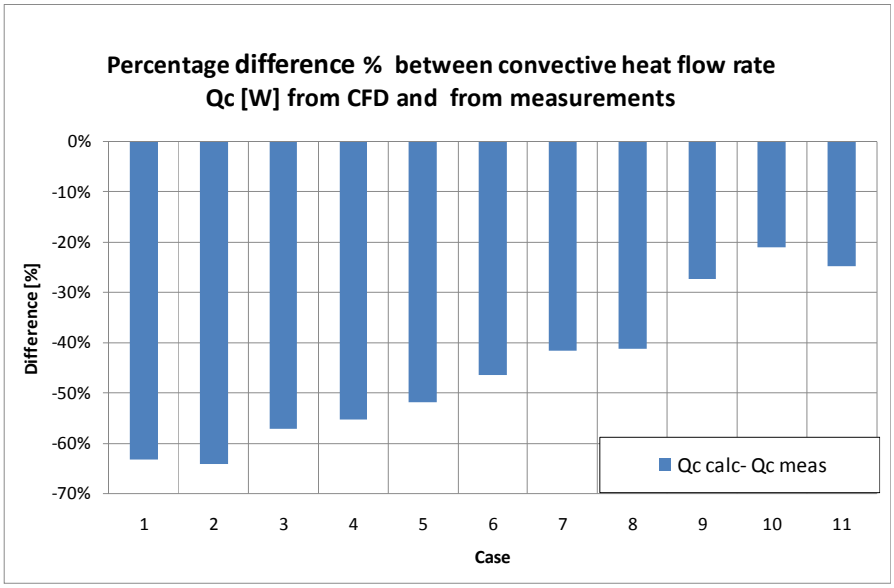

Figure 8. 13 Difference [%] between measured and calculated heat flow rates Qc [W]

8.2.2 Thermal comfort evaluation

Thermal comfort parameters were investigated by means of CFD simulations, using the grid type n° 1 or type n° 2. For all the cases model n° 1, with real size of the table, was adopted.

Temperature, air velocity and all the three components of velocity were available in all the volume at the end of each simulation (when steady state was reached) and 3 dimensional visualizations were available. This kind of information could give the opportunity to highlight some particular phenomena occurring in the room.

Besides, vertical air temperature and air velocity profiles were calculated in 7 positions at different heights; these positions were the same described in Chapter 6 and reported in Appendix A, therefore a comparison with measured values has been carried out.

Air temperature was calculated from 0.2 m (or 0.1 m for displacement ventilation) until 1.7 m height, while air velocity was calculated from 0.05 m until 1.8 m height, but only from 0.1 m from the floor when grid n °2 was adopted.

Vertical temperature differences between head level (1.1 m) and ankle level (0.1 m) were calculated for the cases with displacement ventilation DV-3 and DV-4

Draught risk DR [%] according to ISO7730 [16] near the floor (0.1 m) and at head level (1.1 m) was calculated for different cases (M1-1, M1-2, M1-5, M2-1, M2-2 , M2-5 , DV-3 and DV-4) using all simulations data, that is air temperature, air velocity and the standard deviation of the velocity (used to calculate turbulence Tu%).

8.2.3 Ventilation effectiveness evaluation

Studies about ventilation effectiveness guaranteed by mechanical ventilation in the model were carried out using grid n° 3 because computational time necessary to reach steady state conditions was in general much higher than that necessary for thermal analysis. The air change rate adopted for mixing ventilation was 1 ACH instead of 0.5 ACH with the aim of maintain the same air velocity at supply air terminals by using a courser grid. Both contaminant removal effectiveness (CRE) and air change efficiency (ACE) were elaborated via CFD, since contaminants were introduced from a source or mixed with primary air depending on the test.

For all the cases model n° 1, with real size of the table and adiabatic contaminant source (if present) was adopted; model n° 2, with smaller table and surface temperature of the

contaminant source assumed (if present) and model n °3, with higher percentage of convective heat transfer from heat gains, were applied only a few times.

Even if in real experiments both R134a and CO_2 were used for the calculation of ventilation effectiveness, for CFD analysis only CO_2 was adopted. The same quantity of carbon dioxide was assumed both for CRE and for ACE studies, in this way the influence of the position from which the gas entered could be evaluated.

It was assumed that the concentration of CO_2 was 5.5 mg/s for all cases of mixing ventilation and 11 mg/s for all cases of displacement ventilation.

Since the gas entered with slightly different mass flow rates depending on the case during the experiments (from 10 mg/s to 12.5 mg/s), the previous assumption introduced a difference with measurements, but at the same time allowed to compare the different boundary conditions.

Contaminant concentration was monitored in the three position P1, P2, P3 (corresponding to the positions C1, C2 and C3 where measurements have been carried out), near the manikin at 1.1 m (in front of the face) and in the extract air terminal (exhaust). For CRE analysis, concentrations were calculated also in other 3 points, at the center of the room (P5) and on the other side of the table with respect to the manikin (P6 and P7), 0.9 m distant from the nearest wall and respectively 2.3 m and 0.5 m from the window. Finally the spatial average of the contaminant concentration in the volume <c> was calculated.

The air quality index was calculated with equation (8.5), where the c_e is the contaminant concentration in the exhaust air, c_i is the concentration in the point and c_s is the contaminant concentration in the supply air (assumed zero).

$$\varepsilon_P^c = \frac{c_e - c_s}{c_i - c_s} \qquad \textit{Eq. 8. 5}$$

Then, contaminant removal effectiveness CRE at different heights (0.6 m, 1.1 m and 1.7m) were calculated as the average of the air quality indices at the same height obtained from the 7 points.

The contaminant removal effectiveness CRE for the whole room was instead calculated as follow:

$$CRE = \frac{c_e - c_s}{< c > - c_s} \qquad \textit{Eq. 8. 6}$$

Therefore the following parameters were determined:

- air quality index in 7 positions (P1, P2, P3, P4, P5, P6 and P7) at 0.6 m, 1.1 m and 1.7 m height from the floor;
- contaminant removal effectiveness CRE at 0.6 m, 1.1 m and 1.7 m height (average of the previous the air quality indices).

The definitions of air change index ε^a_P and air change efficiency (ε^a or ACE) include the concept of "age of air" τ, introduced by Sandlberg in 1981 [17]. The main age of air, that could refers to a the whole room (called $<\tau>$) or to a point τ_P, is a statistical concept based on the age distribution of the air components in a point. The local mean age of air at exhaust coincides with the nominal time constant τ_n, which real definition is the ratio between the room volume V and the ventilation flow rate q_v.

REHVA [18] gives the instruments to calculate all the previous parameter by using the tracer gas decay technique and the measured concentrations at exhaust and in the monitored points. According to these formula the nominal constant time τ_n is calculated as the integral of the concentration decay curve at exhaust divided by the initial concentration, the local mean age of air τ_P as the integral of the concentration decay curve at the point divided by the initial concentration and finally the mean age of air of the room $<\tau>$ is calculated from the time-weighted area under the curve at exhaust. Anyway in this study $<\tau>$ was calculated also from the volume-weighted average contaminant concentration in all the points.

As already explained in Chapter 6, the air change efficiency is defined as the ratio between the lowest possible mean age of air ($\tau_n/2$) and the room mean age of air $<\tau>$, while the air change index is the ratio between the constant time τ_n and the mean local age of air in the point τ_P.

After the calculations of τ_n, τ, τ_P and $<\tau>$, equations (8.7) and (8.8) could be easily applied. The REHVA method was adapted to the case of step up tracer gas method adopted in experiments.

$$\varepsilon^a = \frac{\tau_n}{2 \cdot < \tau >} \qquad \textit{Eq. 8. 7}$$

$$\varepsilon_P{}^a = \frac{\tau_n}{\tau_P} \qquad \textit{Eq. 8. 8}$$

The following parameters were calculated:

- air change efficiency ACE calculated with equation (8.7) and <τ> calculated from the integral of the weighted-volume average concentration when steady state condition was reached (definition n° 1);
- air change efficiency ACE calculated with equation (8.7) and <τ> obtained from the time-weighted area under the contaminant curve at exhaust (definition n° 2), with the REHVA method;
- air change index in positions P1, P2 and P3, placed in the occupied zone at 0.6 m, 1.1 m and 1.7 m height with equation (8.8).

8.3 Results

8.3.1Thermal comfort results

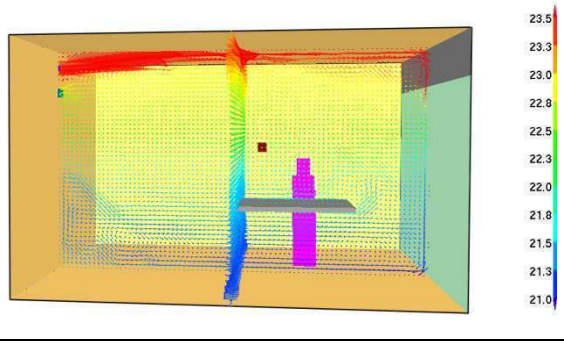

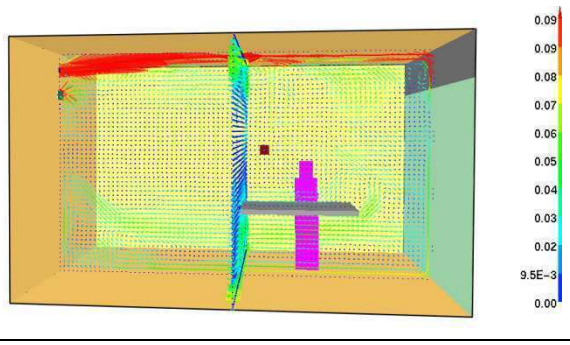

a	*b*

Figure 8. 14 Temperature in [°C](a) and air velocity in [m/s](b) representation along longitudinal and cross section of the room, for a winter case without floor heating (case M1-1)

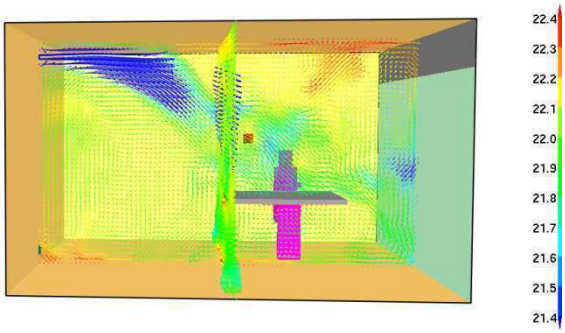

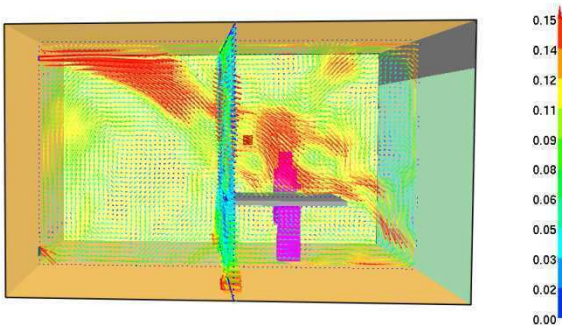

a	*b*

Figure 8. 15 Temperature in [°C](a) and air velocity in [m/s](b) representation along longitudinal and cross section of the room, for a winter case with floor heating (case M2-2)

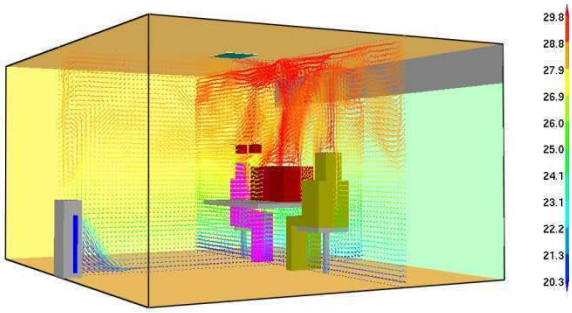

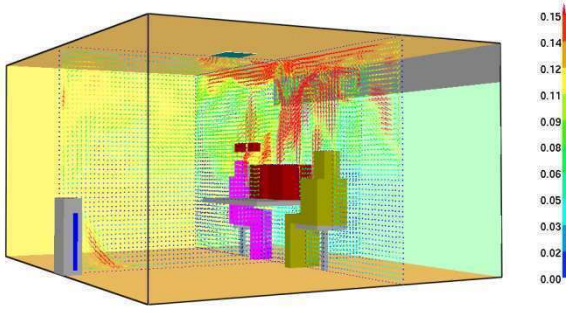

a	*b*

Figure 8. 16 Temperature in [°C](a) and air velocity in [m/s](b) representation along the section crossing supply air terminal and that crossing heat gains, for displacement ventilation (case DV-4)

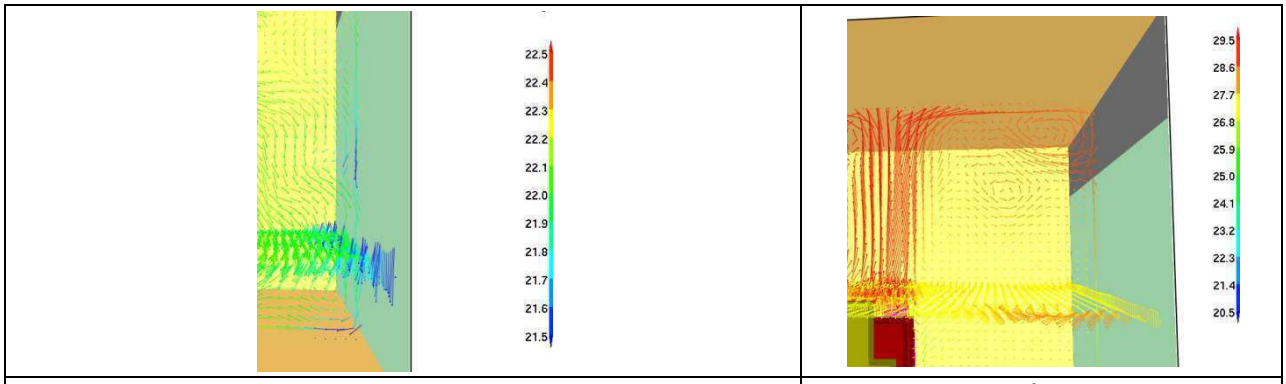

a	*b*

Figure 8. 17 Details of the temperatures in [°C] close to the window in winter (a) and in summer in presence of significant heat gains (b)

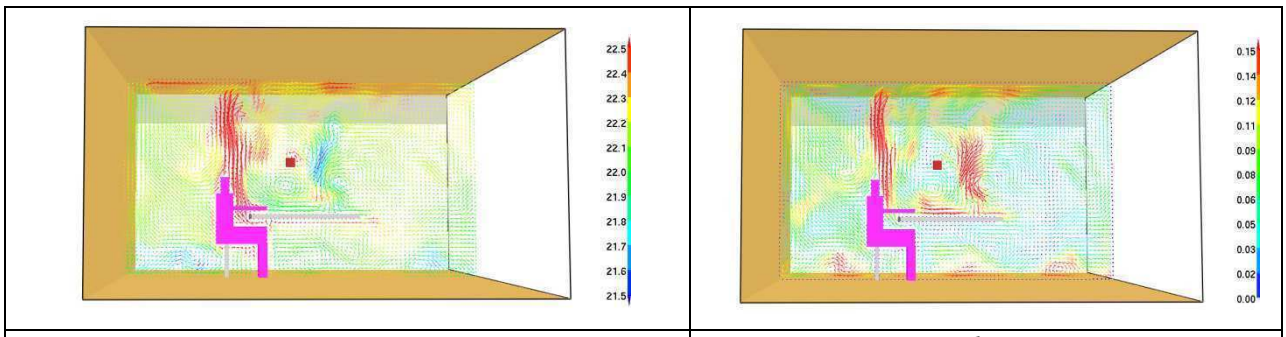

a	*b*

Figure 8. 18 Thermal plume from the manikin in winter case (Case M1-2)- temperatures in [°C], (a) and velocities in [m/s], (b)

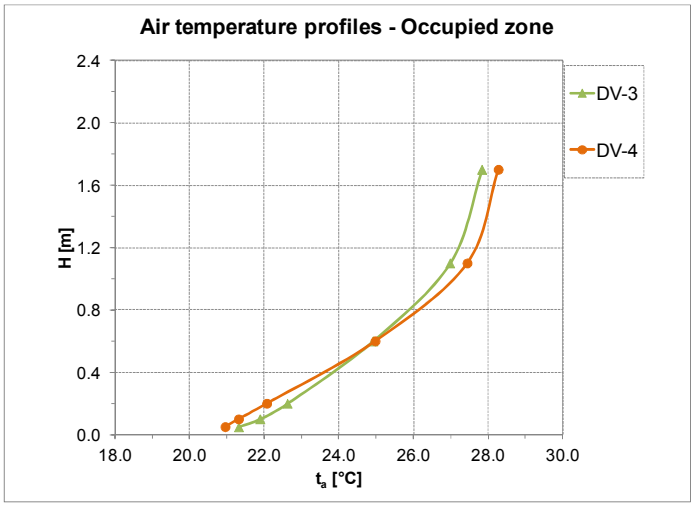

Figure 8. 19 Vertical air temperature profile calculated for displacement ventilation cases in the occupied area (cases DV-3 and DV4)

CFD simulations have been carried out for 8 cases of mixing ventilation and 2 cases of displacement ventilation as described before.

Air temperature and air velocity were studied separately by means of three dimensional representations when steady state was reached, in order to individuate the main features of each condition. Figure 8. 14 and Figure 8. 15 show the air temperature and velocity distribution for 2 cases of mixing ventilation in winter: as easily predictable, when the same air flow rate is introduced in the room at lower supply temperature (Figure 8. 15), the occupied zone is affected by higher velocities (up to 0.15 m/s) and colder temperatures at head level (in the range between 1.m and 1.7 m height). The thermal plume starting from the warm manikin interacts with the cold air and, also for the table presence, a quite complex air flow originates in that area (Figure 8. 18). When warm air is used without floor heating, a clear distinction between the lower level (colder) and the upper level, where temperature are up to 2.5 °C higher, is evident in Figure 8. 14.

Another important aspect in winter condition is the effect of the window: even if not so high velocity values are calculated near the window, the cold air falling down has a determinant role to the resulting air movement, as shown in Figure 8. 15 and Figure 8. 17 (a).

Figure 8. 16 shows the temperature and velocity when displacement ventilation with 2.1 ACH is used in an office during a summer day: the cold air near the flow becomes warmer and rises in correspondence of the heat gains and this determines significant vertical temperature gradient, as shown also in Figure 8. 19. In this case the warm air from the window interacts with the warm air from the heat gains, determining a vortex flow as shown in Figure 8. 17 (b).

Vertical air temperature difference $\Delta\theta$ between head (1.1 m) and ankle level (0.1 m) were calculated in seven positions for both case DV-3 and case DV-4. Results confirms that case DV-4 is out of category C of thermal comfort (ISO 7730) if the occupied zone of the room is considered, because $\Delta\theta$ are higher than 4°C. For case DV-3 vertical air temperature differences $\Delta\theta$ obtained from measurements were quite different than those from calculations, even if a better agreement was found in the positions S1, S2 and S7 near the window.

Vertical temperature and air velocity profiles are similar to those obtained from experiments for all the cases (Appendix B); anyway it is evident that with simulation vertical air temperature profiles for the seven positions are similar to each other, except when cold air jet comes directly to the point. Air velocity are generally lower than 0.1 m/s, except near the supply air terminal.

Regards floor cooling cases with mixing ventilation, vertical profiles were obtained by means of two different grids for the reasons explained before; it is evident that in the conjunction zone the curve is deflected.

Calculated DR [%] according to ISO 7730 from simulations are in general comparable with those calculated from experiments for all the 4 cases of mixing ventilation (Table 8. 7 and Table 8. 8): when warm air is used (cases 1 and 3) DR [%] is near zero; when cold air is used (cases 2 and 5) draught risk exists but it less than 10 % (category A) for both simulations and experiments. In regards to displacement ventilation cases, draught rating values from simulations are very close to those obtained from experiments at 1.1 m height, but some differences exist at 0.1 m height (Table 8. 9).

Table 8. 6 Calculated and measured vertical air temperature difference Δθ [°C] between head (1.1m) and ankle level (0.1 m) for 7 positions and maximum value Δθ in the occupied zone

$\Delta\theta_{1.1\text{-}0.1}$ - DV - CFD				**$\Delta\theta_{1.1\text{-}0.1}$ - DV - Experiments**			
Position	Height	Case 3	Case 4	Position	Height	Case 3	Case 4
S1	1.1 m-0.1m	4.9	6.5	S1	1.1 m-0.1m	3.7	3.7
S2	1.1 m-0.1m	5.0	6.3	S2	1.1 m-0.1m	4.2	5.3
S3	1.1 m-0.1m	5.0	6.2	S3	1.1 m-0.1m	0.9	5.3
S4	1.1 m-0.1m	5.2	6.4	S4	1.1 m-0.1m	1.2	5.0
S5	1.1 m-0.1m	5.1	6.3	S5	1.1 m-0.1m	0.9	5.0
S6	1.1 m-0.1m	5.1	6.0	S6	1.1 m-0.1m	1.1	4.7
S7	1.1 m-0.1m	4.9	6.1	S7	1.1 m-0.1m	4.0	5.4
Average occupied zone				**Average occupied zone**			
Max Δθ		5.2	6.4	Max Δθ		1.2	5.3

Table 8. 7 Calculated draught rating DR [%] according to ISO 7730 at 1.1m height in 7 positions and for the occupied zone, from calculated values and from measurements, for 4 cases with system M1

		Draught rating M1 - CFD				**Draught rating M1 - Experiments**			
Position	Height	Case 1	Case 2	Case 3	Case 5	Case 1	Case 2	Case 3	Case 5
S1	1.1 m	0.0	0.8	0.0	1.9	0.1	0.0	0.0	0.9
S2	1.1 m	0.0	0.7	0.0	2.6	0.0	1.5	0.0	0.4
S3	1.1 m	0.0	2.6	0.0	1.6	0.0	7.3	0.0	0.0
S4	1.1 m	0.0	2.6	0.0	0.0	0.0	5.1	0.4	0.0
S5	1.1 m	0.0	0.0	0.0	0.0	0.0	4.3	0.0	0.0
S6	1.1 m	0.0	0.7	0.0	3.8	0.0	2.4	0.0	2.0
S7	1.1 m	0.0	2.9	0.0	0.1	0.1	2.6	0.0	0.0
		Average - occupied zone				**Average - occupied zone**			
Average	1.1 m	0.0	1.5	0.0	1.3	0.0	4.8	0.1	0.5

Table 8. 8 Calculated draught rating DR [%] according to ISO 7730 at 1.1m height in 7 positions and for the occupied zone, from calculated values and from measurements, for 4 cases with system M2

		Draught rating M2 - CFD				**Draught rating M2 - Experiments**			
Position	Height	Case 1	Case 2	Case 3	Case 5	Case 1	Case 2	Case 3	Case 5
S1	1.1 m	0.0	0.0	0.0	1.8	0.6	0.0	0.1	0.7
S2	1.1 m	0.0	1.4	0.0	2.8	1.1	0.1	0.0	0.1
S3	1.1 m	0.0	2.8	0.0	1.4	1.4	4.6	0.0	2.1
S4	1.1 m	0.0	1.5	0.0	0.0	0.0	5.7	0.0	0.6
S5	1.1 m	0.0	0.0	0.0	0.0	0.0	2.5	0.0	0.4
S6	1.1 m	0.0	1.2	0.7	3.6	0.1	2.3	0.0	6.3
S7	1.1 m	0.0	0.0	0.0	0.6	0.0	1.0	0.0	0.6
		Average - occupied zone				**Average - occupied zone**			
Average	1.1 m	0.0	1.4	0.2	1.3	0.4	3.8	0.0	2.4

Table 8. 9 Calculated draught rating DR [%] according to ISO 7730 at 1.1m height in 7 positions and for the occupied zone, from calculated values and from measurements, for 2 cases with system DV

Draught rating DV - CFD				**Draught rating DV - Experiments**			
Position	Height	Case 3	Case 4	Position	Height	Case 3	Case 4
S1	0.1 m	0	0	S1	0.1 m	2.6	1.9
	1.1 m	0	0		1.1 m	0.9	0.8
S2	0.1 m	0	0	S2	0.1 m	3.5	3.7
	1.1 m	1.1	0.9		1.1 m	0	1.1
S3	0.1 m	0	0	S3	0.1 m	3.1	3.6
	1.1 m	2.1	0.7		1.1 m	0	0.6
S4	0.1 m	1.1	0	S4	0.1 m	2.4	3.6
	1.1 m	2.2	2.2		1.1 m	3	2.6
S5	0.1 m	0	0	S5	0.1 m	5.5	7.8
	1.1 m	0	2.4		1.1 m	3.2	3.1
S6	0.1 m	0	0	S6	0.1 m	1	8.6
	1.1 m	0	0		1.1 m	0	0
S7	0.1 m	0	0	S7	0.1 m	1.4	1.6
	1.1 m	1	0.9		1.1 m	0.9	1
Average - occupied zone				**Average - occupied zone**			
Average	0.1 m	0.3	0	Average	0.1 m	3	5.9
	1.1 m	1.1	1.3		1.1 m	1.5	1.5

8.3.2 Ventilation effectiveness results

Contaminant removal effectiveness

Contaminant removal effectiveness values calculated via CFD are higher than 1.7, that is that ventilation effectiveness is very high according to simulations. Figure 8. 20 shows that mixing ventilation with extract air terminals near the floor could guarantee CRE values higher than displacement ventilation at 1.1 m and 1.7 m height; anyway if one considers the contaminant removal effectiveness for the whole room CRE (Figure 8. 21) the difference is not so evident.

Figure 8. 22 and Table 8. 11 show the influence of extract air terminals (exhaust) position on contaminant removal effectiveness with the same boundary conditions when mixing ventilation is used for heating or cooling; the choice of exhaust near the floor is always better since the percentage difference varies from + 25. 6% when floor heating is adopted, up to 118 % with floor cooling and + 130.6 % when heating is only with warm air. From experimental studies, exhaust near the floor was better only for the heating cases, not for the cooling cases. Details of the correspondence between the abbreviations in the previous figure and the boundary conditions are reported in Chapter 6.

In regards to displacement ventilation, simulations confirm experimental results : if ventilation rate increases from 2.1 ACH of case DV-4 to 3 ACH of case DV-3 with similar boundary conditions, CRE increases from 2.42 to 3.99 at 1.1 m height and from 2.16 to 2.24 at 1.7 m height (Table 8. 10).

Table 8. 10 shows the contaminant concentration at exhaust when steady state is reached, the one used in equation (8.5); even if the gas mass introduced is the same, with system M2 the contaminant concentrations at exhaust are heavily higher than those with system M1.

Contaminant removal effectiveness calculated via simulation were compared with those calculated via measurements for all the cases and in positions P1, P2 and P3, for which experimental data were available. Figure 8. 23 shows that predicted contaminant removal effectiveness values are always higher than measured values for all the 6 cases of mixing ventilation and this difference is more evident for system M2 with exhaust at low level (the difference is up to 3.88). For all the cases with system M1 the difference between predicted CRE and experimental CRE is in the range from 0.45 (with case M1-1) to 1.88 (with case M1-2).

In order to investigate the influence of the gas temperature and of the edge of the table, for case M1-5 and M2-5 simulations were carried out also with model n° 2; it was found that contaminant removal effectiveness decreases of about 1.0 ACE when cold gas enters the room, no obstacles are down the source and exhaust is at low level (M2-5). On the contrary, when exhaust is at high level, model n° 2 guarantees the same CRE of model n° 1 (Figure 8. 24).

In regards to displacement ventilation, predicted CRE are on average similar to CRE obtained from measurements (Figure 8. 25); a significant difference between the zone near the manikin (P1 and P3) and the rest of the occupied zone (P2) can be observed, even if not so evident as for measured CRE values.

Table 8. 10 Calculated contaminant removal effectiveness [-] for the room, at 1.1m and 1.7 m height (CRE), ventilation rate (ACH), gas mass flow rate introduced [mg/s] and steady state concentration at exhaust [ppm], for all cases and with CFD model n°1

CASE	CRE	CRE [-]		ACH	CO_2	Cs exhaust
	[-]	h=1.1m	h= 1.7m	[h^{-1}]	[mg/s]	[ppm]
M1-1	1.49	1.78	1.85	1	5.5	842.0
M1-2	2.06	2.09	2.13	1	5.5	655.0
M1-5	1.75	1.77	1.85	1	5.5	599.0
M2-1	3.58	4.12	4.57	1	5.5	1167.0
M2-2	2.54	2.63	2.64	1	5.5	964.0
M2-5	3.69	3.86	3.84	1	5.5	1169.0
DV-3	3.33	3.99	2.24	3	11	524.0
DV-4	2.96	2.42	2.16	2.1	11	786.0

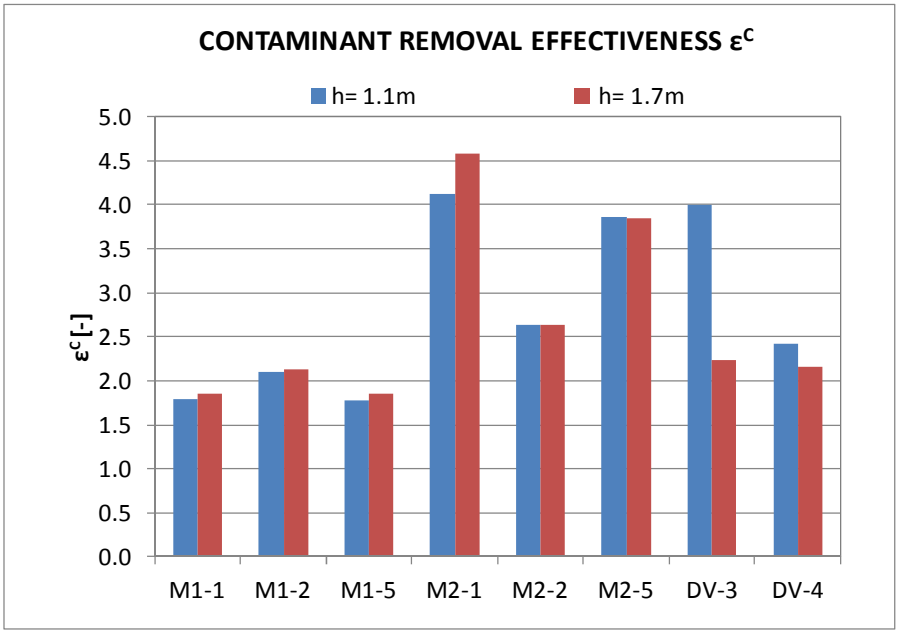

Figure 8. 20 Contaminant removal effectiveness CRE [-] calculated at 1.1m height and at 1.7 m height for all the cases of mixing ventilation and displacement ventilation, with model n° 1

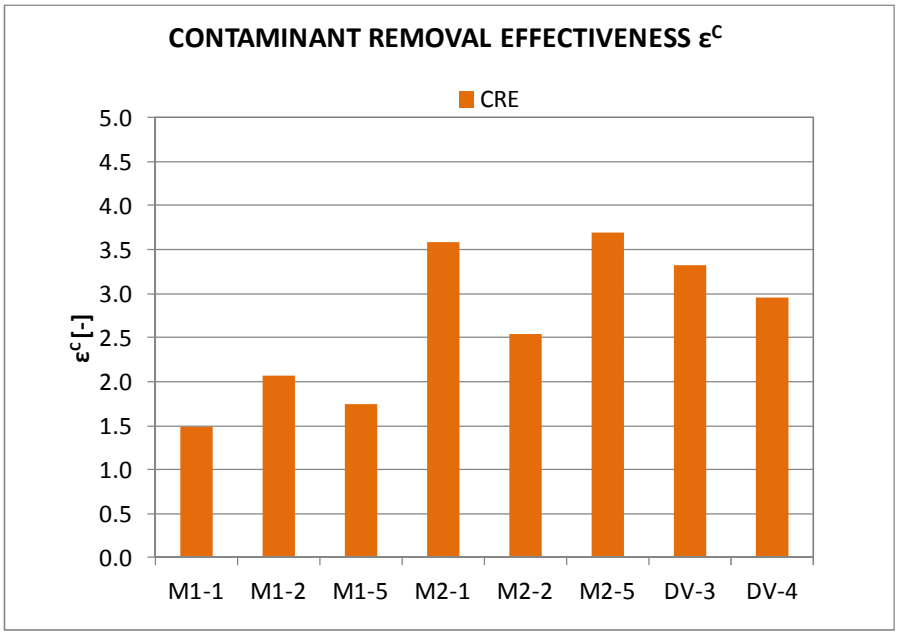

Figure 8. 21 Contaminant removal effectiveness CRE [-] for the whole room calculated for all the cases of mixing ventilation and displacement ventilation, with model n° 1

Table 8. 11 Contaminant removal effectiveness [-] with the same boundary conditions and different positions of exhaust and percentage difference between exhaust at low level and exhaust at high level, with model n° 1

BOUNDARY CONDITIONS	**Exhaust high level**	**Exhaust low level**	**difference**
Wall - T supply 19°C, 0.5 ACH, Floor cooling	1.77	3.86	118.1%
Wall-T supply 30°C, 0.5 ACH	1.78	4.12	130.6%
Wall-T supply 17°C, 0.5ACH, Floor heating	2.09	2.63	25.6%

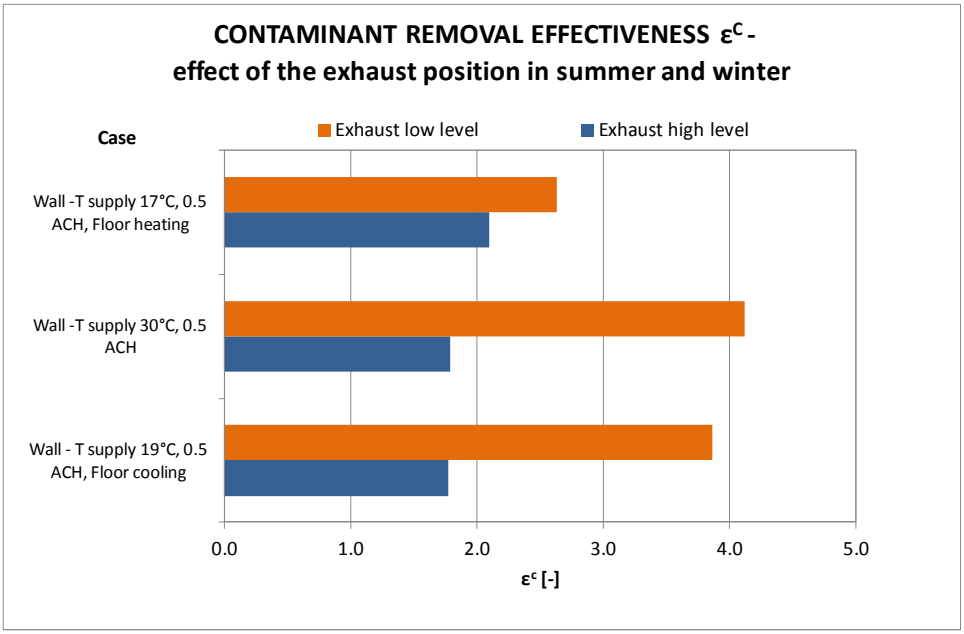

Figure 8. 22 Contaminant removal effectiveness [-]calculated at 1.1 m height for three cases of mixing ventilation from the wall with and without floor heating or with floor cooling, air change of 0.5 ACH, supply air temperature at 17°C, 19°C or 30°C and exhaust at high level near the ceiling or at low level near the floor, with model n° 1

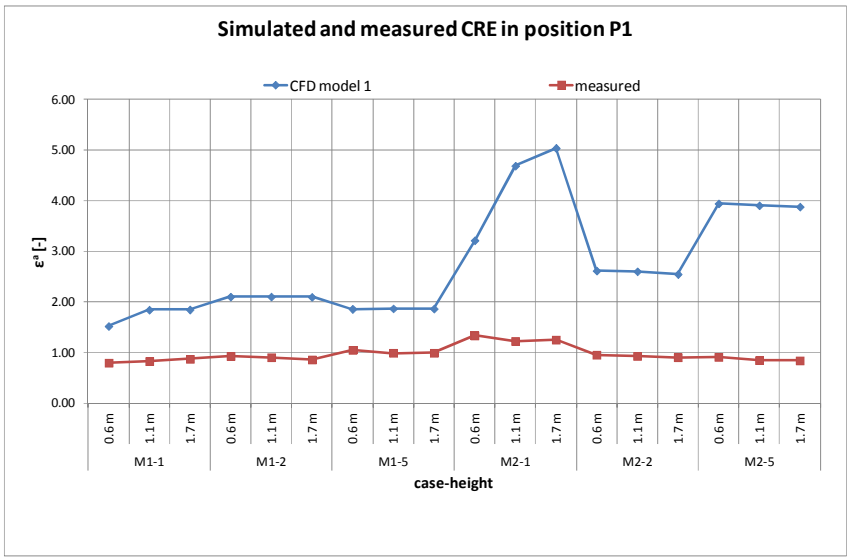

a

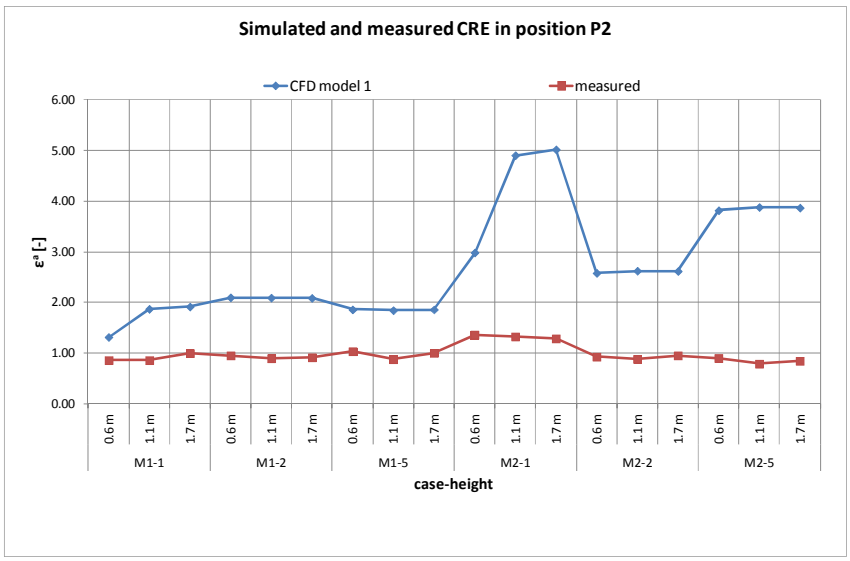

b

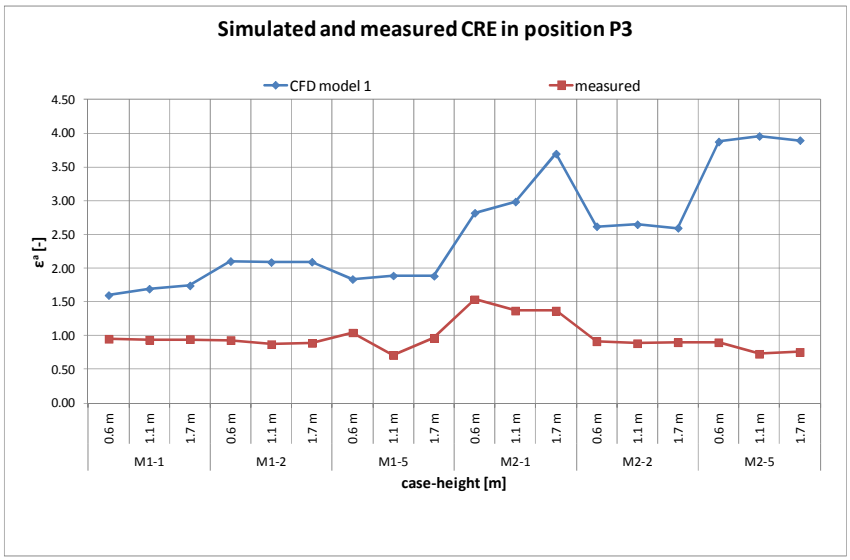

c

Figure 8. 23 Contaminant removal effectiveness [-] in position P1 (a) and position P2 (b) and position P3 (c) at 0.6 m, 1.1m and 1.7 m height, for 6 cases of mixing ventilation (M1-1, M1-2, M1-5, M2-1, M2-2 and M2-5) obtained from measurements and with CFD model n°1

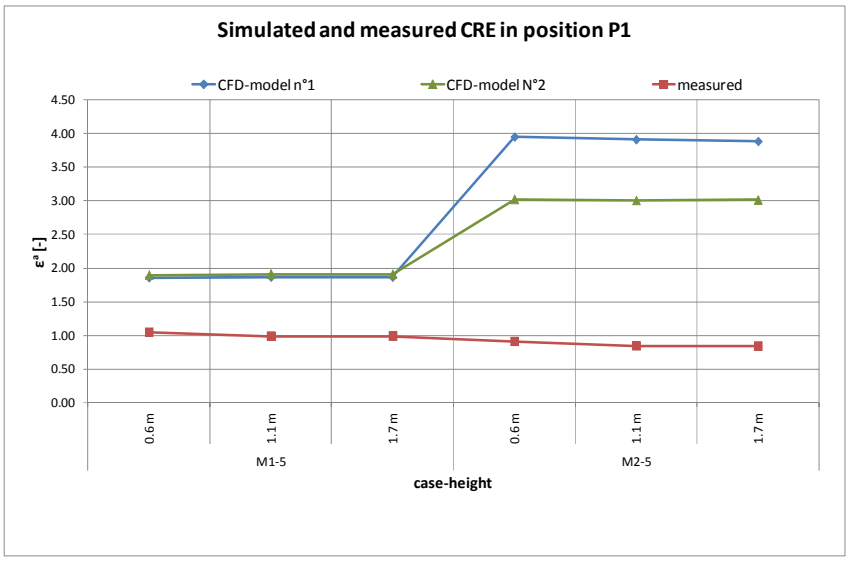

Figure 8. 24 Contaminant removal effectiveness [-] in positions P1 at 0.6 m, 1.1m and 1.7 m height obtained from measurements, for mixing ventilation cases M1-5 and M2-5 and with two CFD models

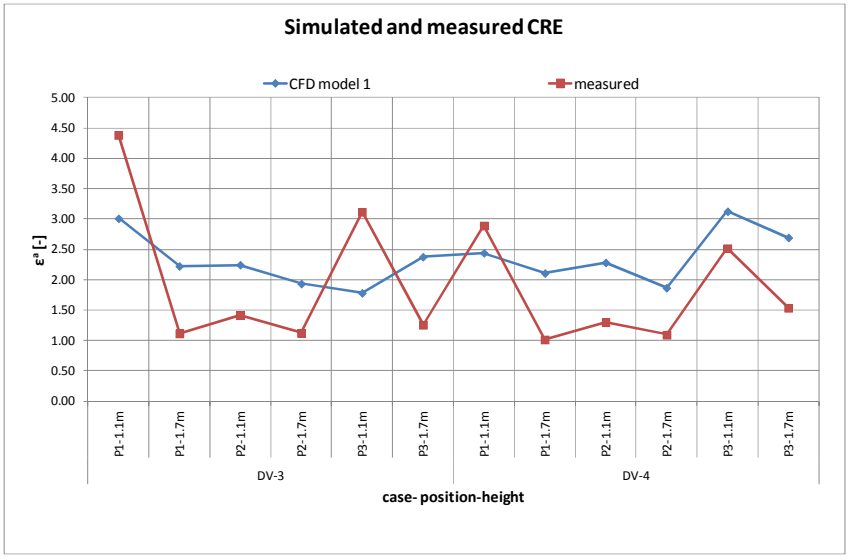

Figure 8. 25 Contaminant removal effectiveness [-] in positions P1, P2 and P3 at 1.1m and 1.7 m height, for displacement ventilation cases DV-3 and DV-4 obtained from measurements and with CFD model n°1

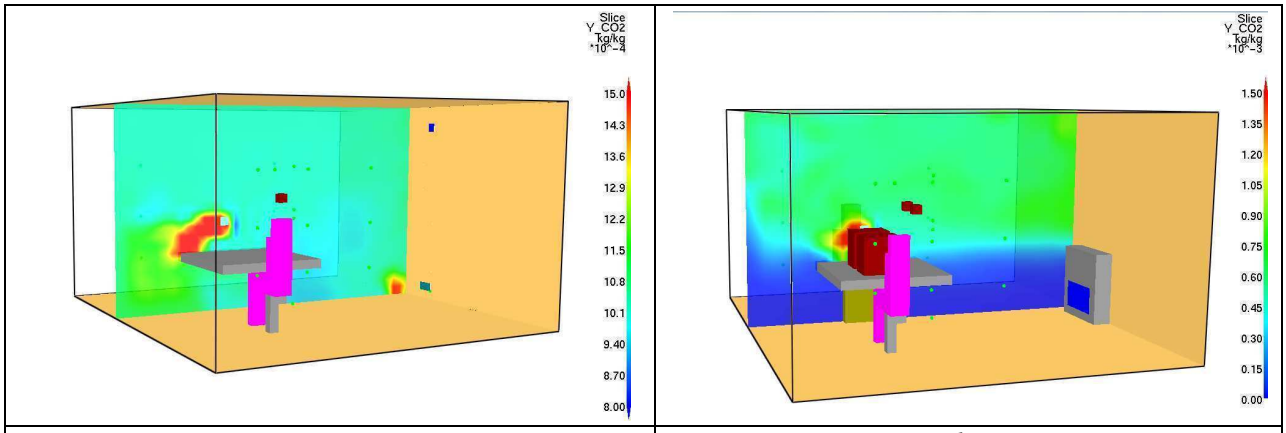

a | *b*

*Figure 8. 26 Examples of contaminant concentrations along the section crossing the source for CRE analysis expressed in [Kg/Kg * 10^{-4}] for case M2-2 (a) and in [Kg/Kg * 10^{-3}] for case DV-4 (b)*

Air change efficiency and air change index

The average local air change index calculated at 1.1 m height and at 1.7 m height is from 92 % to 107 % for all the cases, as reported in Table 8. 12. The maximum is with case M1-1 and in general the cases of mixing ventilation seems to ensure higher level (M1-1, M1-2, M2-1, M2-2) in winter than in summer (cases M1-5 and M2-5). Local air change indices calculated for displacement ventilation are between 92% and 106 %. and a difference between 1.1 m and 1.7 m height is visible with higher air flow rates.

Similar considerations could be done for air change index according to the definition n° 1 ($<\tau>$ from the weighted-volume average concentration in the room): values in mixing ventilation are from 46.3 % of case M2-5 to 53.4 % of case M1-1 while in displacement ventilation they are from 45.7% for case DV-3 to 49.4% of case DV-3. When the definition n° 2 is adopted ($<\tau>$ from the time-weighted area under the curve at exhaust) the case M2-1 is the best among all the mixing ventilation cases, with 73.6% of air change index; displacement ventilation is generally better than mixing ventilation, particularly with high air change rates (case DV-3). Anyway an important aspect is the fact that the constant nominal time τ_n and mean age of air $<\tau>$ of mixing and displacement ventilation cases are different (Table 8.12). Moreover, ACE calculated with definition n° 2 are more than 20 percentage points higher than the corresponding ACE with definition n° 1.

Figure 8. 29 and Table 8. 13 show the influence of the extract air terminal (exhaust) positions on the air change index with the same boundary conditions when mixing ventilation is used for heating or cooling: a soft improvement is visible when high level exhaust are adopted in heating (+ 5.1% with warm air) or with floor cooling (+ 4.2%) while with the same configuration with

floor heating the air change index gets worse (-2%). Not exactly the same trend was found in Chapter 6 with experiments, for which extract air terminals at high level were better only for heating (2% with warm air or +8.3% with floor heating).

Contaminant gas concentrations in the exhaust at steady state condition when gas entered from the supply air terminal were compared to those calculated when the source (with the same mass flow rate) was placed in the occupied zone: no differences exist with displacement ventilation while concentrations increase a lot (up to 3 times) if the source is near the table (Figure 8. 33).

Table 8. 12 Calculated air change efficiency ACE [%] according to 2 definitions, average local air change index (ε_P^a) [%], at 1.1m and 1.7 m height, ventilation rate (ACH), gas mass flow rate [mg/s] introduced, constant nominal time (τ_n) in [h], mean age of air <τ> of the room with definition n°1 in [h] and steady state concentration at exhaust (Cs) in [ppm], for all the cases

CASE	ACE [%]	ACE [%]	Average ε_P^a [%]		ACH	CO_2	τ_n	<τ>	Cs exhaust
	Def.1	Def.2	h= 1.1m	h= 1.7m	[h^{-1}]	[mg/s]	[h]	[h]	[ppm]
M1-1	53.40	66.27	107	107	1	5.5	3.93	3.68	403.4
M1-2	50.34	66.16	101	101	1	5.5	3.88	3.86	398.9
M1-5	48.13	61.48	96	96	1	5.5	3.63	3.77	470.5
M2-1	50.73	73.56	102	101	1	5.5	4.26	4.20	654.4
M2-2	51.72	67.40	103	104	1	5.5	3.96	3.83	350.0
M2-5	46.34	65.89	92	92	1	5.5	3.84	4.14	870.6
DV-3	49.38	83.15	92	106	3	11	1.62	1.68	605.5
DV-4	45.70	73.49	99	101	2.1	11	1.38	1.51	758.1

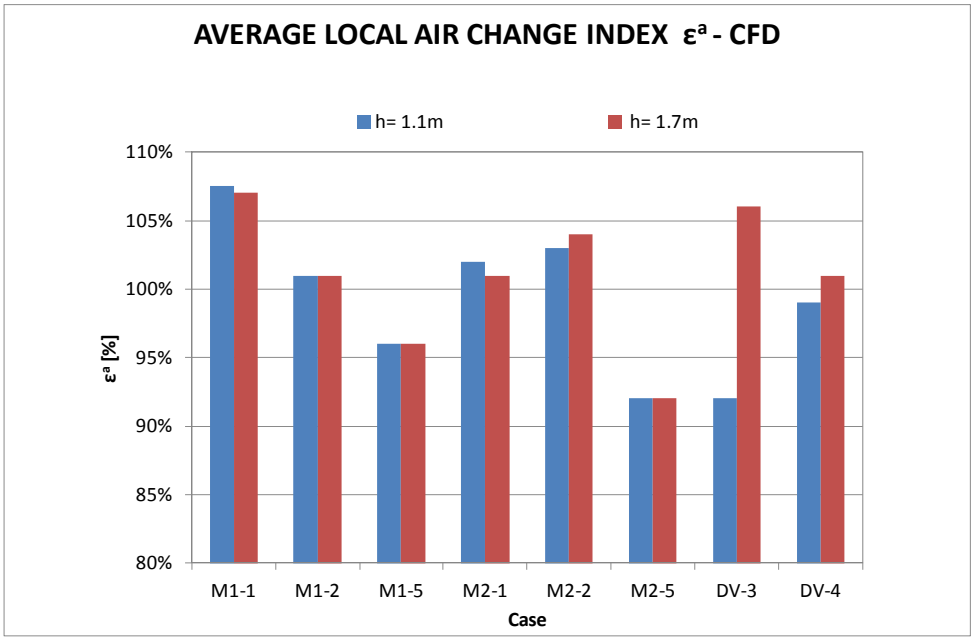

Figure 8. 27 Average local air change index [%] at 1.1m height and at 1.7 m height for all the cases of mixing ventilation and displacement ventilation, with model n°1

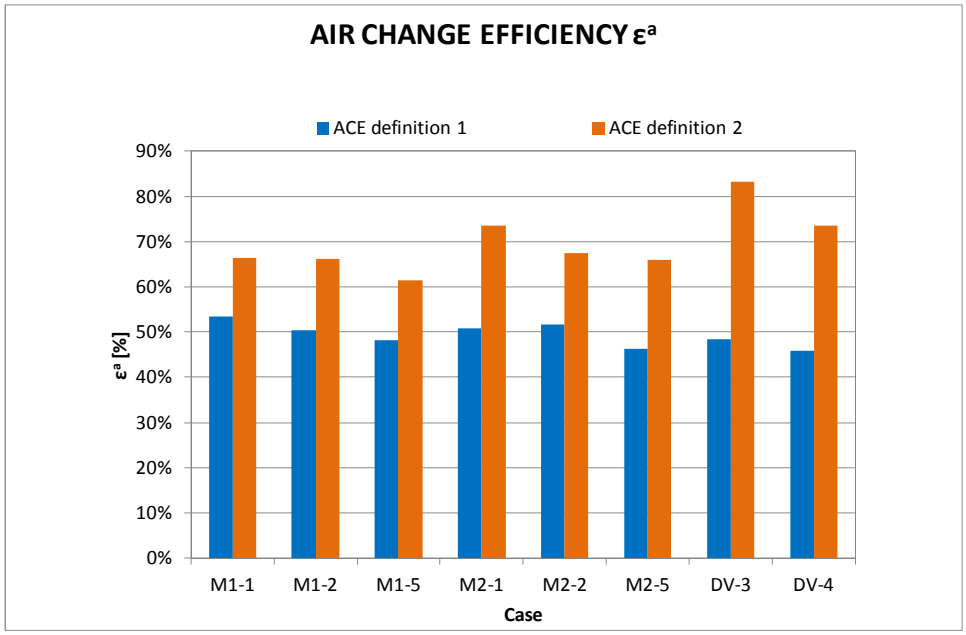

Figure 8. 28 Air change efficiency [%]calculated for all the cases of mixing ventilation and displacement ventilation with 2 different definitions of mean room age of air <τ>

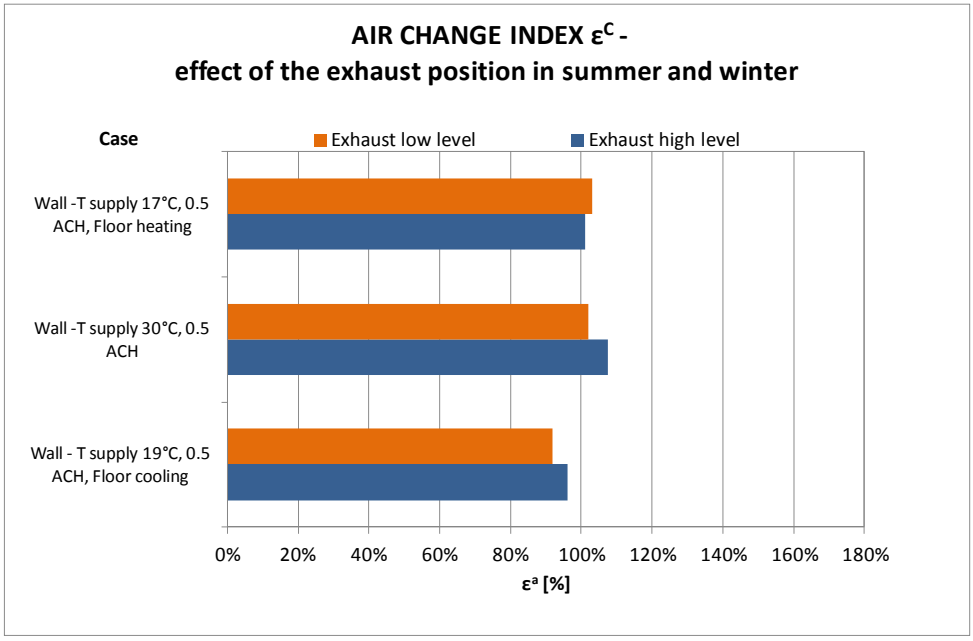

Figure 8. 29 Average local air change index [%]calculated at 1.1 m height for three cases of mixing ventilation from the wall with and without floor heating or with floor cooling, ventilation rate of 0.5 ACH, supply air temperature at 17°C, 19°C or 30°C and exhaust at high level near the ceiling or at low level near the floor, with model n° 1

Table 8. 13 Average local air change index [%] with the same boundary conditions and different position of exhaust and percentage difference between exhaust at low level and exhaust at high level, from simulation results with model n° 1

BOUNDARY CONDITIONS	**Exhaust high level**	**Exhaust low level**	**difference**
Wall- T supply 19°C, 0.5 ACH, Floor cooling	96.0%	92.0%	-4.2%
Wall-T supply 30°C, 0.5 ACH	107.5%	102.0%	-5.1%
Wall-T supply 17°C, 0.5ACH, Floor heating	101.0%	103.0%	2.0%

Local air indices ε_P^a calculated via simulation were compared with those calculated via measurements for all the cases in four points where experimental data were available: at 1.1 m height in positions P1 and in P2, at 1.1m height near the manikin and at 1.7 m height in position P1; results are in Figure 8. 30 and Figure 8. 31.

In regards to mixing ventilation cases, predicted ε_P^a are in the range of measured ε_P^a, that is from 90% to 106%, even if a perfect correspondence is not maintained for cases M1-1, M2-2 and M2-5.

About displacement ventilation, predicted ε_P^a almost coincides with experimental ε_P^a at a certain distance from the manikin (position P2 at 1.1 m and P1 at 1.7 m height) but differs greatly near the manikin, where the thermal plume is present. An additional study was carried out with model n° 3 for case DV-4 assuming an higher percentage of convective heat flow rate (80% of the total) in order to identify a possible reason for the evident air chance index difference near the manikin. Anyway Figure 8. 32 shows that results with model n° 3 are equal to the those obtained with model n°1 and this excludes that the percentage of convective heat flow rate could be a determinant factor for ventilation effectiveness with the model adopted.

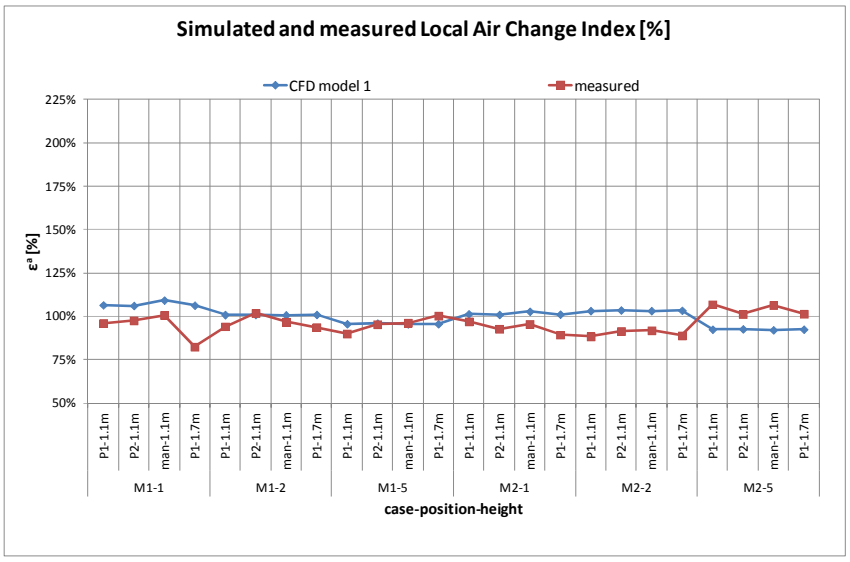

Figure 8. 30 Local air change index [%] calculated at 1.1 m height (P1, P2 and near the manikin) and at 1.7 m height (P1) for 6 cases of mixing ventilation (M1-1, M1-2, M1-5, M2-1, M2-2 and M2-5), obtained from measurements and with CFD model n°1

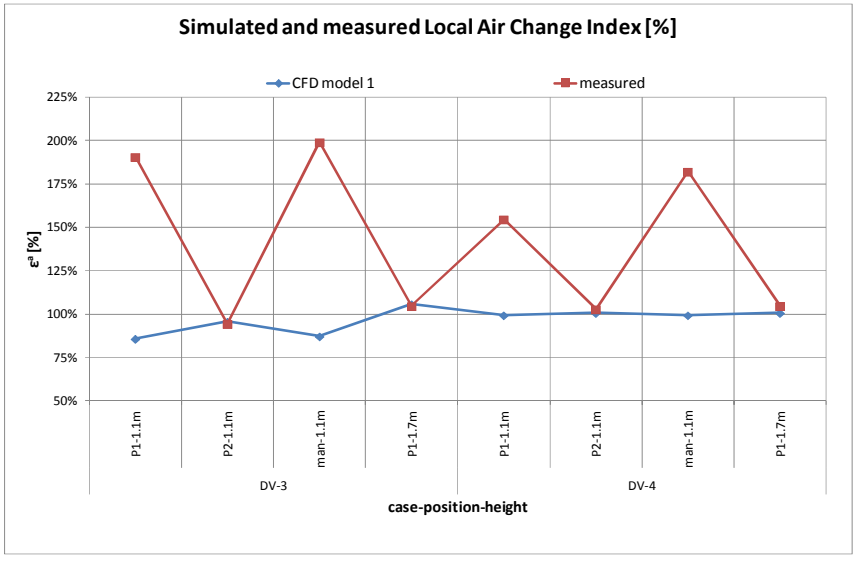

Figure 8. 31 Local air change index [%] calculated at 1.1 m height (P1, P2 and near the manikin) and at 1.7 m height (P1) for displacement ventilation cases DV-3 and DV-4, obtained from measurements and with CFD model n°1

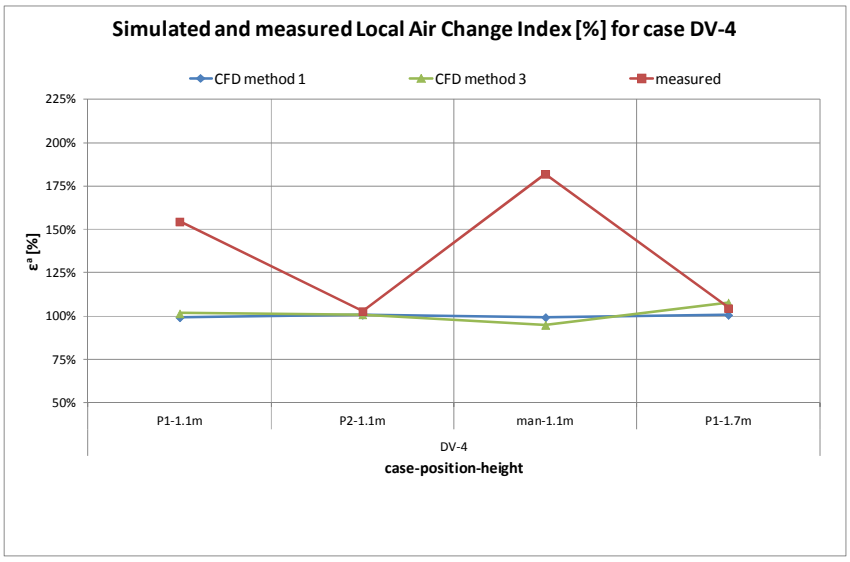

Figure 8. 32 Local air change index [%] calculated at 1.1 m height (P1, P2 and near the manikin) and at 1.7 m height (P1) for case DV-4,obtained from measurements and with two CFD models

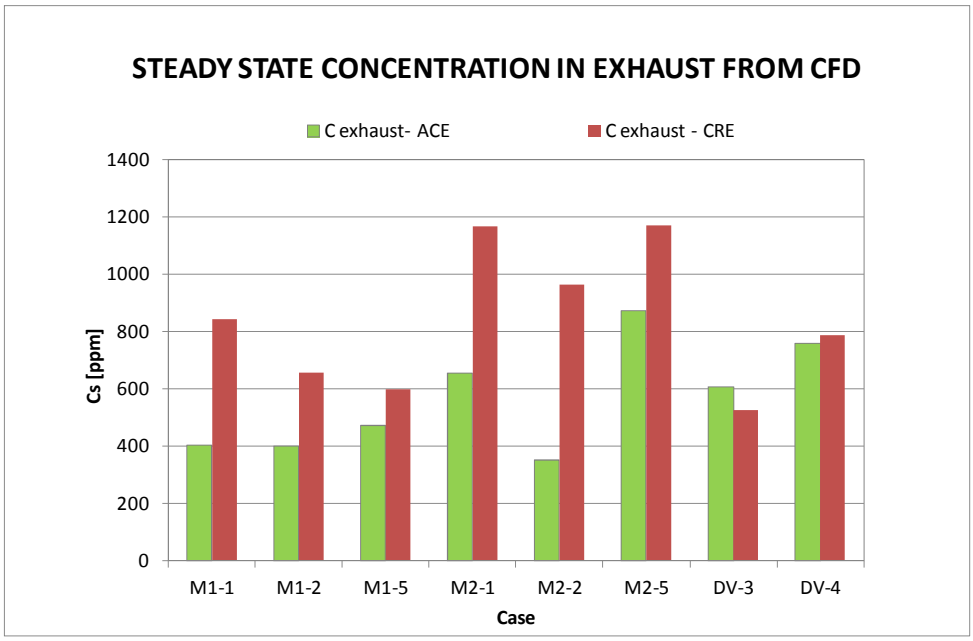

Figure 8. 33 Steady state concentrations[ppm] at exhaust obtained with the same gas mass flow rate when air change efficiency (ACE) and contaminant removal effectiveness (CRE) were calculated from simulations, for all the cases and with model n°1

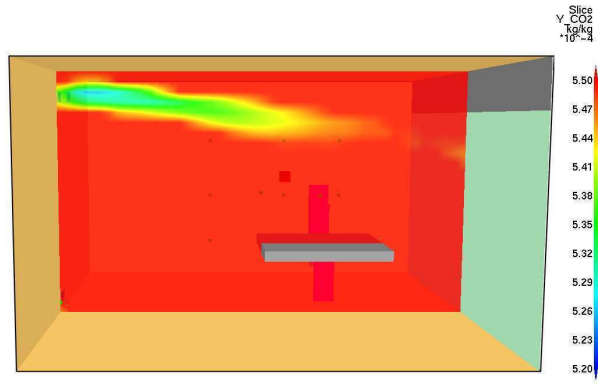

a

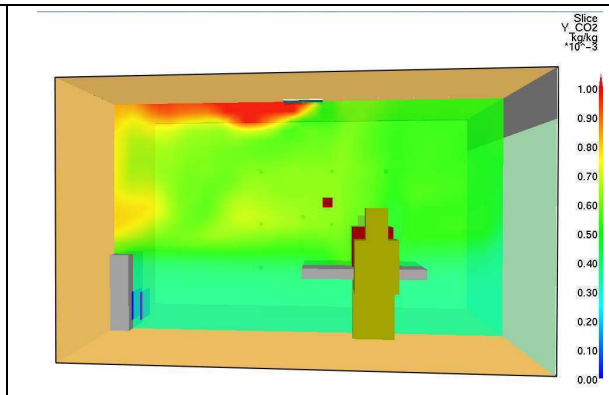

b

*Figure 8. 34 Examples of contaminant concentrations along longitudinal section for ACE analysis expressed in [Kg/Kg * 10^{-4}] for case M21-2 (a) and in [Kg/Kg * 10^{-3}] for case DV-4 (b)*

8.4 Discussions

Thermal comfort

The predicted thermal environment by means of the CFD model was in agreement with measurements for all the chosen conditions. Draught rating DR [%] calculated via simulation were comparable with experimental results, even if for displacement ventilation measured velocity close to the floor were less than measured velocity and, consequently, draught rating risk slightly differed from experimental data. Anyway this discrepancy did not affect the category for thermal comfort and it represents an inevitable consequence of the displacement terminal modeling.

Predicted vertical air temperature profiles were on average similar to the corresponding measured profiles for all the conditions; anyway it is evident that simulation strongly reduces the relative difference between the positions, that is FDS model is less influenced by positions regarding temperatures.

The choice of grid type n° 3 (Figure 8. 5) was successful for improving the model taking into account the real heat transfer from the cooled floor together with the measured temperature near the floor. The particular study carried out with case M1-3 in order to evaluate the better equation for natural convection from the floor related to the chosen size cell, was an effort to minimize the difference between convective heat transfer calculated from CFD and from measurements and, at the same time, the measured and calculated temperatures at the centre of

the closest cells. The problem derives from the way FDS allows the user to impose natural convection from a surface.

In a study about indoor thermal environment, the choice of course grids near the floor affects the temperature profile just in the most interesting zone for comfort: for this reason the maximum size cell was 0.2 m.

Similar studies could be done for natural convection from heating floor (case M1-2 and M2-1) but because of the lower floor heat flow rate (20 W/m^2) and of the lower vertical temperature differences with experimental profiles, it was chosen to adopt grid n° 1.

Natural convection from the wall in the model should be affected by the same problem that occurs at the floor; anyway it was found that heat transfer coefficients adopted by FDS for the hot window did not change significantly if the cell closest to the window was 0.1 m or 0.05 m size, probably because the warm air movement towards the ceiling limited the horizontal temperature difference close to the window. In any case a study similar to that carried out for the floor cooling case was not possible for window because of the lack of experimental data.

Internal heat gains given as net heat flow rate from the manikin and from the desk lamp allowed to take into account different boundary conditions in the thermal analysis. But with displacement ventilation, to better control the complex thermal plumes from different internal heat gains, it was decided to impose convective and radiant heat flows; the same decision was done for ventilation effectiveness analysis in order to focus on contaminant spread mechanisms only.

Ventilation effectiveness

Contaminant removal effectiveness values calculated for mixed ventilation cases via CFD significantly differed from those obtained from experiments. This difference was particularly evident for system M2, with exhaust near the floor. CRE parameter is directly proportional to the exhaust concentration and directly connected to contaminant source conditions and positions: the reasons of disagreement with experimental data should be find in a not completely correct modeling of the source (e.g. gas mass flow rate, gas temperature and position) or of the exhaust. By changing the boundary conditions of the gas source and reducing the table size, it was found that contaminant removal effectiveness values decreased with system M2 while did not change with system M1.

The air supply terminals were different for the two systems: the Simplified Boundary Condition method was applied alone for system M1 and with a sort of Prescribed Velocity method for M2, but this should not influence the air quality in the occupied zone, sufficient distant from the supply air terminal, because the jet momentum and supply air temperature were the same.

The carbon dioxide dosing adopted for simulation was not assumed exactly the same of the measured one in order to have the same mass flow rate for each case and make comparisons between them: but this choice could affect the results.

Another important aspect is the air change rate: simulations considered 1.0 ACH and no infiltration from external environment, but measurements were carried out with 0.5 ACH and air infiltration was estimated in the range of 0.20÷0.28 ACH by means of constant injection tracer gas technique [19]. External air was characterized by different carbon dioxide concentrations during the experimental period, and this could influence the results when so low ventilation rates were adopted.

On the contrary, with higher ventilation rates and displacement ventilation systems, contaminant removal effectiveness from the model was on average similar to experimental results, even if the better air quality at 1.1 m height near the manikin (P1 and P3) was more evident with experiments than with simulations.

CFD studies highlighted the importance of the of air change efficiency definition in making comparisons between cases: if one takes the time-weighted integral of contaminant concentration at exhaust instead of the integral of the volume-weighted average concentration in order to calculate the mean local age of the room $<\tau>$, different conclusions about air change efficiency ACE should be done. With definition n° 1 air change efficiency was sometimes less than 50% , that is signal of short-circuit [18] and displacement ventilation was not clearly good for air quality improvement. With definition n° 2, displacement ventilation was definitely better for ventilation effectiveness (>70%), as expected [18], but at the same time ACE for mixed ventilation were much higher than 50% as expected for fully mixed flow [18]. Anyway the second definition seems to be the most appropriate to compare different cases and the more useful for eventual further comparisons with experimental data (only the contaminant concentration at exhaust is required).

Air change efficiency as well of local air change index were determined using carbon dioxide instead of R134a but this is not a problem for making comparisons with measurements because this parameters represent the ability to replace air in the room.

Local air change index from simulations was in the same range of that calculated from experiments, even if the correspondence was not maintained in particular positions. According to this parameter it is not easy to define if exhaust is better near the floor or near the ceiling: simulations confirmed that local air change index is slightly higher when exhaust is at high level with heating ventilation, as found with experiments, but small differences with experimental results were found with floor cooling/heating systems.

From experiments, ventilation effectiveness near the manikin in displacement ventilation was visible higher than in the rest of the room but this did not happen for simulations, even using a higher convective heat flow percentage from internal heat gains. This represents a limit of the model because the complex air flow movement near the manikin was not well predictable with a simple discretization like grid type n° 1 with cell 10 cm size.

8.5 Conclusions

Experimental studies on air distribution in room with mechanical ventilation and radiant heating or cooling systems have been completed by using a computational fluid dynamic program. This studies focused on thermal comfort parameters and ventilation effectiveness. Eight cases of mixed ventilation from a wall mounted air terminal in a residential room and two cases of displacement ventilation in an office were chosen among the twenty cases available from experiments.

CFD models were built in order to take into account all geometrical features and the boundary conditions of real tests, in a compatible way with limits of the program FDS used in this work.

A particular study bases on measurements was carried out for floor cooling cases with low ventilation rates and a new procedure to introduce natural convection in the CFD model was developed. Three kinds of grids were adopted depending on the problem.

Results showed a good agreement for thermal comfort results, particularly for draught rating DR [%] at 1.1 m height; air vertical temperature profiles were in the range of measured ones, but no relative differences between the positions was visible like in measurements.

It was found that the contaminant removal effectiveness prediction when exhaust was near the floor was strongly influenced by the conditions of the gas entering the room and by the obstacles near the source.

Air change efficiency was calculated with two different definitions of room mean age of air.

Finally, results showed a good agreement of local air change index from simulations with experiments, even if the complex phenomena around internal heat loads when displacement ventilation was used could be not well appreciated with the adopted grid.

8.6 References

[1] Nielsen, P.V. 1973. Berechnung der Lufbewegung in einem zwangsbelüfteten Raum, Gesundheits-Ingenieur.

[2] Catalina, T., Virgone, J., Kuznik, F. 2009.Evaluation of thermal comfort using combined CFD and experimentation study in a test room equipped with a cooling ceiling . Building and Environment 44 (2009) 1740–1750.

[3] Causone, F. , Olesen, B.W., Corgnati, S.P. 2010. Floor Heating with Displacement Ventilation: An Experimental and Numerical Analysis, HVAC&R RESEARCH, Vol. 16 n°2, 2010

[4] McGrattan, K. et al., Fire Dynamic Simulator (version 5), Technical Reference Guide, NIST special publication 1018-5, 2010.

[5] De Carli, M., Scarpa, M., Tomasi, R., Villi, G. 2011. Evaluation of radiant system performance enhancement by means of primary air. Roomvent 2011 Conference, Trondheim, Norway.
[
[6] Musser, A., McGrattan, K., Palmer, J. Evaluation of a fast, simplified, Computational Fluid Dynamic Model for solving Room Airflow Model, NISTIR 6760, NIST, 2001.

[7] EN 15251. 2007. Indoor environmental input parameters for design and assessment of energy performance of buildings-addressing indoor air quality, thermal environment, lighting and acoustics. CEN, Brussels.

[8] Smagorinsky, J. 1963. General Circulation Experiments with the Primitive Equations. I. The Basic Experiment. Monthly Weather Review, 91(3):99–164, March 1963.

[9] Zhang, W., Ryder, N., Roby, R.J, Carpenter. D. Modeling of the Combustion in Compartment Fires Using Large Eddy Simulation Approach. In Proceedings of the 2001 Fall Technical Meeting, Eastern States Section. Combustion Institute, Pittsburgh, Pennsylvania, December 2001.

[10] Werner, H., Wengle, H.1991. Large-eddy simulation of turbulent flow over and around a cube in a plate channel. In 8th Symposium on Turbulent Shear Flows, pages 155–168, 1991.

[11] Forney, G. P. Smokeview (Version 5) - A Tool for Visualizing Fire Dynamics Simulation Data Volume II: Technical Reference Guide. NIST special publication 1017-2, 2010.

[12] Nielsen, P.V. et al., RHEVA Guidebook n°10. 2004. Computational Fluid Dynamics in ventilation design.

[13] Gosman, A.D., Nielsen, P.V., Restivo, A., Whitelaw, J.H. 1980. The flow Properties of Rooms With small Ventilation Openings, Journal Of Fluid Engineering, (1980), Vol.102, pp.316-322.

[14] ASHRAE 1997. Handbook of Fundamentals – SI Edition. American Society of Heating, Refrigerating, and Air-Conditioning Engineers, Inc. Atlanta, GA.

[15] Olesen, B W, Michel, E., Bonnefoi, F, De Carli, M. 2000. Heat Exchange coefficient between floor surface and space by floor cooling-Theory or a Question of Definition. ASHREE Transactions 2000, 106 Pt.1

[16] ISO 7730:2005. Ergonomics of the thermal environment — Analytical determination and interpretation of thermal comfort using calculation of the PMV and PPD indices and local thermal comfort criteria.

[17] Sandberg, M. What is ventilation efficiency? Building and Environment, Vol. 19, n°2, pp. 123-135.

[18] Mundt, E. et al. RHEVA Guidebook n°2. 2004.Ventilation effectiveness.

[19] ASTM 1995. ASTM Standard E741-95. Test method for determining air change in a single zone by means of tracer gas dilution. Philadelpia: American Society for Testing and Material.

9 Overall discussions and conclusions

Radiant systems for heating and cooling represent a good solution for energy savings; in fact the low temperature difference between the surface and the room that they ensure fits well with high efficiency energy solutions and renewable sources like heat pumps, free cooling and thermal solar collectors. On the other hand, the low temperature differences between the surface and the room could guarantee high thermal comfort and for this reason floor radiant systems are recommended for residential environments. The heat loads normally present in offices can be efficiently removed by means of cooled ceiling panels or cooled floors; in this case mixed ventilation or, as an alternative, displacement ventilation systems are recommended in order to provide for primary air and to increase the cooling capacity when necessary.

The determination of thermal performance of water based surface heating and cooling systems requires the definition of heat transfer coefficients between indoor surfaces and the room. Literature reports different equations, based on measurement procedures or on detailed calculations. In Chapter 2 a critical review on convective heat transfer coefficients has been presented and equations for calculating these coefficients for each case of heating/cooling from floor, ceiling and wall have been proposed.

The energy performance of radiant systems and their behavior under transient conditions due to presence of daily solar radiation, internal gains and human occupancy have been numerically investigated. A numerical model able to perform the detailed simulation of the dynamic behaviour of water based surface embedded heating and cooling systems, already developed by the research group, has been validated by using experimental data and presented in this work. In order to perform the validation under real use boundary conditions, a specific procedure to set heating/cooling load profiles aimed to simulate different climatic conditions which have to be faced by ceiling radiant panels has been carried out and presented in Chapters 3 and 4. The results from simulations show that the presented model can predict the real room conditions and that results are not affected by the use of variable or fixed convective heat transfer coefficients.

When radiant systems are used for cooling, an appropriate ventilation system should be adopted in the room in order to dehumidify and to avoid condensation on surfaces at low temperatures. The interaction between the primary air entering the room and a radiant cooled ceiling has been examined in this work. The possible performance enhancement of radiant ceiling coupled with

ventilation caused by the increase of convective heat transfer coefficients has been investigated based on CFD (Computational Fluid Dynamics) analysis, as shown in Chapter 5.

As a result, it was found a modest enhancement of the total heat transfer coefficients at the ceiling surface when primary air is provided, while the ceiling cooling capacity globally did not increase.

In order to limit the cooling capacity of the AHU and consequently costs, ventilation rates should be limited; in this way air velocities in the room and thus draught risk decrease but, at the same time, the system's ability to remove air-borne contaminants and to replace fresh air decreases. In low energy buildings the heating demand for space is decreasing, therefore ventilation system can be used also for heating purposes. In order to evaluate indoor climate in a typical room or an office when mechanical ventilation is combined with floor heating/cooling systems, an experimental study has been carried out in a fully scale test room and presented in Chapter 6. Different sets of mixed ventilation for residential rooms in winter and summer conditions and different ventilation rates from a displacement diffuser in a typical office room during cooling season have been examined. Thermal comfort parameters like air temperature vertical gradients, operative temperatures, velocity vertical profiles have been measured in different positions in the room, in order to characterize the occupied zone. Besides, ventilation effectiveness, expressed as contaminant removal effectiveness and as air change index has been determined.

Results show that mixing ventilation with low flow rates coupled with floor heating/cooling systems guarantees high levels of thermal comfort, even though the temperature of the floor during cooling season could cause local discomfort if it is too low with respect to the reference temperature of the room. Furthermore it was found that mixing ventilation with low ventilation rate in residential rooms can guarantee acceptable ventilation effectiveness values both during heating season and during cooling season. However, contaminant removal effectiveness and air change index have been found to be strongly dependent on the boundary conditions and on the positions of the extract air terminal units. Displacement ventilation guarantees high ventilation effectiveness, even using modest air flow rates. But when high ventilation rates are adopted, the risk of local discomfort due to high vertical air temperature differences between head and ankle level exists. Finally, results showed that radiant temperature asymmetry due to warm ceiling is a potential risk of discomfort when the floor temperature is lower than the reference temperature in the room, regardless of the type of ventilation system (displacement or mixing ventilation).

Carbon dioxide is normally used as indicator of human bioeffluents and its concentration in the room is usually used to check the air quality in low polluted buildings. The effect of the supply and extract air terminal units positions on the contaminant distributions in an office equipped with cooled ceilings has been predicted using numerical simulations (CFD) in Chapter 7. Mixed ventilation has been compared with different displacement ventilation solutions, adopting floor outlets or a displacement unit from a wall. Contaminant removal effectiveness, percentage of dissatisfied PD% in different positions of the occupied zone and a discomfort index for the whole office have been calculated. Results showed that with displacement ventilation exhaust should be placed on the ceiling above the occupied zone and that displacement ventilation units could guarantee lower contaminant concentration at the breathing zone if terminals are on a wall.

Even though CFD technique represents a valid tool to predict indoor climate in rooms, CFD models need to be validated by a comparison with experimental data, since different complex phenomena taking place in the room are difficult to expect by means of calculation alone. A CFD model for air distribution in rooms equipped with mixed or displacement ventilation combined with heating/cooling floor systems has been built and presented in Chapter 8. It has been validated by comparison with experimental measurements in a fully scale test room representing a typical residential room or a typical occupied office. Results showed that the model was suitable to evaluate thermal environment and to predict thermal comfort parameters. The model was also correct in the prediction of ventilation effectiveness expressed as local air change index in the occupied zone, except very close to the internal heat gains. The prediction of contaminant removal effectiveness was in agreement with experimental data in case of displacement ventilation; however, when mixed ventilation with low flow rates was adopted, calculated contaminant removal effectiveness values were quite different than the corresponding values derived by experiments and they were heavily influenced by the conditions of the contaminants and by the obstacles near the contaminant sources.

In conclusion, different aspects of radiant systems for heating and cooling and their interaction with ventilation systems have been studied in this work through experiments and numerical calculations. A numerical model suitable for the analysis of radiant system behavior to transient conditions has been validated using experimental data. Furthermore CFD techniques have been exploited in order to predict a possible performance enhancement of radiant systems due to ventilation and to predict the effects of supply and extract air terminal units on air quality in an office cooled by the ceiling. Finally a CFD model able to predict air distribution in a room equipped with radiant systems and mechanical ventilation has been built up and validated by

using experimental results obtained in fully scale test room; by using this model, thermal comfort and ventilation effectiveness could be suitably predicted for both mixing and displacement ventilation.

In the future, the results and the numerical models presented in this work could be exploited for further analysis of energy performance under transient conditions and indoor climate concerning other rooms in residential and office buildings equipped with radiant systems for heating and cooling combined with mechanical ventilation.

APPENDIX A – VERTICAL PROFILES OF AIR TEMPERATURES and AIR VELOCITIES

System M1 (Mixing ventilation):

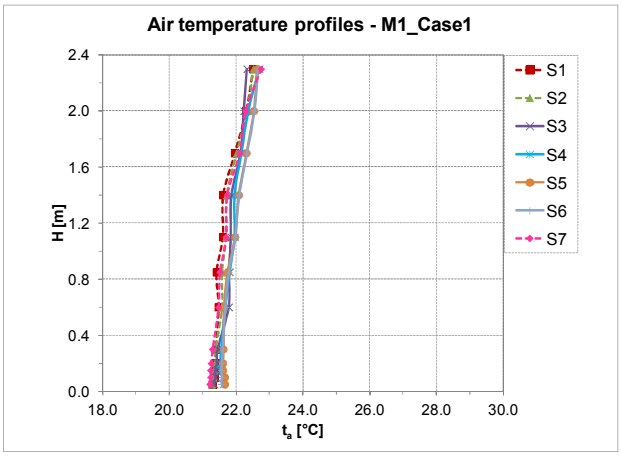

a

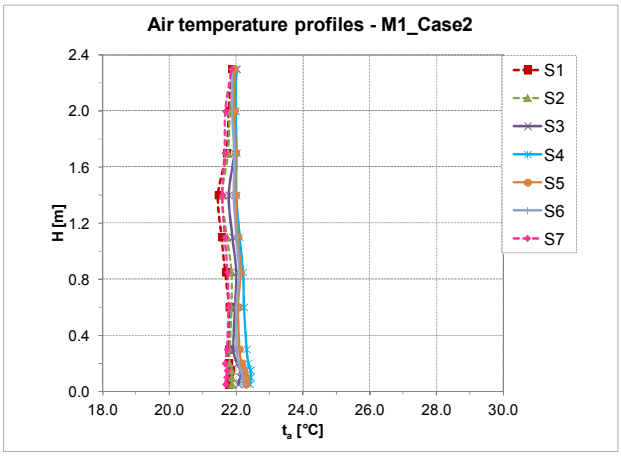

b

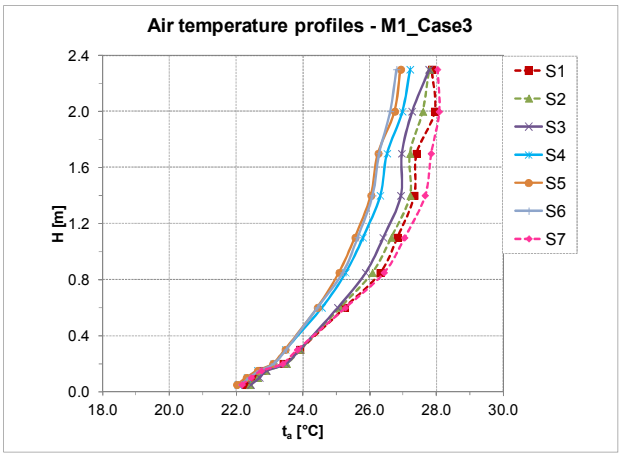

c

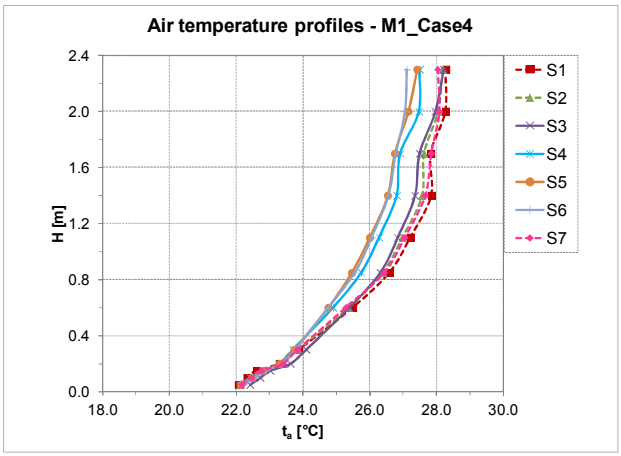

d

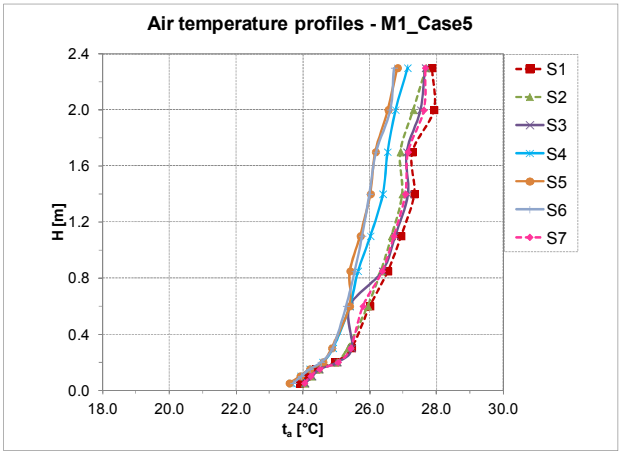

e

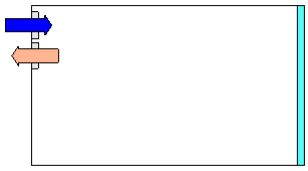

Figure A1 Air temperature vertical profiles for all cases (case 1 (a), case 2 (b), case3 (c) case 4 (d) case 5 (e)) of system M1 measured in the occupied zone (continuous line) and close to the window (dotted line)

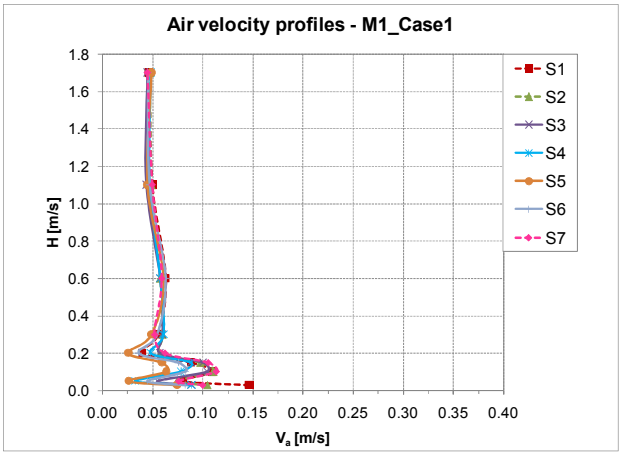

a

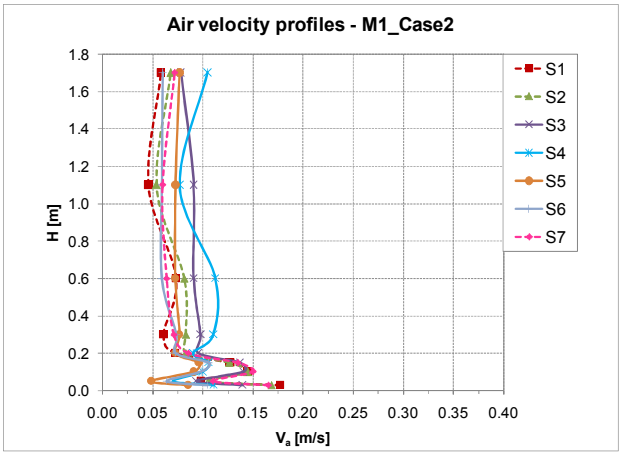

b

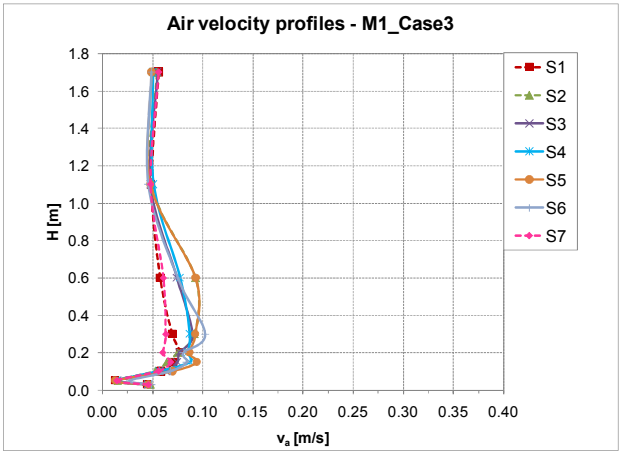

c

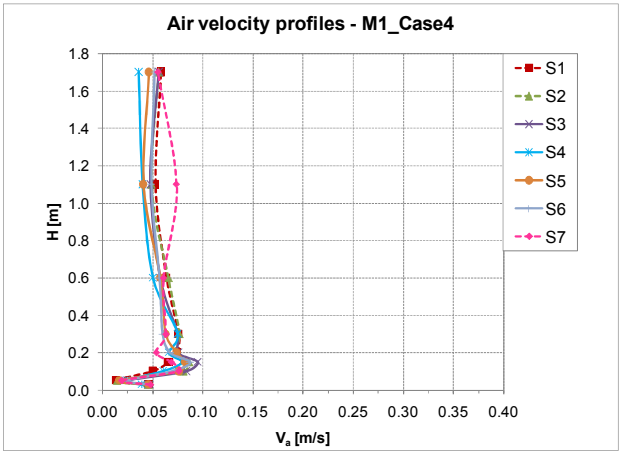

d

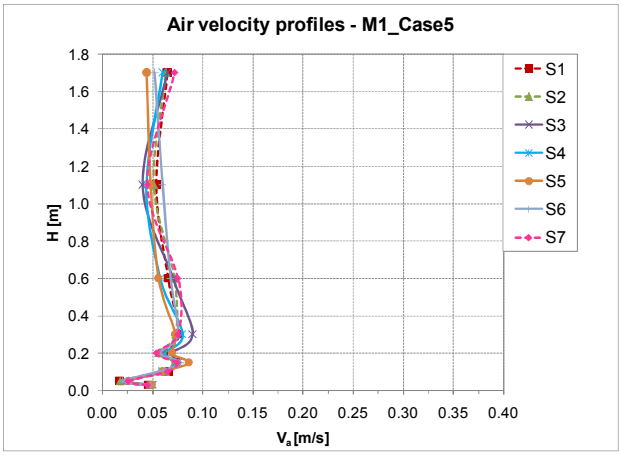

e

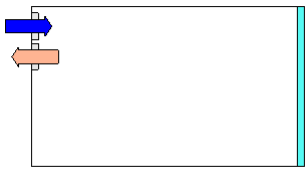

Figure A2 Air velocity vertical profiles for all cases (case 1 (a), case 2 (b), case3 (c) case 4 (d) case 5 (e)) of system M1 measured in the occupied zone (continuous line) and close to the window (dotted line)

System M2 (Mixing ventilation):

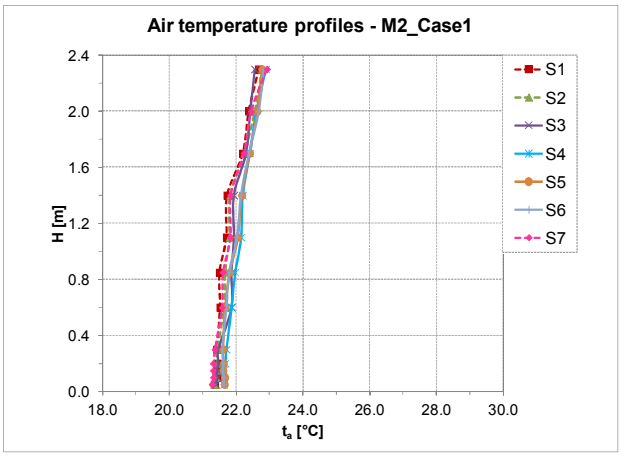

a

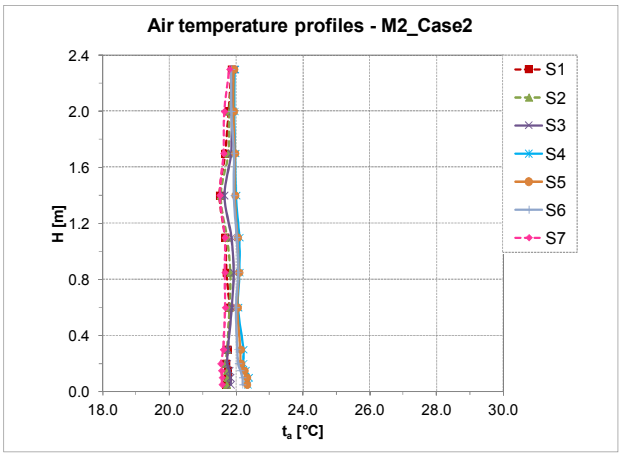

b

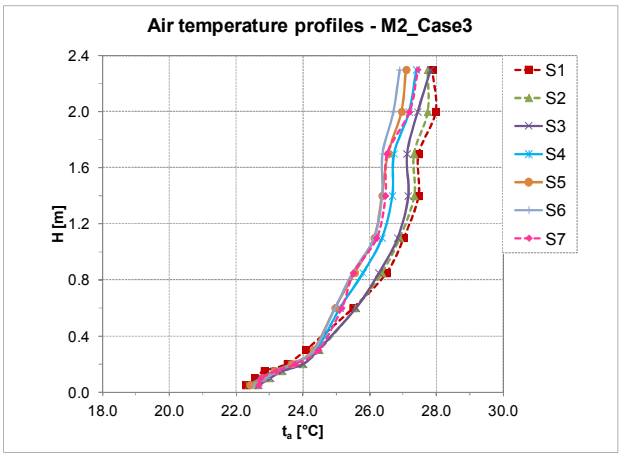

c

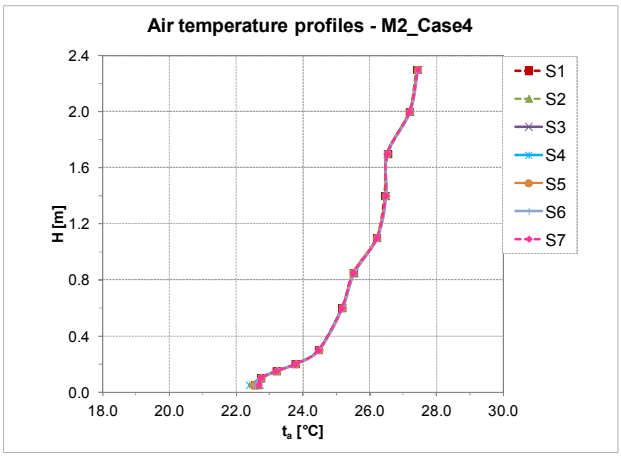

d

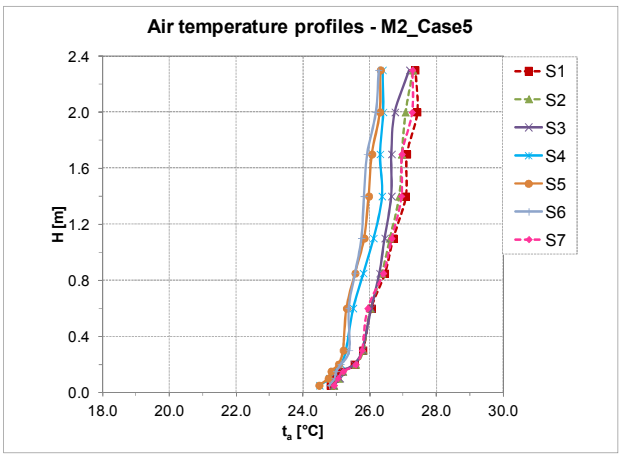

e

Figure A3 Air temperature vertical profiles for all cases (case 1 (a), case 2 (b), case3 (c) case 4 (d) case 5 (e)) of system M2 measured in the occupied zone (continuous line) and close to the window (dotted line)

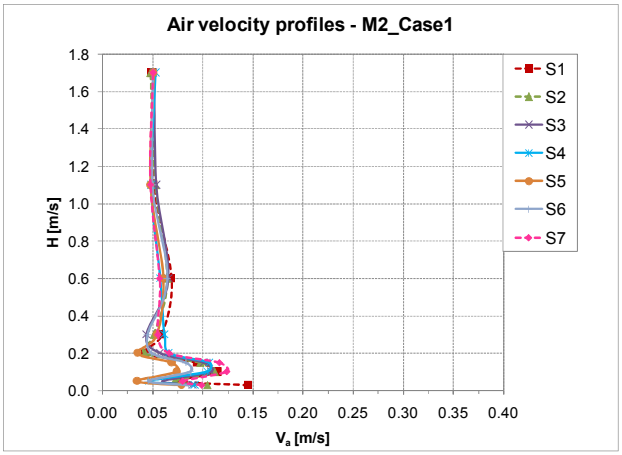

a

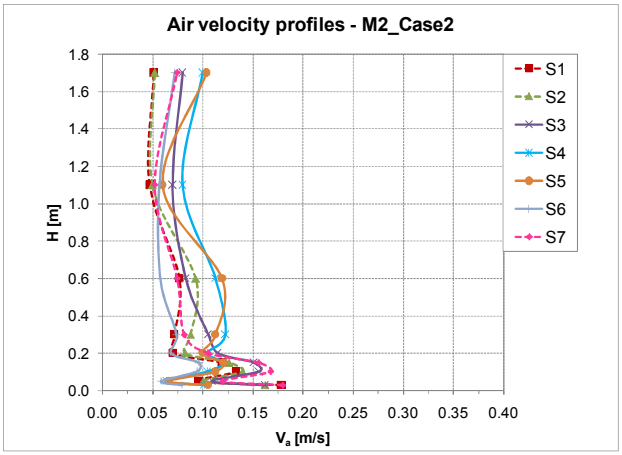

b

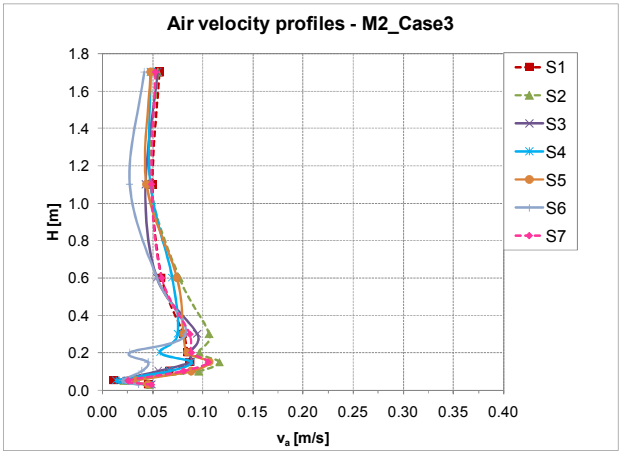

c

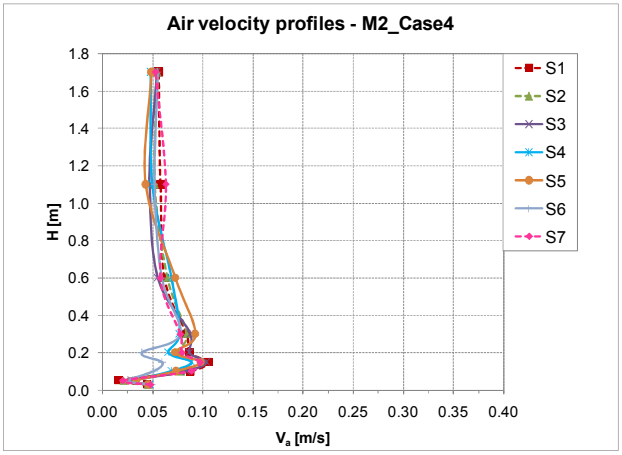

d

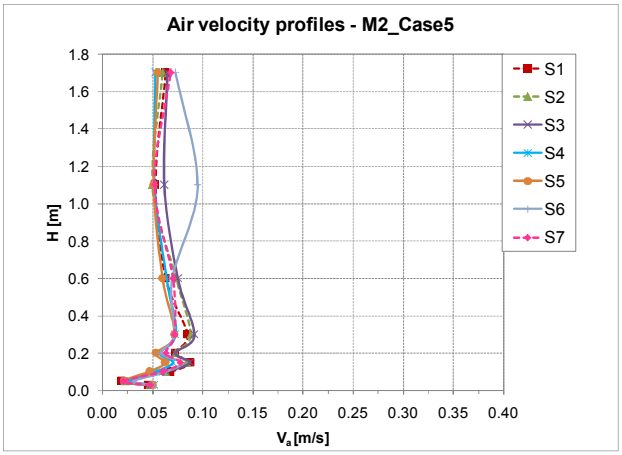

e

Figure A4 Air velocity vertical profiles for all cases (case 1 (a), case 2 (b), case3 (c) case 4 (d) case 5 (e)) of system M2 measured in the occupied zone (continuous line) and close to the window (dotted line)

System M3 (Mixing ventilation):

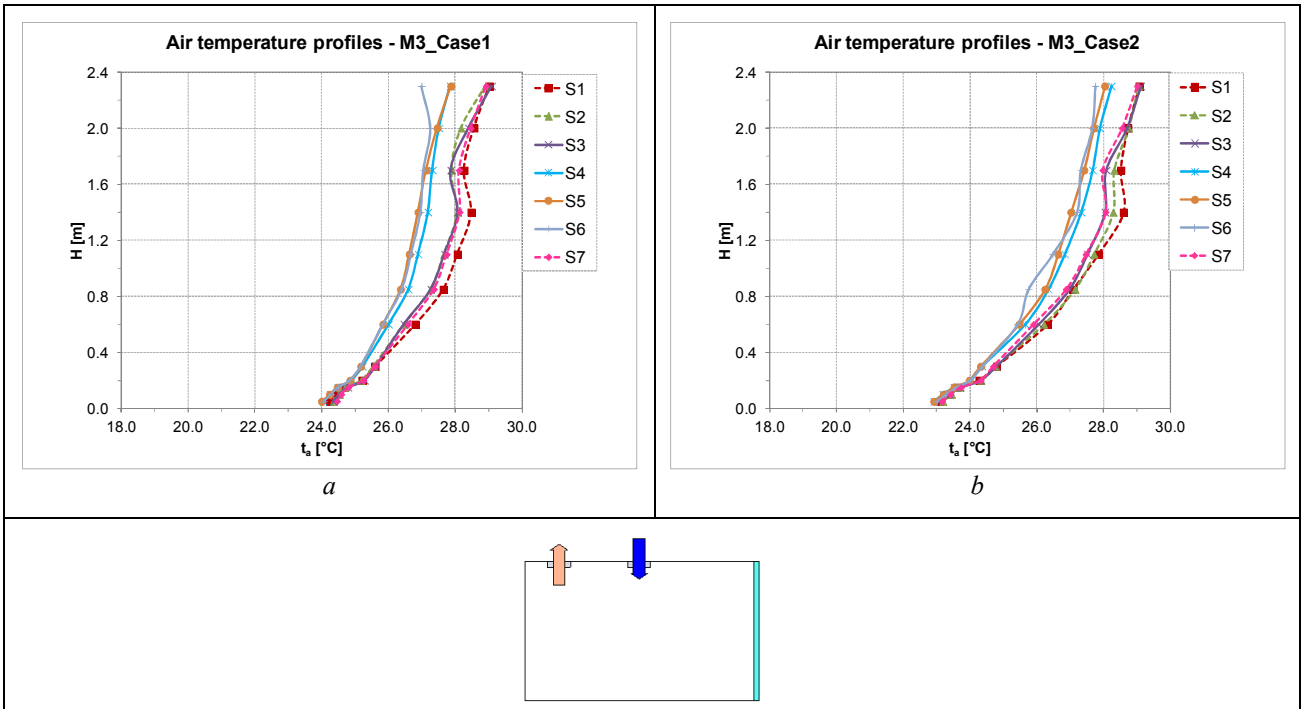

Figure A5 Air temperature vertical profiles for all cases (case 1 (a), case 2 (b)) of system M3 measured in the occupied zone (continuous line) and close to the window (dotted line)

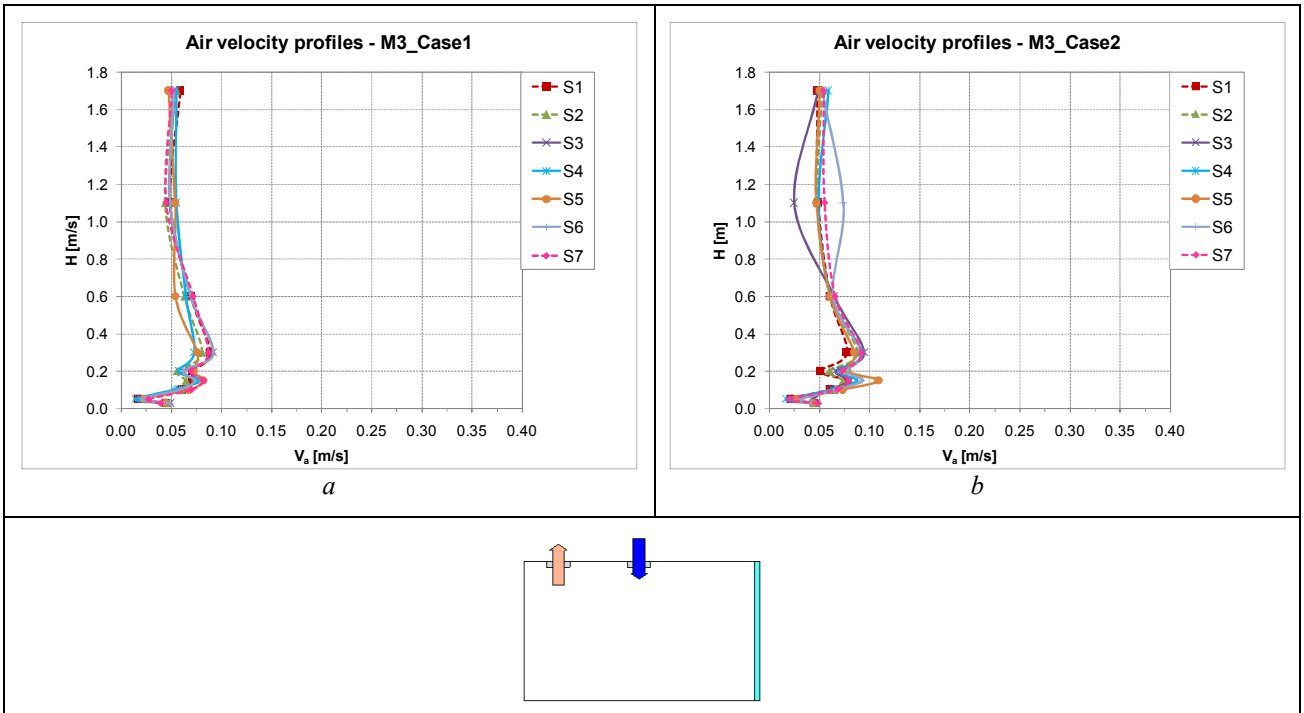

Figure A6 Air velocity vertical profiles for all cases (case 1 (a), case 2 (b)) of system M3 measured in the occupied zone (continuous line) and close to the window (dotted line)

System M4 (Mixing ventilation):

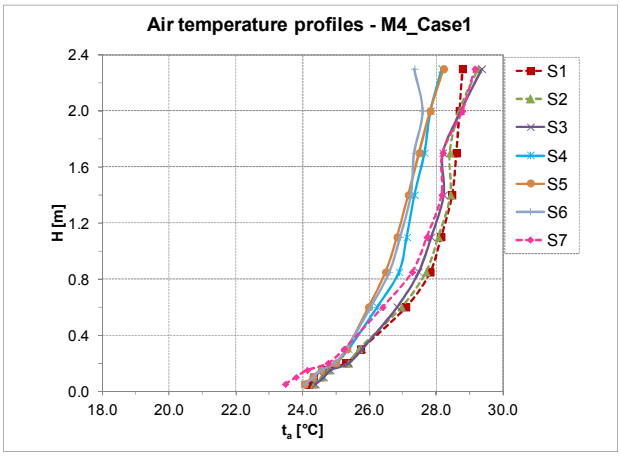

a

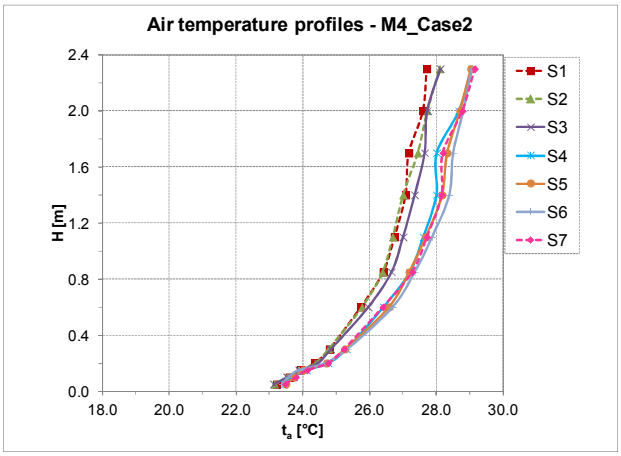

b

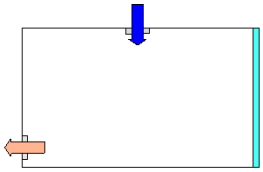

Figure A7 Air temperature vertical profiles for all cases (case 1 (a), case 2 (b)) of system M4 measured in the occupied zone (continuous line) and close to the window (dotted line)

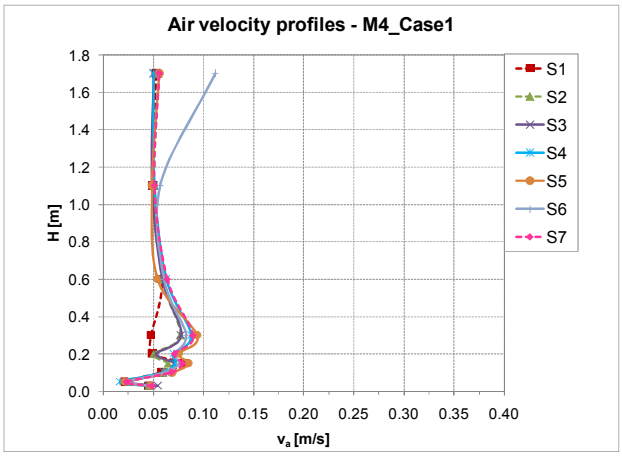

a

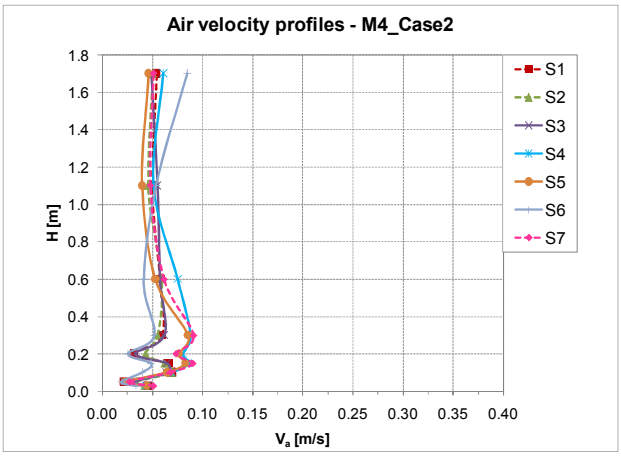

b

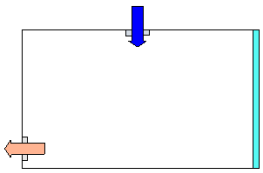

Figure A8 Air velocity vertical profiles for all cases (case 1 (a), case 2 (b)) of system M4 measured in the occupied zone (continuous line) and close to the window (dotted line)

System DV (Displacement ventilation):

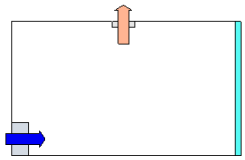

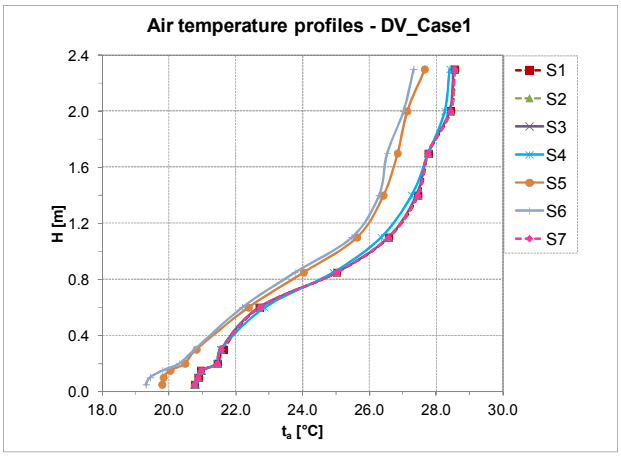

a

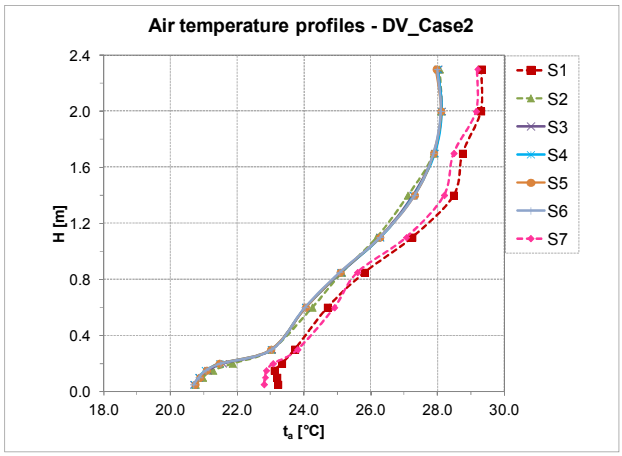

b

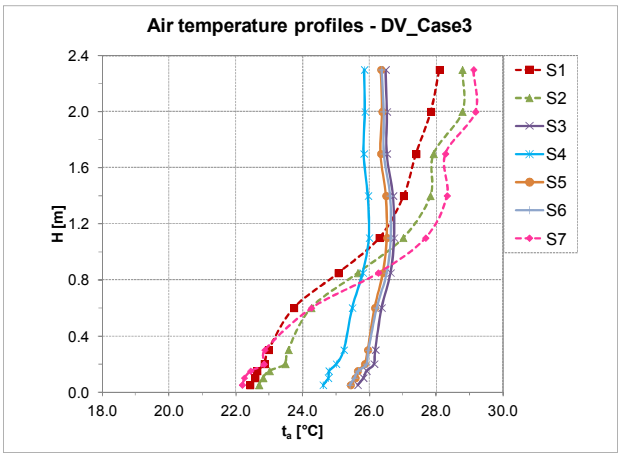

c

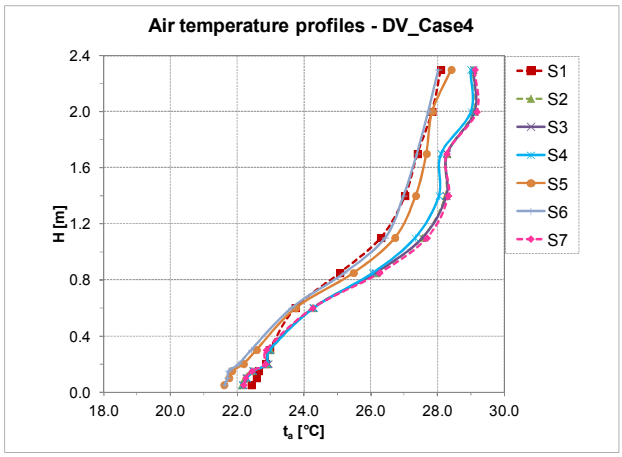

d

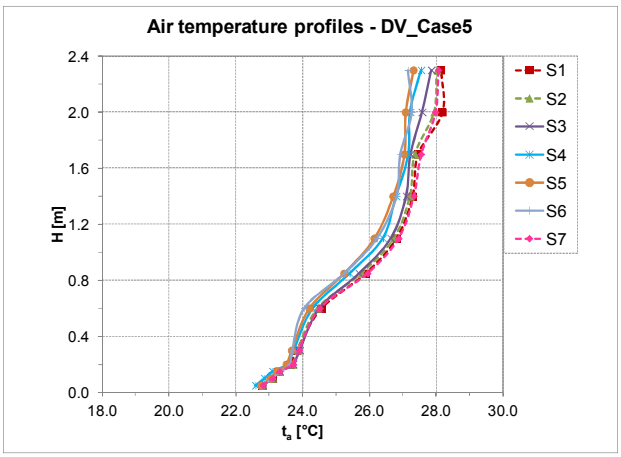

e

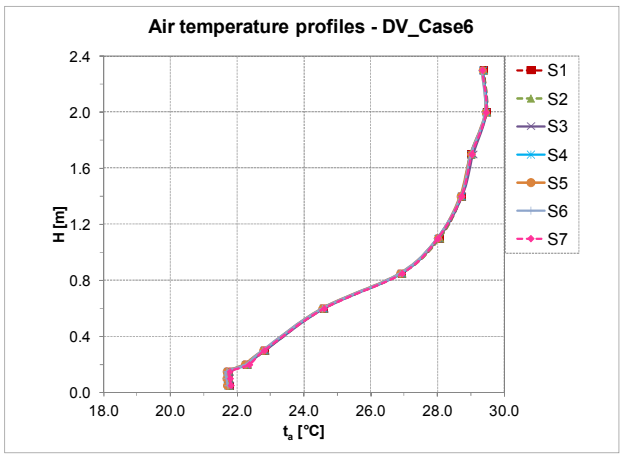

f

Figure A9 Air temperature vertical profiles for all cases (case 1 (a), case 2 (b), case3 (c) case 4 (d) case 5 (e) and case 6 (f)) of system DV measured in the occupied zone (continuous line) and close to the window (dotted line)

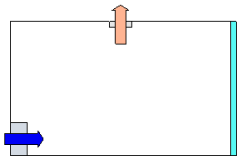

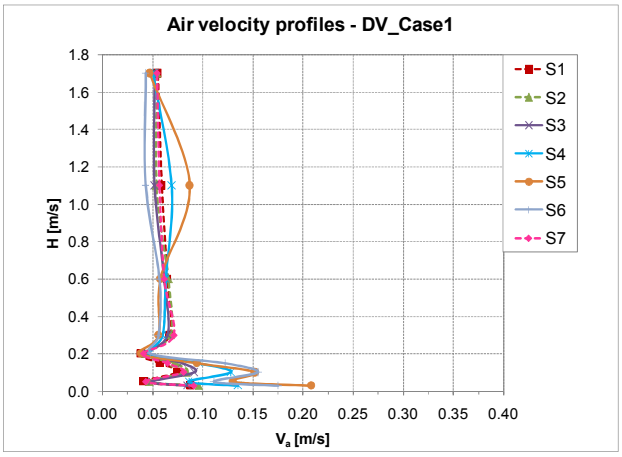

a

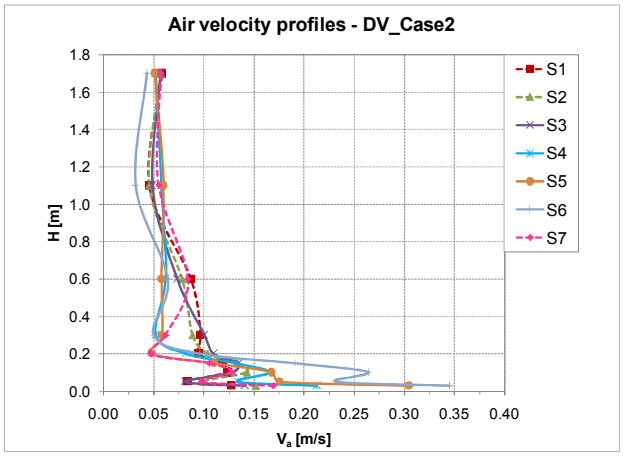

b

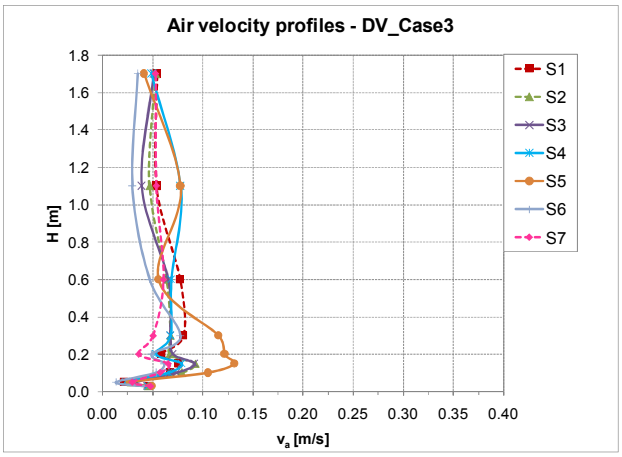

c

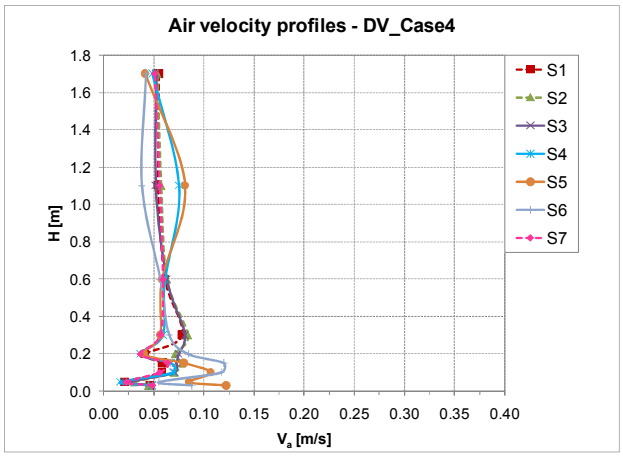

d

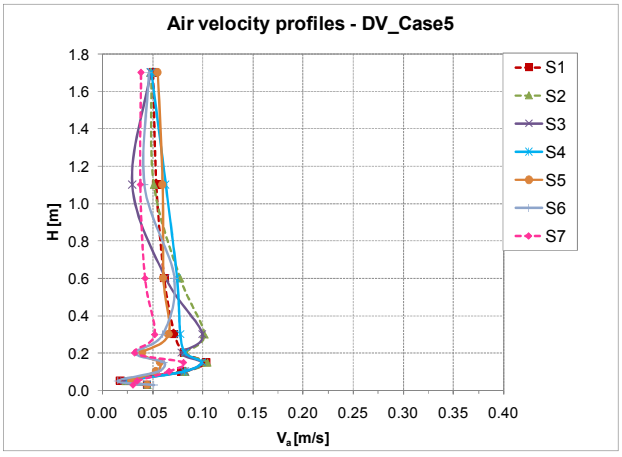

e

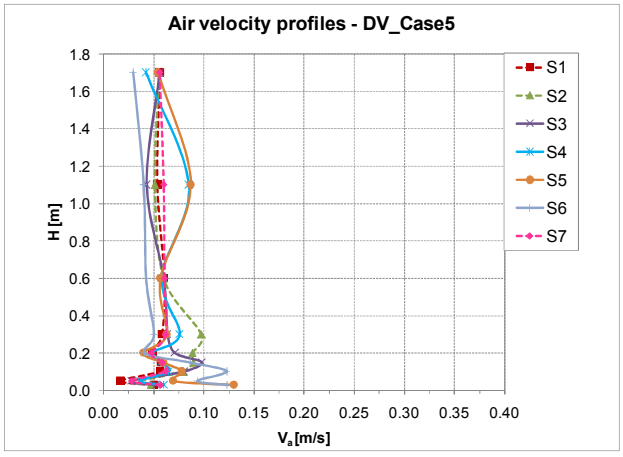

f

Figure A10 Air velocity vertical profiles for all cases (case 1 (a), case 2 (b), case3 (c) case 4 (d) case 5 (e) and case 6 (f)) of system DV measured in the occupied zone (continuous line) and close to the window (dotted line)

APPENDIX B – CALCULATED VERTICAL PROFILES OF AIR TEMPERATURES and AIR VELOCITIES FROM CFD RESULTS

System M1 (Mixing ventilation):

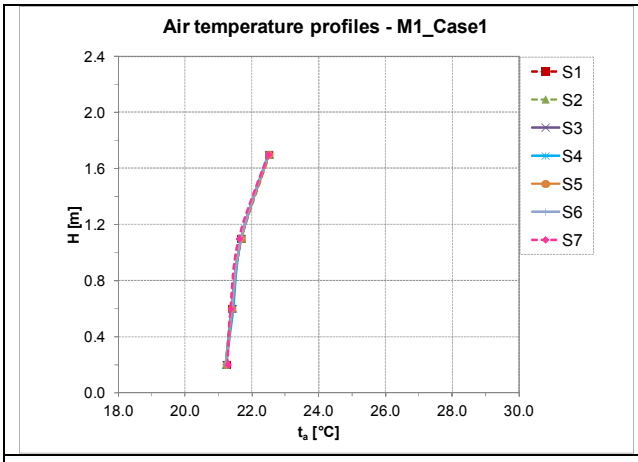

a

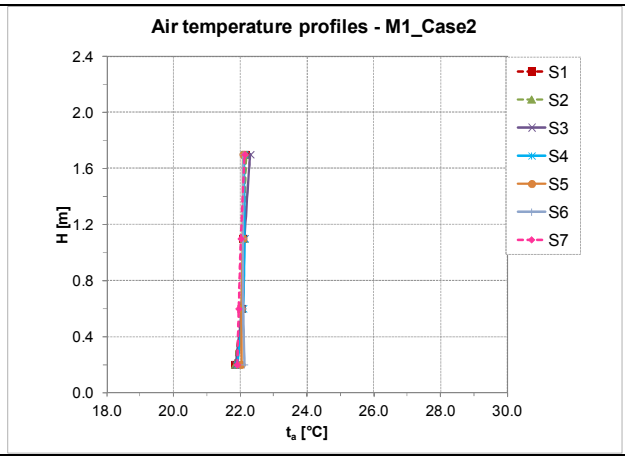

b

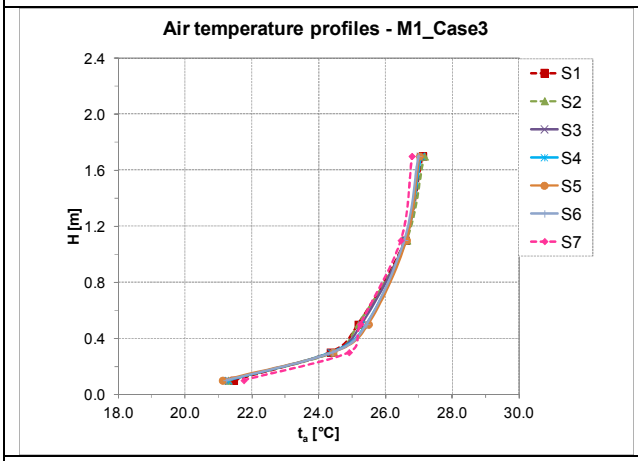

c

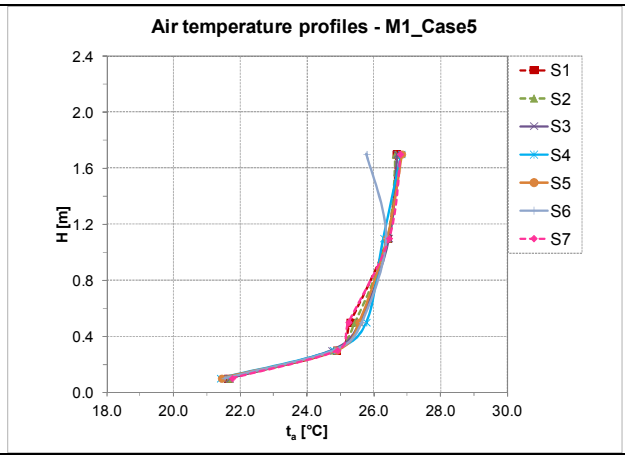

d

Figure B1 Air temperature vertical profiles for case 1 (a), case 2 (b), case3 (c) and case 5 (d) of system M1 in the occupied zone (continuous line) and close to the window (dotted line)

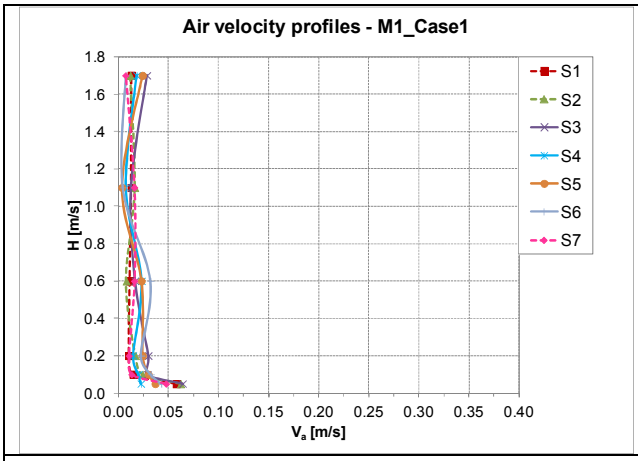

a

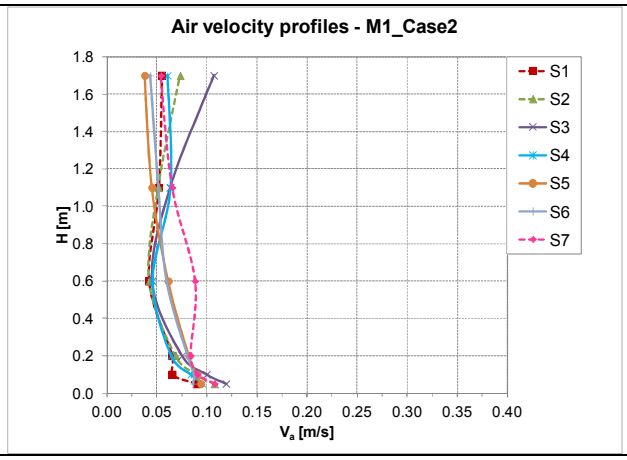

b

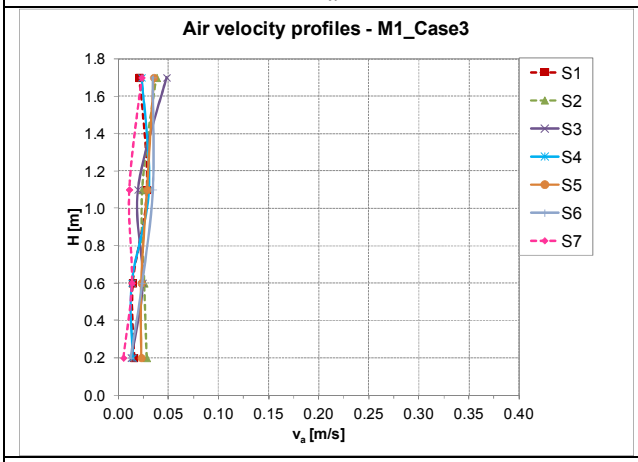

c

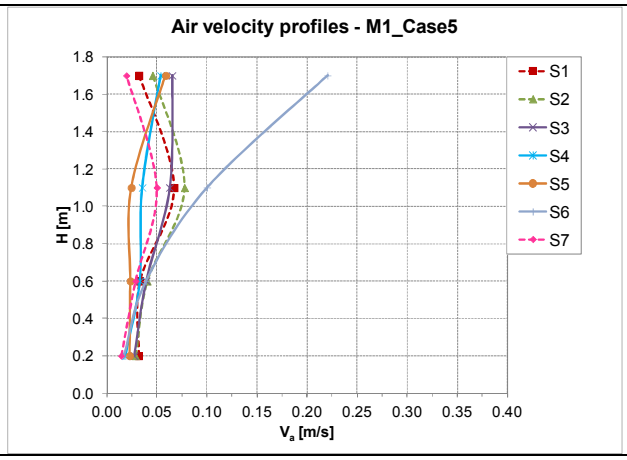

d

Figure B1 Air velocity vertical profiles for case 1 (a), case 2 (b), case3 (c) case 5 (d) of system M1 in the occupied zone (continuous line) and close to the window (dotted line)

System M2 (Mixing ventilation):

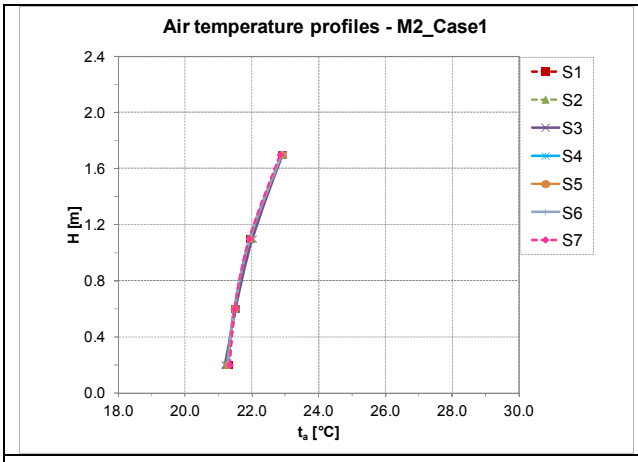

a

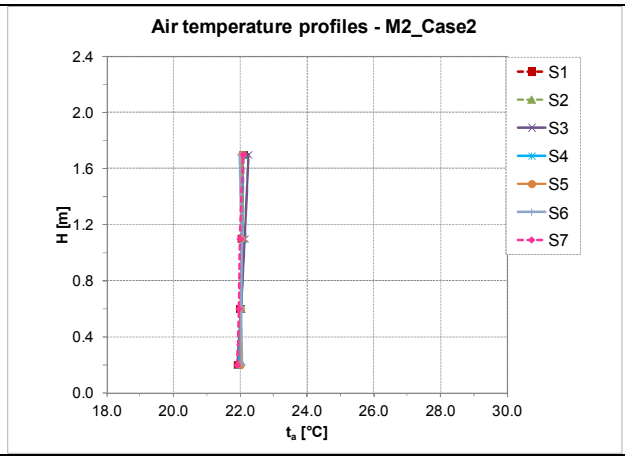

b

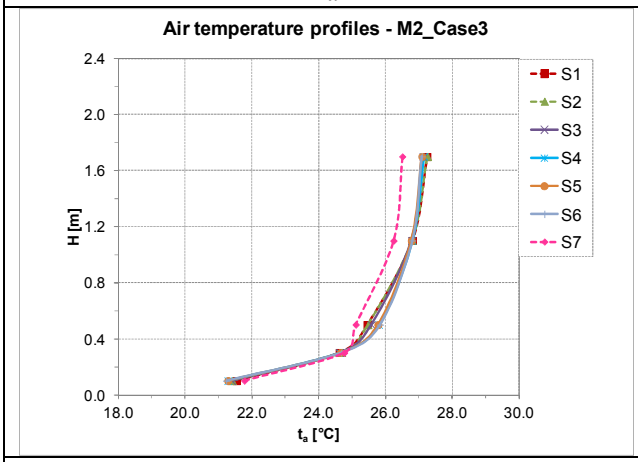

c

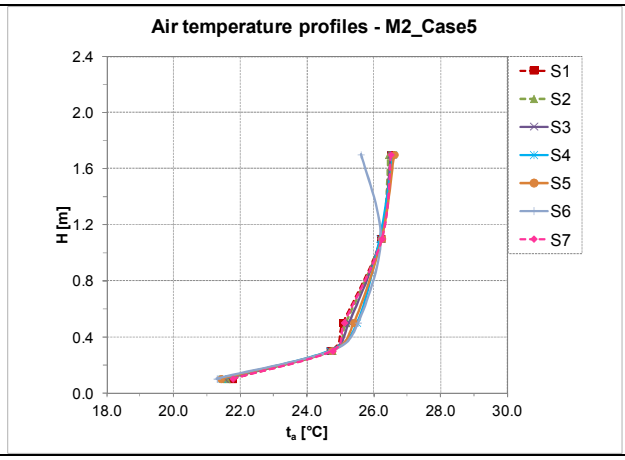

d

Figure B3 Air temperature vertical profiles for case 1 (a), case 2 (b), case3 (c) and case 5 (d) of system M2 in the occupied zone (continuous line) and close to the window (dotted line)

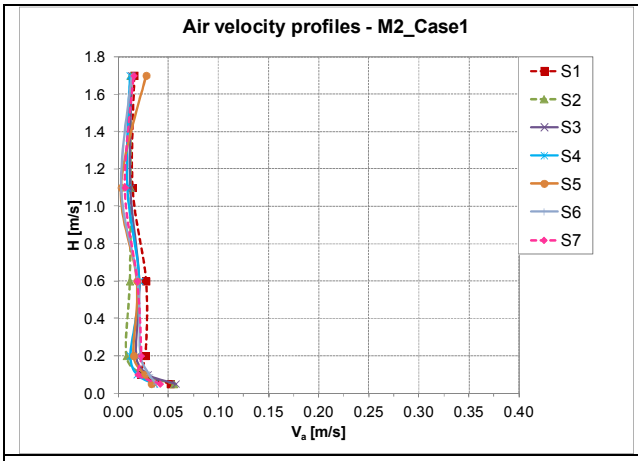

a

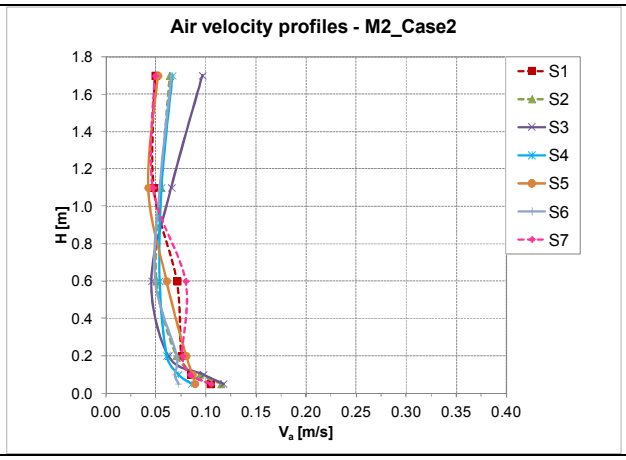

b

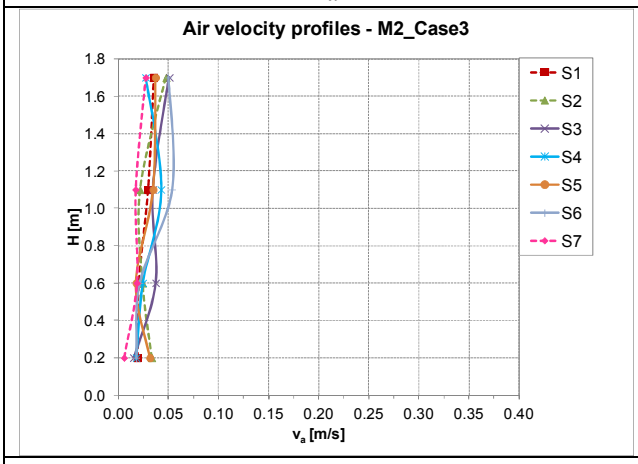

c

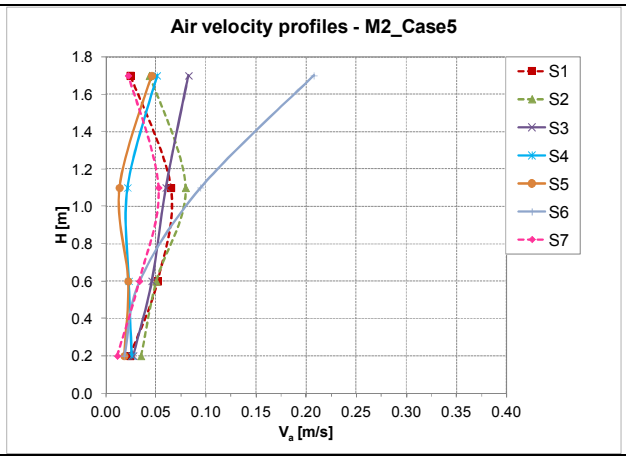

d

Figure B4 Air velocity vertical profiles for case 1 (a), case 2 (b), case3 (c) and case 5 (d) of system M2 in the occupied zone (continuous line) and close to the window (dotted line)

System DV (Displacement ventilation):

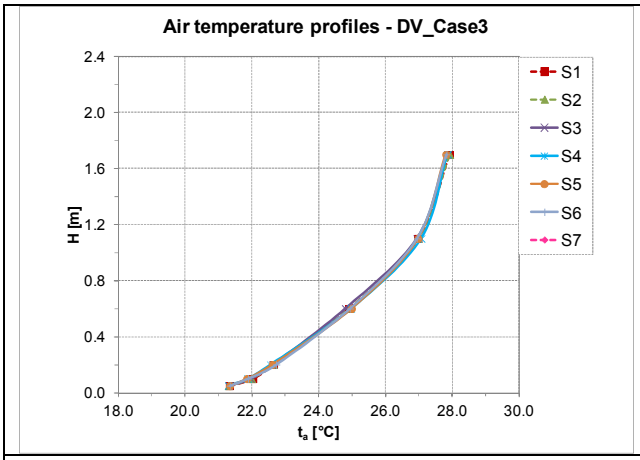

a

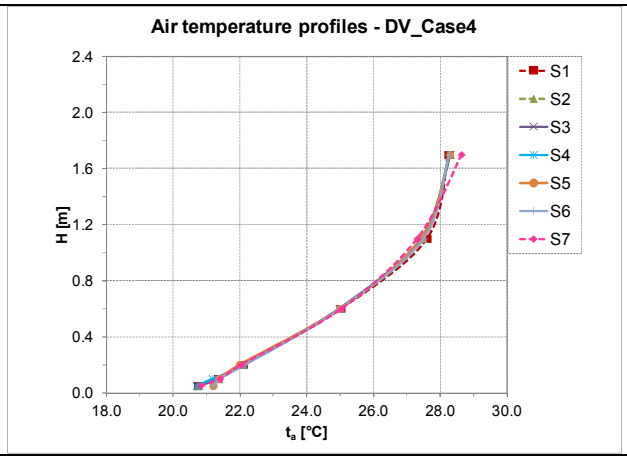

b

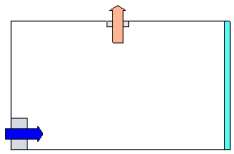

Figure B5 Air temperature vertical profiles for case 3(a) and case 4 (b) of system DV in the occupied zone (continuous line) and close to the window (dotted line)

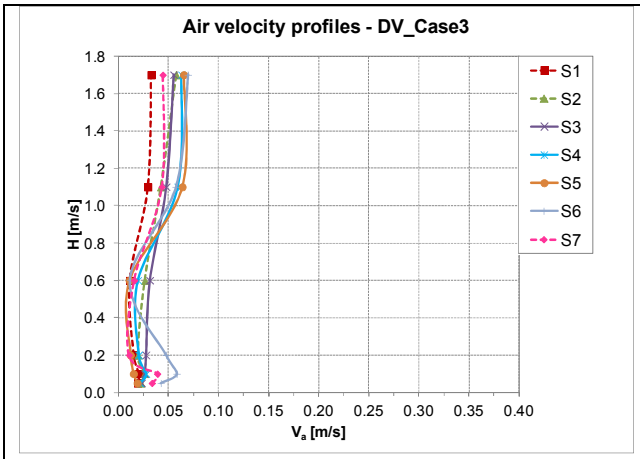

a

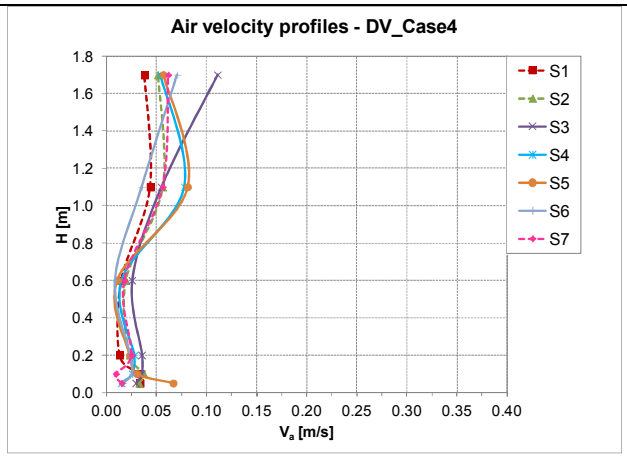

b

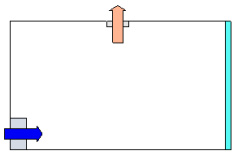

Figure B6 Air velocity vertical profiles for case 3(a) and case 4 (b) of system DV in the occupied zone (continuous line) and close to the window (dotted line)

APPENDIX C – VENTILATION EFFECTIVENESS PARAMETERS FROM CFD RESULTS

Table C1 Contaminant removal effectiveness [-] calculated in 7 positions at 0.6 m, 1.1 m and at 1.7 m height, average for each height for all the simulations; the "*" refers to method n°2

		Position							average
CASE	**Height[m]**	**P1**	**P2**	**P3**	**P4**	**P5**	**P6**	**P7**	
M1-1	**0.60**	1.52	1.31	1.60	-	-	1.16	1.37	1.39
	1.10	1.84	1.87	1.69	1.57	1.76	1.84	1.92	1.78
	1.70	1.85	1.91	1.74	1.70	1.92	1.91	1.94	1.85
M1-2	**0.6**	2.10	2.10	2.11	-	-	1.88	2.06	2.05
	1.1	2.10	2.09	2.09	2.10	2.12	2.08	2.07	2.09
	1.7	2.10	2.09	2.09	2.10	2.28	2.14	2.09	2.13
M1-5	**0.6**	1.86	1.86	1.84	-	-	1.76	1.71	1.81
	1.1	1.87	1.84	1.89	1.89	1.78	1.43	1.72	1.77
	1.7	1.87	1.86	1.88	1.87	1.91	1.78	1.76	1.85
M2-1	**0.60**	3.22	2.98	2.82	-	-	1.37	2.93	2.66
	1.10	4.69	4.91	2.99	3.00	4.32	4.35	4.56	4.12
	1.70	5.04	5.02	3.70	3.22	5.18	4.96	4.90	4.57
M2-2	**0.6**	2.62	2.58	2.62	-	-	2.58	2.60	2.60
	1.1	2.60	2.62	2.65	2.64	2.68	2.63	2.61	2.63
	1.7	2.55	2.62	2.60	2.59	2.92	2.64	2.59	2.64
M2-5	**0.6**	3.95	3.82	3.88	-	-	3.46	3.85	3.79
	1.1	3.91	3.88	3.96	4.00	4.25	3.36	3.67	3.86
	1.7	3.88	3.87	3.90	3.90	4.15	3.65	3.54	3.84
DV-3	**0.6**	17.85	21.09	32.37	-	-	31.32	13.69	23.26
	1.1	3.01	2.24	1.78	12.31	2.38	3.41	2.77	3.99
	1.7	2.22	1.93	2.38	2.74	1.99	1.97	2.47	2.24
DV-4	**0.6**	13.51	8.02	38.03	-	-	8.95	8.60	15.42
	1.1	2.44	2.28	3.13	2.87	2.03	2.09	2.07	2.42
	1.7	2.11	1.87	2.69	2.51	1.92	2.04	2.00	2.16
M1-5*	**0.6**	1.90	1.90	1.87	-	-	1.75	1.70	1.82
	1.1	1.91	1.89	1.93	1.93	1.81	1.50	1.73	1.81
	1.7	1.91	1.90	1.92	1.92	1.96	1.84	1.80	1.89
M2-5*	**0.6**	3.02	2.91	2.92	-	-	2.48	2.99	2.86
	1.1	3.01	3.00	3.05	3.09	3.34	2.44	2.85	2.97
	1.7	3.01	3.01	3.02	3.02	3.26	2.85	2.74	2.99

Table C2 Local air change index [%] calculated in 3 positions at 0.6 m, 1.1 m and at 1.7 m height and near the manikin at 1.1m height, average value for each height, for all the simulations; the "**" refers to method n° 3

	Position					average
CASE	**Height[m]**	**P1**	**P2**	**P3**	**manikin**	
M1-1	**0.60**	109.7%	108.9%	109.0%	-	109.2%
	1.10	106.5%	106.2%	108.2%	109.2%	107.5%
	1.70	106.4%	105.8%	107.7%	-	106.7%
M1-2	**0.6**	100.9%	100.8%	100.9%	-	100.9%
	1.1	100.9%	100.9%	100.8%	100.7%	100.8%
	1.7	101.0%	100.9%	101.0%	-	101.0%
M1-5	**0.6**	95.7%	96.6%	96.4%	-	96.2%
	1.1	95.7%	96.0%	95.5%	95.6%	95.7%
	1.7	95.7%	95.6%	95.6%	-	95.6%
M2-1	**0.60**	102.8%	102.2%	103.1%	-	102.7%
	1.10	101.3%	101.0%	102.3%	102.8%	101.9%
	1.70	101.1%	100.9%	102.1%	-	101.4%
M2-2	**0.6**	103.2%	103.4%	103.3%	-	103.3%
	1.1	103.2%	103.6%	103.4%	103.2%	103.4%
	1.7	103.4%	103.6%	103.5%	-	103.5%
M2-5	**0.6**	92.4%	93.0%	92.7%	-	92.7%
	1.1	92.5%	92.7%	92.1%	92.2%	92.4%
	1.7	92.5%	92.5%	92.4%	-	92.5%
DV-3	**0.6**	87.6%	87.4%	86.3%		87.1%
	1.1	85.8%	95.6%	98.8%	87.2%	91.5%
	1.7	105.8%	111.6%	100.5%		105.8%
DV-4	**0.6**	77.7%	81.3%	73.8%		77.5%
	1.1	99.4%	100.8%	96.5%	99.4%	99.0%
	1.7	100.7%	102.2%	99.0%		100.6%
DV-4**	**0.6**	89.4%	91.2%	86.6%	-	89.0%
	1.1	100.7%	100.1%	101.8%	99.1%	100.4%
	1.7	104.9%	106.3%	97.6%	-	102.8%

ACKNOWLEDGEMENTS

I'm very grateful to my supervisor, Prof. Michele De Carli, who gave me the opportunity to better understand what is the scientific research methodology during my Ph.D, giving me guidance and support a as well as his great experience and friendship.

I would like to express my gratitude to my co-advisor, Prof. Bjarne W. Olesen, who welcomed me at DTU with great cordiality, offering me his remarkable experience and assistance.

I would like to sincerely thank my parents and my brothers Luca and Marco, for their love and support.

I'm grateful to Angela, researcher at DTU, because she has been a fantastic friend and because her constant presence was indispensable during experiments in DTU and during the elaboration of data.

I wish to thank Prof. Roberto Zecchin, for the assistance and the advises he gave me during my university studies and my Ph.D period in Padova.

Thanks to Angelo, Giacomo and Massimiliano, researchers at my University, for their patience and precious help during these three years.

Thanks to Michal from Slovak University of Technology, with whom I shared the preparation and the execution of experimental tests in DTU; our different points of view and previous experiences certainly improved the final results!

I'm grateful to all the staff in DTU that allowed me to work in a pleasant and friendly environment, in particular Mrs. Snjezana, administrative officer at DTU, as well as Peter and Nico, engineer and technician at DTU.

Thanks to Daniela from Politecnico di Torino, for the fantastic exchange of information and experience, besides the friendship, during the period in the same office in DTU.

Thanks to the Ph.D students working in my Department in Padova, for their friendship not only when I was in Italy but also when I was in Denmark!

I would like to thank Franco, librarian at Department of Applied Physics in Padova, for his precious help to find out literature papers even though not very recent.

My sincere thanks to RHOSS S.p.A for the opportunity to carry out experiments in the test room for radiant systems placed at their laboratory; in particular I would like to remind Edi Pasut for his skills and courtesy.